

Slide ✓



DNA 2849F  
JULY 1972

PIFR-72-105

THEORETICAL STUDIES OF  
INTENSE RELATIVISTIC ELECTRON BEAM-PLASMA INTERACTIONS  
FINAL REPORT

AD 745369

by  
Sidney Putnam

Headquarters  
Defense Nuclear Agency  
Washington, D.C. 20305

Approved for public release;  
distribution unlimited.

SA

NATIONAL TECHNICAL  
INFORMATION SERVICE

PHYSICS INTERNATIONAL COMPANY  
2700 MERCED STREET • SAN LEANDRO, CALIF. 94577 • PHONE 357-4610 (415) • TWX 891-9689 (415)



390

Unclassified

Security Classification

| DOCUMENT CONTROL DATA - R&D  |   |  |
|--|---|--|
| <i>(Security classification of title, body of abstract and indexing annotation must be entered when the overall report is classified)</i>  |   |  |
| 1 ORIGINATING ACTIVITY (Corporate-author)<br>Physics International Company<br>2700 Merced Street<br>San Leandro, California 94577  |   | 2a. REPORT SECURITY CLASSIFICATION<br>Unclassified |
|  |   | 2b. GROUP<br>NA                                    |
| 3 REPORT TITLE<br>Theoretical Studies of Intense Relativistic Electron<br>Beam-Plasma Interactions   |   |  |
| 4 DESCRIPTIVE NOTES (Type of report and inclusive dates)<br>Final Report   |   |  |
| 5. AUTHOR(S) (Last name, first name, initial)<br>Putnam, Sidney  |   |  |
| 6. REPORT DATE<br>January 1972   | 7a. TOTAL NO. OF PAGES<br>401   | 7b. NO. OF REFS<br>147                             |
| 8a. CONTRACT OR GRANT NO.<br>DASA-01-68-C-0096   | 9a. ORIGINATOR'S REPORT NUMBER(S)<br>PIFR-72-105  |  |
| b. PROJECT NO.<br>c. NWER Subtask LA 013-02  | 9b. OTHER REPORT NO(S); (Any other numbers that may be assigned<br>this report)<br>DNA 2849F          |  |
| 10 AVAILABILITY/LIMITATION NOTICES<br>Approved for public release; distribution unlimited  |   |  |
| 11. SUPPLEMENTARY NOTES  | 12. SPONSORING MILITARY ACTIVITY<br>Headquarters<br>Defense Nuclear Agency<br>Washington, D.C., 20305 |  |
| 13 ABSTRACT A comprehensive survey of intense relativistic electron beam physics is presented, including detailed discussions of selected topics. The beam-generated plasma is characterized through charge production rules for calculation of gas breakdown times, conductivity at breakdown, and current neutralization. Longitudinal electrostatic instability theory is reviewed in the context of typical beam-plasma parameters and a model explaining the low-pressure transverse instability (the frozen hose) is given. Transport phenomenology without external fields and with external linear pinch and solenoidal fields is discussed and models are developed to define efficient beam transport conditions. Transient electromagnetic (EM) fields are calculated for the finite geometry of the beam-drift chamber and simple rules are given to estimate the EM fields in a finite cavity. Exact EM fields are numerically calculated for a beam penetrating a plasma in a conducting pipe (the current neutralization problem) and for a beam penetrating an end-plate into a neutral gas (the injection problem). Weakly turbulent beam-plasma heating theory is summarized and consistency requirements relating beam and plasma parameters are outlined. Low pressure beam transport and collective ion acceleration are discussed in detail and a model of synchronized ion acceleration is presented. |   |  |

ia

Unclassified  
Security Classification

| 14 | KEY WORDS  | LINK A |    | LINK B |    | LINK C |    |
|----|--|--------|----|--------|----|--------|----|
|    |  | ROLE   | WT | ROLE   | WT | ROLE   | WT |
|    | Intense electron beams<br>Beam-generated plasmas<br>Collective ion acceleration<br>Beam stability<br>Beam transport<br>Beam-generated electromagnetic fields<br>Plasma heating |        |    |        |    |        |    |

**INSTRUCTIONS**

1. **ORIGINATING ACTIVITY:** Enter the name and address of the contractor, subcontractor, grantee, Department of Defense activity or other organization (*corporate author*) issuing the report.
- 2a. **REPORT SECURITY CLASSIFICATION:** Enter the overall security classification of the report. Indicate whether "Restricted Data" is included. Marking is to be in accordance with appropriate security regulations.
- 2b. **GROUP:** Automatic downgrading is specified in DoD Directive 5200.10 and Armed Forces Industrial Manual. Enter the group number. Also, when applicable, show that optional markings have been used for Group 3 and Group 4 as authorized.
3. **REPORT TITLE:** Enter the complete report title in all capital letters. Titles in all cases should be unclassified. If a meaningful title cannot be selected without classification, show title classification in all capitals in parenthesis immediately following the title.
4. **DESCRIPTIVE NOTES:** If appropriate, enter the type of report, e.g., interim, progress, summary, annual, or final. Give the inclusive dates when a specific reporting period is covered.
5. **AUTHOR(S):** Enter the name(s) of author(s) as shown on or in the report. Enter last name, first name, middle initial. If military, show rank and branch of service. The name of the principal author is an absolute minimum requirement.
6. **REPORT DATE:** Enter the date of the report as day, month, year, or month, year. If more than one date appears on the report, use date of publication.
- 7a. **TOTAL NUMBER OF PAGES:** The total page count should follow normal pagination procedures, i.e. enter the number of pages containing information.
- 7b. **NUMBER OF REFERENCES:** Enter the total number of references cited in the report.
- 8a. **CONTRACT OR GRANT NUMBER:** If appropriate, enter the applicable number of the contract or grant under which the report was written.
- 8b, 8c, & 8d. **PROJECT NUMBER:** Enter the appropriate military department identification, such as project number, subproject number, system numbers, task number, etc.
- 9a. **ORIGINATOR'S REPORT NUMBER(S):** Enter the official report number by which the document will be identified and controlled by the originating activity. This number must be unique to this report.
- 9b. **OTHER REPORT NUMBER(S):** If the report has been assigned any other report numbers (*either by the originator or by the sponsor*), also enter this number(s).
10. **AVAILABILITY/LIMITATION NOTICES:** Enter any limitations on further dissemination of the report, other than those

imposed by security classification, using standard statements such as:

- (1) "Qualified requesters may obtain copies of this report from DDC."
- (2) "Foreign announcement and dissemination of this report by DDC is not authorized."
- (3) "U. S. Government agencies may obtain copies of this report directly from DDC. Other qualified DDC users shall request through \_\_\_\_\_."
- (4) "U. S. military agencies may obtain copies of this report directly from DDC. Other qualified users shall request through \_\_\_\_\_."
- (5) "All distribution of this report is controlled. Qualified DDC users shall request through \_\_\_\_\_."

If the report has been furnished to the Office of Technical Services, Department of Commerce, for sale to the public, indicate this fact and enter the price, if known.

11. **SUPPLEMENTARY NOTES:** Use for additional explanatory notes.

12. **SPONSORING MILITARY ACTIVITY:** Enter the name of the departmental project office or laboratory sponsoring (*paying for*) the research and development. Include address.

13. **ABSTRACT:** Enter an abstract giving a brief and factual summary of the document indicative of the report, even though it may also appear elsewhere in the body of the technical report. If additional space is required, a continuation sheet shall be attached.

It is highly desirable that the abstract of classified reports be unclassified. Each paragraph of the abstract shall end with an indication of the military security classification of the information in the paragraph, represented as (TS) (S) (C) or (U).

There is no limitation on the length of the abstract. However, the suggested length is from 150 to 225 words.

14. **KEY WORDS:** Key words are technically meaningful terms or short phrases that characterize a report and may be used as index entries for cataloging the report. Key words must be selected so that no security classification is required. Identifiers, such as equipment model designation, trade name, military project code name, geographic location, may be used as key words but will be followed by an indication of technical context. The assignment of links, roles, and weights is optional.

ib

DNA 2849F

JULY 1972

PIFR-72-105

**THEORETICAL STUDIES OF  
INTENSE RELATIVISTIC ELECTRON BEAM-PLASMA INTERACTIONS**

**FINAL REPORT**

Details of illustrations in  
this document may be better  
studied on microfiche

by

Sidney Putnam

This work was supported by the Defense  
Nuclear Agency under NWER subtask LA 013-02.

Headquarters  
Defense Nuclear Agency  
Washington, D.C. 20305

Approved for public release;  
distribution unlimited.

Prepared by  
Physics International Company  
2700 Merced Street  
San Leandro, California 94577

DASA 01-68-C-0096

## ABSTRACT

A comprehensive survey of intense relativistic electron beam physics is presented, including detailed discussions of selected topics. The beam-generated plasma is characterized through charge production rules for calculation of gas breakdown times, conductivity at breakdown, and current neutralization. Longitudinal electrostatic instability theory is reviewed in the context of typical beam-plasma parameters and a model explaining the low-pressure transverse instability (the frozen hose) is given. Transport phenomenology without external fields and with external linear pinch and solenoidal fields is discussed and models are developed to define efficient beam transport conditions. Transient electromagnetic (EM) fields are calculated for the finite geometry of the beam-drift chamber and simple rules are given to estimate the EM fields in a finite cavity. Exact EM fields are numerically calculated for a beam penetrating a plasma in a conducting pipe (the current neutralization problem) and for a beam penetrating an endplate into a neutral gas (the injection problem). Weakly turbulent beam-plasma heating theory is summarized and consistency requirements relating beam and plasma parameters are outlined. Low pressure beam transport and collective ion acceleration are discussed in detail and a model of synchronized ion acceleration is presented.

## FOREWORD

The material of this report is an updated revision and extension of work performed mostly during a one-year contract (1968-1969) with the Defense Nuclear Agency (DNA). Much of the research was originally published as Physics International Company quarterly reports and as a final report, PIFR-105, April 1970, all of which have been submitted to DNA.

The major addition to PIFR-105 included here is the new work on beam propagation in external solenoidal and linear pinch fields. The viewpoint of the treatment on neutral gas propagation without external fields has been somewhat modified to give more emphasis to coupled beam dynamics and electromagnetic fields through explicit inclusion of the effects of beam transverse energy; the beam current density is emphasized as an important parameter in beam-plasma phenomenology, in addition to the more commonly used  $v/\gamma$  ratio. The collective ion acceleration model material has also been slightly revised from the original report version, and includes a more detailed discussion of ion acceleration cutoff mechanisms.

I have tried to present a rather comprehensive survey of the entire intense beam field in this revision, and, to this end, have included a brief survey of diode physics and a summary of steady state beam equilibrium models as well as a discussion of turbulent plasma heating. The style of the report is hopefully expository and at a level useful as an introduction to the field. I have perhaps given too phenomenological an approach for many tastes in the report, but in many cases no other work exists. Moreover, in this new and very complicated field it has been my experience that such a viewpoint is often more relevant, at least to gross beam behavior, than highly quantitative analytical treatments which necessarily require many impractical assumptions to be analytically amenable. It is likely that as the field advances and diagnostic techniques become more sophisticated, detailed theoretical descriptions will have to rely on numerical simulation.

It is a pleasure to acknowledge the technical guidance and criticism of many individuals. I would especially like to thank Dr. Andrew Sessler of the Lawrence Berkeley Laboratory, Berkeley, California, who has given freely of his time and offered invaluable criticism and guidance throughout the program. Dr. William T. Link, who was the leader of the Beam Physics Group at Physics International Company during the original program conception, encouraged me to embark upon a beam research program in support of the experimental activities, and Mr. David dePackh of the Naval Research Laboratory, Washington, D.C. supported the need for such a program and gave personal encouragement.

Preceding page blank

I wish to acknowledge many helpful discussions with my colleagues at Physics International: Drs. Gerold Yonas, Philip Spence, David Sloan, James Benford, Charles Stallings, and John Guillory, and Messrs. John Creedon, Bruce Ecker, and John Rander. Professor Wulf Kunkel of the Lawrence Berkeley Laboratory has also offered many useful criticisms and suggestions.

I should like to thank my wife, Joyce Putnam, for her valuable assistance in numerical analysis. To Mrs. Lila Lowell for typing endless equations and to Mrs. Pat Shand for major production assistance, I also extend my deepest gratitude.

Dr. Jonathan Wachtel, currently at Yeshiva University, New York, N.Y., acted as the original contract monitor and his active interest provided much support. I express my appreciation to Lt. Col. Robert Sullivan and Major Benjamin Pellegrini of DNA for their support as well as patience with respect to many delays.

Physics International Company made possible completion of some of the material with company support and the Theoretical Group of the Lawrence Berkeley Laboratory provided use of computer facilities and hospitality for the author as a participating guest member.

## CONTENTS

|  | <u>Page</u> |
|--|-------------|
| SECTION 1 INTRODUCTION   | 1-1         |
| 1.1 Basic Concepts of Beam-Plasma Interactions--Historical Survey  | 1-4         |
| 1.2 Discussion of Report   | 1-14        |
| REFERENCES   | 1-25        |
| SECTION 2 GENERAL BEAM PLASMA INTERACTION PHENOMENOLOGY  | 2-1         |
| 2.1 Diode Physics  | 2-1         |
| 2.2 Electromagnetic Fields in Finite Cavities  | 2-16        |
| 2.3 Exact EM Solutions for Beam Penetrating an Endplate in a Finite Radius Chamber ( $f_e = 0$ )                           | 2-26        |
| 2.4 Charge Production in Neutral Gases   | 2-34        |
| 2.5 Plasma Conductivity  | 2-49        |
| 2.6 Current Neutralization   | 2-55        |
| 2.7 Some Beam Dynamics   | 2-64        |
| 2.8 Some Topics in Beam Stability  | 2-86        |
| 2.9 Plasma Channeling  | 2-103       |
| 2.10 Summary of Beam Transport Phenomenology   | 2-105       |
| 2.11 Plasma Heating  | 2-161       |
| REFERENCES   | 2-177       |
| SECTION 3 ELECTRODYNAMIC CALCULATIONS  | 3-1         |
| 3.1 Basic Equations  | 3-1         |
| 3.2 Exact EM fields for a Beam in a Long Pipe Filled with Constant Conductivity Plasma--The Current Neutralization Problem | 3-10        |

CONTENTS (cont.)

|  | <u>Page</u> |
|--|-------------|
| 3.3 The Closed Cavity Problem  | 3-48        |
| 3.4 Single Endplate, Zero Conductivity<br>Problem--The Injection Problem                       | 3-77        |
| 3.5 Beam in a Long Pipe with Plasma<br>Conductivity Varying with Distance<br>Behind Beam Front | 3-104       |
| REFERENCES   | 3-111       |
| SECTION 4 COLLECTIVE ION ACCELERATION BY INTENSE<br>ELECTRON BEAMS IN LINEAR GEOMETRY          | 4-1         |
| 4.1 Experimental Results   | 4-4         |
| 4.2 Some Suggested Acceleration Models   | 4-9         |
| 4.3 The Localized Pinch Model  | 4-22        |
| REFERENCES   | 4-51        |
| SECTION 5 SUMMARY  | 5-1         |

## ILLUSTRATIONS

| <u>Figure</u> |   | <u>Page</u> |
|---------------|---|-------------|
| 1.1           | Electron beam-gas interaction as a function of pressure   | 1-5         |
| 2.1           | The critical current geometry   | 2-4         |
| 2.2           | Impedance collapse phenomenology  | 2-8         |
| 2.3           | Parapotential flow model  | 2-11        |
| 2.4           | Comparison of theoretical [Equation (2.12)] and experimental results for impedance of diode pinched flow. For this comparison, experimental data were restricted to $dI/dt = 0$ . Experimental points correspond to various $r_c/d$ and $V_0$ values. | 2-13        |
| 2.5           | Beam chamber geometry   | 2-17        |
| 2.6           | Fields for a uniform electron beam in a closed cavity   | 2-19        |
| 2.7           | Sketches of $E_z$ fields with and without ions  | 2-24        |
| 2.8           | Open ended pipe geometry  | 2-27        |
| 2.9           | The longitudinal electric field ( $E_z$ ) on axis for a beam penetrating an end plate in a finite radius cavity   | 2-29        |
| 2.10          | The longitudinal electric field ( $E_z$ ) on axis for a beam penetrating an end plate in a finite radius cavity ( $t = 2$ nsec)   | 2-30        |
| 2.11          | The longitudinal electric field ( $E_z$ ) on axis for a beam penetrating an end plate in a finite radius cavity ( $t = 5$ nsec)   | 2-31        |

Illustrations (continued)

| <u>Figure</u>   | <u>Page</u> |
|---|-------------|
| 2.12 The geometry of electrostatic field calculation for a beam emerging from an infinite conducting plane                  | 2-33        |
| 2.13 Plot of $E/p$ versus $P t_i$ for air   | 2-43        |
| 2.14 Plot of $E/p$ versus $P t_i$ for helium  | 2-44        |
| 2.15 Mean ionization time versus pressure for air   | 2-45        |
| 2.16 Phenomenology of charge production in neutral gas  | 2-46        |
| 2.17 A. V. Phelps electron drift velocity data for dry air  | 2-56        |
| 2.18 Conductivity versus time after beam injection sketch for two representative pressures                                  | 2-59        |
| 2.19 Comparison of measured and calculated net currents (Reference 2.23)  | 2-60        |
| 2.20 Beam envelope motion   | 2-66        |
| 2.21 Electron beam-gas interaction as a function of pressure  | 2-68        |
| 2.22 Minimum constant radius versus $\epsilon$ for 4-MeV, $6 \times 10^4$ A electrons (beam in pinch mode).                 | 2-71        |
| 2.23 A sketch of beam-plasma system longitudinal velocity distributions   | 2-87        |
| 2.24 Experimental test setup  | 2-95        |
| 2.25 "Frozen hose" instability of a pinched beam  | 2-96        |
| 2.26 (a) Instability wavelength as a function of $(v/\gamma)^{-1/2}$ , $d \ll D$ : (b) Instability wavelength in guide tube | 2-98        |

Illustrations (Continued)

| <u>Figure</u>  | <u>Page</u> |
|--|-------------|
| 2.27 Transverse instability of a highly pinched beam where $t_B \sim t_p \gg t_r$ .  | 2-99        |
| 2.28 Transverse instability of high pressure pinched beam  | 2-100       |
| 2.29 Fluting instability of a hollow beam  | 2-102       |
| 2.30 The experimental geometry for injection into a plasma channel   | 2-104       |
| 2.31 Electrostatic potential in drift chamber ( $t < \tau_N$ ).  | 2-109       |
| 2.32 Experimental configuration of Z-pinch apparatus and beam-generating diode   | 2-116       |
| 2.33 Magnetic field profiles at times of beam injection. $R_C$ is beam cathode radius, arrows indicate damage radii of transported beams | 2-118       |
| 2.34 The beam return current in a pinch where $t_d \gg t_p$  | 2-120       |
| 2.35 Sketch of beam propagation in collapsing pinch  | 2-121       |
| 2.36 Pinched phase beam injection  | 2-123       |
| 2.37 The expanding pinch model   | 2-126       |
| 2.38 Two dimensional penetration of pinch field by beam  | 2-129       |
| 2.39 A magnetic field profile for transport of a 1 MeV, 2 megampere beam at $10^5$ A/cm <sup>2</sup>                                     | 2-132       |
| 2.40 Perpendicular velocity components in combined $B_\theta$ and $B_z$ magnetic fields  | 2-136       |
| 2.41 Beam penetrating a neutral gas with $B_z$   | 2-141       |

Illustrations (Continued)

| <u>Figure</u>  | <u>Page</u>          |
|--|----------------------|
| 2.42 Cross section of beam chamber showing secondary electron orbits when $r_t \geq R$   | 2-145                |
| 2.43 Cross section of beam chamber showing secondary electron orbits when $a \lesssim r_t \lesssim R$                                | 2-148                |
| 2.44 Secondary electron return currents at various stages of electrical neutralization with $B_z$ fields                             | 2-151                |
| 2.45 Charge transport efficiency at 1/2 meter for three current densities  | 2-160                |
| 3.1 The radial and longitudinal profiles for $j_{bz}$  | 3-11                 |
| 3.2 Cavity geometry  | 3-52                 |
| 3.3 The u dependence for $j_{bz}$  | 3-54                 |
| 3.4 Open-ended pipe geometry   | 3-78                 |
| 3.5 $E_z$ versus t at various distances from the end-plate (a through k)   | 3-83<br>thru<br>3-94 |
| 3.6 $E_z$ versus t at $z = 50$ cm  | 3-95                 |
| 3.7 (a) The longitudinal electric field ( $E_z$ ) on axis for a beam penetrating an end plate in a finite radius cavity (t = 1 nsec) | 3-97                 |
| (b) The longitudinal electric field ( $E_z$ ) on axis for a beam penetrating an end plate in a finite radius cavity (t = 2 nsec)     | 3-98                 |
| (c) The longitudinal electric field ( $E_z$ ) on axis for a beam penetrating an end plate in a finite radius cavity (t = 5 nsec)     | 3-99                 |
| 3.8 The conductivity function  | 3-104                |

Illustrations (Continued)

| <u>Figure</u> |   | <u>Page</u> |
|---------------|---|-------------|
| 4.1           | Schematic of linear beam experiment   | 4-5         |
| 4.2           | Proton pulse separation versus pressure   | 4-8         |
| 4.3           | The beam profile at the start of ion acceleration in the UMG model                                | 4-21        |
| 4.4           | The localized pinch acceleration model  | 4-23        |
| 4.5           | Sketch of the beam envelope in region 1   | 4-30        |
| 4.6           | Longitudinal electric fields of the synchronous ion density enhancement                           | 4-36        |
| 4.7           | Bunching in a slowly moving open-ended potential well   | 4-39        |
| 4.8           | Bunching near the anode with a partially closed well  | 4-41        |
| 4.9           | Beam-front velocity as a function of distance from the anode for a beam penetrating a neutral gas | 4-44        |

## SECTION 1

### INTRODUCTION

The electron accelerator technology necessary to generate the electron beams to which the research of this report is directed is relatively new--five or six years old. The beam currents of interest are in the tens of kiloamperes to megampere range, with kinetic energies from a few hundred kilovolts to about 15 MeV. The beam pulse widths vary from 20 nsec to approximately 200 nsec. We are thus dealing with intense, relativistic or near-relativistic, pulsed electron beams with total energies ranging from kilojoules to megajoules and power levels up to  $10^{13} \sim 10^{14}$  watts.

Much of the initial (and continuing) development of the pulsed power technology for intense electron beam accelerators was by J. C. Martin and his co-workers at the Atomic Weapons Research Establishment, Aldermaston, England. Table 1.1 lists beam parameters of some accelerators designed at Physics International Company (PI) which more or less cover the range of available machines. Other organizations in the United States besides PI with high current electron beam accelerators and active research efforts in the intense beam field are the Naval Research Laboratory, Ion Physics Corporation, Sandia Laboratories, Cornell University, and Maxwell Laboratories. Several accelerators have also been constructed or are currently under development in the Soviet Union, notably at the Institute of Nuclear Physics, Novosibirsk, the Joint Institute of Nuclear Research, Dubna, and at the Lebedev Physics Institute.

TABLE 1.1  
ELECTRON BEAM ACCELERATORS BY PHYSICS INTERNATIONAL

| <u>Machine</u> | <u>Electron Energy (MeV)</u> | <u>Current (kiloamperes)</u> | <u>Pulse Width FWHM (nsec)</u> |
|----------------|------------------------------|------------------------------|--------------------------------|
| 312            | 2                            | 25                           | 20                             |
| 738            | 0.2 to 1.5                   | 100 to 250                   | 40 to 50                       |
| 1140           | 4 to 6                       | 50 to 85                     | 70                             |
| 1590           | 6 to 10                      | 300                          | 65                             |
| B <sup>3</sup> | 0.4 to 8                     | 200 to 400                   | 65                             |
| DML            | 0.1 to 0.15                  | 100 to 300                   | 40                             |
| PIML           | 0.15 to 0.3                  | 200 to 300                   | 50                             |
| Mini-Marx      | 0.6                          | 10 <sup>3</sup>              | 25                             |
| Snark          | 1                            | 10 <sup>3</sup>              | 70                             |
| Aurora         | 15 to 20                     | 1.6 x 10 <sup>3</sup>        | 120                            |

As one might expect, the beams and their self-generated plasmas are a new regime in physics. The beam-plasma investigations of the past have been concerned with the physics of plasmas perturbed by beams of milliampere currents, whereas accelerator physics has been a study of beams of even smaller currents slightly perturbed by plasma or collective many particle effects. In our case the beam and plasma are strongly coupled and most problems are inescapably transient. Many intense beam problems are really problems of partially (space-charge) compensated plasmas, a fascinating field of physics rapidly emerging in collective ion acceleration studies, ion source development, and in some new plasma containment system proposals.

Most of the accelerator development and beam research in the past has been directed toward intense X-ray source applications and studies of material response from rapid energy deposition. The emphasis in these areas has been on efficient beam transport and control of beam energy density. Recently considerable interest has arisen regarding use of intense beams in several new areas: controlled thermonuclear reactor (CTR) applications, high power microwave generation, collective ion acceleration, and highly stripped ion production, to mention a few.

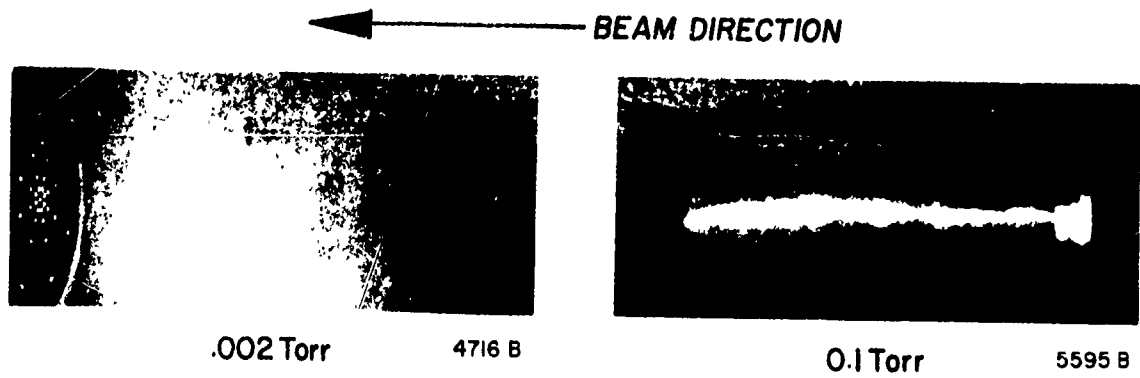
Intense beams offer many possibilities as a direct or supplemental CTR plasma heating energy source and recent experimental evidence of Altyntsev, et al. (Reference 1.1) suggests regimes of strong beam-plasma energy coupling at interesting CTR plasma densities (up to  $10^{14}/\text{cm}^3$ ). Turbulent beam-plasma heating is currently an active research area (Reference 1.2). Fleischman, et al. (Reference 1.3) at Cornell have demonstrated beam induced field reversal in an Astron configuration using a pulsed intense beam and preliminary work on toroidal injection has also

been reported (Reference 1.4). A fruitful merging of intense beam and CTR research can be anticipated in the future as these and other techniques are developed.

Linear beam collective ion acceleration methods show promise of being able to generate high fluxes of accelerated heavy ions. Many such schemes have been proposed during the last decade, notably by the Soviets (see, e.g., Rabinovich, Reference 1.5), but their exploitation has awaited development of the electron accelerator technology. The Graybill-Uglum discovery (Reference 1.6) of beam-generated and accelerated ions with energies up to eight times the beam kinetic energy has renewed interest in these approaches and has already demonstrated the potential for the process as a highly stripped ion source. Higher charge state ions are preferentially bunched and accelerated. Moreover, several kilojoules of ion pulse energy can be extrapolated from the data using higher energy electron accelerators currently within the state of the art.

#### 1.1 BASIC CONCEPTS OF BEAM-PLASMA INTERACTIONS--HISTORICAL SURVEY

The first quantitative work demonstrating the dominant influence of the beam-generated plasma on overall beam properties in the drift chamber was performed by Graybill and Nablo of the Ion Physics Corporation (IPC) (Reference 1.7). They reported a strong dependence of beam current density and propagation efficiency on background gas pressure. Their results, plus the open shutter photography of beam-plasma channels, performed by Link (Reference 1.8) showed pressure regimes where, with increasing pressure from about  $10^{-3}$  torr in air, the beam blew up radially, pinched, drifted in nearly straight lines, and re-pinched again in the 100 torr range. (See Figure 1.1). The open shutter photography also indicated gross stability features of beam propagation.



Reproduced from  
best available copy.

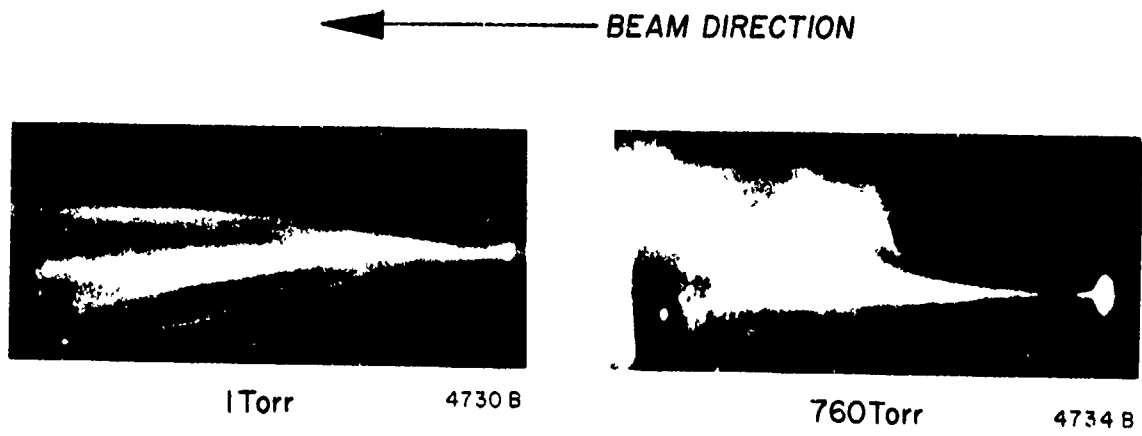


Figure 1.1 Electron beam-gas interaction as a function of pressure

A partial interpretation of the beam behavior was made by Graybill and Nablo using the Lawson uniform beam model (Reference 1.9). Assuming paraxial beam trajectories, the radial equation of motion for a beam electron, including effects of the radial electric space charge and self-magnetic fields, is

$$\frac{d^2 r}{dz^2} = -\frac{2}{\beta^2} (v/\gamma) (f_e - 1/\gamma^2) r/a^2 \quad (1.1)$$

$$v \equiv N r_0 = \frac{I \text{ (amperes)}}{17,000 \text{ (amperes)} \beta_L}$$

$N$  = number of beam electrons/length

$I$  = beam current

$\beta_L c$  = average longitudinal ( $z$ ) velocity of electrons  $\approx \beta c$  in Lawson model

$\gamma$  = relativistic factor

$r_0$  = classical electron radius =  $e^2/m_0 c^2$

$a$  = beam radius

$f_e \equiv -\rho_{ion}/\rho_e$  = fractional electrical neutralization

$\rho_{ion}$  = background ion charge density

$\rho_e$  = electron charge density

The equation indicates  $f_e > 1/\gamma^2$  is required to avoid beam space charge blowup, and, if the background pressure were sufficiently low so that collisional ionization could not achieve  $f_e \gtrsim 1/\gamma^2$  over a substantial portion of the beam pulse, the beam would not propagate. The radial blowup and beam pinching were interpreted in terms of space charge neutralization using the Lawson model.

The model was unable to explain the drifting beam mode at 0.5 to 1 torr pressure, however. The nearly straight line motion of filamentary beams in this pressure range, as evidenced by the beam self photos, was suggestive of complete force neutralization, and Dr. David Sloan of PI first suggested the concept of current neutralization. The rising beam current generates a  $\frac{dB_0}{dt}$ , or inductive, longitudinal electric field which drives plasma electrons in a direction to neutralize the beam current. Link made an ad hoc modification of the radial equation of motion in the Lawson model to account for current neutralization:

$$\frac{d^2 r}{dz^2} \approx \frac{2v}{\beta^2 \gamma a^2} \left[ 1 - f_e - \beta^2 (1 - f_m) \right] r$$

$f_m$  = fractional magnetic neutralization =  $I_p/I_b$   
 $I_p$  = plasma return current enclosed at the beam edge

If  $f_e \approx f_m \approx 1$ , the electrons drift in a force-free environment.

In order that  $f_m \approx 1$ , one immediately realizes that the beam-generated plasma must be a good conductor; i.e., the gas must breakdown. Gaseous discharge theory and experiment suggest, however, that a 0.1 torr pressure gas probably has a higher breakdown conductivity than at 1 torr. The question then arose as to why the 0.1 torr range showed pinched beams with maximum magnetic field or minimum current neutralization. Creedon (Reference 1.10) used the breakdown data of Felsenthal and Proud (Reference 1.11) to estimate breakdown times due to avalanching caused by the inductive electric field. He suggested that the time of breakdown with respect to the beam current rise was the important parameter, as long as the conductivity in the pressure

regime remained high enough to give magnetic diffusion times exceeding the beam pulse width. In other words, when the gas breaks down, the magnetic field level frozen in the plasma is that due to the beam current at the time of breakdown. Breakdown at nearly peak beam currents will result in  $f_m \sim 0$  and breakdown very early in the pulse gives  $f_m \sim 1$ . At high pressures (> few torr) the plasma conductivity drops and, even though breakdown occurred early in the pulse, the beam current is not substantially neutralized. These ideas essentially completed the basic interpretation of the Graybill-Nablo and Link data.

Yonas and Spence (Reference 1.12) subsequently performed careful measurements of gas breakdown times as a function of pressure and developed a semi-empirical magnetic diffusion model to relate the net current to the beam current profile. Their model directly utilized breakdown time measurements of Felsenthal and Proud, (F-P) but their beam parameters required extrapolation of the F-P data beyond its range of validity at low pressures. Moreover, the charge production calculations of Creedon gave much too high plasma densities at the measured lower pressure breakdown times of Jonas and Spence. A charge production model was proposed by the author (Reference 1.13 and 1.14) to explain these discrepancies and to give a physical basis for the good empirical agreement with F-P data in the 1 torr range. The model basically suggests that electron avalanching is unimportant until  $f_e = 1$ . The space charge fields are too high ( $10^5$  to  $10^6$  V/cm) for avalanching, i.e., the secondary electrons generated by collisional ionization become relativistic and, moreover, their motion is primarily radial out of the beam channel. This simple modification allowed consistent estimates of breakdown times in agreement with the Jonas-Spence data.

As higher current electron accelerators were developed, the Alfvén-Lawson current limit (Reference 1.15) for existence of a uniform beam with a given kinetic energy was approached. This limit is  $v/\gamma \sim 1$  for a space charge neutralized beam, independently of the beam radius. There are several physical interpretations of this limit:

$$1) \quad v/\gamma \sim \frac{\langle \beta_t^2 \rangle}{\langle \beta_L^2 \rangle}$$

$$2) \quad v/\gamma \approx \frac{a}{r_L}$$

$$3) \quad v/\gamma \approx \frac{E_{e.m.}}{E_{kin}}$$

where

$$\langle \beta_t^2 \rangle c^2 = \text{average transverse electron velocity squared}$$

$$\langle \beta_L^2 \rangle c^2 = \text{average longitudinal electron velocity squared}$$

$$r_L = \text{Larmor radius of gyration of beam electrons in the beam self-magnetic field at the beam edge}$$

$$E_{e.m.} = \text{electromagnetic field energy/beam particle or per unit length}$$

$$E_{kin} = \text{kinetic energy/beam particle or per unit length}$$

Most researchers emphasized interpretation (2) which states that when  $v/\gamma \sim 1$ , electrons will turn around over the radius of the beam; i.e., not propagate. Graybill, Uglum, and Nablo (Reference 1.16) performed experiments which showed such beams would not propagate, and for a time, the beam physics community was

astir with questions about the feasibility of propagating beams with currents higher than the Alfvén limit. The author suggested (Reference 1.17) that current neutralization would allow propagation of  $v/\gamma > 1$  beams as long as  $v_{\text{net}}/\gamma < 1$ , where  $v_{\text{net}}$  includes the beam current and the backstreaming plasma current. Moreover, Hammer and Rostoker (Reference 1.18) derived a hollow beam equilibrium model (no current neutralization) which removed the  $v/\gamma \sim 1$  limitation of an orbital interpretation. Production and propagation of  $v/\gamma > 1$  beams was first reported by Yonas and Spence (Reference 1.12) and later by Andrews et al. at Cornell (Reference 1.19).

We also have suggested that the third interpretation of  $v/\gamma$  is the dominant limitation on efficient beam propagation (Reference 1.13). When  $v_{\text{net}}/\gamma > 1$ , the electromagnetic self energy dominates the beam kinetic energy, independently of the details or orbit dynamics. Beams then strongly interact with cavities, degrading their kinetic energy at the beam front over distances comparable to the beam radius either by the space charge field, or, in the case of electrical neutrality and partial current neutralization, by the inductive field.

The average transverse beam particle energy is comparable to the longitudinal or streaming energy when  $v/\gamma \sim 1$  and roughly so when  $v_{\text{net}}/\gamma \sim 1$  (interpretation 1). J. C. Martin and D. Forster of his group were probably the first to emphasize the importance of beam transverse energy (Reference 1.20) and Yonas et al. subsequently performed careful measurements of the average beam transverse energy (Reference 1.12). They also ascribed the relatively poor beam transport efficiency (30 to 40 percent over meter distances) of  $v/\gamma \gg 1$  beams (even with  $v_{\text{net}}/\gamma < 1$ ) in neutral gases to loss of higher transverse energy beam components. The rapid gas breakdown requirement for good

current neutralization is in conflict with the requirement for a high net magnetic field to contain beam transverse energy. A "cold" beam ( $\langle \beta_t^2 \rangle / \langle \beta_L^2 \rangle \ll 1$ ) with  $v_{\text{net}}/\gamma \ll 1$  is thus required for efficient transport in neutral gases or pre-ionized plasmas.

To illustrate the implications of the statement further, we can assume injection into a preionized plasma of high conductivity, thereby assuring that  $v_{\text{net}}/\gamma \ll 1$ . The cold beam requirement means that the injected beam electrons must be nearly paraxial. We are then led to the concept of the critical diode current,  $I_c$ , first introduced by Friedlander, et al. (Reference 1.21):

$$I_c \approx 8500 \beta \gamma (r_c/d),$$

with  $r_c$  the cathode radius and  $d$  the anode-cathode gap spacing. Physically this current is the value at which an electron emitted at the cathode edge would strike the anode tangentially under the influence of the self-magnetic field, and with neglect of the radial electric field. If  $I \ll I_c$  in the diode, the beam is cool, and the onset of pinching occurs around  $I \sim I_c$ . The diode peak voltage places a minimum value upon  $d$  to avoid impedance collapse over the beam pulse width. This restriction in turn places a minimum value upon  $r_c$  for a cold beam. In other words, efficient transport in neutral gases or pre-ionized plasmas places an upper limit on beam current density. Benford and Ecker (Reference 1.22) have demonstrated major beam energy loss upon injection of high current density ( $\sim 10^5$  A/cm<sup>2</sup>) beams into a pre-ionized plasma. The loss occurred within a few centimeters of the anode. The need to transport high  $v/\gamma$ , high current density beams thus led to investigation of external field propagation techniques.

Roberts and Bennett (Reference 1.23) first transported a relativistic beam ( $v/\gamma \sim 0.2$ ) in a linear pinch plasma. They observed nearly complete current neutralization and reported efficient transport. Their work was extended by Benford and Ecker (Reference 1.24), who transported hot beams ( $v/\gamma \gtrsim 7$ ,  $\sim 10^5$  A/cm<sup>2</sup>) with efficiencies  $> 90$  percent. They also proposed a single particle orbit theory model to explain the details of beam propagation. This model states that beam propagation is a superposition of injected electron orbits in the undistorted magnetic field of the pinch at injection. Generally speaking, we expect that efficient propagation will occur when charge and current neutralization short out beam self fields, and that any distortion of the external field-plasma system will result in beam energy loss. Single particle orbit model conditions therefore prevail with efficient transport. The single particle orbit model is extended in this report to allow for field-plasma distortion.

Beam propagation in external solenoidal fields was first studied by Andrews, et al. (Reference 1.25) at Cornell using a  $v/\gamma \sim 2$  beam. At present solenoidal transport work is underway at PI, Naval Research Laboratory, Cornell University, Sandia Laboratories, and Maxwell Laboratories (Reference 1.26). An interesting result reported by Stallings (Reference 1.27) is a reduction in transport efficiency as the external field is increased beyond about 9 kilogauss. Lee and Sudan (Reference 1.28) have predicted a drop in current neutralization at high  $B_z$  fields due to incomplete space charge neutralization, and a more restrictive limitation on the solenoidal field is argued in this report.

Several experiments on beam combination and focusing have been reported within the last year. Benford and Ecker have combined two high  $v/\gamma$  beams in a linear pinch plasma (Reference 1.29), and magnetic mirror compression experiments by Davitian, et al., (Reference 1.30), have shown beam area compression of a factor of 3 with  $v/\gamma \sim 2.5$  beams. Cold beam geometrical focusing experiments in a neutral gas transport system have been reported by Kelley at Sandia (Reference 1.31), Martin (Reference 1.32), and Bradley (Reference 1.33).

We have surveyed the experimental and conceptual development of intense beam plasma physics up to this point from the historical perspective of beam transport and energy density control. As we have already mentioned, intense beams are currently being studied for CTR applications and collective ion acceleration. The discovery of collectively accelerated ions by Graybill and Uglum (Reference 1.6) at IPC renewed interest in linear beam collective field acceleration possibilities. Rander, et al. (Reference 1.34) continued the IPC work with the use of nuclear emulsion and magnetic spectroscopic diagnostic techniques and Rander (Reference 1.35) correlated the beam front velocity with the first ion pulse. Several models have been advanced to explain the ion acceleration (Reference 1.36) and a detailed presentation of one of them, the localized pinch model, (References 1.37 and 1.38) is given in this report.

Altyntsev, et al. (Reference 1.1) have reported strong beam plasma energy coupling using a  $v/\gamma \sim 0.1$  beam injected into low density-preionized plasmas ( $10^{11} - 10^{14}/\text{cm}^3$ ). This experiment has generated interest in beam-plasma turbulent heating, and Lovelace and Sudan (Reference 1.2) and Guillory and Benford (Reference 1.39) have recently proposed return

current anomalous plasma heating via ion acoustic modes. The experiment of Andrews et al. (Reference 1.3) on beam injection into an Astron geometry is an important preliminary investigation of beam confinement, as we have previously mentioned.

## 1.2 DISCUSSION OF REPORT

The material of this report is organized into three sections. Section 2 is intended as a comprehensive, essentially self-contained, survey and development of the entire intense beam field. The viewpoint is mainly phenomenological, with an emphasis on defining efficient transport systems. Section 3 is a formulation of the quadrature of the electromagnetic (EM) fields in systems without solenoidal fields. The objective of this work was to explore the role of finite boundaries, finite beam risetime, and transient effects. These effects have not been treated in other theoretical work on current neutralization (Reference 1.40). Section 4 is entirely devoted to an analysis of ion acceleration models and a presentation of the localized pinch model, in particular. The material of this section is a "zero-order" coupled analysis of radial and longitudinal ion-electron electrostatics.

The physics of intense beams can be broken up into several sub-areas which, of course, must be ultimately coupled in a self-consistent fashion:

1. EM field determination; i.e., given the beam current profile, what are the EM fields with appropriate boundary conditions?
2. Characterization of the background gas plasma - charge density and conductivity as a function of time and space.

3. Beam dynamics - formulation of realistic, but tractable equations of motion of beam particles and/or the beam envelope.

4. Beam stability - definition of stable propagation modes (longitudinal electrostatic and transverse modes) and instability growth rates in unstable regimes.

The first part of Section 2 essentially follows the above outline. We start, after a brief review of diode physics, by developing a simple ad-hoc model of beam-generated EM fields in finite cavities, complementary to the exact formulations in Section 3. The model includes EM fields due to variations in beam radius with distance and time, endplates, changes in current with time, and charge neutralization. In particular, we discuss the effects of endplates and variations in charge neutralization upon the longitudinal electric field. Aside from the implicit inductive longitudinal electric field of current neutralization calculations (Reference 1.40), the inductive field estimates used in electron avalanching calculations in neutral gases (References 1.10 and 1.12) and the space charge field estimates in the Rostoker and Graybill and Uglum ion acceleration models (Reference 1.36), the literature of intense beam physics does not consider  $E_z$  fields. (Most calculations pertain to steady state equilibrium configurations.) The model thus gives a more complete characterization of the transient longitudinal electric field in the finite cavities of practical beam problems.

We apply the cavity model in developing a procedure for calculating gas breakdown times in neutral gases. The model of Creedon (Reference 1.10) predicts background plasma charge densities that are too high, according to experimental data, and

Yonas and Spence used the empirical data of Felsenthal and Proud (F-P) (Reference 1.11) in their work on gas breakdown. Our model justifies the data correspondence with F-P on physical grounds with certain E/P (E/P is the electric field pressure ratio) regimes and gives good agreement with experimental breakdown measurements at low E/P regimes where F-P does not. The model recognizes that the high E/P values that exist before space charge neutralization do not lead to significant electron avalanching-secondary electrons become relativistic over distances of the beam radius or less and, moreover, the electric field is primarily radial, driving secondary electrons out of the beam channel. We propose a charge production estimate using collisional ionization only until  $f_e \approx 1$ , then using the inductive field for avalanche calculations. The model has one undetermined parameter, the ratio of the background plasma secondary electron density to beam electron density at breakdown. Empirical determination of this parameter from one data point gave agreement with Yonas and Spence data at other pressures. Once gas breakdown times are calculated, the conductivity after breakdown and the fractional magnetic neutralization can be estimated. The charge production model also predicts that beam transverse temperature should affect current neutralization and preliminary data tends to support this result.\*

Section 2.7 considers beam envelope motion in some detail using the analytically tractable Kapchinskij-Vladimirskij envelope equation for beams with finite emittance. Limits on beam focussing imposed by finite emittance are discussed. A review

\* Private communication, J. C. Martin, January 1971.

of high  $v/\gamma$  beam equilibrium models is also included.

The physical implications of the dimensionless ratio  $v/\gamma$  used to characterize beams are outlined and it is argued that current neutralization accounts for experimental results showing propagation of  $v/\gamma > 1$  beams. This interpretation was first suggested during the program (Reference 1.17) and is now commonly accepted in the beam physics community. We have further proposed that the dominant restriction on high  $v/\gamma$  beam propagation is electromagnetic; i.e., even with current neutralization,  $v_{\text{net}}/\gamma < 1$  in order that the beam not seriously degrade its kinetic energy to magnetic field energy. This restriction is dominant in the sense that it obtains nearly independently of the beam current density distribution in radius. The original propagation limit on uniform beams,  $v/\gamma \sim 1$ , or the Alfvén criterion, is essentially an orbital limitation for forward drift of the electrons. Hammer and Rostoker (Reference 1.40) removed this orbital limitation in principle by deriving self-consistent "hollowed-out" current distributions.

The longitudinal ES instability work of several authors is summarized in Section 2.8, and we conclude that instability heating of plasmas has not been important in most beam transport experiments. Transverse instability modes of low pressure (0.1 torr) beams are then discussed and a phenomenological model is argued which allows predictions of the instability wavelengths in good agreement with the data. This model is the "frozen-hose" model, first proposed by the author (Reference 1.41). The model stems from a recognition of the need to utilize two characteristic times in instability growth of beams in neutral gases. Early times are defined as times before breakdown where the plasma is

nonconducting and post breakdown times are usually resistive with characteristically longer growth times. This model led to the concept of plasma channeling (Reference 1.13) and a necessary criterion for beam combination in neutral gas systems.

The role of beam transverse energy is emphasized in the summary of neutral gas transport phenomenology of Section 2.10.1. A criterion is derived giving upper limits on beam electron transverse energy at injection, and it is shown that this criterion amounts to a restriction on current density. The transverse energy containment criterion can also be expressed in terms of a dimensionless parameter,  $\beta$ , analogous to the plasma  $\beta$ :

$$\beta \equiv \text{beam and plasma transverse energy/volume}/(B_{\theta}^{\text{net}})^2/8\pi$$

Inasmuch as  $B_{\theta}^{\text{net}}$ , the net magnetic field including current neutralization, is not a beam parameter, current density is perhaps a more convenient parameter for beam characterization, in addition to the  $v/\gamma$  ratio (which is independent of beam radius).

Transport phenomenology in linear pinch ( $B_{\theta}$ ) fields is covered in Section 2.10.2 and conditions are outlined for validity of single particle orbit transport. In the single particle model the beam propagation is a superposition of injected beam electron orbits in the undistorted magnetic field of the pinch plasma at injection. We consider pinch field-plasma distortion induced by transverse pressure imbalance due to the beam. An "inverse snow-plow" model is developed which allows estimation of the distortion time scale for given beam and pinch parameters. This work is the first modeling of distortion of intense beam plasmas and fields within the diffusion approximation. Plasma and field

lines expand while maintaining nearly constant enclosed magnetic flux. The criteria for single particle orbit theory are compared with the experimental data of Benford and Ecker (Reference 1.24) and it is shown that their use of such a model is consistent with experimental conditions.

The discussion of transport phenomenology concludes with a preliminary outline of solenoidal field transport. A simple uniform beam model explicitly considers paramagnetic and diamagnetic beam and plasma effects due both to gyrorotation and rotation about the system axis induced by space charge and  $B_0$  fields. A diode flow model appropriate to large aspect ratio diodes where the radial electric field effects are negligible shows that  $v/\gamma > 1$  beams are net paramagnetic and also gives the maximum ratio of  $B_0$  to  $B_z$  for uniform current density flow. Diamagnetism and paramagnetism in the transport system are related to  $f_e$  and  $f_m$ , and are shown to be additional beam energy loss mechanisms. Also proposed is a new model giving upper limits on the applied  $B_z$  field for efficient transport. The model carries over ideas of current neutralization in the  $z$  direction to theta currents. The perpendicular conductivity at breakdown has to be large enough to allow theta plasma currents to neutralize the beam theta currents. This condition in general gives a lower  $B_z$  field level for efficient transport than the criterion of Lee and Sudan (Reference 1.28) regarding destruction of  $z$  current neutralization by high  $B_z$  fields.

Section 2 concludes with a summary of turbulent plasma heating and a proposal for an intense neutron and X-ray source using collectively accelerated deuterium ions. The turbulent heating discussion outlines conditions necessary for consistent estimates of anomalous plasma heating. Simple formulas for maximum plasma electron temperature estimates are derived.

The determination of the EM fields generated by general beam current distributions (accelerated and non-accelerated) in finite cavities is discussed in Section 3. We consider in detail the EM fields of constant velocity beams with finite risetimes, pulse width and decay time in circular conducting pipes with and without endplates. The EM quadrature is in a convenient form for looking at endplate effects, and can easily be reduced to the cases with one or no endplate. Numerical evaluations are given for two interesting beam problems--the current neutralization problem (Section 3.2) and the beam injection into a cavity problem (Section 3.4).

The current neutralization problems considered by other authors pertain to semi-infinite beams in infinite homogeneous plasmas (Reference 1.40). The beam has a zero riselength and is suddenly "switched on" at  $t=0$ . Our work is the first exploration of the effects of finite boundaries and finite beam risetimes, and we explicitly determine the fields near the beam head. The blunt beam and highly conducting plasma limits, which are the cases treated by other authors, are quantitatively defined in terms of beam, plasma, and chamber parameters.

A current neutralization problem is evaluated for a beam in a finite radius drift tube which gives closed form expressions for the EM fields and contains the dominant terms of more general radial current density distribution profiles. The fields are plotted as a function of distance behind the beam head in the beam front region and show the essential role of the conducting boundary in determining the electric field attenuation behind the beam front in weakly conducting plasmas (plasmas where the plasma skin depth is of the order of the chamber radius).

The  $E_z$  field is plotted in Section 3.4 for a beam injected into a neutral-gas-filled cavity (zero conductivity) and the effects of the endplate and finite drift tube radius are exhibited. We derive criteria for negligible endplate influence on beam fields. It turns out that endplates have two effects on the  $E_z$  field; the sign and magnitude may be substantially altered (this effect is primarily electrostatic), and the accelerated surface charges of the conducting boundaries give rise to precursor radiation. If the beam is highly relativistic (travelling at nearly  $c$ ) the precursor radiation induces field oscillation in the beam front region. The conditions for neglect of endplate effects are that the precursor radiation front be far in front of the beam head, and secondly, that the beam front and region of interest be far beyond the  $E_z$  field-reversal point near the chamber endplate. An approximate expression is given for the point behind the beam head where the  $E_z$  field reverses direction. The formula involves both the chamber radius and the relativistic  $\gamma$  factor of the beam.

The collective ion acceleration discussion of Section 4 considers in detail some implications of experimental data with respect to models of Rostoker, Graybill and Uglum, and Wachtel and Eastlund (Reference 1.36). The Rostoker model attributes ion acceleration to space charge fields near the front of a beam penetrating a neutral gas. Acceleration of the space charge well is due to a decreasing charge neutralization time caused by precursor radiation and electrons, and Rostoker argues a particular time history of well acceleration which gives ion energies independent of mass, in accordance with the data. Acceleration terminates when the well has accelerated to a value where the space charge field is no longer adequate to trap ions.

Graybill and Uglum also suggest a one-dimensional accelerating space well model. Ion acceleration in their model does not occur at the beam front, but begins near the anode window of the drift chamber after  $f_e$  exceeds  $1/\gamma^2$ . In our opinion they do not argue an accelerated well, however, but only a constant velocity well moving at a rate determined by the gas breakdown time.

Wachtel and Eastlund have proposed the Veksler "inverse Cerenkov" acceleration process as an explanation of observed ion acceleration. The Veksler theory assumes existence of an ion bunch whose dimensions are small compared to the resonant plasma wavelength,  $\lambda \approx 2\pi v_b/\omega_p$ ;  $v_b$  is the beam electron velocity and  $\omega_p$  is the beam plasma frequency. In order to extend the Veksler theory to a non-bunched ion distribution (the background ion charge distribution) they somewhat arbitrarily define an ion bunch as ions within the Debye sphere. The problem of the longitudinal phase stability of the accelerating bunch is not considered; i.e., the ion bunch is assumed to be rigid. We estimate limits upon ion energies due to excitation of longitudinal electrostatic streaming instabilities and conclude that the maximum ion kinetic energy is too small to explain the data. This approach obviates the necessity of arguing initial formation of an ion bunch in order to apply the Veksler theory.

A new model of ion acceleration, the localized pinch model (LPM), is discussed, and it is argued that the model gives the most comprehensive agreement with presently established features of the data. In particular, the model can explain multiple ion pulses; i.e., acceleration can occur either near the beam front or behind it. The model proposes a two-dimensional electromagnetic acceleration mechanism, in contrast to the one-dimensional

electrostatic models of Rostoker and Graybill and Uglum. Moreover, LPM includes a self-synchronizing mechanism to keep the ions in phase with the accelerating fields. The one-dimensional models do not have this feature; the potential well, in a sense, happens to accelerate properly to give partial trapping. The synchronization is achieved in the LPM by the electric field associated with a non-adiabatic pinching of the beam envelope. The presence of the ion bunch locally shorts out the radial electric space charge field and the magnetic field then causes the beam to contract. A longitudinal electric field in the direction of electron flow results from the higher electron charge density in the constricted region. With typical parameters of ion acceleration experiments the pinching field is large enough to degrade the electron kinetic energy over distances of a few beam radii, giving rise to additional electron bunching. This latter bunching provides longitudinal phase stability.

The rise length of the ion charge density enhancement of the bunch must be of the order of the beam radius to allow rapid (non-adiabatic) contraction of the beam envelope, and thereby generate high enough fields to degrade the electron kinetic energy. It is shown that the space charge well near the anode window can form sharply defined bunches and a criterion for bunching is derived which translates to an upper limit on gas pressure for ion acceleration.

Various possible acceleration cutoff mechanisms are considered in the context of experimental data and it is suggested that ion depletion is a likely explanation. The background ion currents generated by the accelerating fields around the ion bunch deplete the ion supply behind the bunch and an electrostatic well is then re-established near the anode window, terminating

further acceleration. As collisional ionization continues the process repeats. Experiments are proposed to identify the nature of the acceleration cutoff mechanism.

## REFERENCES

### SECTION 1

- 1.1 A. Altyntsev and others; JETP Letters, 1971, Vol. 13, page 139; Unclassified.
- 1.2 R. Lovelace and R. Sudan; Physical Review Letters, 1971, Vol. 27, page 1256; Unclassified; A. Altyntsev and others; IAEA Conference on Plasma Physics and Controlled Nuclear Fusion Research, Madison, Wisconsin, 1971, IAEA/CN-28, Paper E20; Unclassified.
- 1.3 M. Andrews and others; Physical Review Letters, 1971, Vol. 27, page 1428; Unclassified.
- 1.4 G. Meixel and others; Bulletin of the American Physical Society, 1971, Vol. 16, page 1251; Unclassified.
- 1.5 M. Rabinovich; Lebedev Physics Institute, March 1969, Preprint Number 36; UCRL Translation 1398, Lawrence Berkeley Laboratory, Berkeley, California; Unclassified.
- 1.6 S. Graybill and J. Uglum; Journal of Applied Physics, 1970, Vol. 41, page 236; Unclassified.
- 1.7 S. Graybill and S. Nablo; Applied Physics Letters, 1966, Vol. 8, page 18; Unclassified.
- 1.8 W. Link; IEEE Transactions on Nuclear Science, 1967, Vol. NS-14, page 777; Unclassified.
- 1.9 J. Lawson; Journal of Electronics and Control, 1957, Vol. 3, page 507; Unclassified and 1958, Vol. 5, page 146; Unclassified.
- 1.10 J. Creedon; PIIR-17-67, March 1967; Physics International Company, San Leandro, California; Unclassified.
- 1.11 P. Felsenthal and J. Proud; Physical Review, 1965, Vol. 139, page A1796; Unclassified.

- 1.12 G. Yonas and P. Spence; PIFR-106, October 1968 and PIFR-106-2, August 1969, Physics International Company, San Leandro, California; Unclassified.
- 1.13 S. Putnam; PIFR-105, April 1970; Physics International Company, San Leandro, California; Unclassified.
- 1.14 S. Putnam; PIIR-29-71, June 1971; Physics International Company, San Leandro, California; to be published in IEEE Transactions on Nuclear Science, Eleventh Symposium on Electron, Ion, and Laser Beam Technology, Boulder, Colorado, held in May 1971; Unclassified.
- 1.15 H. Alfven; Physical Review, 1939, Vol. 55, page 425; Unclassified.
- 1.16 S. Graybill and others; Bulletin of the American Physical Society, Series II, 1968, Vol 13, page 56; Unclassified.
- 1.17 S. Putnam PIQR-105-1, August 1968, Physics International Company, San Leandro, California; Unclassified.
- 1.18 D. Hammer and N. Rostoker; Physics of Fluids, 1970, Vol. 13, page 1831; Unclassified.
- 1.19 M. Andrews, and others; Applied Physics Letters, 1970, Vol. 16, page 98; Unclassified.
- 1.20 G. Yonas; private communication, February 1970.
- 1.21 F. Friedlander and others; DASA-2173, September 1968, Defense Atomic Support Agency, Washington, D.C.; Unclassified.
- 1.22 J. Benford and others; PIIR-10-70, December 1969, Physics International Company, San Leandro, California; Unclassified: Accepted for publication in Physics of Fluids.
- 1.23 T. Roberts and W. Bennett; Plasma Physics, 1968, Vol. 10, page 381; Unclassified.
- 1.24 J. Benford and B. Ecker; Physical Review Letters, 1971, Vol. 26, page 1160; Unclassified.
- 1.25 M. Andrews and others; Physics of Fluids, 1970, Vol. 13, page 1322; Unclassified.

- 1.26 C. Stallings; PIFR-227/295, September 1971, Physics International Company, San Leandro, California; Unclassified: J. Block and others; to be published in Proceedings of IEEE Eleventh Symposium on Electron, Ion and Laser Beam Technology, Boulder, Colorado, May 1971; Unclassified: J. Bzura and S. Linke; Bulletin of the American Physical Society, 1970, Vol. 15, page 1452; Unclassified: P. Bolduc and E. Patterson, Bulletin of the American Physical Society, 1971, Vol 16, page 1230; Unclassified.
- 1.27 C. Stallings, S. Shope and J. Guillory; to be published; see also Reference 1.26; Unclassified.
- 1.28 R. Lee and R. Sudan; Physics of Fluids, 1971, Vol. 14, page 1213; Unclassified.
- 1.29 J. Benford and B. Ecker, PIFR-227/294, September 1971, Physics International Company, San Leandro, California; Unclassified: to be published in Physical Review Letters.
- 1.30 H. Davitian and others; Bulletin of the American Physical Society, 1970, Vol. 15, page 1452; Unclassified.
- 1.31 J. Kelley, Bulletin of the American Physical Society, 1971, Vol. 16, page 1230; Unclassified.
- 1.32 J. C. Martin, M. Goodman, T. Storr and H. Herbert; January 1971, Paper presented at DASA Simulation Meeting, Washington, D.C.; Unclassified.
- 1.33 L. Bradley and others; to be published in Proceedings of IEEE Eleventh Symposium on Electron, Ion, and Laser Beam Technology, Boulder, Colorado, May 1971; Unclassified.
- 1.34 J. Rander and others; Physical Review Letters, 1970, Vol. 24, page 283; Unclassified.
- 1.35 J. Rander; Physical Review Letters, 1970, Vol. 25, page 893; Unclassified.
- 1.36 N. Rostoker; Report No. LPS 21, 1969, Laboratory for Plasma Studies, Cornell University, Ithaca, New York; Unclassified: J. Wachtel, B. Eastlund, Bulletin of the American Physical Society, 1969, Vol. 14, page 1047; Unclassified: S. Graybill and others; DASA Report 2477, June 1970, Defense Atomic Support Agency, Washington, D.C.; Unclassified.

- 1.37 S. Putnam; Physical Review Letters, 1970, Vol. 25, page 1129; Unclassified.
- 1.38 S. Putnam; IEEE Transactions on Nuclear Science, June 1971, Vol. NS-18, page 496; Unclassified.
- 1.39 J. Guillory and G. Benford; "Estimates of Dense Plasma Heating by Stable Intense Electron Beams," submitted to Plasma Physics; Unclassified.
- 1.40 S. Chandrasekhar; "The Electromagnetic Wake Following a Pulse of Charged Particles," July 1961, IDA Report; Unclassified: S. Yadavalli; Physics of Fluids, 1965, Vol. 8, page 956; Unclassified: J. Cox and W. Bennett; Physics of Fluids, 1970, Vol 13, page 182; Unclassified: D. Hammer and N. Rostoker, Physics of Fluids, 1970, Vol. 13, page 1831; Unclassified.
- 1.41 S. Putnam; PIIR-7-68, March 1968, Physics International Company, San Leandro, California; Unclassified: also, references 1.13 and 1.14.

## SECTION 2

### GENERAL BEAM PLASMA INTERACTION PHENOMENOLOGY

In this section we discuss a wide range of topics in intense beam-plasma physics from a point of view which hopefully will be practically useful, i.e., we emphasize basic physics and show how relatively simple models can describe most of the gross features of beam-plasma interactions. We begin the discussion with a summary of the present status of high current diode physics.

#### 2.1 DIODE PHYSICS

2.1.1 Space-Charge Limited Flow. All of the pulsed relativistic beam diodes for currents higher than a few thousand amperes have field emission-initiated electron flow. A variety of cathode surfaces have been used--needles, milled metal with grooves, razor blades, roll pins, etc. As a general rule, when the macroscopic electric field level at the cathode surface reaches  $2-3 \times 10^5$  V/cm, field emission occurs from microscopic whiskers or roughened edges. The whiskers vaporize, creating a "plasma cathode" that can essentially emit with a zero work function up to the space charge limit. The emitted current density is then limited to a value for which the associated space-charge cloud in the anode-cathode gap reduces the electric field to zero at the cathode. (The thermal energy of the plasma electrons is negligible compared to the applied voltage.)

All analysis of diode flow has been confined to steady state flow where  $di/dt = 0$ ,  $I$  is the diode current. In practice, inductive effects decreases the electron kinetic energy during current rise. The kinetic energy of electrons entering the drift chamber is usually obtained as a function of time by subtracting the inductive voltage drop  $(L \frac{dI}{dt})^*$  from the measured diode voltage profile. The inductance,  $L$ , may be determined experimentally using a load resistor of approximately the same radius as the beam. A further inductive correction resulting from beam pinching  $(I \frac{dL}{dt})$  may be necessary for rapidly contracting beam envelopes.

A diode should, of course, be matched to the generator for maximum energy transfer. In steady state, this means that the diode impedance should equal the generator internal impedance. We must determine the type of electron flow to achieve proper diode impedance. The two types of flow of greatest practical relevance to high-current diodes without external magnetic fields are planar space-charge limited, or Langmuir-Childs flow (Reference 2.1), and parapotential flow (Reference 2.2 through 2.4). A rough transition criterion is whether or not the current is to exceed the so-called critical current (References 2.3 and 2.4):

$$I_c \approx 8500 \sqrt{\gamma_0^2 - 1} (r_c/d) \quad (2.1)$$

where

$I_c$  = critical current in amperes

$\gamma_0$  = electron total energy/ $m_0 c^2$

$m_0$  = electron rest mass

$r_c$  = cathode radius

$d$  = anode-cathode gap spacing

\*  $L$  is the effective beam-diode chamber inductance.

The critical current is the current level at which the self-magnetic field of the beam becomes large enough to cause the electrons at the beam edge to impinge tangentially on the anode. The derivation of Equation (2.1) is quite simple--we include it here to indicate the approximate nature of the criterion.

We assume a cylindrically symmetric diode as indicated in Figure 2.1, and neglect the radial electric field. This neglect is probably not too serious for large aspect-ratio ( $r_c/d$ ) geometry. Moreover, we take  $B_\theta$  constant for the outermost electrons. Again, this approximation is not severe for large aspect-ratio diodes. The radial equation of motion for the outermost electrons is then

$$\frac{d}{dt} (\gamma v_r) = -\left(\frac{e}{m_0}\right) v_z \frac{B_\theta}{c} \quad (2.2)$$

with

$$B_\theta \approx \frac{2I}{cr_c}$$

$v_r$  = radial velocity component

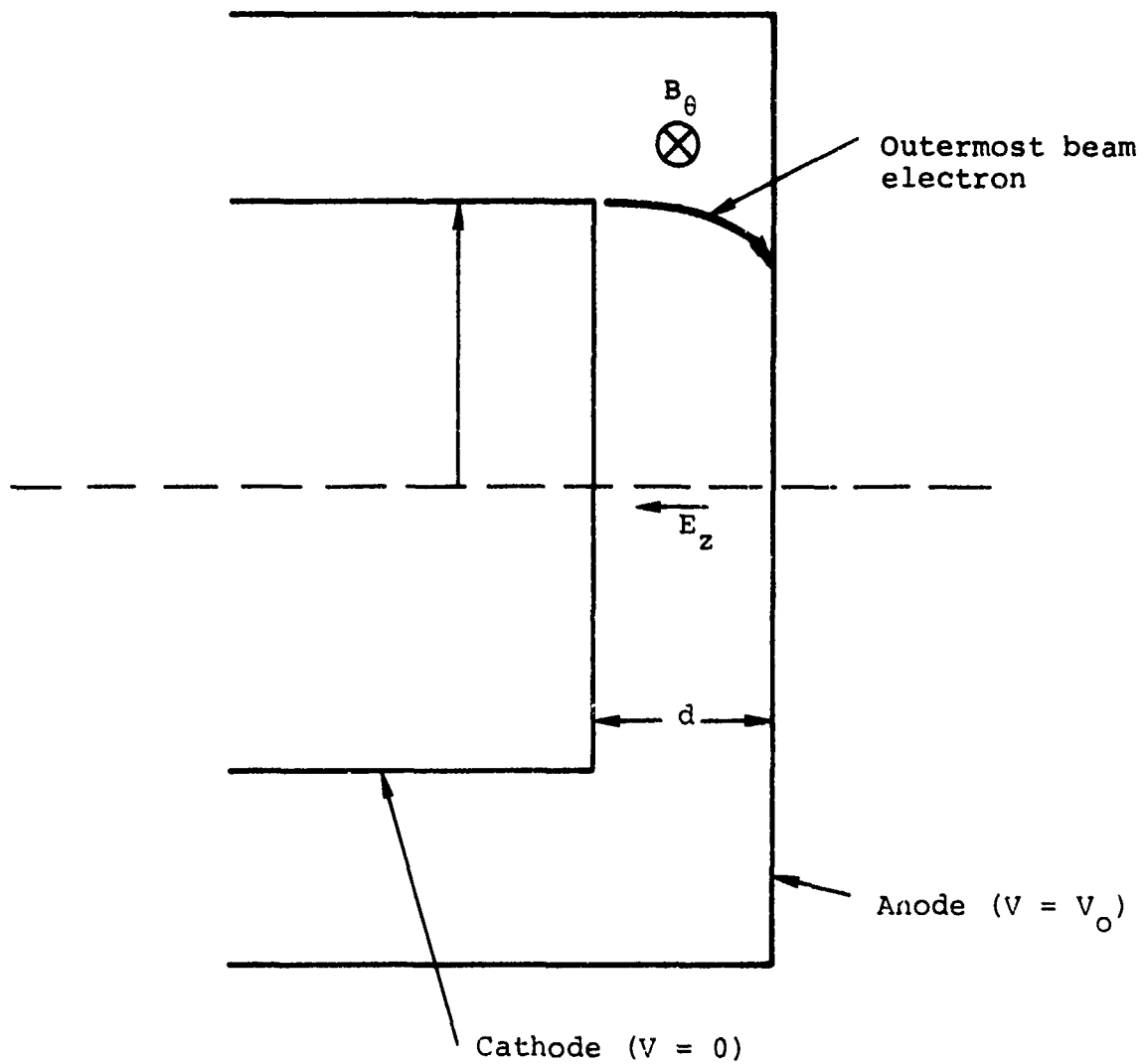
Integrating,

$$\beta_r = \frac{v_r}{c} = \frac{eB_\theta z}{\gamma m_0 c} \quad (2.3)$$

At the anode, grazing incidence means  $\beta_r = \beta$ ,

$$\beta_r = \frac{\sqrt{\gamma_0^2 - 1}}{\gamma_0} \quad (2.4)$$

with  $\gamma_0$  corresponding to the anode potential,  $V_0$ . Substituting for  $B_\theta$  in Equations (2.3) and (2.4) gives Equation (2.1).



$E_z$  = longitudinal electric field  
 $B_\theta$  = self-magnetic field of beam  
 $V$  = potential  
 $r_c$  = cathode radius

Figure 2.1 The critical current geometry

In spite of the approximations above,  $I_c$  is a useful experimental guide for onset of beam pinching for intermediate  $(r_c/d)$  values. Clark and Linke (Reference 2.5) have shown that pinching starts at about 80 percent of  $I_c$  for diode impedances in the 5 to 10 ohm range and  $(r_c/d) \gtrsim 6$ . However, experiments by Ecker at Physics International (Reference 2.6) using  $(r_c/d) \sim 20$  have shown that no appreciable pinching occurs at  $I_c$ , which is perhaps not surprising in view of the derivation--the criterion merely states that the flow is no longer laminar and that outer electron trajectories start to cross near the anode. If  $(r_c/d) \sim 1$ , one would not expect the derivation to be meaningful.

Below  $I_c$  the diode flow will be essentially one-dimensional and laminar. Then one uses the Langmuir-Child impedance:

$$\begin{aligned} Z_{L.C.} &= \frac{136}{\sqrt{V_0}} (d/r_c)^2 && \text{(non-relativistic)} && (2.5) \\ &= 960 (d/r_c)^2 && \text{(ultra-relativistic)} \end{aligned}$$

where  $Z$  is in ohms,  $V_0$  in megavolts, and the cathode is assumed to be a uniformly emitting circular disk.\* If  $(r_c/d)$  is determined from

$$I_c Z_{L.C.} \approx V_0 \quad (2.6)$$

or

$$(r_c/d) \approx 1.16 \frac{\sqrt{\gamma_0^2 - 1}}{(V_0)^{3/2}} \quad \begin{array}{l} \text{(non-relativistic)} \\ \text{(cold beam)} \end{array} \quad (2.7)$$

we theoretically have a minimum impedance, "cold beam" diode; i.e., the transverse electron kinetic energy should be zero,

---

\* See Reference 2.3 for a discussion of relativistic planar space charge flow.

or at least very small. In practice, Equation (2.7) "works" only if the current density is not too high--of the order of a few kiloamperes/cm<sup>2</sup> or less. (The current density is entirely determined by the diode voltage and gap spacing when Equation (2.6) is satisfied.) If the current density exceeds  $\sim 10^4$  A/cm<sup>2</sup>, the anode window vaporizes, forming a plasma which can both supply an ion current and, also effectively close the gap.

Let us first consider the case where the anode behaves as a high-density plasma with a relatively sharp boundary, stationary over times of interest. The ions are accelerated back to the cathode by the electric field, and we have the case of bipolar space charge flow. As shown by Langmuir (Reference 2.7), the constant in Equation (2.5) is now reduced. In the case of zero work function for ion emission from the anode plasma, the electric field at the anode, as well as the cathode, is zero. Defining

$j_o$  = electron current density in absence of positive ions  
 $j_e$  = electron current density with positive ions  
and  $j_i$  = positive ion current,

Langmuir shows (non-relativistically) that

$$\left(\frac{j_e}{j_o}\right)^{1/2} \approx \left(\frac{3}{4}\right) \int_0^1 \frac{d\omega}{\left(\sqrt{\omega} + \alpha \sqrt{\omega - 1 - \alpha}\right)^{1/2}} \quad (2.8)$$

where

$$\alpha = \frac{j_i}{j_e} \left(\frac{\eta_e}{\eta_i}\right)^{1/2}$$

$\eta_e$  ( $\eta_i$ ) = charge to mass ratio for electrons (ions).

The completely space charge limited case is  $\alpha = 1$ , and numerical integration of the integral above then gives  $j_e = 1.86 j_o$ . We thus see that the maximum ion current in the space charge limit is

$$j_i \cong (1.86) j_o \left( \frac{\eta_i}{\eta_e} \right)^{1/2} \quad (\text{non-relativistically})$$

$$z \approx \frac{73}{\sqrt{V_o}} \left( \frac{d}{r_c} \right)^2 \quad (\text{bipolar flow}) \quad (2.9)$$

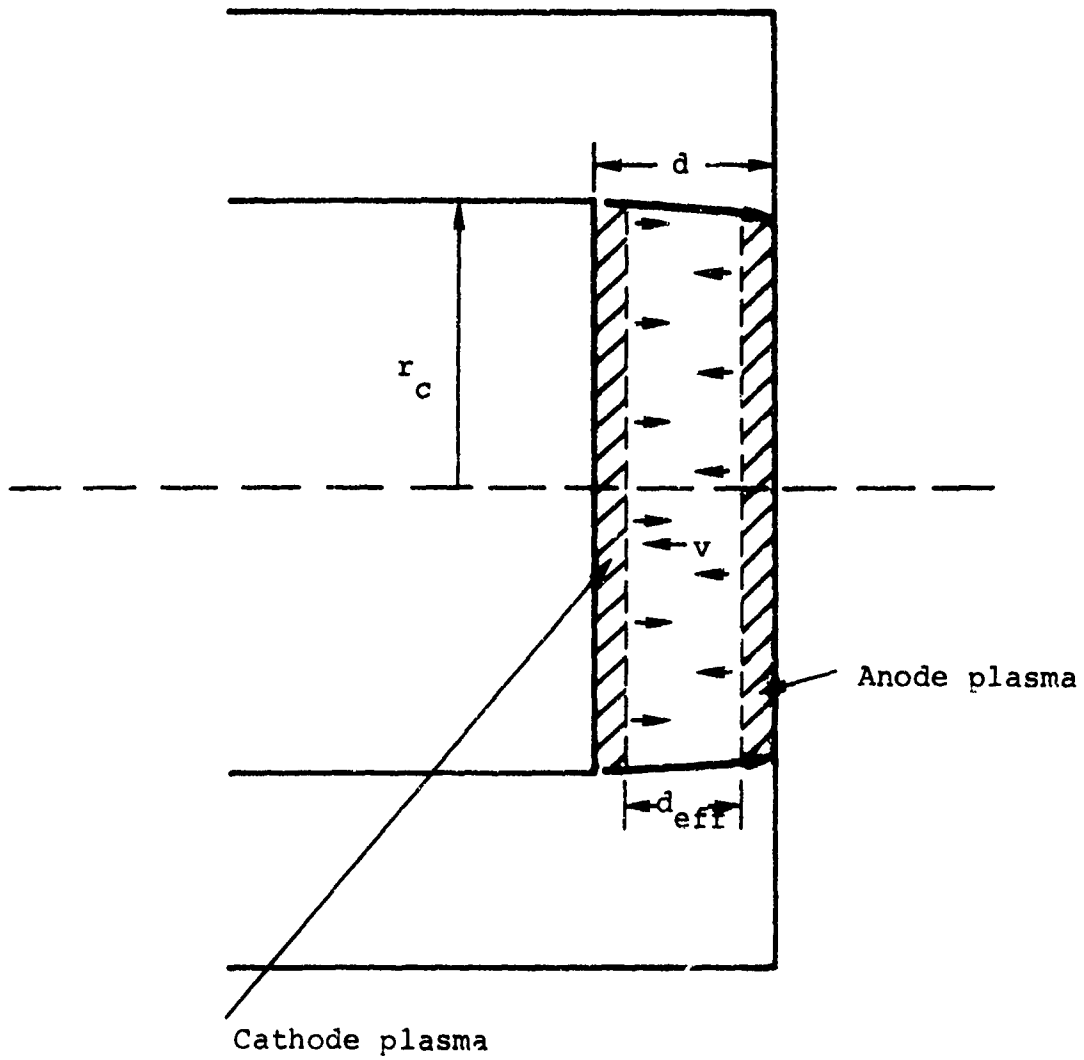
If one is interested in accelerating ions in the diode (and recovering them through a hole in the cathode, for example), the energy efficiency of the process in space charge flow,  $\epsilon$ , would maximally be

$$\epsilon \equiv \frac{\int v_o j_i dt}{\int v_o j_e dt} \quad (2.10)$$

$$= \left( \frac{\eta_i}{\eta_e} \right)^{1/2}$$

For Deuterons,  $\epsilon \approx 1.65$  percent. Recently, Friedman, et al., have performed preliminary experiments on ion acceleration in the diode, using a laser to form a high temperature anode plasma (Reference 2.8). Ion acceleration in the diode may indeed be a useful way to obtain high ion currents, providing impedance collapse of the diode and contamination effects from ions other than the desired specie are not serious problems.

In high-current diodes where the beam pinches ( $I > I_c$ ), not only does the beam form an anode ion source as discussed above, but the anode plasma appears to explode and the high-density plasma moves hydrodynamically toward the cathode (see Figure 2.2). This effective gap closure gives an impedance that drops with time. Loda and Spence (Reference 2.9) have obtained



- $d$  = actual geometrical gap spacing
- $d_{\text{eff}}(t)$  = effective anode-cathode gap
- $v$  = anode plasma velocity

Figure 2.2 Impedance collapse phenomenology

an empirical fit of diode impedance versus time by assuming a constant velocity anode plasma moving at typical material motion velocities (a few cm/ $\mu$ sec) observed with framing cameras.

One can also expect cathode plasma motion to close the gap, but if the beam pinches appreciably, it is reasonable that anode plasma motion dominates. These ideas of gap closure have led to the use of hollow ring cathodes with pinched beams to extend the time before impedance collapse. The anode plasma then takes longer to short the gap, and diodes with an initial gap of a few millimeters can be made to hold impedance for 100 to 150 nsec.

To summarize the above discussion, we expect for  $I \lesssim I_c$  that the diode impedance will initially follow Equation (2.5)

$$Z_{L.C.} \approx \frac{136}{\sqrt{V_0}} \left( \frac{d}{r_c} \right)^2$$

When the anode becomes a plasma, the impedance should drop to

$$Z \approx \frac{73}{\sqrt{V_0}} \left( \frac{d}{r_c} \right)^2$$

as bipolar space-charge limited flow is established. If the anode plasma moves hydrodynamically, the impedance should further decrease as

$$Z \propto \left( d_{\text{eff}} \right)^2 \propto (d - vt)^2$$

with  $v$  the velocity of the anode plasma. The time scales of the above phenomena depend on the current density or electron energy absorbed in the anode.

2.1.2 Parapotential Flow (PPF). When diode current exceeds the critical current, the self-magnetic field causes the beam to pinch and planar space-charge flow is no longer an adequate approximation. The suggestion of a parapotential flow (along equipotentials) was first advanced by D. C. dePackh (Reference 2.2). Friedlander, et al. (Reference 2.3), and Creedon (Reference 2.4) have carried out similar calculations. We follow Creedon's exposition here.

The basic assumption of the PPF model is that the impedance of the gap is essentially determined by self-consistent flow along equipotentials within a region extending from the cathode shank to a region slightly in front of the anode. If the anode is an equipotential (conductor), electrons must cross equipotentials in a small region near the anode. The model has an undetermined parameter since it does not treat flow all the way across the diode. Figure 2.3 shows a sketch of flow lines. Creedon approximates flow lines by cones converging to a point at the anode. By assuming azimuthal symmetry and force balance along each equipotential,

$$\vec{E} = -\frac{\vec{v}}{c} \times \vec{B},$$

where  $\vec{E}$  is the electric field and  $\vec{v}$  is the velocity associated with the flow line, a solution of Poisson's equation gives an expression for the diode steady-state current:

$$I = \frac{8500 \gamma_m \ln \left[ \gamma_m + \sqrt{\gamma_m^2 - 1} \right]}{\ln \left( \tan \frac{\theta_m}{2} \right) - \ln \left( \tan \frac{\delta}{2} \right)} \quad (2.11)$$

2.1.2 Parapotential Flow (PPF). When diode current exceeds the critical current, the self-magnetic field causes the beam to pinch and planar space-charge flow is no longer an adequate approximation. The suggestion of a parapotential flow (along equipotentials) was first advanced by D. C. dePackh (Reference 2.2). Friedlander, et al. (Reference 2.3), and Creedon (Reference 2.4) have carried out similar calculations. We follow Creedon's exposition here.

The basic assumption of the PPF model is that the impedance of the gap is essentially determined by self-consistent flow along equipotentials within a region extending from the cathode shank to a region slightly in front of the anode. If the anode is an equipotential (conductor), electrons must cross equipotentials in a small region near the anode. The model has an undetermined parameter since it does not treat flow all the way across the diode. Figure 2.3 shows a sketch of flow lines. Creedon approximates flow lines by cones converging to a point at the anode. By assuming azimuthal symmetry and force balance along each equipotential,

$$\vec{E} = -\frac{\vec{v}}{c} \times \vec{B},$$

where  $\vec{E}$  is the electric field and  $\vec{v}$  is the velocity associated with the flow line, a solution of Poisson's equation gives an expression for the diode steady-state current:

$$I = \frac{8500 \gamma_m \ln \left[ \gamma_m + \sqrt{\gamma_m^2 - 1} \right]}{\ln \left( \tan \frac{\theta}{2} \right) - \ln \left( \tan \frac{\delta}{2} \right)} \quad (2.11)$$

where  $\gamma_m$  is the relativistic factor for the outer flow line along  $\theta_m$ , and the minimum angle flow line is  $\theta = \delta$ . It turns out that the solution requires a current flowing interior to  $\theta = \delta$ , which is termed the bias current,  $I_b$ . Specification of any one of the parameters  $\theta_m$ ,  $\gamma_m$ , or  $I_b$  determines the other two.

Creedon suggests

$$\tan \delta = \frac{r_c}{d}$$

$$\theta_m = \pi/2$$

$$\gamma_m = \gamma_0 \text{ (corresponding to anode voltage)}$$

and, substituting in Equation (2.11)

$$I^{(PPF)} = 8500 \left(\frac{r_c}{d}\right) \gamma_0 \ln[\gamma_0 + (\gamma_0^2 - 1)^{1/2}], \left(\frac{r_c}{d}\right) \gg 1 \quad (2.12)$$

Equation (2.12) is also the solution which minimizes the bias current. This solution would appear to require flow along the cathode shank, since the inner flow line is taken as emanating from the outside edge of the cathode. Recent experimental data of Ecker (Reference 2.10) shows reasonably good agreement with Equation (2.12) (Figure 2.4). His investigations of emission from hollow ring cathodes confirmed another aspect of Creedon's parameter choice; namely, that  $\delta$  is essentially determined by the ratio of  $r_c/d$ . By removing inner emission surfaces of the cathode, very little change in the steady-state impedance was observed.

3. The current density is non-uniform and peaked in the center when  $B_z \approx B_0$ , even when no appreciable beam pinching occurs (Reference 2.10). A tentative explanation of this effect is that the outer electrons have a lower longitudinal velocity. Certainly this would be the case if the electrons roughly follow field lines--the pitch angle of outer field lines is larger due to the larger self field. When  $B_z < B_0$ , the impedance is somewhat insensitive to cathode area whereas if  $B_z \gg B_0$ , the current density again becomes nearly uniform as the field lines "straighten out." The diode impedance then follows Langmuir-Childs.

## 2.2 ELECTROMAGNETIC FIELDS IN FINITE CAVITIES\*

An understanding of the nature of the electromagnetic (EM) fields generated by intense beams in finite closed conducting cavities is fundamental to a description of charge production in neutral gases and beam transport phenomenology. For orientation, we first discuss a simple quasistatic model to estimate EM fields including the influence of cavity endplates, variations in beam radius and charge/length, and density of the background charge. Plasma effects are included here only in terms of electrical (space charge) neutralization. We assume the beam energy and current profiles are specified as a function of space and time, and do not consider coupling to orbit or beam envelope equations. The immediate utility of the equations below is that one can estimate EM limits on beam-transport efficiency for desired beam and chamber parameters, excluding current neutralization effects (in this section). Exact solutions of Maxwell's equations for beams penetrating finite cavities are given in Sections 3.3 and 3.4.

---

\* This section includes material reported in References 2.13 and 2.14.

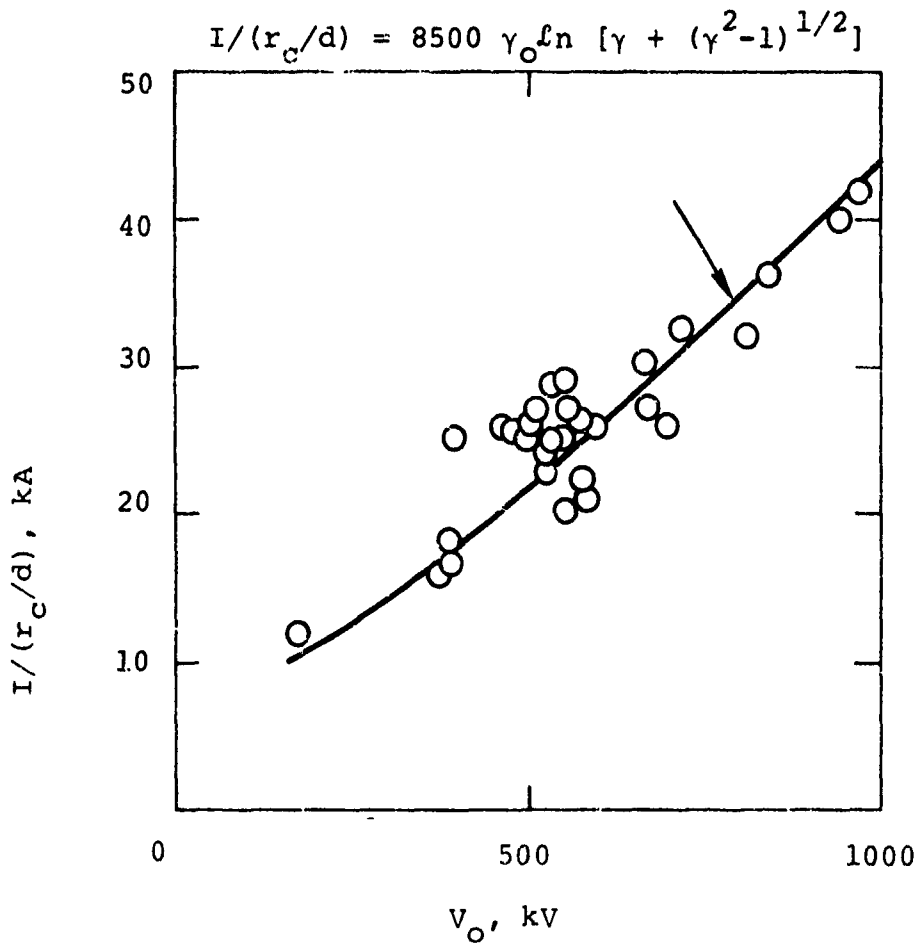


Figure 2.4 Comparison of theoretical [Equation (2.12)] and experimental results for impedance of diode pinched flow. For this comparison, experimental data were restricted to  $dI/dt = 0$ . Experimental points correspond to various  $r_c/d$  and  $V_0$  values.

1. There is an applied magnetic field level above which no appreciable beam pinching occurs. Hammer, et al. (Reference 2.11), have empirically found that if

$$\frac{B_z}{B_\theta} > \left(\frac{\gamma}{v}\right) \left(\frac{r_c}{2d}\right) \quad (2.13)$$

pinching is inhibited.  $B_z$  is the applied longitudinal magnetic field value and  $B_\theta$  is the maximum azimuthal self-field of the beam. dePackh (Reference 2.12) has numerically solved the electron orbit equations, neglecting diamagnetic effects and electric fields, and obtains the criterion

$$\frac{B_z}{B_\theta} > \sqrt{2} \left(\frac{\gamma}{v}\right)^{1/2} \quad (2.14)$$

It should be noted that both of these equations involve the parameter

$$v = \frac{I \text{ (amps)}}{17,000 \beta_L}$$

and the longitudinal velocity,  $\beta_L c$ , has to be "guessed."

2. The beam rotates in the diode, indicating the existence of a macroscopic theta motion. The azimuthal acceleration results from forces

$$F_\theta \propto \frac{e}{c} (v_r B_z - v_z B_r)$$

and radial velocity, of course, may result from either pinching due to the self-magnetic field, or from radial electric fields near the cathode. The radial electron field gives rise to diamagnetic rotation whereas the  $B_\theta$  field generates paramagnetic theta currents. We discuss these effects in more detail in Section 2.10.3.

3. The current density is non-uniform and peaked in the center when  $B_z \approx B_0$ , even when no appreciable beam pinching occurs (Reference 2.10). A tentative explanation of this effect is that the outer electrons have a lower longitudinal velocity. Certainly this would be the case if the electrons roughly follow field lines--the pitch angle of outer field lines is larger due to the larger self field. When  $B_z \lesssim B_0$ , the impedance is somewhat insensitive to cathode area whereas if  $B_z \gg B_0$ , the current density again becomes nearly uniform as the field lines "straighten out." The diode impedance then follows Langmuir-Childs.

## 2.2 ELECTROMAGNETIC FIELDS IN FINITE CAVITIES\*

An understanding of the nature of the electromagnetic (EM) fields generated by intense beams in finite closed conducting cavities is fundamental to a description of charge production in neutral gases and beam transport phenomenology. For orientation, we first discuss a simple quasistatic model to estimate EM fields including the influence of cavity endplates, variations in beam radius and charge/length, and density of the background charge. Plasma effects are included here only in terms of electrical (space charge) neutralization. We assume the beam energy and current profiles are specified as a function of space and time, and do not consider coupling to orbit or beam envelope equations. The immediate utility of the equations below is that one can estimate EM limits on beam-transport efficiency for desired beam and chamber parameters, excluding current neutralization effects (in this section). Exact solutions of Maxwell's equations for beams penetrating finite cavities are given in Sections 3.3 and 3.4.

---

\* This section includes material reported in References 2.13 and 2.14.

The geometry is shown in Figure 2.5. Azimuthal symmetry is assumed and the theta component of the beam current is taken zero. Direct integration of the Maxwell equation:

$$\nabla \times \vec{E} = -\frac{1}{c} \frac{\partial \vec{B}}{\partial t}$$

gives

$$E_z = - \int_r^R \frac{\partial E_r}{\partial z} dr' - \frac{1}{c} \int_r^R \frac{\partial B_\theta}{\partial t} dr' \quad (2.15)$$

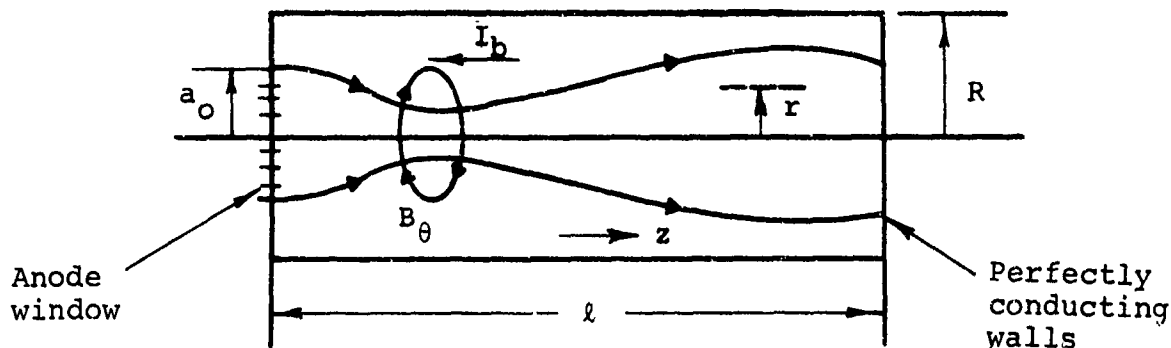


Figure 2.5 Beam chamber geometry.

where the boundary condition  $E_z = 0$ ,  $r = R$  has been imposed. In the quasistatic limit, the displacement current in the calculation of  $B_\theta$  is neglected and the radial electric field is assumed to be obtainable from the electrostatic (ES) potential. It is thus required that the time for light to travel twice the longest chamber dimension be small compared to times of interest. The ES potential can be determined exactly:

$$\phi = \int_0^R r' dr' \int_0^{\ell} dz' G(r, r', z, z') \rho(r', z') \quad (2.16)$$

with

$$G(r, r', z, z') = \frac{8\pi}{R} \sum_{n=1}^{\infty} \frac{J_0\left(\frac{\lambda_n r}{R}\right) J_0\left(\frac{\lambda_n r'}{R}\right)}{\lambda_n [J_1(\lambda_n)]^2 \sinh\left(\frac{\lambda_n \ell}{R}\right)}$$

$$\begin{cases} \sinh\left(\frac{\lambda_n}{R}\right) z \sinh\frac{\lambda_n}{R}(\ell - z'), & z \leq z' \\ \sinh\left(\frac{\lambda_n}{R}\right)(\ell - z) \sinh\frac{\lambda_n}{R} z', & z \geq z' \end{cases} \quad (2.17)$$

The charge density is  $\rho$  (esu/cm<sup>3</sup>) and  $\lambda_n$  are the roots of  $J_0(x)$ . An ad hoc approximation for  $E_r$  is now made to avoid the complications of Equation 2.16. The spirit of the approximation is to note from the exact expression the term dropping off most slowly in  $z$ , and then to find an approximate normalization factor. The chamber radius  $R$  is to be restricted to a range such that the  $z$  dependence is reasonably accurate for small  $z$ . This implies that  $1 < R/a \leq 10$ , and  $1 \leq R \leq 10$  length units, which is henceforth considered the range for  $R$ . Assuming a uniform beam current density and that the scale variation in  $z$  for beam parameters is large compared to  $R/2.4$  near the endplates or compared to the beam radius "far away" from the beam endplates (paraxial approximation), take

$$\begin{aligned} E_r &= f(z) \frac{2\lambda}{a^2} r, \quad r \leq a \\ &= f(z) \frac{2\lambda}{r}, \quad r \geq a \end{aligned} \quad (2.18)$$

with  $f(z) = 0$ ,  $z = 0, \ell$ . The beam charge/length (which may also have a  $z$  dependence) is denoted by  $\lambda$ . Equation (2.18) is exact at  $z = \ell/2$  for  $\lambda$  constant. Two cases of interest are

$$(1) \quad \ell \lesssim R \longrightarrow f(z) \approx \frac{4z(\ell-z)}{\ell^2}$$

$$(2) \quad \ell > R \tag{2.19}$$

$$f(z) \approx \frac{1 - e^{-2.4 z/R}}{(1 - e^{-2})}, \quad z \lesssim 2(R/2.4)$$

$$= 1, \quad 2(R/2.4) \leq z \leq \ell - 2R/2.4$$

$$= \frac{1 - e^{-2.4(\ell-z)/R}}{1 - e^{-2}}, \quad \ell - 2R/2.4 \leq z \leq \ell$$

The  $E_r$  profile for these two cases are sketched in Figure 2.6.

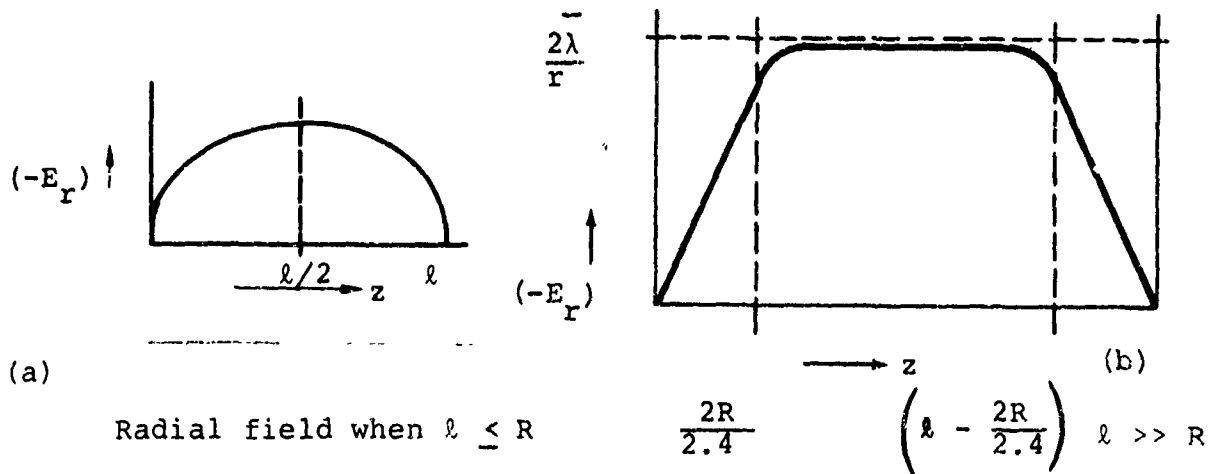


Figure 2.6 Fields for a uniform electron beam in a closed cavity.

Returning to Equation (2.15), and using

$$B_{\theta} = \frac{2I}{ca^2} r, \quad r < a$$

$$= \frac{2I}{cr}, \quad r \geq a$$

an expression for  $E_z(0, z, t)$  is obtained when  $\ell < R$ :

$$E_z(0, z, t) = - 2 \overbrace{\frac{\partial \lambda}{\partial z} \left( \frac{1}{2} + \ell n \left( \frac{R}{a} \right) \right)}^{(1)} \frac{4z(\ell-z)}{\ell^2} + \overbrace{\frac{2\lambda}{a} \frac{\partial a}{\partial z} \left( \frac{4z(\ell-z)}{\ell^2} \right)}^{(2)}$$

$$- 2\lambda \overbrace{\left( \frac{1}{2} + \ell n \left( \frac{R}{a} \right) \right) \frac{4}{\ell^2} (\ell-2z)}^{(3)} - \overbrace{\frac{2}{c} \frac{\partial I}{\partial t} \left( \frac{1}{2} + \ell n \left( \frac{R}{a} \right) \right)}^{(4)}$$

$$+ \overbrace{\frac{2}{c^2} \frac{I}{a} \frac{\partial a}{\partial t}}^{(5)} \tag{2.20}$$

If  $R \ll \ell$ , a similar evaluation for  $E_z$  can be made using Equation (2.19).

The terms of Equation (2.20) can be identified as follows:

- (1) Electrostatic due to a variation in beam charge density/length modulated by end plate surface charges
- (2) Electrostatic due to a variation of beam radius with  $z$  modulated by end plate surface charges

(3) Electrostatic due to induced (positive) surface charges at the end plates which terminate the field lines of adjacent beam (negative) charges

(4) Changing magnetic flux due to current variation ( $L \, dI/dt$ )

(5) Changing magnetic flux due to containment of current within a time varying radius ( $I \, dL/dt$ )

It is interesting to note that without end plates, (set  $z = \ell/2$ ), Equation (2.20) reduces to

$$E_z(0, z, t) = \frac{2}{\gamma_L} \frac{\partial \lambda}{\partial u} \left( \frac{1}{2} + \ln \left( \frac{R}{a} \right) \right), \quad (2.21)$$

(no end plates)

$$u = \beta_L ct - z$$

$$\gamma_L = 1 / \sqrt{1 - \beta_L^2}$$

$\beta_L c$  = average forward streaming velocity of beam electrons,

if not referring to the beam head or tail and if a constant beam radius with varying charge/length is assumed. Equation (2.21) can be rewritten for the case  $I_b = I^P (1 - e^{-\alpha u})$ ,  $I^P$  = peak beam current:

$$E_z \Big|_{r=0} \text{ (V/cm)} = \frac{(-) 4}{\gamma^2 \beta_L^2} \frac{I^P \text{ (amps)}}{t_r \text{ (nsec)}} \left( \frac{1}{2} + \ln R/a \right) e^{-\alpha u} \quad (2.22)$$

We have defined ( $\alpha^{-1}$ ) as a two e-folding current rise length:

$$\alpha \beta_L c t_r = 2$$

For  $I^P = 5 \times 10^4$  amps,  $t_r = 20$  nsec,  $\gamma = 3$ ,  $R = 6$ ,  $a = 1$ , and  $\beta_L \cong 0.8$ ,  $E_z \cong 4 \times 10^3 e^{-\alpha u}$  V/cm.

If we are within the current rise portion of a beam of electrons ( $\partial\lambda/\partial u < 0$ ) streaming in the positive  $z$  direction Equation (2.21) shows that  $E_z$  is in the negative  $z$  direction; i.e., in a direction to accelerate the front electrons, and is opposite in sign to the  $E_z$  field behind the head when the beam emerges from a conducting endplate. We remark that if one transforms to the beam frame in the problem with no endplates, uses Gauss's law for the now electrostatic problem, and then transforms back to the lab frame, one also obtains Equation (2.21). To include displacement-current effects, second and higher order derivatives of  $\lambda$  with  $z$  must be included in the electrostatic problem in the beam frame. These examples point to a sufficient condition for the validity of Lenz's law--changing magnetic flux induces an electric field tending to drive current producing fields to oppose the change in flux; i.e.,  $\partial E_r/\partial z$  be negligible over the length of interest.

The effects of ions at rest can easily be included in the above equations by replacing  $\lambda$  by  $\lambda(1-f_e)$ ;  $f_e \equiv -|\rho_{ion}/\rho_{electron}|$  is the fractional electrical neutralization.

If we take  $f_e = f_e(u)$ , then Equation (2.20) gives for constant beam radius:

$$E_z(0, u) = +2 \left( \frac{1}{2} + \ln R/a \right) \left[ \frac{\partial \lambda}{\partial u} \left( \frac{1}{\gamma_L^2} - f_e \right) - \lambda \frac{\partial f_e}{\partial u} \right] \quad (2.23)$$

and  $E_z$  reverses sign when

$$\lambda \frac{\partial f_e}{\partial u} = \left( \frac{1}{\gamma_L^2} - f_e \right) \frac{\partial \lambda}{\partial u} \quad (2.24)$$

If both  $\lambda$  and  $f_e$  increase linearly behind the beam front, Equation (2.24) is satisfied when  $f_e = 1/2\gamma_L^2$ . Figure 2.7 shows qualitatively the effects of ions upon  $E_z$ .

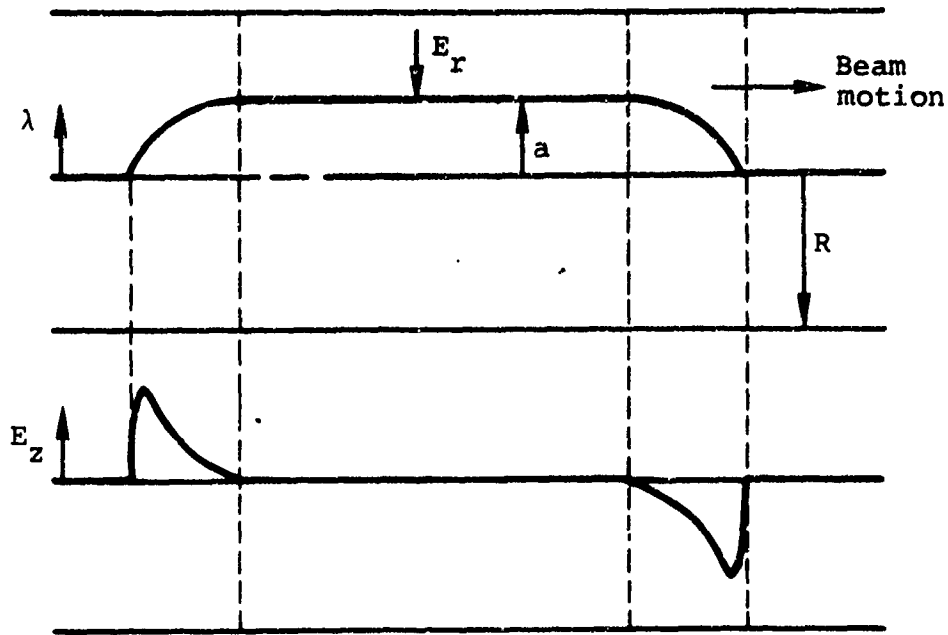
If  $f_e \cong$  constant or a function of  $t$ , and the ions are again assumed to have no  $z$  directed velocity, we see that

$$E_z = 0 \quad \text{if} \quad f_e = \frac{1}{\gamma_L^2} \quad (2.25)$$

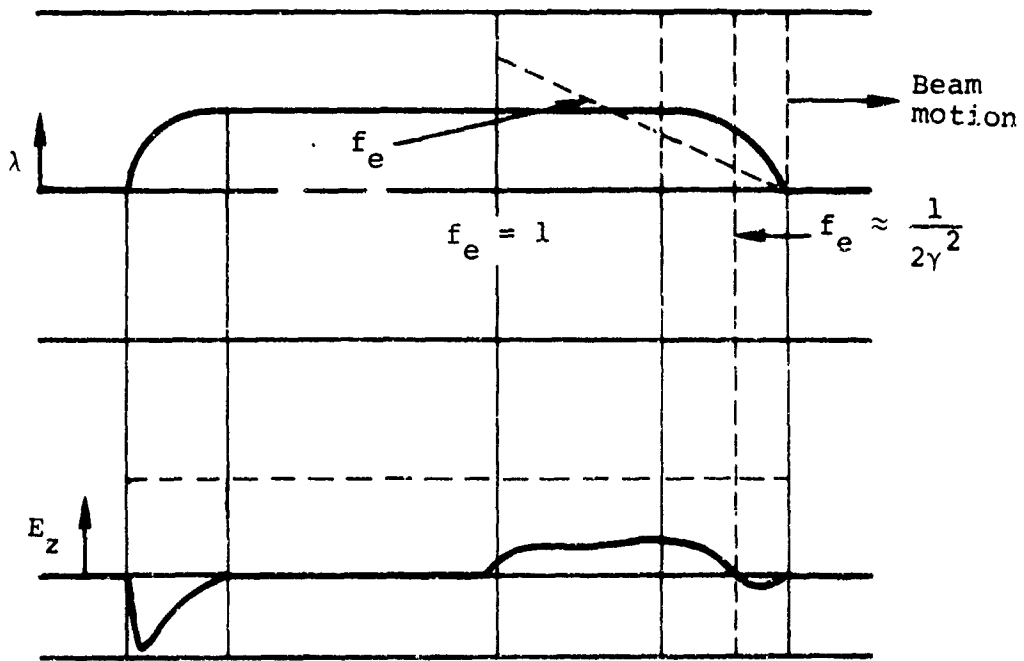
This is also the condition for radial force neutralization of the primary beam electrons. Thus, if Equation (2.25) is satisfied, the primary beam electrons may drift in a force-free environment. In other words,  $f_e = 1/\gamma_L^2$  is a condition for beam "transparency."

On first glance one might suspect that if the gas pressure could be adjusted to maintain  $f_e \cong 1/\gamma_L^2$  during a substantial portion of the beam risetime, very little energy loss would occur in beam transport. However, as discussed in Section 4,  $f_e \cong 1/\gamma_L^2$  is the condition for ion acceleration, or, in other words the beam may be unstable. Physically, Equation (2.25) may be understood by recalling that

$$E_z = - \frac{\partial \phi}{\partial z} - \frac{1}{c} \frac{\partial A_z}{\partial t}$$



Long conducting pipe, no ions,  $f_e = 0$



Long conducting pipe,  $f_e$  increases linearly behind beam front.

Figure 2.7 Sketches of  $E_z$  fields with and without ions.

where  $\phi$  is the scalar potential and  $A_z$  is the z component of the vector potential. In a rising current region of the beam profile  $\partial\phi/\partial z$  and  $\partial A_z/\partial t$  are oppositely directed. The presence of ions such that  $f_e \approx 1/\gamma_L^2$  is the condition that  $\partial\phi/\partial z$  is shorted out enough to exactly balance the inductive  $\partial A/\partial t$  term.

Equations (2.21) through (2.25) have been derived assuming a constant beam radius with  $z$  and  $t$ . Let us return to Equation (2.20) and look at terms 2 and 5, again neglecting endplate effects or restricting  $z$  to values about  $l/2$ . Denote these terms by  $\overline{E}_z$ :

$$\overline{E}_z(0, z, t) = \frac{2}{a} \left[ \lambda(1-f_e) \frac{\partial a}{\partial z} + \frac{\lambda \beta_L c}{c^2} \frac{\partial a}{\partial t} \right] \quad (2.26)$$

If  $a = a(u)$ ,  $u > 0$ ,

$$\begin{aligned} \overline{E}_z(0, z, t) &= \frac{2\lambda}{a} \frac{\partial a}{\partial u} \left[ f_e - 1 + \beta_L^2 \right] \\ &= \frac{2\lambda}{a} \frac{\partial a}{\partial u} \left( f_e - \frac{1}{\gamma_L^2} \right) \end{aligned} \quad (2.27)$$

When  $f_e = 1/\gamma_L^2$ ,  $\overline{E}_z = 0$ , and we conclude that changes in radius with  $u$ , or the distance behind the beam head, also lead to  $E_z = 0$  if the positive ion charge density follows the beam radius changes. If they do, the ion envelope velocity is, of course, equal to the propagating velocity of the electron beam envelope.

To summarize the above field discussion, we remark that the fields have been determined in a quasi-static approximation which requires that the time scale of interest be long compared to time for light signals to travel twice the longest system dimension.

We have made an ad hoc approximation for  $E_r$  to include endplate effects that places a lower limit on the scale of  $z$  variation of beam parameters. Our  $E_z$  expressions have been obtained for  $r = 0$ ; if we assume that  $E_z$  does not vary over the beam radius, our error at the beam edge,  $r = a$ , is using

$$\left(\frac{1}{2} + \ln\left(\frac{R}{a}\right)\right)_{r=0} \text{ form} \quad \text{instead of} \quad \left(\ln\left(\frac{R}{a}\right)\right)_{r=a} \text{ form}$$

for terms 1, 3, and 4 of Equation (2.20). If  $R \approx a$ , this error is not serious; in any case, we are overestimating  $E_z$  and any beam distortion due to  $E_z$  would be less than our results. When  $f_e \approx 1$  everywhere, the electrostatic contributions of the EM fields vanish, leaving only the inductive components [terms 4 and 5 of Equation (2.20)]. The endplates can now be ignored.

### 2.3 EXACT EM SOLUTIONS FOR BEAM PENETRATING AN ENDPLATE IN A FINITE RADIUS CHAMBER ( $f_e = 0$ ) - A SUMMARY OF RESULTS

The discussion above assumes that the beam has already traversed the drift chamber. Now to be considered are exact solutions of Maxwell's equations for a beam penetrating a chamber endplate; sufficient conditions will be presented to justify neglect of endplate effects. The material discussed is of interest for low-pressure beam transport in ion acceleration modes when electrostatic fields dominate, and it shows the importance of finite chamber boundaries. The details of the calculations are given in Section 3.4.

An end plate has two effects on the EM fields. One, primarily electrostatic, is to reverse the direction of  $E_z$  near the end plate and short out the radial electric field. The other is to generate a radiated field component as surface charges are accelerated by the beam. This field gives rise to precursor fields traveling at the velocity of light and, under certain conditions, to oscillatory fields near the beam front. The geometry for the calculations is shown in Figure 2.8.

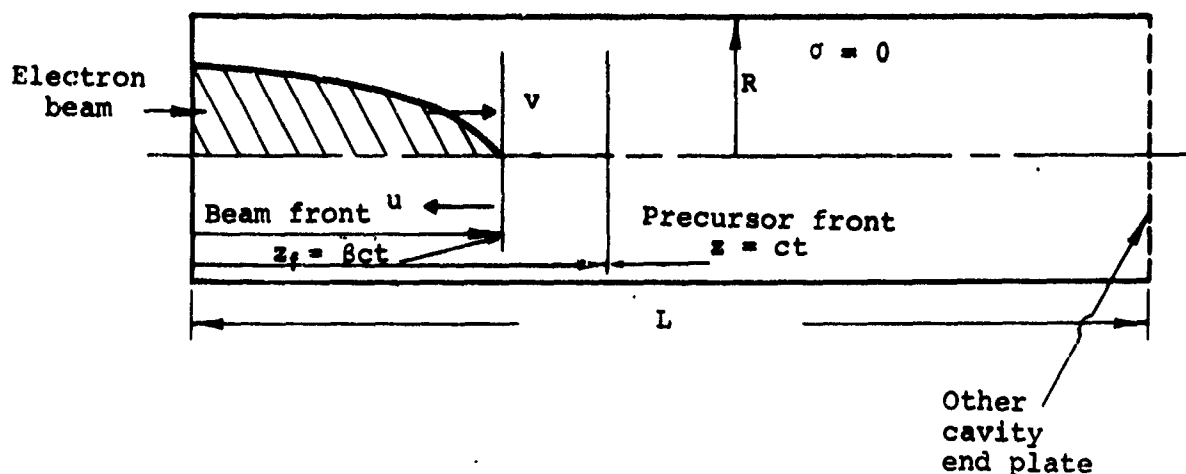


Figure 2.8 Open ended pipe geometry.

A sufficient criterion for neglect of field oscillation is that

$$\sqrt{(ct)^2 - z_f^2} \gg R/2.4, \quad 1 \lesssim R \lesssim 10 \text{ length units} \quad (2.28)$$

where  $z_f$  is the beam front position. Another way of stating Equation (2.28) is that the light signal must have traveled "far beyond" the beam front. One would therefore not expect this

effect to be important for low-energy beams. A typical oscillation amplitude, for example, would be  $\sim 10^3$  V/cm with  $5 \times 10^4$  A 1-MeV beam, 20-nsec risetime, and 1-cm radius in a 6-cm-radius pipe.

The reversal of the sign of  $E_z$ , as compared to the case without end plates, is perhaps the most important influence of the end plate, since this effect can seriously degrade the beam energy and reduce the front velocity. The beam "blows up" radially, resulting in large energy losses. Figures 2.9, 2.10 and 2.11 show the  $E_z$  field on axis for a beam with current in the positive z direction penetrating an end plate. In order to illustrate the details of the ES field near the end plate, an undistorted "slow" beam was chosen.\* The parameters are

$$\beta_L \approx 1/30$$

$$t_R \approx \text{risetime} \approx 0.1 \text{ nsec}$$

$$R = 6 \text{ cm}$$

$$a \approx 1 \text{ cm (Gaussian radial current variation)}$$

$$I^P = \text{peak current} \approx 1.77 \times 10^3 \text{ amperes. (The ES field scales linearly with peak charge/length.)}$$

The reversal of the sign of  $E_z$  occurs at the crossover distance,  $z_c$ , and can be estimated from

$$z_c \approx [(R/2.4) \ln 2\gamma + \gamma z_f] / (\gamma + 1), \quad (2.29)$$

\* In order that the field calculations be self-consistent with beam motion,  $v/\gamma - 1 \ll 1$ . Section 2.10.1 discusses beam front motion when this condition is violated. Scaling of field values for other beam parameters is discussed in Section 3.4.1.

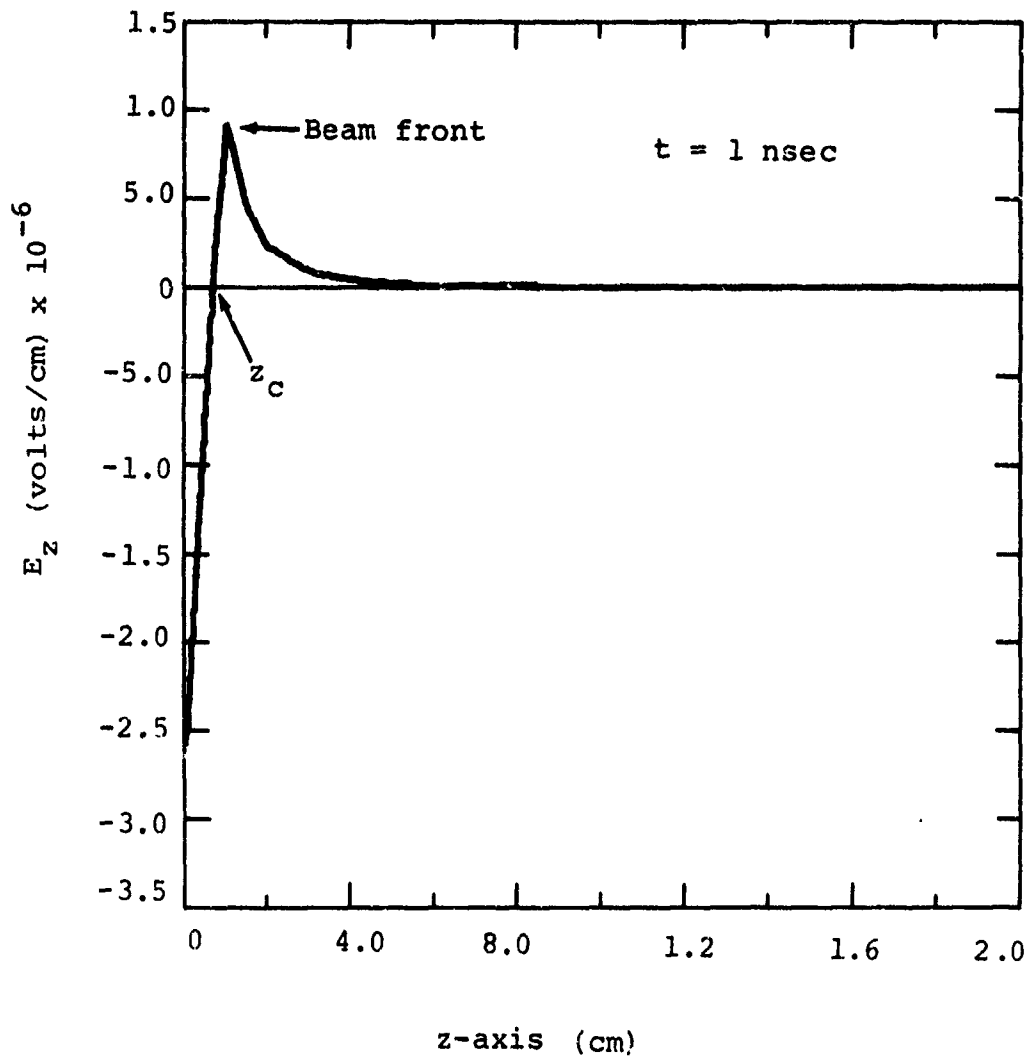


Figure 2.9 The longitudinal electric field ( $E_z$ ) on axis for a beam penetrating an end plate in a finite radius cavity ( $t = 1$  nsec).

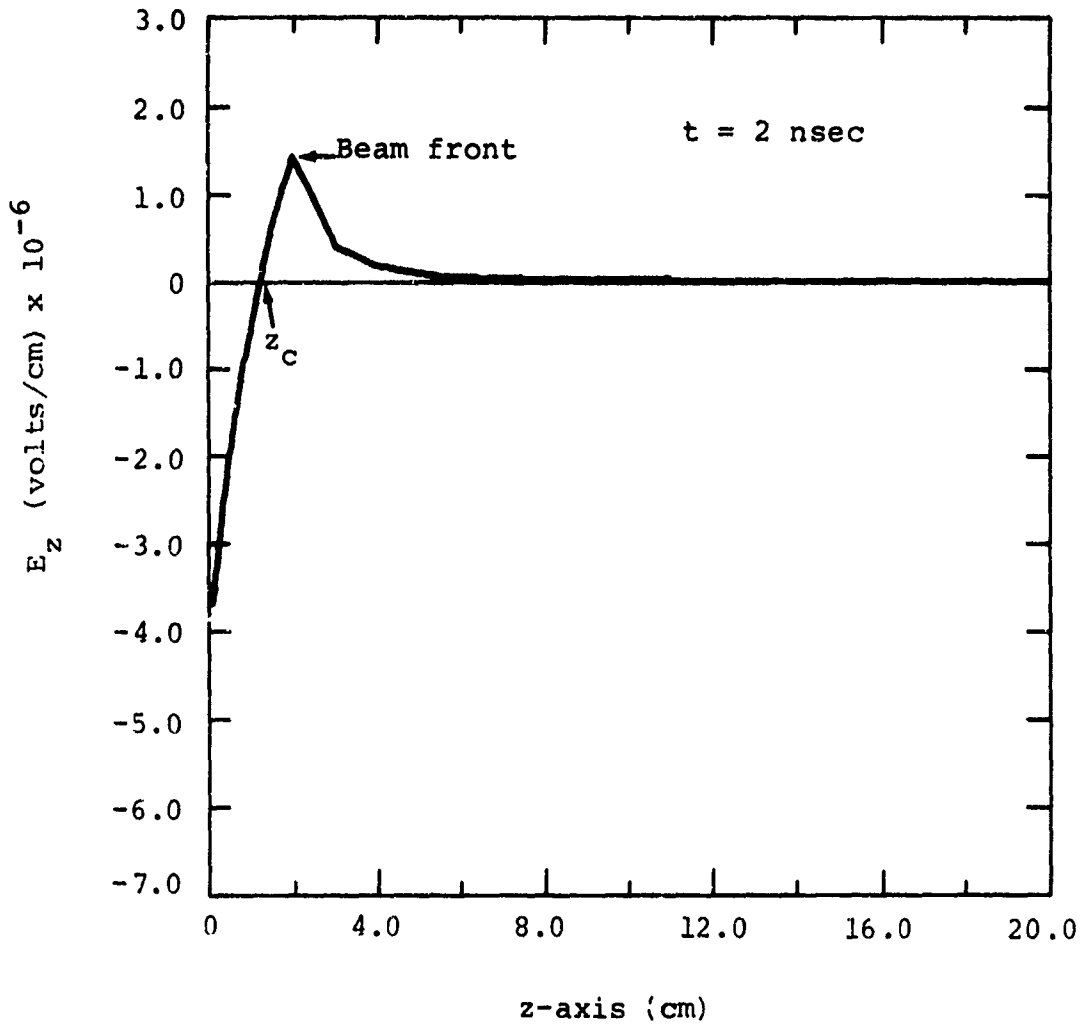


Figure 2.10 The longitudinal electric field ( $E_z$ ) on axis for a beam penetrating an end plate in a finite radius cavity ( $t = 2$  nsec).

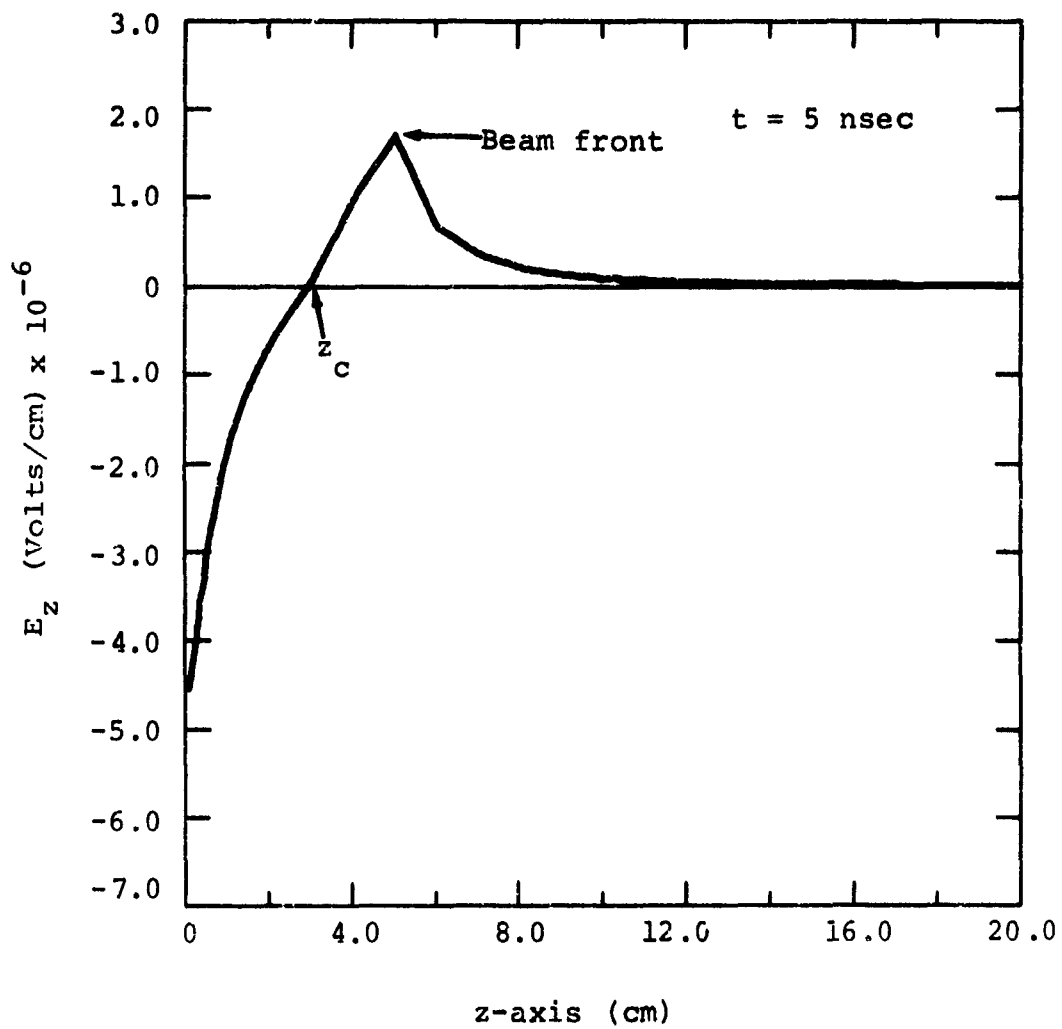


Figure 2.11 The longitudinal electric field  $E_z$  on axis for a beam penetrating an end plate in a finite radius cavity ( $t = 5$  nsec).

where  $z_f$  is the beam front position ( $\approx$  time in nanoseconds in the above example). Equation (2.29) is valid for a "blunt" beam when  $z_c \lesssim 2R/2.4$ . In order to neglect the electrostatic endplate effect on the beam fields, it is therefore required that

$$ct/\gamma, z_f, z \gg R/2.4 \quad (2.30)$$

When  $R \rightarrow \infty$ , one can also derive a manageable expression for the  $E_z$  field. A straightforward electrostatic image method calculation (Figure 2.12) gives for the potential,  $\phi$ , on axis ( $r = 0$ )

$$\begin{aligned} \phi(z,L) &= \frac{2\lambda}{a^2} \left\{ \frac{1}{2} \left[ (L+z)^2 - (L-z)^2 - 2z^2 \right] + \int_{-z}^{L-z} d\omega \sqrt{a^2 + \omega^2} \right. \\ &\quad \left. - \int_z^{L+z} d\omega \sqrt{a^2 + \omega^2} \right\} \\ &= \frac{\lambda}{a^2} \left\{ 2z(2L-z) + (L-z) \sqrt{a^2 + (L-z)^2} - (L+z) \sqrt{a^2 + (L+z)^2} \right. \\ &\quad + 2z\sqrt{a^2 + z^2} + a^2 \left[ \ln \left( L-z + \sqrt{a^2 + (L-z)^2} \right) \right. \\ &\quad + \ln \left( z + \sqrt{a^2 + z^2} \right) - \ln \left( \sqrt{a^2 + z^2} - z \right) \\ &\quad \left. \left. - \ln \left( L+z + \sqrt{a^2 + (L+z)^2} \right) \right] \right\} \quad (2.31) \end{aligned}$$

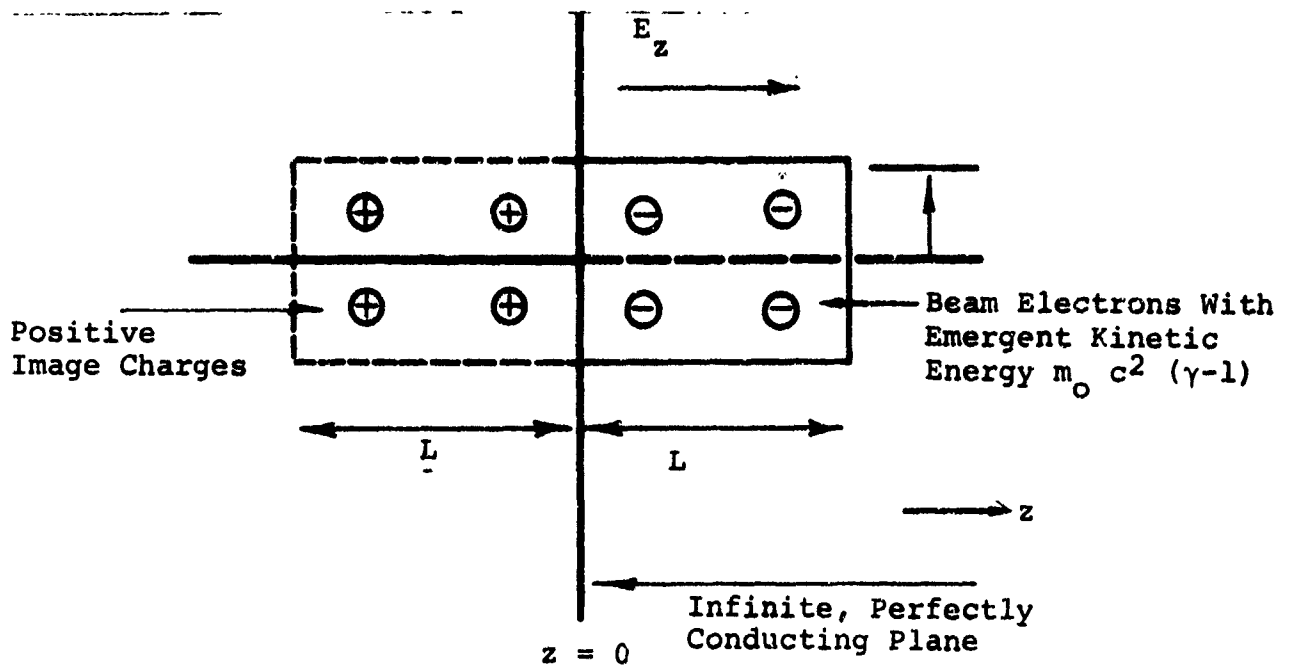


Figure 2.12 Geometry of electrostatic field calculation for a beam emerging from an infinite conducting plane.

where  $\lambda$  is the charge/length and is assumed constant from  $z = 0$  to  $z = L$ . The charge density has also been taken uniform in radius out to  $r = a$ . The expression for  $E_z$  follows directly from Equation (2.31):

$$E_z = - \frac{\partial \phi}{\partial z}$$

$$= - \frac{2\lambda}{a^2} \left\{ 2(L-z) + 2\sqrt{a^2 + z^2} - \sqrt{a^2 + (L-z)^2} - \sqrt{a^2 + (L+z)^2} \right\}$$

(2.32)

We see that  $E_z$  reverses sign and the potential well depth is maximum for  $z = z_c$  given by

$$(L-z_c) + \sqrt{a^2 + z_c^2} = \frac{1}{2} \left[ \sqrt{a^2 + (L-z_c)^2} + \sqrt{a^2 + (L+z_c)^2} \right]$$

(2.33)

## 2.4 CHARGE PRODUCTION IN NEUTRAL GASES

For the purposes of a discussion of charge production processes, one needs to realize that typical intense beams in neutral gas-filled drift chambers have electrostatic (ES) space charge fields in the  $10^5$  to  $10^6$  V/cm range before electrical neutralization and inductive fields of the order of a few keV/cm after  $f_e \approx 1$ . As shown previously, the ES fields are primarily longitudinal near the anode window and the downstream chamber endplate, and primarily radial within a region of length  $\approx 2$  ( $R/2.4$ ) away from and interior to both the endplates. Depending on beam energy and current risetimes, the ES field near the anode window, which is always in a direction to degrade the beam kinetic energy, may slow beam electrons down, sharpening the front, causing the beam to "blow up" radially, and effectively decreasing the current risetime. We then have a situation where a relatively sharp beam front precedes an ion charge neutralization front.\* This process effectively moves the anode down the chamber, maintaining a primarily longitudinal space charge field behind the beam front until, e.g.,  $f_e \sim 1/2 \gamma_L^2$  in the case discussed in Equation (2.24), and then primarily radial until  $f_e \approx 1$ . Both the value of the ES field and its direction depend on the "sharpness" of the beam and ion fronts, and may be inferred from Sections 2.2 and 2.3, using a superposition of fields from an electron and equivalent ion beam. As the beam collisionally ionizes the gas, the secondary electrons move out of the beam channel, leaving positive ions to neutralize the beam space charge over a time scale  $\tau_N$ . When the ES fields are primarily longitudinal, the  $v_z B_\theta$  force accelerates them out of the channel, or when primarily radial, the electric field does.

---

\* These remarks are amplified in Section 2.10.1.

During  $\tau_N < t < t_r$ ,  $t_r$  the current risetime, the electric field is inductive dominated, longitudinal, and drops to values of the order of a few keV/cm. We argue below in a charge production model that it is this inductive electric field which has a major effect upon charge production through electron avalanching. The exponentiation of secondary electron density during avalanching causes the gas to break down, giving rise to the phenomenon of current neutralization.

The plasma charge density may also be enhanced by the influence of ES instability-generated electric fields if the beam parameters (temperature or velocity spread) and plasma density are such as to allow rapid growth of instability oscillations. We defer a discussion of instability heating to Section 2.8.1.

2.4.1 Direct Collisional Ionization. Good working values for the impact ionization cross section ( $\sigma_{ion}$ ) for beams with energy in the MeV range are given in Table 2.1 (Reference 2.15).

TABLE 2.1

IONIZATION CROSS SECTIONS

| Gas            | $\sigma_{ion}$ (cm <sup>2</sup> ) |
|----------------|-----------------------------------|
| H <sub>2</sub> | $2 \times 10^{-19}$               |
| He             | $2 \times 10^{-19}$               |
| Ne             | $4 \times 10^{-19}$               |
| A              | $9 \times 10^{-19}$               |
| N <sub>2</sub> | $2.6 \times 10^{-18}$             |
| Air            | $2.6 \times 10^{-18}$             |

Using the cross sections above, the time for attainment of electrical neutrality,  $\tau_N$ , can be estimated. If we assume

singly charged stationary ions and that the secondary electrons escape "instantaneously" from the beam channel, the ion charge density,  $\rho_i$  is given by

$$\begin{aligned} \frac{d\rho_i}{dt} &= 3.53 \times 10^{16} j_b \sigma_{ion} P \\ &= 3.53 \times 10^{16} \frac{I_b}{\pi a^2} (c/10) \sigma_{ion} P \end{aligned} \quad (2.34)$$

with

$j_b$  = beam current density (assumed uniform) (statamps/cm<sup>2</sup>)

$I_b$  = beam current in amperes

$a$  = beam radius (cm)

$P$  = gas pressure in Torr

Integrating Equation (2.34) using  $I_b = g(t) I^P$ ,  $I^P$  = peak current in amperes,

$$\rho_i(t) = \frac{(3.53)(10^{16})}{\pi} (c/10) \sigma_{ion} P I^P \int_0^t dt' \left( \frac{g(t')}{a^2(t')} \right) \quad (2.35)$$

The electron beam charge density,  $\rho_e$ , is

$$\rho_e = \frac{I^P g(t)}{(10) \pi a^2 \beta_L}$$

so

$$\begin{aligned} f_e(t) &\equiv - \frac{\rho_{ion}}{\rho_e} \\ &= 3.53 \times 10^{16} \sigma_{ion} cP \frac{a^2 \beta_L}{g(t)} \int_0^t \frac{g(t') dt}{a^2(t')} \end{aligned} \quad (2.36)$$

The time  $\tau_N$  to attain  $f_e = 1$  can easily be obtained from Equation (2.36) for the linear current rise case ( $g(t) = t/t_z$ ) when no appreciable change in beam radius occurs over  $\tau_N$ :

$$\tau_N \text{ (nsec)} \approx \frac{0.7}{\beta_L P \text{ (torr)}} \frac{\sigma_{\text{ion}} \text{ (air)}}{c_{\text{ion}} \text{ (gas)}} \quad (2.37)$$

Let us now briefly examine the assumption that secondary electrons instantaneously escape from the beam channel. The secondary electron orbit equations are

$$\begin{aligned} \frac{d}{dt} (\gamma v_r) &= -\frac{e}{m_0} \left( E_r - \frac{v_z B_\theta}{c} \right) \\ \frac{d}{dt} (\gamma v_z) &= -\frac{e}{m_0} \left( E_z + \frac{v_r B_\theta}{c} \right) \end{aligned} \quad (2.38)$$

where  $v_r$  ( $v_z$ ) = radial (longitudinal) velocity component of secondary electrons. The energy equation is

$$\frac{d\gamma}{dt} = -\frac{e}{m_0 c^2} (E_r v_r + E_z v_z) \quad (2.39)$$

These equations can be solved analytically with specified fields only in a few cases.

First, we note from inspection of Equation (2.38) that the radial acceleration will always be outward (positive) until

$$\beta_z \equiv \frac{v_z}{c} = (E_r / B_\theta) \quad (2.40)$$

If the beam charge density is uniform in radius,

$$\frac{E_r}{B_\theta} = \frac{1-f_e}{\beta_L}$$

Thus, since  $\beta_z < 1$ , the secondary electrons will escape to "infinity" unless

$$f_e > 1 - \beta_L \quad (2.41)$$

If  $E_z \approx 0$  ( $f_e \approx 1/\gamma_L^2$ ) and  $E_r, B_\theta$  are only functions of  $r$ , Equations (2.38) and (2.39) can be solved analytically for the turning radius,  $r_t$ , at which the secondary electron reverses radial velocity. Denoting quantities referring to the initial coordinates and velocities of secondary electrons with the subscript "1,"

$$\begin{aligned}
 (\gamma v_r)^2 = & (\gamma v_r)_1^2 - \frac{2e}{m_0 c^2} \left\{ \int_{r_1}^r dr' \left[ \gamma_1 - \frac{e}{m_0 c^2} \int_{r_1}^{r'} E_r(r'') dr'' \right] E_r(r') \right. \\
 & + \frac{e}{m_0 c^2} \int_{r_1}^r \left[ B_\theta(r') \int_{r_1}^{r'} B_\theta(r'') dr'' \right] dr' \\
 & \left. - \int_{r_1}^r (\gamma v_z)_1 \frac{B_\theta}{c}(r') dr' \right\} \quad (2.42)
 \end{aligned}$$

and

$$\left. \begin{aligned}
 \gamma(r) &= \gamma_1 - \frac{e}{m_0 c^2} \int_{r_1}^r E_r(r') dr' \\
 \gamma v_z &= (\gamma v_z)_1 - \frac{e}{m_0 c^2} \int_{r_1}^r B_\theta(r') dr'
 \end{aligned} \right\} \quad (2.43)$$

Let us evaluate Equations (2.42) and (2.43) for  $\gamma_1 = 1$  in the uniform beam case, assuming  $r_t > a$ , the beam radius. We obtain

$$\begin{aligned}
 \gamma v_z &= \frac{2|I|}{m_0 c^2} e \left( \frac{1}{2} - \frac{r_1^2}{2a^2} + \ln \frac{r}{a} \right) \\
 \gamma(r) &= 1 + \left( 1 - \frac{f_e}{\beta_L} \right) 2|I| \frac{e}{m_0 c^2} \left( \frac{1}{2} - \frac{r_1^2}{2a^2} + \ln \frac{r}{a} \right)
 \end{aligned}$$

These two equations can be solved for  $r_t$ :

$$r_t = a \exp \frac{1}{2} \left\{ \frac{2(1-f_e)}{v(1-\alpha^2)} - 1 + (r_1/a)^2 \right\} \quad (2.44)$$

with

$$\alpha \equiv \frac{1-f_e}{\beta_L}$$

If we take a 1 MeV electron beam,  $v \approx 3$ ,  $f_e \approx 1/\gamma^2$ , and  $r_1 = a/2$ , Equation (2.44) gives  $r_t \approx 12a$ . In other words, when chamber radius  $R$  is  $< 12a$ , the secondary electrons would hit the wall (at relativistic velocities). If we blandly ignore the effects of  $E_z$  when  $f_e > 1/\gamma^2$ , a criterion for secondary electrons to be lost to the chamber wall is

$$2 \ln R/a \leq \frac{2(1-f_e)}{v(1-\alpha^2)} + \frac{r_1^2}{a^2} - 1 \quad (2.45)$$

Numerical orbit calculations are required to more carefully justify the assumption that secondary electrons escape from the beam channel over times short compared to  $\tau_N$  when  $f_e \lesssim 1$ . Experimental observations of beam envelope profiles using  $\tau_N$  from Equation (2.37) show that the assumption at least gives a good working estimate of space charge neutralization times.

**2.4.2 Electron Avalanching and Gas Breakdown.** Relativistic electrons create secondaries with energies in the few electron volt range. The ionization cross-section for further ionization by these secondaries is in the  $10^{-16} \text{ cm}^2$  range and, if the beam induced electric field is large enough to accelerate the secondaries to ionization energies for the background gas atoms in a distance of the order of a mean free path, these secondaries create more electron-ion pairs--the condition for gas breakdown.

In order that avalanching influence plasma generation in the beam channel, the radial electric (space charge) field of the beam cannot be too large, or in other words, the radial electric field must be low enough to keep the transit time over a distance of the beam radius not significantly smaller than the mean ionization time for secondary avalanching.

If  $f_e \approx 1$ , this condition is fulfilled. Moreover, when  $f_e > 1/\gamma_L^2$  the beam is in a pinching condition, so the space charge blowup is terminated and the beam radius can be assumed roughly constant in avalanche calculations. The charge production equation for secondary electrons can be written from the Townsend discharge theory as

$$\frac{dn_p}{dt} = \underbrace{\alpha \frac{I(t)}{\pi a^2}}_{\text{collisional ionization}} + \underbrace{\frac{n_p}{t_i(t)}}_{\text{avalanche term}} - \underbrace{\nabla \cdot \vec{\Gamma}}_{\text{transport term}} \quad (2.46)$$

where  $n_p$  is the secondary electron density/cm<sup>3</sup>

$I(t)$  = the beam current in amperes

$a$  = the beam radius in cm.

$t_i$  = mean ionization time

$$= \left( \langle v_{ion} \rangle - \langle v_a \rangle \right)^{-1}$$

$v_{ion}$  = ionization frequency

$v_a$  = electron oxygen attachment frequency in air

$\langle \rangle$  denotes a value averaged over the secondary electron velocity distribution and the background gas velocity distribution

$\Gamma$  = the particle transport current out of the volume element due to the electric field (mobility current) and diffusion

$$\alpha = \begin{cases} 5.8 \times 10^{17} \text{ P (Torr) air (N}_2\text{)} \\ 8.8 \times 10^{16} \text{ P (Torr) He} \end{cases} \left. \begin{array}{l} \text{number of ion pairs/} \\ \text{cm}^3/\text{sec/amp/cm}^2 \end{array} \right\}$$

and  $\alpha$  is obtained using the ionization cross sections in Table 2.1\*. The mean ionization time is a function of the E/P (electric field/pressure) ratio and since E varies with t,  $t_i = t_i(t)$ . We can integrate Equation (2.46) assuming  $a \approx$  constant, and neglecting the transport term,

$$n_p(t) = \frac{\alpha e}{\pi a^2} \int_{t_0}^t e^{-\int_{t_0}^{t'} \frac{dt''}{t_i}} I(t') dt' + n_p(t_0) e^{\int_{t_0}^t \frac{dt'}{t_i}} \quad (2.47)$$

$n_p$  is the secondary electron density at  $t = t_0$ . If we break up the time intervals into segments with approximately constant electric fields,  $t_i =$  constant, and if  $I = I^P t/t_r$ , a linear current rise to a peak current  $I^P$ ,

$$n_p(t) = \frac{5.8 \times 10^{17} \text{ P (Torr) } I^P \text{ (amps)}}{\pi (a(\text{cm}))^2} \frac{(t_i)^2}{t_r} \left( e^{t/t_i - t/t_i - 1} \right) + n_p(t_0) e^{t/t_i} \text{ (air)} \quad (2.48)$$

with all times in seconds.

\*  $t_i = t_i$  (only collisional ionization),

$$n_p(t) = 2.9 \times 10^{17} \text{ P} \frac{I^P}{\pi a^2} \frac{t^2}{t_r} \text{ (air)} \quad (2.49)$$

Equation 2.46 neglects recombination effects. These are not important at pressures corresponding to high conductivity breakdown.

The mean ionization times have been plotted as a function  $E/P$  from the data of Felsenthal and Proud\* (Reference 2.16) by J. Creedon (Reference 2.17). Figures 2.13 and 2.14 compare air and helium, and Figure 2.15 shows the mean ionization time in air plotted as a function of pressure for two typical electric field values.

A model of charge production is now argued to estimate breakdown times. Secondary electron orbit sketches and typical field magnitudes are summarized in Figure 2.16 for a beam in a drift chamber. The figure indicates that beam-driven electric fields vary several orders of magnitude from the time of front arrival to gas breakdown time,  $t_B$ , and that the highest fields exist for  $t < \tau_N$ . In fact, these fields are usually sufficiently high at pressures of interest for efficient beam propagation (0.1 to 1 torr) that the secondary electrons become relativistic over distances of the order of the beam radius and the ionization cross section drops to values around  $10^{-18}$   $\text{cm}^2$ . This can be compared to typical Townsend discharge theory where cross sections are used for electrons with energies up to the kilovolt range ( $\sim 10^{-16}$   $\text{cm}^2$  cross section). Moreover, until  $f_e \cong 1$  is achieved, the secondary electron motion is primarily radial and the flow is out of the beam channel. Thus, it seems reasonable to neglect avalanching in the beam channel until  $f_e \cong 1$ . When  $t > \tau_N$ ,  $|E| \cong E_z \cong 10^3$  V/cm, (typically), we consider avalanche effects to be important and the electric field is inductive. With these arguments in mind, an ad hoc charge production calculation procedure for high current electron beams is outlined:

---

\*The reader is cautioned about extrapolation of their data to off-the-curve points, particularly toward the high  $E/P$  values. These authors carefully delineate the validity of their measurements.

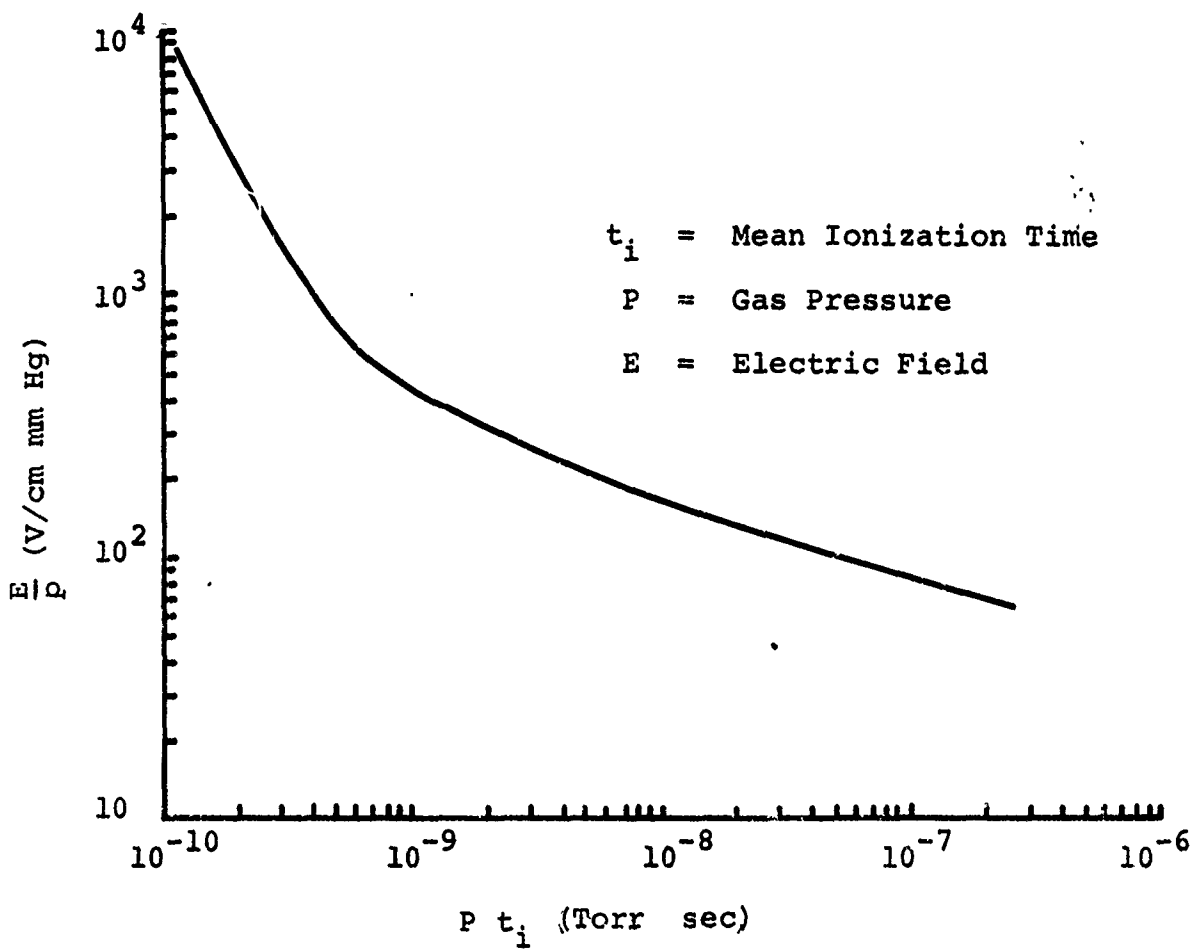


Figure 2.13 Plot of  $E/p$  versus  $P t_i$  for air.

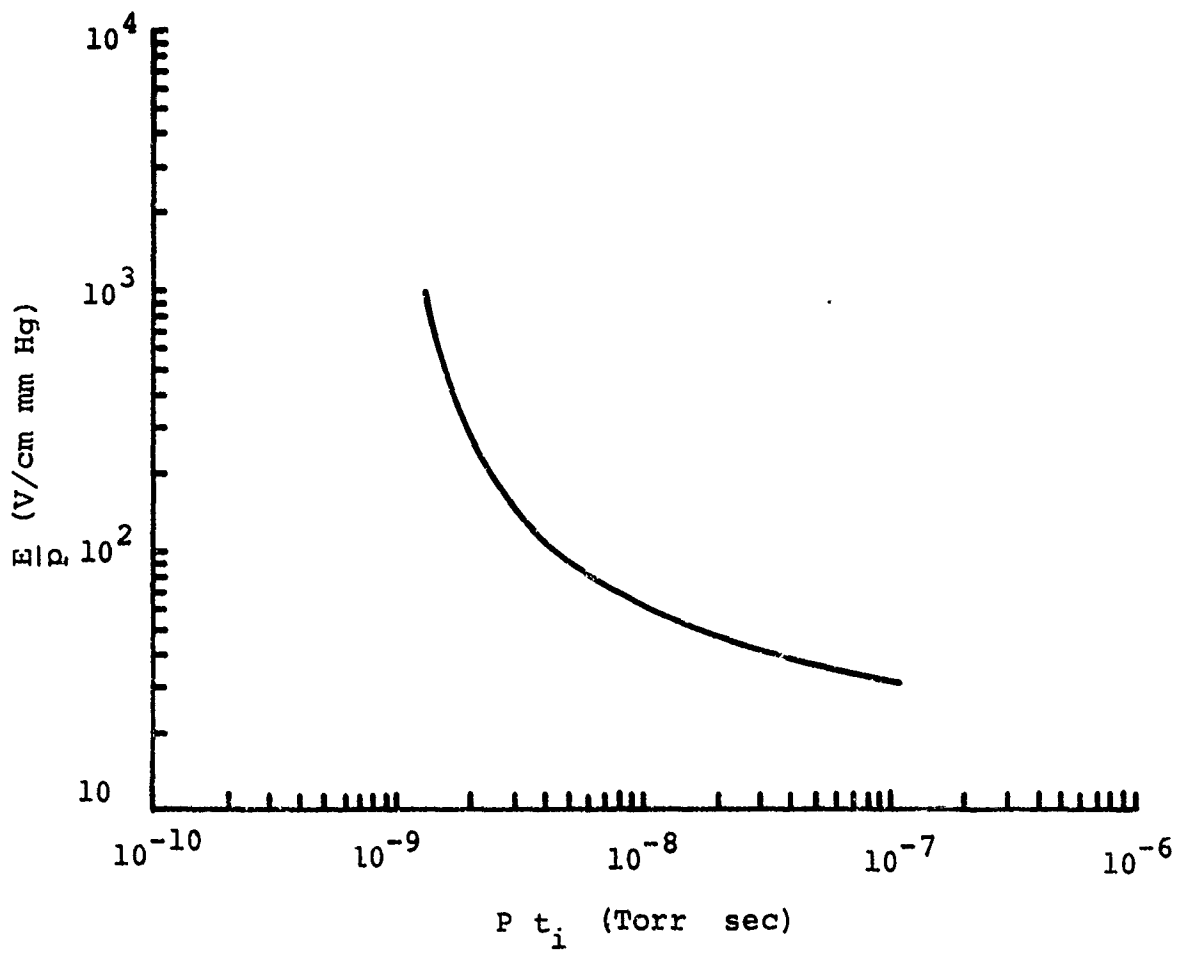


Figure 2.14 Plot of  $E/p$  versus  $P t_i$  for helium.

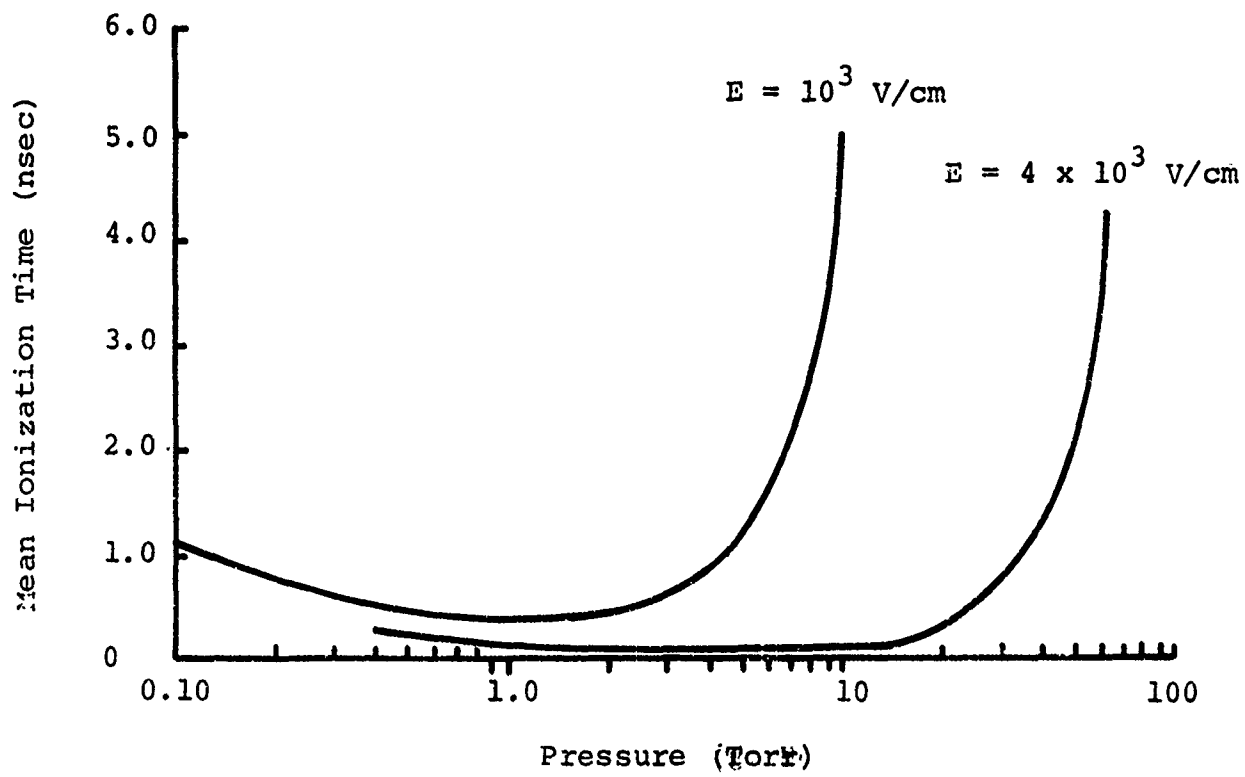


Figure 2.15 Mean ionization time versus pressure for air.

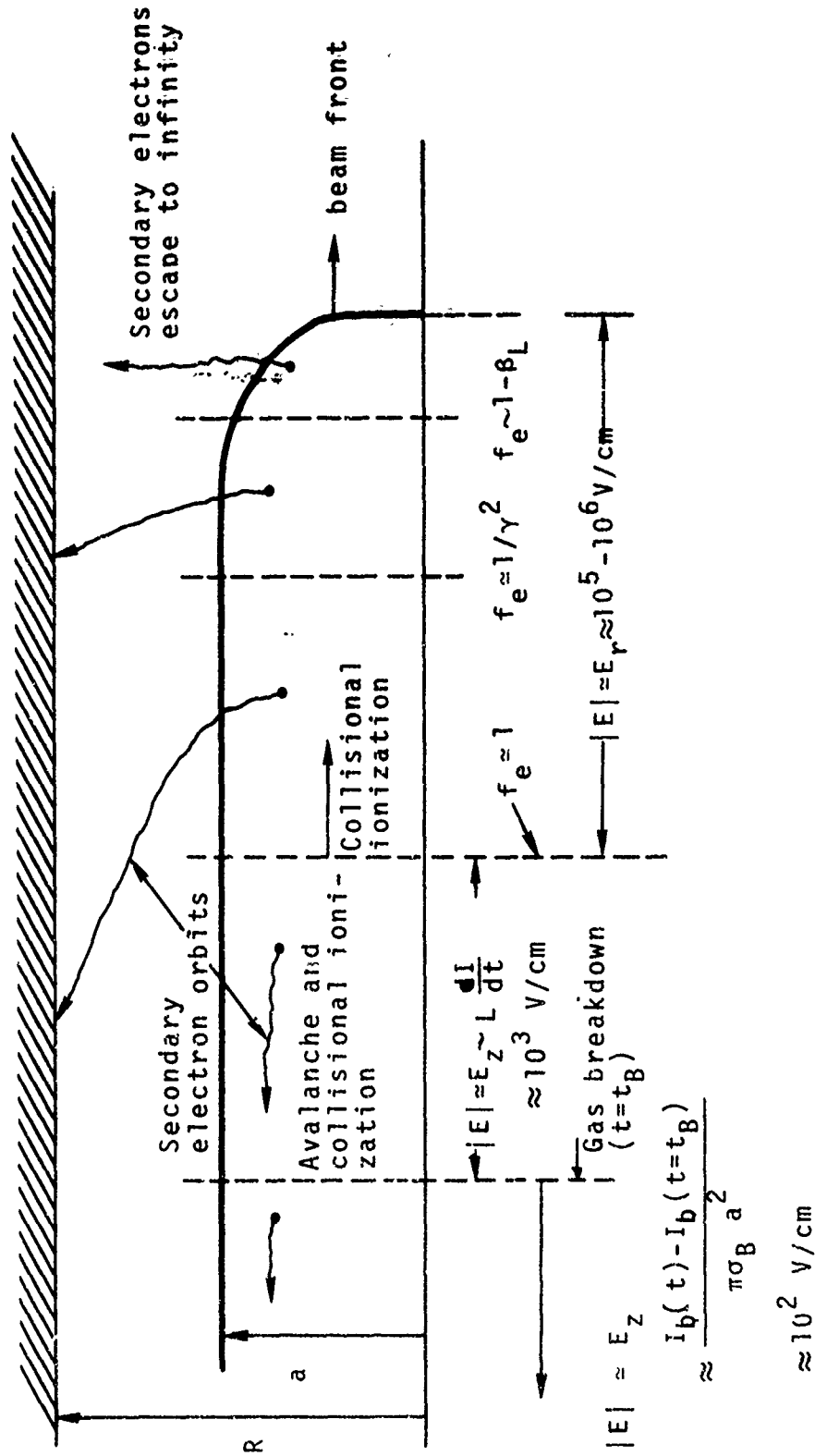


Figure 2.16 Phenomenology of charge production in neutral gas.

- a.  $\tau_N$ , the time for  $f_e \approx 1$ , is calculated from collisional ionization ( $\tau_N$  (nsec)  $\cong 0.7/\beta_L P$  (torr) for air).
- b. From the time the beam front arrives at the point of interest up to  $t = \tau_N$ , secondary electrons escape instantaneously out of the beam channel; no significant electron avalanching occurs within the beam channel.
- c. From  $t = \tau_N$  to  $t = t_B$ , the breakdown time,

$$E_z \text{ (V/cm)} \approx \frac{2I^P \text{ (amps)}}{t_r \text{ (nsec)}} (1/2 + \ln R/a),$$

assuming a linear current rise,

$$\begin{aligned} R &= \text{chamber radius} \\ a &= \text{beam radius} \\ t_r &= \text{beam risetime} \end{aligned}$$

Using  $E_z$  above and the pressure of interest,  $t_i$ , the mean ionization time (Townsend discharge theory), can be determined from Figure 2.13.

- d. Neglecting the transport term and assuming  $E_z$  constant, in Equation (2.48) gives

$$n_e^s (t - \tau_N) = \frac{\alpha I^P}{\pi a^2} \left( \frac{t_i}{t_r} \right) \left[ e^{(t-\tau_N)/t_i} (t_i + \tau_N) - (t + \tau_N) \right]$$

e. Breakdown is defined as  $n_e^s(t_B) = \delta n_b(t_B)$   
 Empirically determined  $\delta \approx 226$

f.  $t_B$  is obtained from the transcendental equation:

$$\frac{e^{(t_B - \tau_N)/t_i}}{t_B} \approx \frac{80}{P \text{ (torr)}} \frac{1}{t_i \beta_L} \frac{1}{(t_i + \tau_N)} \quad \text{for air} \quad (2.50)$$

(All times are in nanoseconds.)

Breakdown time calculations from the above are compared with Yonas and Spence data in Table 2.2 (Reference 2.18). The beam parameter range over which the above model is relevant is not clear, inasmuch as detailed breakdown data exists only from the Yonas and Spence work. It is quite likely that widely different beam parameters would require adjustment of the charge multiplication factor,  $\delta$ .

TABLE 2.2

BREAKDOWN TIME CALCULATIONS

| <u>P</u><br>(torr) | <u><math>\tau_N</math></u><br>(nsec) | <u><math>t_i</math></u><br>(nsec) | <u><math>t_B</math></u><br>(nsec)<br>Calculated | <u><math>t_B</math></u><br>(nsec)<br>Measured |
|--------------------|--------------------------------------|-----------------------------------|---|---|
| 0.1                | 13.0                                 | 1.0                               | 20.7  | 20  |
| 0.3                | 4.3                                  | 0.47                              | 7.8   | 10  |
| 0.5                | 2.6                                  | 0.34                              | 5.1   | 5   |

Agreement is within  
 experimental error

Parameters

$I^P = 4 \times 10^4$  amperes  
 $t_r = 20$  nsec  
 $E_z = 2 \times 10^3$  volts/cm

$a^2 = 2.5 \text{ cm}^2$   
 $\beta_L = 0.54$   
 $\gamma = 1.5$   
 $R = a$

After gas breakdown the plasma becomes a good conductor and the electric field typically drops to the few hundred V/cm range or less. An estimate of further ionization can then be made from

$$\frac{dn_p(t)}{dt} \approx \frac{\sigma E_z^2}{\Delta W_{ion}}, \quad t > t_B \quad (2.51)$$

where  $\sigma$  is the plasma conductivity after breakdown and  $\Delta W_{ion}$  is the energy required to create an electron-ion pair  $\approx 33$  eV/ion pair  $\approx 5.3 \times 10^{-11}$  erg/ion pair. Equation (2.51) would, of course, apply until the gas is fully ionized or the driving field becomes negligible. In Section 2.6 we estimate the  $E_z$  of Equation (2.51).

## 2.5 PLASMA CONDUCTIVITY

In order to use the concept of conductivity in a meaningful sense and thereby simplify the plasma dynamics enormously, we have to carefully characterize the plasma parameters and the electric fields; an intense beam, self-generated plasma system typically has electric fields varying several orders of magnitude over the beam pulse width and, of course, the gas changes from an unionized state to perhaps a fully-ionized, heated plasma. We are most interested in the necessary conditions to use a scalar, dc conductivity--the simplest case.

Before the gas is fully ionized, the conductivity contains contributions both from electron-neutral and electron-ion collisions. An often-used rule to calculate the effective conductivity is

$$\frac{1}{\sigma_T} = \frac{1}{\sigma_{e,n}} + \frac{1}{\sigma_{e,i}} \quad (2.52)$$

with

$$\begin{aligned}\sigma_T &= \text{total conductivity} \\ \sigma_{e,i} &= \text{electron-ion conductivity} \\ \sigma_{e,n} &= \text{electron-neutral conductivity}\end{aligned}$$

The scalar conductivity components are defined as

$$\begin{aligned}\sigma_{i,j} &= \frac{n_p e^2}{m_o} \frac{1}{\nu_{i,j}} = \frac{\omega_p^2}{4\pi} \frac{1}{\nu_{i,j}} \\ &= 2.53 \times 10^8 \frac{n_p}{\nu_{i,j}} \text{ (sec}^{-1}\text{)}, *\end{aligned} \quad (2.53)$$

where  $n_p$  = plasma electron density ( $\text{cm}^{-3}$ )

$\omega_p$  = electron plasma frequency

$\nu_{i,j}$  = momentum transfer collision frequency ( $\text{sec}^{-1}$ )  
for (i,j) 90 degree scattering to direction of  
electric field.

We list several restrictions upon use of Equation (2.53) which have to be considered in intense beam applications.

1.  $\nu_{i,j} \gg \omega_m$  (dc approximation),  $\omega_m$  = maximum angular frequency of EM field components with "appreciable" amplitude. Otherwise, electron inertial effects are important and

$$\sigma = \sigma(\omega) = \frac{\omega_p^2}{4\pi} \left[ \frac{\nu_{i,j}}{(\nu_{i,j})^2 + \omega^2} - i \frac{\omega}{(\nu_{i,j})^2 + \omega^2} \right] \quad (2.54)$$

\*

$$\sigma \text{ (mho/cm)} \approx \frac{\sigma \text{ (sec}^{-1}\text{)}}{10^{12}}$$

Typically,  $\omega_m \approx \frac{2\pi}{t_p} \lesssim 10^8/\text{sec}$ . The beam pulse width is  $t_p$ .

2.  $v_{i,j} \gg \omega_c$  (scalar approximation),  $\omega_c \approx$  cyclotron frequency of secondary electrons in magnetic fields. Otherwise we must use a tensor conductivity and, for a Lorentz gas,

$$\sigma_{\perp} \approx \sigma_{\parallel} \left[ \frac{1}{1 + \left( \frac{\omega_c}{v_{i,j}} \right)^2} \right] \quad (2.55)$$

where  $\sigma_{\perp}$  ( $\sigma_{\parallel}$ ) is the conductivity perpendicular (parallel) to the magnetic field lines.  $\sigma_{\parallel}$  is given by Equation (2.53). When no external magnetic fields are applied, the "cyclotron" frequency is the Larmor or betatron frequency of the net  $B_{\theta}$  field (including current neutralization). This field is zero on axis and a maximum near the beam edge. When beam transport efficiency is high, the net current is typically such that  $B_{\theta}^{\text{net}}(r=a) \lesssim$  few kilogauss. If we take  $B_{\theta}^{\text{net}} \lesssim 2$  kilogauss,  $\omega_c \lesssim 3 \times 10^{10}/\text{sec}$ .

The collision frequency above has been tacitly assumed to be strictly collisional, either electron neutral or electron-ion. When the beam-plasma system is unstable to longitudinal electrostatic oscillations, an effective collision frequency,  $\nu_{\text{eff}}$ , can be used in weakly turbulent plasmas to give a so-called anomalous conductivity. This collision frequency represents wave-particle scattering and may be orders of magnitude higher than  $\nu_{e,n}$  or  $\nu_{e,i}$ . If the instability wave energy is dissipated by collisions rapidly enough so that non-linear regimes and particle trapping do not occur,  $\nu_{\text{eff}}$  is taken of order of the fastest linear instability growth rate,  $\text{Im}(\omega)$ . We therefore additionally require for validity of Equation (2.53):

$$v_{e,i} (\text{sec}^{-1}) \approx 6 \times 10^{-5} n_p T_e^{-3/2} \quad (2.61)$$

giving

$$\sigma_{e,i} (\text{sec}^{-1}) \approx 4.2 \times 10^{12} T_e^{3/2} \quad (2.62)$$

The two conductivity components above are equal when

$$\frac{n_p}{N_0} \approx 10^{-4} (T_e)^2$$

assuming  $\langle \sigma_m \rangle \approx 10^{-16} \text{ cm}^2$ . Thus, from Equation (2.52),  
 $\sigma \approx \sigma_{e,i}$  if

$$\left( \frac{n_p}{N_0} \right) \gg 10^{-4} (T_e)^2 \quad (2.63)$$

As an example of the application of the above remarks, let us estimate the conductivity after gas breakdown for the Yonas and Spence beam parameters of Table 2.2. We obtain the electron plasma density at breakdown from our charge production model [ $n_p(t_B) \approx 200 n_b(t_B)$ ,  $n_b$  = beam electron number density] and assume a temperature of  $T_e \approx 10$  volts. From Equation (2.63)  $n_p/N_0 \approx 10^{-2}$  is the equal  $\sigma_{e,i}$  and  $\sigma_{e,n}$  plasma electron to background gas density ratio. The calculations are given in Table 2.3.

TABLE 2.3

CONDUCTIVITY ESTIMATES AT GAS BREAKDOWN

| <u>P (torr)</u> | <u><math>N_0</math> (<math>\text{cm}^{-3}</math>)</u> | <u><math>n_p(t_B)</math></u> | <u><math>n_p/N_0</math></u> | <u><math>\sigma(t \approx t_B)</math> (<math>\text{sec}^{-1}</math>)</u>                 |
|-----------------|---|------------------------------|-----------------------------|--|
| 0.1             | $3.5 \times 10^{15}$                                  | $4 \times 10^{14}$           | $\sim 10^{-1}$              | $\sigma \approx \sigma_{e,i} \approx 1.3 \times 10^{14}$                                 |
| 1.0             | $3.5 \times 10^{16}$                                  | $4 \times 10^{13}$           | $\sim 10^{-2}$              | $\sigma = \sigma_{e,i}^{1/2} \approx \sigma_{e,n}^{1/2}$<br>$\approx 6.5 \times 10^{13}$ |

of a transverse magnetic field, but presumably could be important near the axis of a  $B_0$  field system where  $B_\theta \approx 0$ . If  $n_p \approx 3.5 \times 10^{15} / \text{cm}^3$ ,  $p \approx 0.1$  torr, fully ionized,  $T_e \sim 10$  volts,  $Z = 1$ , (conditions for rapid gas breakdown and good beam transport), Equation (2.57) gives  $E_z \leq 700$  V/cm. Such a field would correspond to plasma current densities,  $j_p$ , of  $\sim 7 \times 10^4$  amps/cm<sup>2</sup>, assuming  $\sigma = \sigma_{e,i}$  and  $T_e \lesssim 10$  volts. The highest beam current densities yet attained in the drift chamber are  $\sim 10^5$  amps/cm<sup>2</sup>. Thus, the  $E_z$  field limitation for Equation (2.56) will usually allow use of a scalar conductivity giving essentially complete current neutralization of the highest current density beams.

Returning to Equation (2.38), we obtain expressions for  $\sigma_{e,n}$  and  $\sigma_{e,i}$ . The electron-neutral collision frequency is defined as

$$v_{e,n} = N_0 \langle \sigma_m v \rangle \approx N_0 \langle \sigma_m \rangle v_t, (v_t > v_d) \quad (2.58)$$

where  $v$  is the electron velocity,  $N_0$  is the background gas neutral density,  $\langle \sigma_m \rangle$  is the electron distribution-averaged momentum transfer cross section. Equation (2.58) may be rewritten using Equation (2.56) as

$$v_{e,n} (\text{sec}^{-1}) \approx 2.1 \times 10^{24} \langle \sigma_m \rangle \sqrt{T_e} (\text{eV}) P (\text{torr}) \quad (2.59)$$

giving

$$\sigma_{e,n} (\text{sec}^{-1}) \approx 1.2 \times 10^{-16} \frac{n_p}{\langle \sigma_m \rangle \sqrt{T_e}} \frac{1}{P (\text{torr})} \quad (2.60)$$

Typically  $\langle \sigma_m \rangle \sim 10^{-15} - 10^{-16}$  cm<sup>2</sup>, and may be obtained for various gases from electron mobility measurements (References 2.20 and 2.21). The electron-ion collision frequency for  $Z = 1$  ions (Reference 2.22) is

$$v_{e,i}(\text{sec}^{-1}) \approx 6 \times 10^{-5} n_p T_e^{-3/2} \quad (2.61)$$

giving

$$\sigma_{e,i}(\text{sec}^{-1}) \approx 4.2 \times 10^{12} T_e^{3/2} \quad (2.62)$$

The two conductivity components above are equal when

$$\frac{n_p}{N_o} \approx 10^{-4} (T_e)^2$$

assuming  $\langle \sigma_m \rangle \approx 10^{-16} \text{ cm}^2$ . Thus, from Equation (2.52),  
 $\sigma \approx \sigma_{e,i}$  if

$$\left( \frac{n_p}{N_o} \right) \gg 10^{-4} (T_e)^2 \quad (2.63)$$

As an example of the application of the above remarks, let us estimate the conductivity after gas breakdown for the Yonas and Spence beam parameters of Table 2.2. We obtain the electron plasma density at breakdown from our charge production model [ $n_p(t_B) \approx 200 n_b(t_B)$ ,  $n_b$  = beam electron number density] and assume a temperature of  $T_e \approx 10$  volts. From Equation (2.63)  $n_p/N_o \approx 10^{-2}$  is the equal  $\sigma_{e,i}$  and  $\sigma_{e,n}$  plasma electron to background gas density ratio. The calculations are given in Table 2.3.

TABLE 2.3

CONDUCTIVITY ESTIMATES AT GAS BREAKDOWN

| <u>P (torr)</u> | <u><math>N_o</math> (<math>\text{cm}^{-3}</math>)</u> | <u><math>n_p(t_B)</math></u> | <u><math>n_p/N_o</math></u> | <u><math>\sigma(t \approx t_B)</math> (<math>\text{sec}^{-1}</math>)</u>         |
|-----------------|---|------------------------------|-----------------------------|--|
| 0.1             | $3.5 \times 10^{15}$                                  | $4 \times 10^{14}$           | $\sim 10^{-1}$              | $\sigma \approx \sigma_{e,i} \approx 1.3 \times 10^{14}$                         |
| 1.0             | $3.5 \times 10^{16}$                                  | $4 \times 10^{13}$           | $\sim 10^{-2}$              | $\sigma = \sigma_{e,i}/2 \approx \sigma_{e,n}/2$<br>$\approx 6.5 \times 10^{13}$ |

These estimates, of course, suffer from the uncertainty in  $T_e$ , but the conclusion that the conductivity at 1 torr is lower than at 0.1 torr is supported by experimental data on plasma current decay rates (Reference 2.23).<sup>\*</sup> The change in  $\sigma$  after breakdown will depend on the value of  $\sigma(t = t_B)$ , or equivalently, the power input to the plasma after breakdown. At  $p = 1$  torr, we would expect the plasma ionization to continue and the conductivity to increase somewhat. Detailed measurements of plasma densities and temperatures are needed to verify these remarks.

A plot of electron drift velocity in air as a function of  $E/P$  for an electron-neutral dominated collision frequency is given in Figure 2.17, from which  $\sigma_{e,n}$  can be inferred:

$$\sigma_{e,n} \approx 1.4 \times 10^{-7} \frac{v_d n_p}{E(\text{V/cm})} \quad (2.64)$$

## 2.6 CURRENT NEUTRALIZATION

We have already discussed space charge neutralization and its influence upon the electric fields. When  $f_e > 1/\gamma^2$  (or  $1/2 \gamma^2$ , depending on the variation of  $f_e$  with space and time behind the beam front), the  $E_z$  field is in a direction to drive secondary electrons back to the anode, i.e., oppositely to the beam electrons. The radial electric field component is still large, however, and the secondary electrons are driven out of the beam channel until  $f_e \approx 1$ . After  $f_e \approx 1$ , the field is inductive ( $L \, dI/dt$ ) and we argued in the charge production model the use of the inductive field for electron avalanching calculations. The plasma electron "supply" is not large enough to provide a substantial secondary electron current until gas breakdown occurs,

<sup>\*</sup> If plasma parameters at breakdown are such that  $\sigma_{e,n}$  always dominates, this conclusion is, of course, also true.

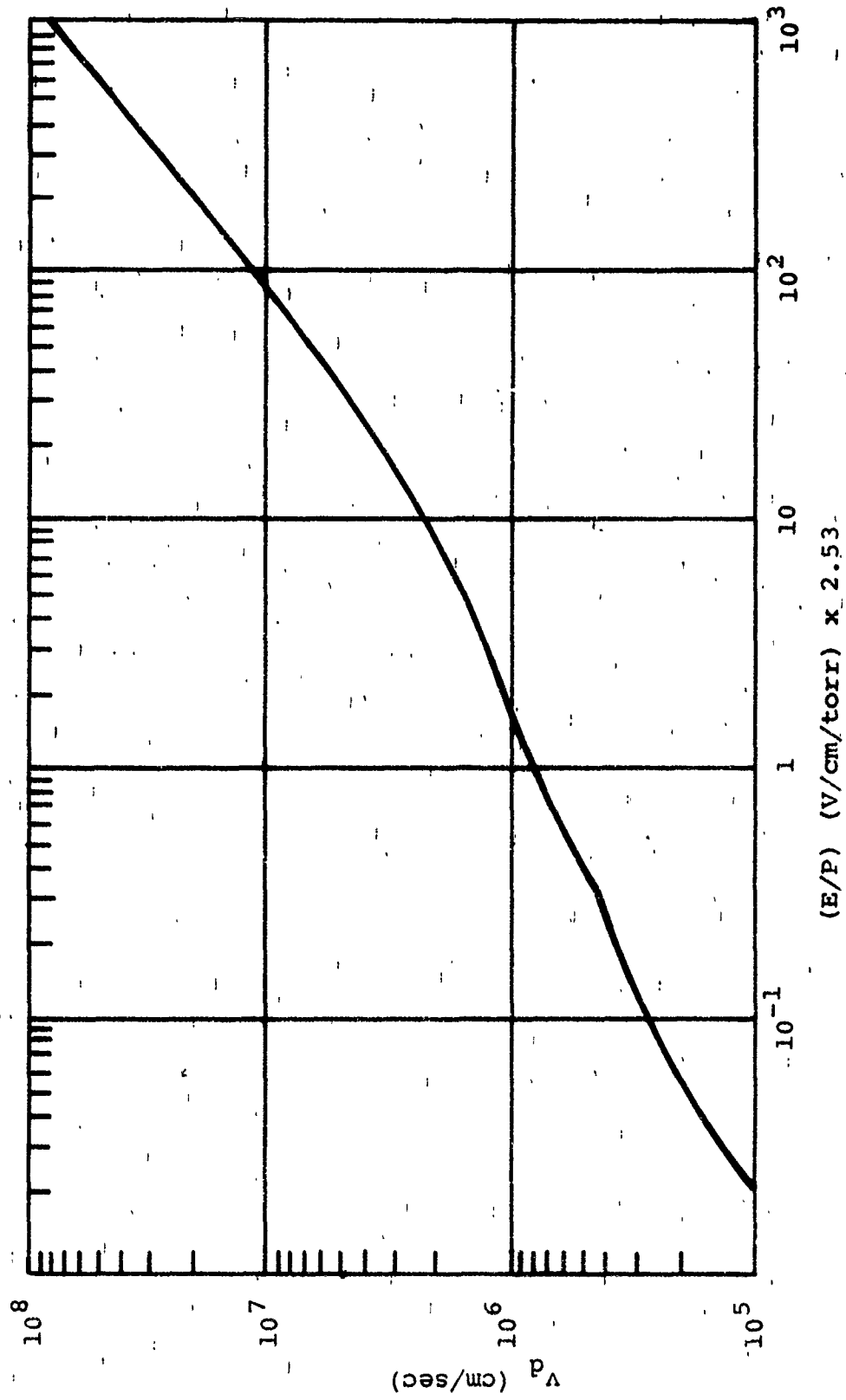


Figure 2.17 A. V. Phelps electron drift velocity data for dry air

after which time the net current in the chamber is held more or less constant over the remainder of the beam pulse. In other words, the beam current may be neutralized by the plasma return current. We argue below a simple model to estimate the degree of current neutralization for beams injected into a neutral gas.

If the gas is a good conductor after breakdown, as is usually the case, the time scale for further changes in the magnetic field, assuming a constant conductivity, is the magnetic diffusion time,  $t_d$ :

$$t_d \text{ (sec)} \approx \frac{4\pi \sigma a^2}{c^2} \quad (2.65)$$

$\sigma$  in ( $\text{sec}^{-1}$ ). This is the time scale for changes in the magnetic field to diffuse a distance of the order of the beam radius,  $a$ . When the gas breaks down, the beam current has reached a certain value depending on time of breakdown and has an associated  $B_\theta$  value. The magnetic field after breakdown changes from this  $B_\theta$  value over a time scale of  $t_d$ . If  $\sigma_B \gtrsim 10^{13}/\text{sec}$ , e.g.,  $a \cong 1 \text{ cm}$ , Equation (2.65) gives  $t_d \gtrsim 130 \text{ nsec}$ . Thus, if  $t_d \gg t_p$ , the beam pulse width, the magnetic field and net current remain approximately constant and equal to values at breakdown. The magnetic field is then "frozen" or clamped and the plasma return currents adjust to the changing beam current to keep the net current constant. An estimate of  $E_z$  driving the plasma return current for  $t > t_B$  is

$$E_z \approx \frac{I_b(t) - I_b(t_B)}{\pi \sigma_B a^2}, \quad (t_d \gg t_p) \quad (2.66)$$

where  $I_b$  = beam current.

We define the fractional magnetic neutralization,  $f_m$ :

$$f_m \equiv \frac{I_p (r = a)}{I_b} = 1 - \frac{I_b (t_B)}{I_b (t)} \quad (2.67)$$

$I_p$  is the plasma return current over the beam cross section. For strictly inductive electric fields,  $f_m < 1$ . An estimate of  $f_m$  can be made from the charge production rules of Section 2.4, which give an estimate of  $t_B$ , and therefore  $I_b(t_B)$ .

In order to achieve high current neutralization, we need to fulfill two conditions:

1. The conductivity at breakdown,  $\sigma_B$ , must be high ( $t_d > t_p$ )
2. Breakdown must occur early in the pulse ( $t_B < t_r$ ).

In the 0.1 to 1 torr pressure range, the second point is usually dominant. At higher pressures current neutralization will drop because  $\sigma_B$  decreases. These remarks are summarized in Figure 2.18, where we see that  $f_m \approx 0$  at 0.1 torr, even though  $\sigma_B$  is higher than  $\sigma_B$  at 1 torr (refer to Table 2.3).

Yonas et al. (Reference 2.23), have utilized the ideas discussed above to approximately calculate the net current versus time for a given beam-current profile. They break up the beam profile into a current-rise region, a "flat top," and a decay, and use the magnetic diffusion equation with this type of an approximate source term (beam current) to calculate the net current. Figure 2.19 shows an example of their calculated net currents versus measured net current.

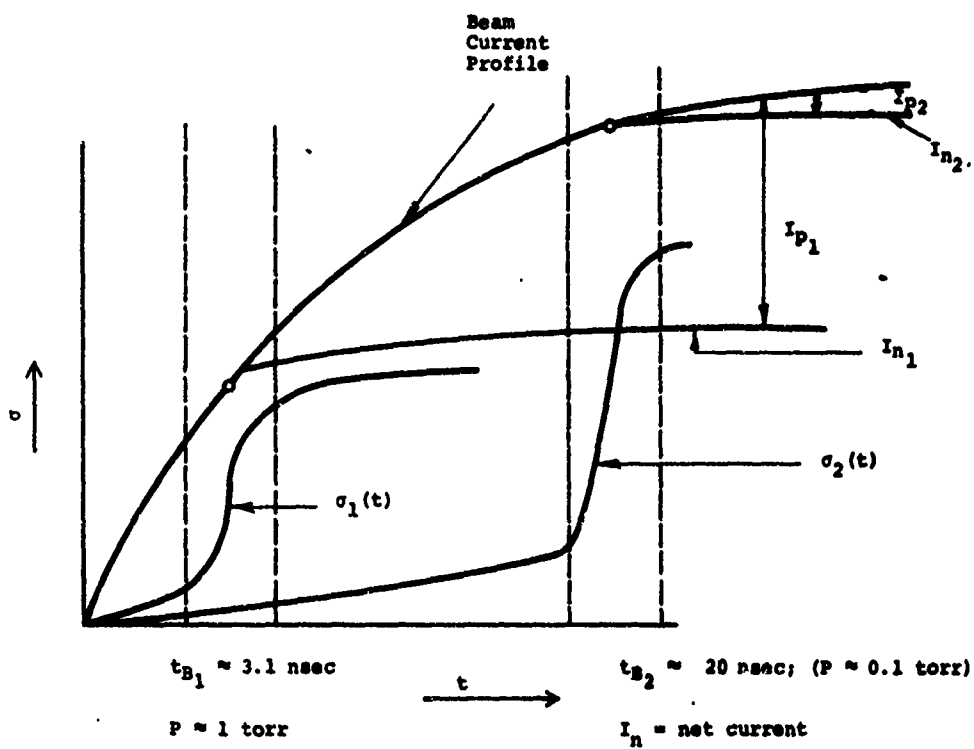


Figure 2.18 Conductivity versus time after beam injection sketch for two representative pressures.

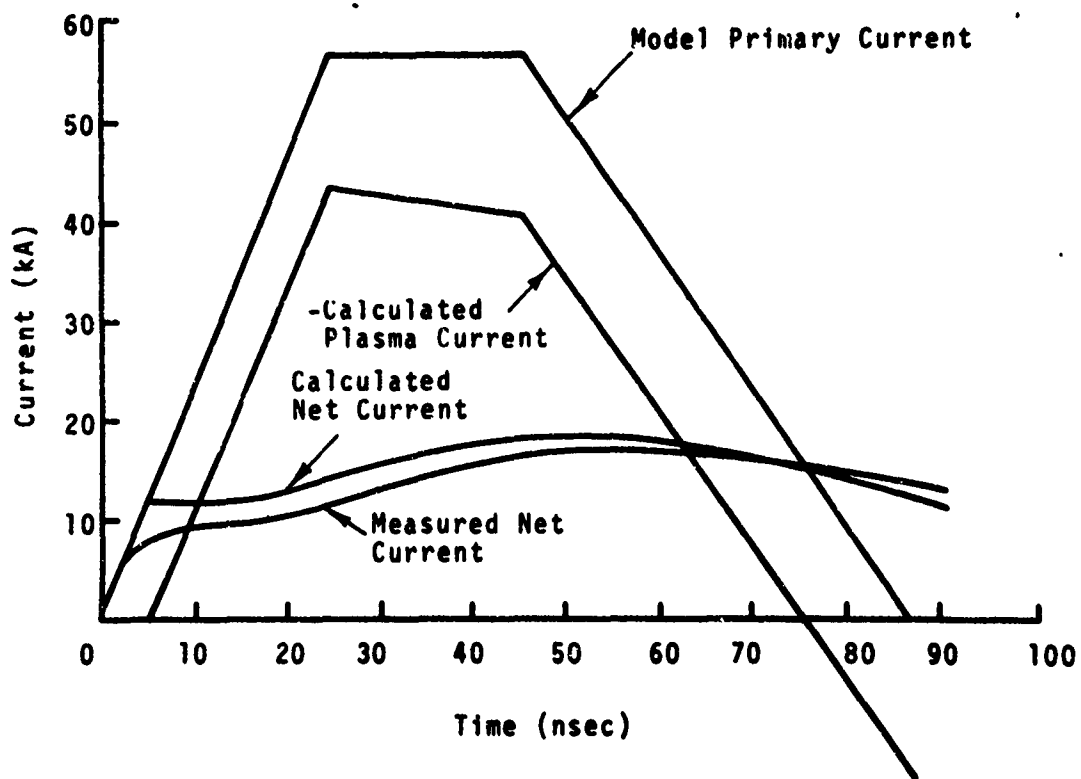


Figure 2.19 Comparison of measured and calculated net currents (Reference 2.23).

We now present a summary of an exact EM calculation showing current neutralization. Several authors have discussed the current neutralization problem under various assumptions (Reference 2.24). All calculations assume a constant conductivity plasma (except, recently, Swain, Reference 2.25), an assumption which therefore restricts them to injection into preionized plasmas; i.e., they completely miss the point for neutral gas current neutralization phenomena discussed above. The most practically relevant calculations for preionized gas injection are given in Section 3.3 where a finite risetime beam in a finite radius chamber is considered. We summarize below the results of these calculations.

2.6.1 Beam Injected Into a Preformed Plasma. We make the following assumptions in the calculations:

- a. Azimuthal symmetry
- b.  $B_z \approx 0$ ,  $j_{b\theta} = 0$
- c. Undistorted beam moving at constant velocity,  $\beta_L c \approx v$ .
- d.  $j_{bz} = j_b =$  beam longitudinal current density  
 $= f(r) g(u)$ ,  $u \equiv \gamma(vt - z)$ .
- e.  $g(u) = (1 - e^{-\alpha u})$ ,  $(\alpha^{-1})$  is the e-folding current riselength.

Equation (3.64) of Section 3 gives us the vector potential  $A = A_z$ , from which we obtain  $B_\theta = -\partial A / \partial r$ , and the net current

$$I_n(r, u) = \frac{c}{2} r B_\theta(r, u) = 4\pi C_1 r \sum_{n=1}^{\infty} H_n G_n(u) \frac{J_1\left(\frac{\lambda_n}{R} r\right)}{J_1\left[\left(\lambda_n\right)\right]^2} \quad (2.68)$$

where  $J_0$  ( $J_1$ ) is the zero (first) order Bessel function,  $\lambda_n$  are the roots of  $J_0(x)$ ,  $R$  is chamber radius, and  $H_n$  is the radial form factor:

$$H_n = \frac{1}{2R^2 b^2} \frac{R}{\lambda_n} e^{-(\lambda_n/2Rb)^2} \quad \text{for } f(r) = C_1 e^{-b^2 r^2}, \quad (2.69)$$

$$R \gg \frac{1}{b},$$

$$= \frac{a}{\lambda_n} J_1 \left( \frac{\lambda_n}{R} a \right) \quad \text{for } f(r) = C_1 H(a-r) \quad (2.70)$$

H is the Heaviside function, and for  $u > 0$ ,

$$G_n(u) \equiv 1 - \left( \frac{\lambda_n}{R} \right)^2 \left( \frac{1}{\alpha - \eta_1} \right) \left[ \frac{\alpha e^{-\xi_1 u}}{\eta_1^2 \sqrt{\xi}} - \frac{e^{-\alpha u}}{\alpha + \eta_2} \right] \quad (2.71)$$

$$\xi = k^2 + \left( \frac{\lambda_n}{R} \right)^2$$

$$k = \frac{2\pi\sigma\beta_L\gamma_L}{c}$$

$$\eta_1 = \sqrt{\xi} - k$$

$$\eta_2 = \sqrt{\xi} + k$$

Equation (2.71) assumes  $\alpha \neq \eta_1$ . We note from Equation (2.71) that when  $u \gg 1/\alpha$ ,  $1/\eta_1$ , or, in other words, when we are far behind the beam front  $I_n \rightarrow I_b$ , as it should. For orientation, we mention a typical ordering of the basic system lengths for injection of a 40 nsec risetime, 1 MeV beam into a highly conducting plasma with  $\sigma = 10^{14}$ /sec. Then defining  $\alpha\gamma_L\beta_L c t_r = 2$  gives

$$\alpha = 6 \times 10^{-4} \text{ cm}^{-1}$$

$$k = 6 \times 10^4 \text{ cm}^{-1}$$

$$\eta_1 \approx 8 \times 10^{-5} \lambda_n/R \text{ cm}^{-1}$$

$$\eta_2 \approx 2k = 1.2 \times 10^5 \text{ cm}^{-1}$$

Rather than further discussing specific examples in detail here, we simply remark that the beam-tube plasma has three ordering lengths,  $\alpha$ ,  $\lambda_n^c/R$ , and  $k$ , whose relation to each other substantially affects the form of  $G_n(u)$ . (The value of  $\lambda_n^c/R$  at the cutoff index in the summation is denoted by  $\lambda_n^c/R$ .) Some limits are:

$$1. \text{ low conductivity } \rightarrow k = 2\pi\sigma\beta_L\gamma_L/c \ll \frac{\lambda_1^c}{R} = 2.4/R$$

The variations in  $u$  are now geometrically determined with scale length  $(\lambda_1/R)^{-1}$ . Plasma return currents substantially flow in the chamber wall.

$$2. \text{ high conductivity } \rightarrow k \gg \frac{\lambda_n^c}{R}$$

Plasma return currents are now essentially contained within a skin depth  $(k)^{-1}$  around the beam channel.

Within these two cases are subcases depending on  $\alpha$ . The "blunt" beam case is  $\alpha \gg \eta_2$ , and the "slow risetime" case is  $\alpha \ll \eta_1$ .

The net current expression, Equation (2.68) above, gives exact EM solutions for the constant conductivity case if the beam is undistorted. These approximations are realistic only if the conductivity at injection is sufficiently high to keep the electrical fields small enough to avoid beam distortion and substantial plasma heating. If we are interested in transporting the beam a distance  $L$ , we require

$$eE_z L \ll \text{beam kinetic energy (K.E.)}$$

or

$$\frac{j_p}{\sigma} \approx \frac{j_b}{\sigma} < \frac{K.E.}{Le}, \quad j_p = \text{plasma current density}$$

or

$$\sigma > \frac{j_b Le}{K.E.} \quad (2.72)$$

The other more serious practical restriction for use of the model is that the beam must be "cold" at injection; i.e., the transverse energy must be small enough to be contained by the low net magnetic fields in the plasma. We consider effects of beam transverse temperature in Section 2.10.1.

The EM calculations on current neutralization outlined above may be "fixed up" to cover the case of neutral gas injection with gas breakdown. The way to do this is relatively simple. Take  $\sigma = 0$ ,  $t < t_B$ ,  $\sigma \approx \sigma_B$ ,  $t > t_B$ , and use the initial condition

$$B_\theta [r, u(t_B)] = \frac{2I_b(r, u(t_B))}{cr}$$

The solution consists of the sum of two parts, one the decay of  $B_\theta$  (initial), which is a homogeneous solution of the vector potential equation, and the other a solution of the vector potential equation with the beam current after breakdown as a source term. This latter term has a net current of the form of Equation (2.68).

## 2.7 SOME BEAM DYNAMICS

So far we have considered the EM fields existing in a beam-plasma system and charge production in neutral gases assuming that the beam and gas parameters were specified. In reality, of

course, the beam motion is coupled to the fields. Our viewpoint has tacitly emphasized the longitudinal electric field and we have given expressions to evaluate its magnitude and direction with or without finite chamber boundaries. We are thus in a position to outline conditions for validity of the equations of motion for the beam envelopes and steady-state self-consistent beam equilibria discussed below.

2.7.1 The Kapchinskij-Vladimirskij (K&V) Equation. The K&V equation (Reference 2.26) is a self-consistent equation for the beam envelope including the radial electric space-charge and self-magnetic fields, and finite emittance or transverse beam "temperature." The current density is taken uniform in radius, (but varying in  $z$ ), so the forces on the beam electrons are linear in displacement from the beam axis and the flow is paraxial. While these assumptions are restrictive and render the equation irrelevant to many intense beam applications, the K&V equation is analytically tractable.

The K&V equation for the beam envelope, modified to include current neutralization, is

$$\frac{d^2 a_e}{dz^2} = \frac{2v}{\beta_L^2 \gamma} \left[ 1 - f_e - \beta_L^2 (1 - f_m) \right] \frac{1}{a_e} + \frac{\epsilon^2}{a_e^3} \quad (2.73)$$

where

- $a_e$  = beam envelope electron radius
- $\pi\epsilon$  = beam emittance or  $(r, dr/dz)$  phase space area (cm-rad)

Our inclusion of  $f_m$  is only valid if  $E_z$  is uniform in radius which, in turn, implies that the plasma skin depth is large

compared to the beam radius and that  $\ln R/a > 1$ . We rewrite Equation (2.73) as

$$\frac{d^2 a_e}{dz^2} = \frac{A}{a_e} + \frac{\epsilon^2}{a_e^3} \quad (2.74)$$

where  $A \equiv \frac{2v}{\beta_L^2 \gamma} [1 - f_e - \beta_L^2 (1 - f_m)]$

A first integral of Equation (2.74) can be obtained by multiplying both sides by  $2 da_e/dz$ , giving

$$\frac{da_e}{dz} = \left\{ A \ln \left( \frac{a_e}{a_o} \right)^2 - \epsilon^2 \left( \frac{1}{a_e^2} - \frac{1}{a_o^2} \right) + v_o^2 \right\}^{1/2} \quad (2.75)$$

$a_o$  = beam envelope at plane  $z = z_o$

$$v_o = \left( \frac{\partial a_e}{\partial z} \right)_{z=z_o}$$

Figure 2.20 illustrates these terms. Envelope extrema are obtained from Equation (2.75) by setting  $da_e/dz = 0$ , and the constant radius case is  $da_e^2/dz^2 = 0$ . Garren (Reference 2.27) has numerically calculated beam envelopes using a dimensionless version of the K&V equation.

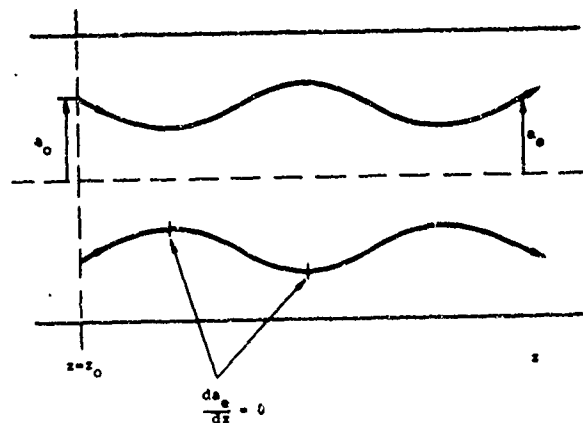


Figure 2.20 Beam envelope motion.

Some of the gross features of beam behavior versus gas pressure can now be qualitatively understood. Figure 2.21 shows some typical beam features ( $I_p \approx 2.5 \times 10^4$  A, 3 MeV) at representative pressures. The beam propagation length in the photos is  $\sim 50$  centimeters. We repeat here some of the arguments of Link (Reference 2.28). Referring to Equation (2.74) we note that the transverse energy term is always  $> 0$ , so unless  $A < 0$  the beam blows up radially. Maximum pinching occurs when  $f_e \approx 1$ ,  $f_m \approx 0$ . Using the charge production rules of Section 2.4, we obtain the following ordering of  $f_e$ ,  $f_m$  over a substantial portion of the beam pulse (pulse width  $\sim 50$  nsec,  $t_r \approx 15$  nsec).

| $P$ (torr) | $\tau_N$ (nsec) | $f_e$    | $t_B$ (nsec) | $f_m$    | $A\beta_L^2 \gamma/2v$                  |
|------------|-----------------|----------|--------------|----------|---|
| $10^{-3}$  | 700             | $\sim 0$ | $\sim$       | $\sim 0$ | $1/\gamma_L^2$<br>(space charge blowup) |
| $10^{-1}$  | 7               | $\sim 1$ | $\sim 8$     | $\sim 0$ | $-\beta_L^2$ (pinch)                    |
| 1          | 0.7             | 1        | $\sim 3$     | 1        | $\sim 0$ (drift)                        |
| 760        | $\sim 0$        | 1        | $\sim$       | $\sim 0$ | $-\beta_L^2$ (pinch)*                   |

\* The beam blowup in Figure 2.21(d) after  $\sim 25$  centimeters is probably due to an instability.

Let us now address the question of beam pinching and equilibrium radii in more detail. We consider two limits on the beam radius or energy density; the steady-state, nonuniform beam envelope case and the steady-state uniform beam envelope case.

Some of the gross features of beam behavior versus gas pressure can now be qualitatively understood. Figure 2.21 shows some typical beam features ( $I_p \approx 2.5 \times 10^4$  A, 3 MeV) at representative pressures. The beam propagation length in the photos is  $\sim 50$  centimeters. We repeat here some of the arguments of Link (Reference 2.28). Referring to Equation (2.74) we note that the transverse energy term is always  $> 0$ , so unless  $A < 0$  the beam blows up radially. Maximum pinching occurs when  $f_e \approx 1$ ,  $f_m \approx 0$ . Using the charge production rules of Section 2.4, we obtain the following ordering of  $f_e$ ,  $f_m$  over a substantial portion of the beam pulse (pulse width  $\sim 50$  nsec,  $t_r \approx 15$  nsec).

| $P$ (torr) | $\tau_N$ (nsec) | $f_e$    | $t_B$ (nsec) | $f_m$    | $A\beta_L^2 \gamma/2v$                  |
|------------|-----------------|----------|--------------|----------|---|
| $10^{-3}$  | 700             | $\sim 0$ | $\sim$       | $\sim 0$ | $1/\gamma_L^2$<br>(space charge blowup) |
| $10^{-1}$  | 7               | $\sim 1$ | $\sim 8$     | $\sim 0$ | $-\beta_L^2$ (pinch)                    |
| 1          | 0.7             | 1        | $\sim 3$     | 1        | $\sim 0$ (drift)                        |
| 760        | $\sim 0$        | 1        | $\sim$       | $\sim 0$ | $-\beta_L^2$ (pinch)*                   |

\*The beam blowup in Figure 2.21 (d) after  $\sim 25$  centimeters is probably due to an instability.

Let us now address the question of beam pinching and equilibrium radii in more detail. We consider two limits on the beam radius or energy density; the steady-state, nonuniform beam envelope case and the steady-state uniform beam envelope case.

Case 1: minimum possible beam radius,  $\frac{da_e}{dz} = 0$ .

Setting  $da_e/dz = 0$  in Equation (2.75), for the envelope extrema, and taking  $A < 0$  for the pinching mode,

$$v_p^2 + |A| \ln \left( \frac{a_o}{a_m} \right)^2 = \frac{\epsilon^2}{a_o^2} \left[ \left( \frac{a_o}{a_m} \right)^2 - 1 \right] \quad (2.76)$$

$a_m$  is the envelope extremum value.

Recalling that  $f_e = 1$ ,  $f_m = 0$  produces tight pinching, and that

$$\left( \frac{a_o}{a_m} \right)^2 > 1$$

for the pinched beam, we write (2.76) as

$$\ln \left( \frac{a_o}{a_m} \right)^2 = \frac{\gamma \epsilon^2 \beta_L^2}{2v a_o^2} \left( \frac{a_o}{a_m} \right)^2 \quad (2.77)$$

where we have assumed  $v_o = 0$ .

Equation (2.77) is a transcendental equation for the minimum beam radius, which gives the physically reasonable (but not realizable) result that a high  $v/\gamma$  beam with low emittance should be focusable into an extremely small spot. In other words, a high current beam produces a strong magnetic field to drive the pinch, and the pinch continues to a very small radius if the transverse pressure is small.

One of the difficulties in achieving tightly pinched high-current beams arises from the fact that  $v/\gamma$  and  $\epsilon$  are not independently variable in real beams. Educted high  $v/\gamma$  beams

invariably have large emittances as a result of the interaction between the electrons and the self-magnetic field of the beams in the diode region. Additional problems arise in the beam chamber. If the beam pinches very rapidly, an axial electric field due to  $I \, dL/dt$  can be produced that is large enough to stop the primary beam in a distance on the order of the beam radius. This effect is discussed in Section 4.

Case 2: constant radius

The beam envelope radius is determined in this case by  $d^2 a_e / dz^2 = 0$ . From Equation (2.74), we obtain with  $A < 0$ ,

$$a = \frac{\epsilon}{\sqrt{|A|}} \quad (2.78)$$

where  $\epsilon$  is the beam emittance in cm-radians. Figure 2.22 shows a graph of Equation (2.78) for a 4 MeV  $6 \times 10^4$  ampere beam with  $f_e = 1$ ,  $I_m = 0$ .

Case 3: constant beam radius with finite ion emittance

In case 2 we tacitly assumed that the ions had no transverse energy. This case can be easily generalized to obtain beam equilibria when ions have finite emittance. We assume that the average longitudinal velocity of the ions  $\beta_{Li} c \ll \beta_L c$ . Then using an equation for ion envelope,  $a_i$ , similar to Equation (2.73) and setting  $a_i = a_e = a_0$  gives

$$a_0^2 = \frac{\gamma}{2v} \frac{1}{\left(1 - \frac{1}{\gamma_L^2}\right)} \left( \epsilon_e^2 \beta_L^2 \gamma m_0 + \epsilon_i^2 \beta_{Li}^2 m_i / Z \right) \quad (2.79)$$

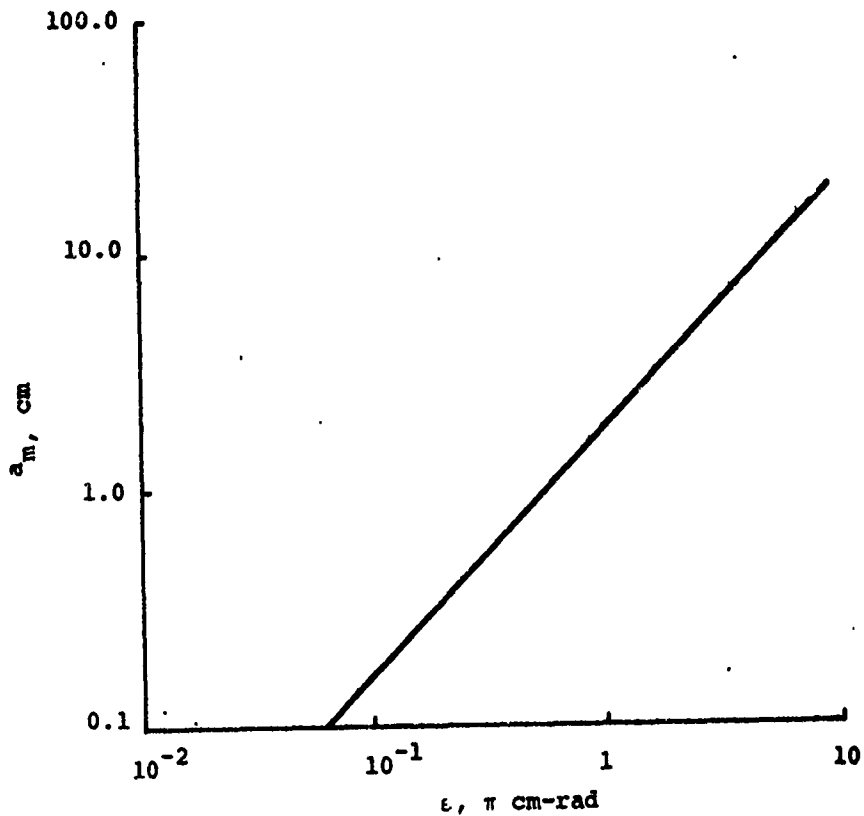


Figure 2.22 Minimum constant radius versus  $\epsilon$  for 4-MeV,  $6 \times 10^4$  A electrons (beam in pinch mode).

where

$\epsilon_i$  = the ion beam emittance

$Z$  = the ion charge state

$m_i$  = the ion mass

The steady-state equilibrium electrical neutralization,  $f_e^0$ , is given by

$$f_e^0 = \frac{1}{\gamma_L^2} + \left(1 - \frac{1}{\gamma_L^2}\right) \frac{\epsilon_e^2 \beta_L^2 \gamma_{m_0}}{\epsilon_i^2 \beta_{Li}^2 m_i/Z + \epsilon_e^2 \beta_L^2 \gamma_{m_0}} \quad (2.80)$$

If  $\epsilon_i \approx 0$ , we obtain  $f_e^0 = 1$  as in case 2.

We can compare Equation (2.80) with the Lawson constant radius, uniform beam model (Reference 2.29) where the beam electrons and ions have non-zero angular momenta. Then

$$f_e^0 = \frac{1}{\gamma_L^2} + \left(1 - \frac{1}{\gamma_L^2}\right) \frac{\langle \beta_{te}^2 \rangle \gamma_{m_0}}{\langle \beta_{te}^2 \rangle \gamma_{m_0} + \langle \beta_{ti}^2 \rangle m_i / Z} \quad (2.81)$$

$$\langle \beta_{te}^2 \rangle c^2 = \text{average electron transverse velocity squared}$$

$$\langle \beta_{ti}^2 \rangle c^2 = \text{average ion transverse velocity squared}$$

We thus see a direct correspondence between the emittance and transverse energy in the uniform beam case.

2.7.2 Beam Envelope Equation With Longitudinal Electric Space Charge Field. The K&V equation has been generalized by Walsh (Reference 2.30) to include  $E_z$  space charge fields due to  $\int \partial E_r / \partial z \, dr'$ .<sup>\*</sup> The modified envelope equation is ( $f_m \approx 0$ )

$$\begin{aligned} \frac{d^2 a}{dz^2} = & \frac{2V}{\beta_L^2 \gamma} \left(1 - f_e - \beta_L^2\right) \frac{1}{a} + \frac{e}{\beta_L^2 \gamma m_0 c^2} \frac{dV}{dz} \frac{da}{dz} \\ & + \frac{e}{2\beta_L^2 \gamma m_0 c^2} \frac{d^2 V}{dz^2} a + \frac{\epsilon^2}{a^3} \end{aligned} \quad (2.82)$$

$V$  is the ES potential on axis ( $r = 0$ ) and  $V$  has been taken as  $V = V(z, 0) + r^2/2 (\partial^2 V / \partial r^2)_{r=0}$  in deriving Equation (2.82).

<sup>\*</sup>The author is indebted to J. D. Lawson for calling his attention to Walsh's work (private communication, August 1971).

In uniform radius flow, Equation (2.82) gives an equation for  $a = a_0$ :

$$\frac{2v}{\beta_L \gamma} \left( f_e - \frac{1}{\gamma_L} \right) = \frac{e a_0^2}{2 \beta_L^2 \gamma m_0 c^2} \frac{d^2 v}{dz^2} + \frac{\epsilon^2}{a_0^2} \quad (2.83)$$

If  $f_e \cong 0$ ,  $\epsilon \cong 0$ ,  $\gamma \approx 1$  (non-relativistic), Equation (2.83) becomes

$$\frac{d^2 v}{dz^2} = - \frac{4I}{\beta_L a^2} \quad (2.84)$$

Using  $\beta_L = \beta = - 2eV/m_0 c^2$  from energy conservation, Equation (2.84) gives the Langmuir-Childs space charge limited flow if  $dV/dz = 0$  at  $z = z_0$ . More general beam envelope profiles or cases have not been calculated using Equation (2.82) to the author's knowledge.

In summary, we have looked at beam envelopes and equilibria for paraxial flow using the K&V equation that ignores  $E_z$  and one special case of a more general, albeit more complicated, equation which includes beam space charge  $E_z$  fields. This latter equation [Equation (2.82)] would not be valid in regions near a chamber endplate. Thus, in both cases, we have to be away from the endplate and interior to a drift chamber unless  $f_e \approx 1$ . If  $f_e \approx 0$ , the potential well in the chamber must be "shallow" enough to allow propagation. Finally, variation in beam current must be slow enough to ignore the inductive fields over distances of interest.

### 2.7.3 v/γ And Beam Propagation-High v/γ Beam Equilibria.

The envelope equations and beam equilibria above are all relevant to "low v/γ" beams; i.e.,  $v/\gamma < 1$ . The flow was assumed paraxial,

which implies that the beam radial velocity components were small compared to longitudinal velocity components. In 1939 Alfven (Reference 2.31) calculated electron trajectories in space-charge-neutralized current flow with uniform current density in radius, and showed that the largest current that could be enclosed giving electron drift in the direction of electrons producing the magnetic field was  $I$  (amps)  $\approx 17,000 \beta\gamma$  or  $v/\gamma \approx 1$ . Lawson (Reference 2.29) generalized this result to include space charge effects and obtained that uniform beam propagation required

$$\frac{2v}{\beta^2 \gamma} \left( f_e - \frac{1}{\gamma^2} \right) \lesssim 1 \quad (2.85)$$

If  $f_e \approx 1$ ,  $v/\gamma \lesssim 1/2$ , which is equivalent to the condition that the Larmor radius of gyration at the beam edge in the self field is equal to  $a/2$ . These propagation limits are independent of the beam radius.

If we are to propagate larger currents than  $I_A = 17,000 \beta\gamma$  it is clear that the current density cannot be uniform beyond a certain radius. Alfven also considered currents due to  $\nabla \vec{B}$  drifts outside the uniform current beam and found that the total current passable through a plane perpendicular to the  $z$  axis is

$$I(r) < I_A (r/a), \quad r > a \quad (2.86)$$

Thus, the current density outside the direct beam must be  $\propto 1/r$ .

Several authors have looked at self-consistent, beam orbit-EM theory to discover steady state configurations allowing  $I > I_c$  to flow within a fixed radius. Their approaches are

essentially similar--an electron distribution function,  $f_0$ , is assumed having a specified functional dependence upon the constants of motion. All quantities vary only with radius (parapotential flow).

Bennett Pinch (Reference 2.32). Bennett derived a self-consistent distribution for an electron beam moving through a counterstreaming ion distribution. He assumed charge neutralization in the center of mass ( $\approx$  ion stream) system, and obtained the relation

$$[I \text{ (stat amps)}]^2 = 2 N k (T_e + T_i) c^2 \quad (2.87)$$

where  $T_e$  ( $T_i$ ) are the transverse electron (ion) temperatures (eV),  $N$  is the number of electrons/cm, and  $k$  is the Boltzmann constant (ergs/eV). Although his model is collisionless, he used the concept of transverse temperature. The particles drift with constant  $z$  velocity and the density varies with radius as

$$n(r) = \frac{n_0}{(1 + n_0 b r^2)^2} \quad (2.88)$$

$n_0$  = density on axis

$$b = \frac{\pi e^2 \beta_L^2}{2k (T_e + T_i)}$$

It is interesting to note that Equation (2.87) is a condition for equilibrium of beam electrons moving through a neutralizing ion background having no  $z$  velocity in the Lawson uniform current density model (Reference 2.29). As discussed previously, Lawson's work is restricted to  $v/\gamma \ll 1/2$ , or equivalently,

$$\frac{\langle \beta_t^2 \rangle}{\beta^2} \ll 1$$

The equivalence requires the correspondence

$$\frac{\gamma}{2} m_o \langle \beta_{te}^2 \rangle c^2 + \frac{1}{2} m_i \langle \beta_{ti}^2 \rangle c^2 + kT_e + kT_i$$

One can also derive the Bennett distribution from MHD theory, as is done in many plasma physics books. Then  $\beta_L c$  is the (constant) fluid drift velocity and  $\langle \beta_t^2 \rangle / \langle \beta_L^2 \rangle \gg 1$ , or  $v/\gamma \gg 1$ .

Hollow Beam Equilibria. Benford, Book, and Sudan (Reference 2.33) have expanded upon Bennett's work, and obtained other solutions using essentially the same distribution function that Bennett used. They assume

$$f_o \propto \exp \left( -\frac{a}{c} H + \alpha P_z \right)$$

$$H = c \left( p^2 + m^2 c^2 \right)^{1/2} - e\phi$$

$$P_z = p_z - \frac{e}{c} A_z$$

$p$  = total particle momentum

$\phi$  = electrostatic potential

$A_z$  = z component of vector potential

$a, \alpha$  = parameters ( $\alpha < a$ )

Their form for  $n(r)$  is

$$n(r) \propto \frac{1}{r^2} \left[ \left( \frac{r}{L} \right)^\eta + \left( \frac{r}{L} \right)^{-\eta} \right]^{-2} \quad (2.89)$$

$\eta$  is an arbitrary positive number and  $L$  is a scale length. Bennett's solution corresponds to  $\eta = 1$ . The particle and current densities diverge at  $r > 0$  when  $\eta < 1$ , and  $\eta > 1$  corresponds to hollowed-out density distributions. An interesting feature of these equilibria is that the space charge

neutralized flow condition with  $\eta > 1$  requires a line current flowing on axis in the opposite direction to the beam current. This backstreaming current is zero for the Bennett case ( $\eta = 1$ ). (cf., the bias current in the parapotential diode model of Section 2.1.)

Another hollow beam equilibrium solution has been derived by Hammer and Rostoker (Reference 2.34). They assume

$$f_0 \propto \delta(H - \epsilon_e) \delta(P_z - \gamma m_0 V_z)$$

with

$$\epsilon_e = \frac{\gamma m_0}{2} v_1^2 - e [\phi(r) - \beta_z A_z]$$

$\beta_z c = V_z$  = an average longitudinal electron velocity, and obtain a solution with most of the current flowing in a thin shell of thickness  $c/\omega_p$ , the electrical skin depth. The beam plasma frequency is  $\omega_p$ . If  $v/\gamma \gg 1$ ,  $I = \sqrt{v/\gamma_0} I_A$ ,  $\gamma_0$  is a relativistic factor at  $r = 0$ . In the Lawson model the propagation limit was  $v/\gamma \sim 1/2$ , which meant physically that the Larmor radius at the beam edge was equal to one-half the beam radius. The HR model has currents confined mostly to a shell of thickness  $c/\omega_p \ll$  outer beam radius. One would therefore expect that a much higher magnetic field could exist before electrons were turned around with radius  $c/2\omega_p$ .

Yoshikawa Model. A beam model allowing arbitrarily high current propagation for neutralized beams has recently been proposed by Yoshikawa (Reference 2.35). The essential feature of this model is that the beam has a macroscopic theta current generating a self-consistent z component of the magnetic field.

An interesting feature of the equilibrium is that electrons move almost parallel to the field lines, so their motion is nearly force-free. The charge density is taken uniform in radius for moderately relativistic beam energies. It is not apparent to this author how one would prepare Yoshikawa's equilibrium. Spontaneous evolution of a high  $v/\gamma$  beam to a state with macroscopic theta currents seems highly unlikely.

2.7.4 Steady State Flow with External  $B_z$  Fields. Steady state, parapotential flow in the presence of  $B_z$  fields has been extensively studied by high power electron gun designers. Their analysis usually proceeds from the assumptions of laminar flow, radial force balance, energy conservation, and conservation of canonical angular momentum in axisymmetric systems. (Also, paraxial ray equation analysis has been used.) Many flow modes have been investigated, falling mainly into two classes, isorotational or rigid rotor beams, and isovelocity or uniform longitudinal velocity in radius beams. Reference 2.1, e.g., contains a detailed discussion of these analyses.

We consider here only a few special cases of  $B_z$  flow. Assuming laminar flow, uniform current and charge densities, and that  $\beta_t \ll \beta_L$ , the radial envelope equation of motion is

$$\frac{d^2 a}{dz^2} = \frac{2v}{\gamma\beta_L^2} \left(1 - f_e - \beta_L^2\right) \frac{1}{a} - a \left(\frac{\omega_L}{\beta_L c}\right)^2 \left[1 - \left(\frac{\phi_0}{\pi a^2 B_z}\right)^2\right] \quad (2.90)$$

where  $\omega_L \equiv$  Larmor frequency = 1/2 cyclotron frequency

$$= \frac{eB_z}{2\gamma m_0 c}$$

$$\phi_0 = 2\pi \int B_z(r', z_0) r' dr' = B_z(z_0) \pi r_0^2 = \text{flux enclosed at "birthplace" of electron now at } a, z.$$

In deriving Equation (2.90) we have used Busch's theorem and assumed  $B_z$  uniform in radius, i.e., negligible beam diamagnetism. In an azimuthally symmetric system, the canonical angular momentum is constant:

$$\gamma m_0 r^2 \dot{\theta} - \frac{e}{c} r A_\theta = \text{constant}, \quad (2.91)$$

$A_\theta$  = theta component of  
vector potential

If  $\dot{\theta} = \omega = 0$  where the electrons are born, and the electrons rotate about the system axis,

$$\omega = \frac{e}{2\pi\gamma m_0 c r^2} \left[ \phi(r) - \phi(r_0) \right] \quad (2.92)$$

Busch's theorem

If  $B_z$  is constant in radius, Equation (2.91) is

$$\begin{aligned} \omega(r) &= \frac{eB_z}{2\gamma m_0 c} \left[ 1 - \left( \frac{r_0}{r} \right)^2 \right] \\ &= \omega_L \left[ 1 - \left( \frac{r_0}{r} \right)^2 \right] \end{aligned} \quad (2.93)$$

The only case of Equation (2.90) we consider is that of solid beam Brillouin flow, which requires  $\phi_0 = 0$ , or that the diode is magnetically shielded. Setting  $d^2 a/dz^2 = 0$  and  $f_e = 0$  gives

$$\omega_L^2 = \frac{2}{\gamma^3} \frac{c^2}{a_0^2} \quad (2.94)$$

and from Equation (2.92), the flow is isorotational. Using radial force balance, and energy conservation, one can easily demonstrate that the flow is also exactly isovelocity. The

practical importance of this flow stems from the above remarks, from the uniform charge density and from the relatively modest  $B_z$  fields required. The perveance

$$\frac{I \text{ (amperes)}}{V \text{ (volts)}^{3/2}}$$

$V$  = potential at the beam edge, is relatively low from the point of view of intense beam physics, however. Non-relativistically, the maximum current flow condition is

$$I \text{ (amps)} \approx 25 \times 10^{-6} V^{3/2} \quad (2.95)$$

Relativistic Brillouin flow has a lower perveance. Neugebauer (Reference 2.36) discusses relativistic Brillouin flow in detail and his calculations show, e.g., that a 720 kA beam with 1 cm radius would only require a  $B_z$  field approximately 3 kilogauss but the potential depression over the beam radius would be ~68 MeV!

If the cathode is immersed in the magnetic field, the flow is no longer isorotational [see Equation (2.93)] and we have the case of hollow beam Brillouin flow; a lower perveance flow than the solid beam case.

A finite beam emittance can be included in the envelope equation following Garren's derivation of the K&V equation. We treat the  $v_\theta B_z$  force term as a linear external focusing force, thereby restricting ourselves to  $\phi_0 = 0$ :

$$\frac{d^2 a}{dz^2} = \frac{2v}{\beta_L^2 \gamma} \left( 1 - f_e - \beta_L^2 \right) \frac{1}{a} - \left( \frac{\omega_L}{\beta_L c} \right)^2 a + \frac{\epsilon^2}{a^3} \quad (2.96)$$

If  $\frac{d^2 a}{dz^2} = 0$ , we obtain for non laminar, but paraxial flow,

$$\omega_L^2 = \frac{\beta_L^2 c^2}{a_0^2} \left[ \frac{2v}{\gamma^2 \beta_L^2} (1 - f_e - \beta_L^2) + \frac{\epsilon^2}{a_0^2} \right] \quad (2.97)$$

The flow is no longer exactly isovelocity.

The above equations all assumed electron rotation about the system axis. If the electron motion is that of a guiding center rotation about the axis, plus a fast cyclotron gyration about the guiding center, it is most convenient to work in rectangular coordinates. Andrews, et al., (Reference 2.37) have considered a non-diamagnetic or paramagnetic uniform beam case with  $\beta_t \ll \beta_L$ , using the two-mass approximation (longitudinal electron mass  $\approx \gamma^3 m_0$ , transverse  $\approx \gamma m_0$ ). The equations of motion are

$$\begin{aligned} \ddot{x} &= -\Omega^2 x + \omega_c \dot{y} \\ \ddot{y} &= -\Omega^2 y - \omega_c \dot{x} \\ \ddot{z} &= \frac{e}{\gamma_L^3 m_0 c} \frac{dA_z}{dt} \approx 0 \end{aligned} \quad (2.98)$$

where  $\Omega^2 = \frac{2v}{\gamma_L} \left(\frac{c}{a}\right)^2 (\beta_L^2 + f_e - 1)$

$\omega_c =$  cyclotron frequency  $= e \frac{B_z}{\gamma_L m_0 c}$

$\gamma_L = 1/\sqrt{1 - \beta_L^2}$

$\beta_L c =$  average longitudinal velocity

The last equation in Equation (2.98) follows from the assumption that  $\beta_t/\beta_L \ll 1$ . A priori, one expects  $\ddot{z} \approx 0$  from the two mass approximation when  $v/\gamma_L \ll 1$ . They show, moreover, an a posteriori justification even when  $v/\gamma \gg 1$  with sufficiently high  $B_z$  fields. By defining  $\xi = x + iy$ , Andrews, et al. combine Equations (2.98) into

$$\xi' - i\omega_c \xi' + \Omega^2 \xi = 0 \quad (2.99)$$

which has a solution of the form

$$\left. \begin{aligned} \xi &= A_+ \exp(i\omega_+ t) + A_- \exp(i\omega_- t) \\ \omega_{\pm} &= \frac{\omega_c}{2} \left\{ 1 \pm \left[ 1 + \left( \frac{2\Omega}{\omega_c} \right)^2 \right]^{1/2} \right\} \end{aligned} \right\} \quad (2.100)$$

Several flow properties follow from Equation (2.99).<sup>\*</sup> If

$$\frac{2\Omega}{\omega_c} < 1$$

the solutions are sinusoidal no matter what  $f_e$  is. When  $\omega_c \gg 2|\Omega|$ ,

$$\begin{aligned} \omega_+ &\approx \omega_c \\ \omega_- &\approx \frac{\Omega^2}{\omega_c} \end{aligned} \quad (2.101)$$

and the solution consists of a fast gyration of frequency  $\omega_c$  about the guiding center that precesses with frequency  $-\Omega^2/\omega_c$ . The sign of  $\Omega^2$  affects the direction of precession. Thus, the particles move at approximately constant radius,  $r_0$ , varying only by the gyroradius  $r_0 (\Omega/\omega_c)^2$ . The flow is consistent with their approximations if

<sup>\*</sup>The solid Brillouin beam case [ $f_e \approx 0$ ,  $\beta_L^2 \ll 1$  (or neglect of  $B_\theta$ )] corresponds to  $\Omega^2/\omega_c = -\omega_c/4$ .

$$\frac{2B_{\theta}(a)}{B_z \beta_L^2} \left| \beta_L^2 + f_e - 1 \right| \ll 1 \quad (2.102)$$

where  $B_{\theta}(a)$  is the beam self-field at the beam edge. Thus, if  $B_z \gg B_{\theta}(a)$ , the flow is predominantly streaming ( $\beta_t/\beta_L \ll 1$ ), no matter what the values of  $f_e$  and  $v/\gamma$  are.\*

Finally, we call attention to some recent work by Toepfer (Reference 2.38) who uses the relativistic fluid equations for electron beam motion. He considers examples of rigid rotor steady state beam flow allowing diamagnetic effects and finite temperature, and gives several numerical plots of radial current profiles.

2.7.5 High  $v/\gamma$  Propagation with Intense Pulsed Beams. All of the high  $v/\gamma$  beam flow modes discussed above were steady state flow and did not consider  $E_z$ . Even if  $E_z$  effects are negligible, it is most certainly likely that the relevance to experimental beam propagation would strongly depend on the preparation of the beam, i.e., the flow generated in the diode. Also, of course, one needs to consider the stability of the various models.

In practical beam transport problems with pulsed beams one has to operate at neutral gas pressures giving good current neutralization, or inject into a preformed plasma, in order to minimize energy loss from beam-generated EM fields. Thus, we are in a regime where the  $E_z$  driving current neutralization is essential and, in principle, the steady state flow patterns would not be relevant until the plasma return currents have died away. These times are in the microsecond regime--much longer than the beam pulse width. When substantial plasma return

\* We also note that the model solutions correspond to force-free electron motion ( $\vec{j} \times \vec{B} = 0$ ).

currents do exist, the  $B_0(r)$  distribution is that of a current sheath around the edge of the beam, a distribution somewhat similar, but not identical, to the hollow beam modes. So, no matter how we prepare the beam in the diode, we would further have to consider evolution through a plasma return current stage to determine and justify a relevant steady state flow pattern for pulsed beams.

We might guess that a beam with plasma return currents will have a  $B_0(r)$  field similar to the hollow beam equilibria with  $f_e \approx 1$  as we have just mentioned. Then, one would not expect a dynamical or orbit limitation on the net  $v/\gamma$ ; i.e.,  $v_{net}/\gamma$  can exceed unity. However, as mentioned in Section 1, the EM limitation on propagation would still "hurt." When  $v_{net}/\gamma > 1$ , the EM field energy/particle exceeds the kinetic energy/particle, or equivalently, beams can lose all their energy over distance of the order of a few beam radii. A simple calculation illustrates this point.

Let us consider a beam injected into a plasma tube with a conductivity low enough that the inductive field of the beam drives a return current giving  $v_{net}/\gamma > 1$ , and take  $f_e = 1$ . In order to propagate efficiently, the power input to the beam-chamber system expended by the beam in setting up the magnetic field associated with  $v_{net}$  must be less than "inertial" power flow of the beam. The power input to the magnetic field is

$$\approx \frac{I_n^2}{c^2} \ln(R/a) \beta c$$

and we must have

$$(\gamma - 1) m_0 c^2 N \beta c \geq \frac{I_n^2}{c^2} \ln (R/a) \beta c, \quad a < R \quad (2.103)$$

where  $N$  = number of beam particles/length =  $v/r_0$   
 $r_0$  = classical electron radius  
 $R$  = chamber radius

in order to avoid substantial beam distortion. Rewriting Equation (2.103) we obtain

$$(\gamma - 1) v \geq v_{net}^2 \beta^2 \ln (R/a)$$

or

$$\left(\frac{v_{net}}{\gamma}\right)^2 < \left(\frac{v}{\gamma + 1}\right) \frac{1}{\ln (R/a)} \quad (2.104)$$

If  $v_{net}/\gamma > 1$ ,  $v/\gamma > 1$ , and with  $\ln (R/a) \sim 1$ , the EM criterion is violated.

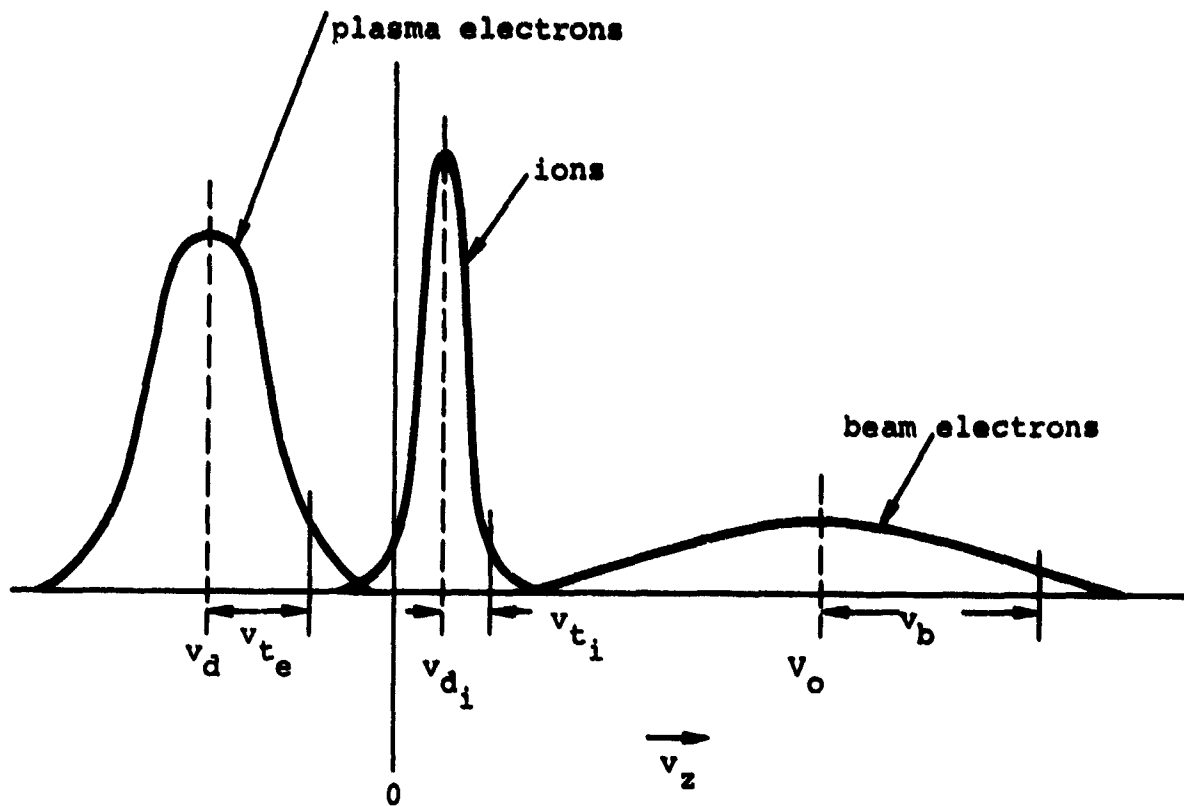
These considerations led the author to suggest that the relevant restriction for practical high  $v/\gamma$  beam transport with pulsed intense beams is  $v_{net}/\gamma \ll 1$  (Reference 2.13). The low pressure beam propagation experiments of Graybill and Nablo (Reference 2.39) have shown beam stopping when  $v_{net}/\gamma \approx v/\gamma \sim 1/2$ . Current neutralization was negligible in these experiments. Yonas and Spence (Reference 2.23) have propagated beams with  $v_{net}/\gamma \ll 1/2$ , but with  $v/\gamma \approx 4-5$  over meter distances.

## 2.8 SOME TOPICS IN BEAM STABILITY

Current interest in beam plasma stability (or instability) focuses in two directions. Efficient beam transport clearly requires a stable beam, whereas plasma heating is enhanced with a weakly-turbulent beam plasma system. We discuss three types of beam plasma instabilities: (1) longitudinal electrostatic, (2) transverse (hose, kink), and (3) filamentation or fluting modes. The transverse hose instability seems to be the most serious for high current beam neutral gas propagation, and the fluting modes for transport with  $B_z$  fields. When considering neutral gas stability we have to recognize that the nature of the beam-generated plasma may change markedly during the pulse, evolving from an unionized gas to an ion-electron plasma ( $t < \tau_N$ ) to a highly ionized few electron volt temperature plasma after breakdown.

2.8.1 Longitudinal Electrostatic (ES) Instabilities. Our discussion will consider the case of a pulsed beam plasma system after gas breakdown, or injection into a preformed plasma. Only linearized theory will be covered, implying that plasma instability wave growth is sufficiently damped by collisions or Landau damping to avoid non-linear regimes and strong particle-wave trapping.

A typical ordering of beam plasma component longitudinal velocity distributions (not to scale) is shown in Figure 2.23. The system is a "hot beam, cold plasma" configuration with the plasma return current flowing oppositely to the beam electrons. The ion drift velocity and thermal speed are negligible compared to the plasma electron quantities. ES instability theory considers two types of instabilities, electron-ion (e-i) relevant



- $v_d$  = drift velocity of plasma electrons
- $v_{d_i}$  = drift velocity of plasma ions
- $v_0$  = average longitudinal beam velocity
- $v_b$  = rms longitudinal velocity spread of beam electrons
- $v_{t_e}$  = thermal velocity of plasma electrons
- $v_{t_i}$  = thermal velocity of plasma ions

Figure 2.23 A sketch of beam-plasma system longitudinal velocity distributions

to interactions between the plasma return current electrons and ions, and electron-electron (e-e) relevant to interactions between beam electrons and plasma electrons. Interactions between beam electrons and plasma ions have a slower growth rate than the e-e mode.

Electron-Ion Modes. The two e-i modes are the ion acoustic (Reference 2.40) and the Buneman mode (Reference 2.41).

Ion-Acoustic (I-A). ( $v_{ti} < v_d < v_{te}$ )

$$\text{Re}\omega \sim 0.1 \left( \frac{m_o}{m_i} \right)^{1/2} \omega_p$$

$$\text{Im}\omega \sim 0.1 \left( \frac{m_o}{m_i} \right)^{1/2} \omega_p \quad (2.105)$$

$$k \equiv 2\pi/\lambda \approx \frac{\omega_p}{2v_d}$$

$\omega_p$  = electron plasma frequency =  $4\pi n_p e^2/m_o$

$n_p$  = plasma electron density

$m_i$  = ion mass

$m_o$  = electron rest mass

$\text{Re}\omega$  = frequency of fastest growing mode

$\text{Im}\omega$  = e-folding growth rate of fastest growing mode

$k$  = wave number of fastest growing mode =  $2\pi/\lambda$

Buneman. ( $v_{te} \gtrsim v_d$ )

$$\text{Re}\omega \sim 0.1 \left( \frac{m_0}{m_i} \right)^{1/3} \omega_p$$

$$\text{Im}\omega \sim 0.1 \left( \frac{m_0}{m_i} \right)^{1/3} \omega_p \quad (2.106)$$

$$k \sim \frac{\omega_p}{v_d}$$

IA waves are essentially due to induced Cerenkov emission from drifting electrons when  $v_d$  exceeds the ion sound speed ( $\approx v_{ti}$ ) and the Buneman instability is an electron-ion counter-streaming mode. The effect of collisions on these modes has recently been considered by Guillory and Benford (Reference 2.42), assuming a Lorentzian electron distribution. Their conclusion is that collisions are unimportant when  $v_{te}/v_d \gtrsim 0.1$ .

Electron-Electron Modes. These modes were first studied by Bludman, Watson, and Rosenbluth (Reference 2.43), who considered only the cold-beam case in the so-called weak-beam approximation ( $n_b/\gamma n_p \ll 1$ ,  $n_b$  is the beam particle density). Their theory assumes a steady state uniform beam in mechanical equilibrium with the plasma.  $E_z$  is zero in zero order so no plasma currents are assumed to be flowing. The plasma is further assumed to be infinite in extent (as it is in the electron-ion mode theory). This approximation is usually not bad since the instability wavelengths are small. A nice discussion of the physics of these modes is given by Lewis (Reference 2.44), and the influence of a beam velocity spread (warm beam) on wave growth is considered in

detail by Bohmer, Chang, and Raether (Reference 2.45), using a Lorentzian beam distribution function.

(i) Cold Beam. Quantitatively defining a cold beam requires a statement about collisional effects. Ascoli (Reference 2.46) gives

$$\frac{v_b}{v_0} < 0.76 \alpha \left( \frac{\omega_p}{v} \right) \quad (2.107)$$

where  $\alpha \equiv \frac{n_b}{\gamma n_p} < 1$ . The numerical calculations of Singhaus (Reference 2.47) show that

$$\left( \frac{v_b}{v_0} \right)^2 < (0.7 \alpha \omega_p / v)^2 \quad (2.108)$$

We define the cold beam limit as the case when Equation (2.108) is satisfied and additionally require that  $v_b/v_0 < \alpha^{1/3}$ .

There are several sub cases within this limit that we now consider.

High-Frequency, Collisionless. ( $k \sim \omega_p/v_0$ ,  $\nu < \text{Im}\omega$ )

$$\begin{aligned} \text{Re}\omega &\sim \omega_p \\ \text{Im}\omega &\sim (\alpha/2)^{1/3} \omega_p \end{aligned} \quad (2.109)$$

High-Frequency, Collisional. ( $k \sim \omega_p/v_0$ ,  $\nu > \text{Im}\omega$ )

$$\begin{aligned} \text{Re}\omega &\sim \omega_p \\ \text{Im} &\sim (\alpha/2\nu)^{1/2} \omega_p^{3/2} \end{aligned} \quad (2.110)$$

Low-Frequency, Collisionless. ( $kV_0 < \omega_p, \text{Im}\omega > \nu$ )

$$\text{Im}\omega = \text{Im}\omega(k) = \alpha^{1/2} kV_0 \quad (2.111)$$

Low-Frequency, Collisional. ( $kV_0 < \omega_p, \nu > \text{Im}\omega$ )

$$\text{Im}\omega = \text{Im}\omega(k) = \omega_p \left( \frac{\alpha \nu kV_0}{2} \right)^{1/2} \quad (2.112)$$

The high frequency modes have a reduced growth rate with large collision frequency whereas the low frequency growth rate is enhanced by collisions.

(ii) Warm Beam. Collisions never completely suppress the instability in the cold beam case but in the warm beam case they may. The warm beam growth occurs within the Singhaus criterion, and with  $(v_b/V_0) \geq \alpha^{1/3}$ . The instability growth is now dependent on beam momentum spread and is "kinetic," rather than "hydrodynamic" as in the cold beam case. The growth rate for fastest growth ( $V_0 k \sim \omega_p$ ) is

$$\text{Im}\omega \cong 0.3 \alpha \left( \frac{V_0}{v_b} \right)^2 \omega_p - \nu_c/2 \quad (2.113)$$

and  $\text{Re}\omega \approx \omega_p$

The modes are stable when the Singhaus criterion (Equation 2.108) is violated:

$$\left( \frac{v_b}{V_0} \right) > \left[ 0.7 \alpha \frac{\omega_p}{\nu} \right]^{1/2} \quad (\text{stable modes}) \quad (2.114)$$

The Singhaus criterion has been experimentally checked by Bohmer, Chang, and Raether (Reference 2.45) using low current beams ( $\sim 400$  mA). They found instability quenching as predicted by the Singhaus criterion. The criterion, if anything, is conservative.

### 2.8.2 Beam Propagation and Longitudinal ES Instabilities.

The growth rates, oscillation frequencies, and wavelengths for fastest growth of ES instabilities have been summarized for various orderings of beam and plasma parameters. We now determine conditions for stable propagation of intense beams. To attain stability of e-e modes, we desired to satisfy Equation (2.114), the Singhaus criterion. Stability requires

$$\frac{0.7 \alpha \omega_p}{v} < \left( \frac{v_b}{v_o} \right)^2$$

Using  $v = v_{e,1} \approx 6 \times 10^{-5} n_p [T_e (\text{eV})]^{-3/2}$  from Equation (2.61) ( $Z=1$ ), we can rewrite the above equations as

$$\left( \frac{n_b}{\gamma n_p} \right) \left( \frac{T_e}{n_p} \right)^{3/2} < 10^{-9} \left( \frac{v_b}{v_o} \right)^2 \quad (\text{e-e stability}) \quad (2.115)$$

with  $n_b/\gamma n_p \ll 1$  (weak beam requirement).

If we take  $v_b/v_o \sim 1$  (hot beam), beam energy 1 MeV ( $\gamma = 3$ ) and current density  $\sim 10^4$  A/cm<sup>2</sup>,  $n_b \approx 2 \times 10^{12}$  electrons/cm<sup>3</sup>, Equation (2.115) says that stability requires  $T_e$  (volts)  $\lesssim 10^{-14} n_p$  (cm<sup>-3</sup>). Efficient beam propagation occurs in the 0.1 to 1 torr range, so if we take  $n_p = 3.5 \times 10^{15}$ /cm<sup>3</sup>,  $T_e \lesssim 35$  volts.

Stability of e-i modes for the plasma return current is equivalent to requiring

$$v_d < v_{te} \left( E < E_c = \frac{2 \times 10^{-12}}{T_e} z n_p \right) \quad (2.116)$$

and, since  $v_d$  may exceed  $v_{ti}$ , ion-acoustic modes must not significantly affect the plasma conductivity. This requirement translates into  $v_{e,i} > \text{Im}(\omega)$  for ion-acoustic modes, or from Equation (2.105)

$$n_p > 4 \times 10^{10} T_e^3 \quad (\text{insignificant I-A effects}) \quad (2.117)$$

for a hydrogen plasma. If  $T_e \lesssim 10$  volts,  $n_p > 4 \times 10^{13}/\text{cm}^3$ , or  $P \gtrsim 0.1$  torr. Using these parameters in Equation (2.116), the  $E_z$  field driving plasma return currents should be less than 700 V/cm.

**2.8.3 Transverse Instabilities--The Frozen Hose Instability.** \* Several authors have recognized that beam instability against transverse bending (hose, kink) may be a serious threat to overall beam stability (Reference 2.48); experimental experience tends to confirm their predictions. Important transverse forces giving rise to instability development are: (a) the attractive electric polarization forces acting between the ion and electron streams, (b) magnetic interstream forces, (c) image focusing forces from the presence of conducting pipes, and (d) a velocity dependent drag force arising from the resistance of the beam-generated plasma to motion of magnetic lines of

\* This material contains the work reported in S. Putnam, Transverse Instabilities of Intense, Relativistic Pinched Electron Beams, PIIR-7-68, Physics International Company, San Leandro, Ca., March 1968.

force as the beam undergoes displacement. When the angular frequency of the perturbation is much less than the plasma conductivity,  $\sigma(\text{sec}^{-1})$ , or when the skin depth,  $s$ , of the magnetic field penetration of the plasma is of the order of a few beam radii or less, we adopt the conventional terminology and refer to the instability as resistive.\* The increasing gas conductivity induced by the rising beam current suggests that a non-resistive behavior may rapidly develop into a resistive mode, particularly if the gas breaks down. Existing theory considers only steady state beams with constant plasma conductivity and no net plasma return currents. More detailed interpretations of the experiments thus require further theoretical work.

Figure 2.24 shows a schematic diagram of the experimental setup to investigate transverse beam instabilities in the low pressure pinched beam mode P( $\sim 0.1$  torr).\*\* The drift chamber was 50-cm long and 25 cm in radius. The electron stream was injected through a 1 mil-aluminum anode window into the electron beam chamber, where the gas (air) pressure was held at 0.1 torr for most runs. Aluminum screen tubes of various radii,  $R$ , were also positioned within the large drift chamber in order to observe the effects of conducting pipes on the pinched beam oscillations. The electron beam was stopped in a graphite calorimeter array placed at the end of the screen tube. The calorimeter array consisted of 25 small blocks covering an area one inch square. Two 90 degree stereo time-integrated photographs were taken of the light emitted from the beam path by the

---

\* Alternatively, the low frequency hose instability limit is defined as  $s(\omega) > \text{beam radius}$ .

\*\* The experimental measurements described here were performed by G. L. Hatch, W. T. Link, J. Murray, and H. F. Ruge.

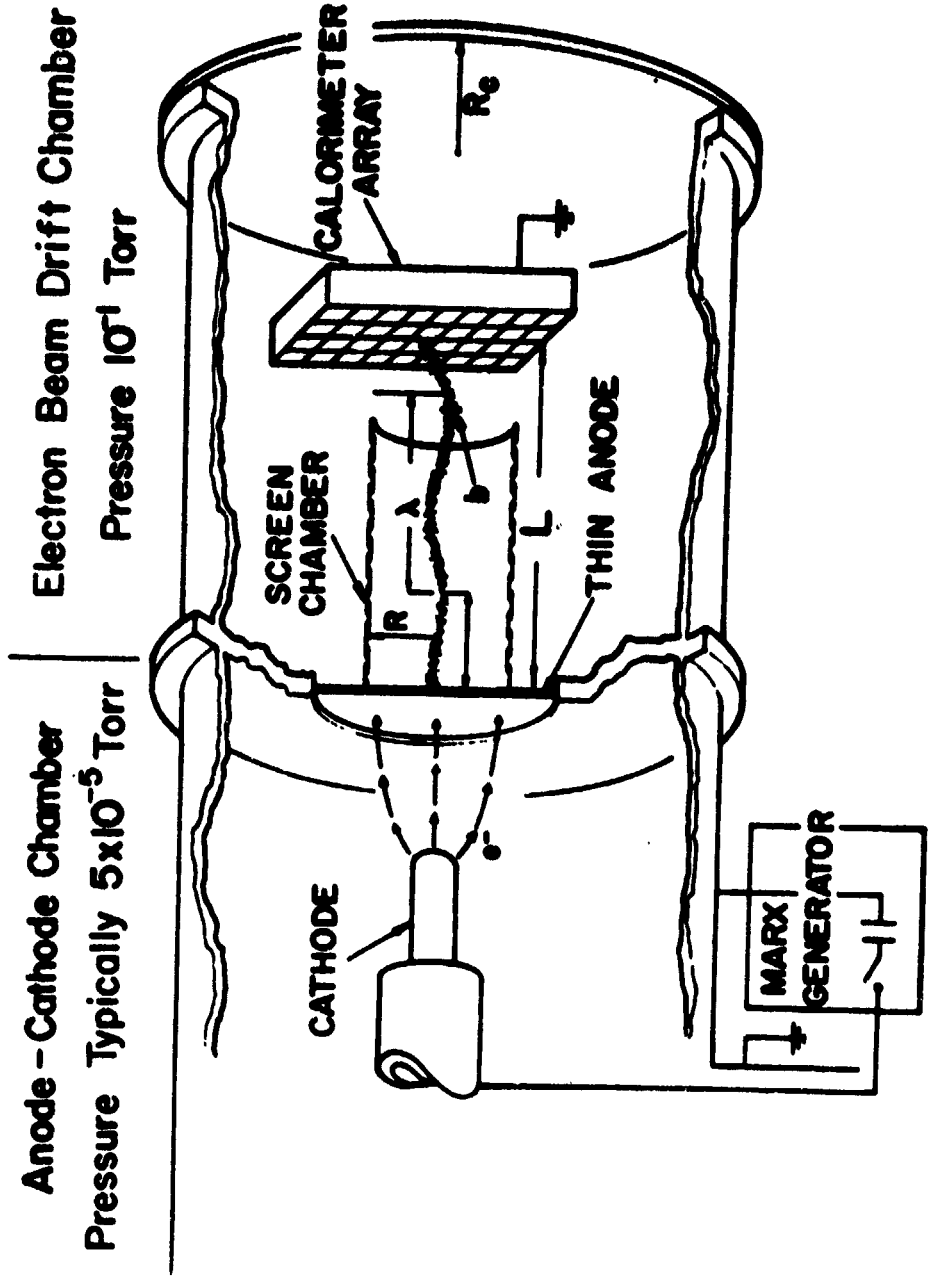


Figure 2.24 Experimental test setup.

line and recombination radiation of the beam-generated plasma. In all cases, the photographs and calorimeter data agreed regarding beam position. The wavelength of the oscillation in the pinched beam was measured from the stereo photographs and the relativistic electron current in the pinch was determined from the calorimetry data in the one inch graphite array.

A typical hose-like beam instability at 0.1 torr is shown in Figure 2.25. A suggestive interpretation is that the instability develops during the early portion of the risetime of the beam current when  $\sigma \lesssim 10^{10} - 10^{11}/\text{sec}$ ,  $s > b/2$ , and non-resistive instability mechanisms predominate. When the conductivity of the background gas rapidly increases at breakdown, the plasma damps the motion or, in other words, lowers the oscillation frequency and increases the growth time, so that the hose appears "frozen" over the intense plasma radiation times ( $\sim$  a few beam pulse widths).



0.1 Torr

4718 S

Figure 2.25 "Frozen hose" instability of a pinched beam.

Rather idealized theoretical models (Reference 2.49), for non-resistive growth predict the wavelength of the fastest growing transverse oscillation modes;  $\lambda_{inst}$ :

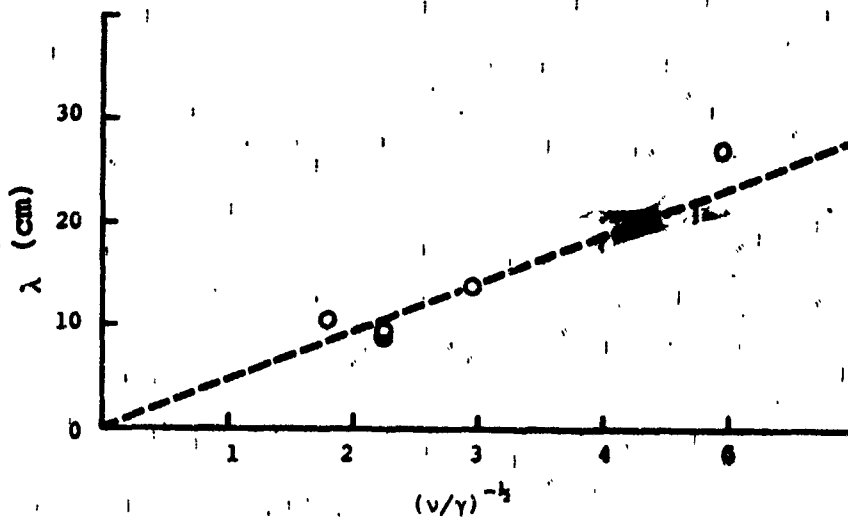
$$\lambda_{inst} \approx \frac{\pi}{\sqrt{2}} \left(\frac{v}{\gamma}\right)^{-\frac{1}{2}} d, \quad d \ll D \quad (2.118)$$

$$\approx \frac{\sqrt{\pi}}{2} \left(\frac{v}{\gamma}\right)^{-\frac{1}{2}} D, \quad d \sim D$$

where  $d(D)$  is the beam (chamber) diameter. Figure 2.26 and 2.27 show experimentally measured wavelengths, showing reasonable agreement with Equation (2.118). After gas breakdown, resistive mode theory (Reference 2.50) suggests a growth rate  $\approx (t_d)^{-1}$  where  $t_d$  is the magnetic diffusion time (Equation 2.65). For  $\sigma \gtrsim 10^{13}/\text{sec}$ ,  $t_d \gtrsim 100$  nsec, and the beam path developed in the non-resistive mode thus appears "frozen" over times of the order of the beam pulse.

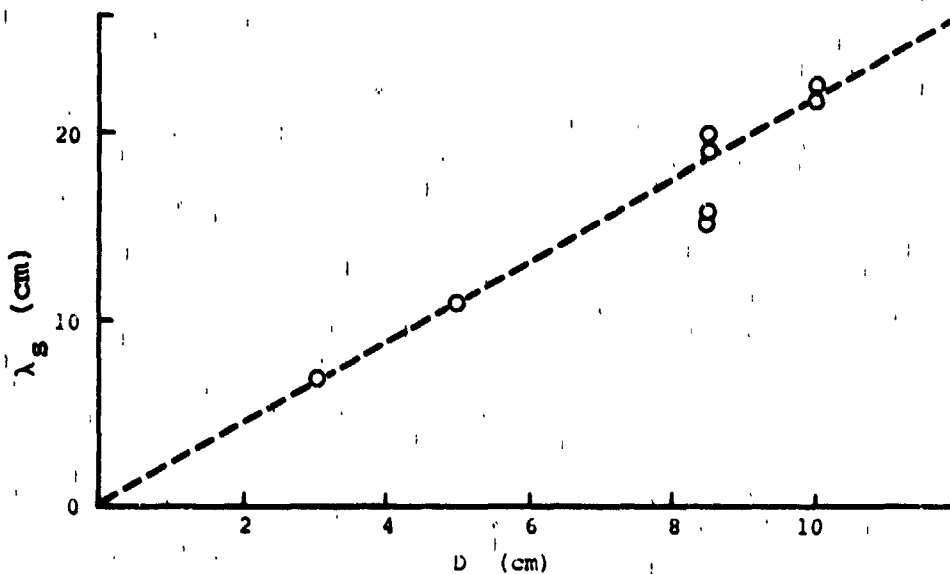
To summarize, a procedure is outlined to estimate instability wavelengths for the low pressure case ( $t_B < t_p$ , the beam pulse width):

- From the charge production rules given in Section 2.42 the gas breakdown time at the pressure of interest can be calculated, and the beam current at breakdown time determined.
- The instability wavelength may be estimated by using the breakdown current value to determine  $v$  in Equation (2.118).
- A qualitative estimate of the "amplitude" of the instability growth can be made from the time of breakdown. Earlier breakdown and lower net currents mean smaller amplitudes. Figure 2.27 shows a pinched beam case where  $t_B > t_r$ .



The values of  $v/\gamma$  are approximate and are obtained from multiple calorimetry. The beam kinetic energy is approximately 3 MeV, the chamber pressure 100  $\mu$ , and  $d = 2$  cm.

Figure 2.26a Instability wavelength as a function of  $(v/\gamma)^{-1/2}$ ,  $d < D$ .



$v/\gamma$  is assumed to have the approximately constant value 0.3. The kinetic energy is approximately 3 MeV, the chamber pressure 100  $\mu$ .

Figure 2.26b Instability wavelength in guide tube.



Figure 2.27 Transverse instability of a highly pinched beam where  $t_p \sim t_p > t_r$ . Beam parameters: pressure 0.01 torr; beam current 25 kA; average kinetic energy  $\sim 3$  MeV; current risetime  $\sim 10$  nsec.

This low pressure behavior is to be contrasted with the transversely unstable, high-pressure ( $P > \sim 100$  torr) propagation where the beam is also pinched, but appears to rapidly blow up into a smeared, filamentary structure (Figure 2.28). Although current neutralization is small for both pinched modes, the plasma conductivity is high at low pressures ( $\sigma \gtrsim 10^{13}$  to  $10^{14}$ /sec) and very low at high pressures because of the high electron plasma collision frequency. The differences in the plasma conductivity suggest markedly different growth-time regimes for transverse instabilities. Thus, as stated previously, before gas breakdown in the low pressure mode, the instability is non-resistive, and, after breakdown, resistive. In the high pressure case, a nonresistive mode would apply throughout the beam pulse.

Reproduced from  
best available copy.



760Torr

4734 B

Figure 2.28 Transverse instability of high pressure pinched beam

2.8.4 Fluting and Filamentation Modes. Recent work with beam propagation in  $B_z$  fields has demonstrated existence of fluting and filamentation instabilities (Hammer, Reference 2.51) and Stallings, Reference 2.52). A typical witness plate damage pattern for such a mode is shown in Figure 2.29. Hammer has considered a picture similar to the picture of the frozen-hose mode. He suggests growth of a classical flute instability (Longmire, Reference 2.53) due to inhomogeneities in the external magnetic field until gas breakdown with a growth time,  $\tau$ :

$$\tau \approx L \sqrt{\frac{\rho}{NP_{\perp}}}$$

- $\rho$  = beam-plasma mass density
- $L$  = scale length of magnetic field inhomogeneities
- $N$  = azimuthal mode number
- $P_{\perp}$  = perpendicular particle pressure

Until breakdown ( $\rho/P_{\perp}$ ) is dominated by beam parameters, and after breakdown, the ion mass dominates  $\rho$ , giving a much slower growth rate. The fluting modes have not been investigated sufficiently at this time to confirm the model. Some theoretical beam-plasma fluting and filamentation instability studies have recently been reported by Striffler and Rammash, (Reference 2.54) and G. Benford, (Reference 2.55).



Figure 2.29 Fluting instability of a hollow beam.

## 2.9 PLASMA CHANNELING

Plasma channeling is the formation of a fairly well-defined plasma region by beam electrons which has the ability to guide subsequent beam electrons along its configuration. Any intense beam will, of course, generate a plasma, but unless certain conditions are fulfilled, the plasma will not act as an effective guide for upstream beam electrons. We discuss these conditions in a simple-minded fashion drawing upon previous discussions of beam-induced plasma conductivity and transverse instabilities, and give some practical implications of plasma channeling.

In order for the plasma to be a plasma channel in our context we require that:

1. The plasma region must have a frozen-in magnetic field level at least high enough to guide beam electrons around the smallest radius of curvature of the channel configuration.
2. The channel must be stable or, from the previous discussion, on the frozen-hose instability,  $t_d \gg$  beam pulse width. These two criteria are usually achieved when the gas breakdown time,  $t_B \lesssim$  beam pulse risetime,  $t_r$ .

The experiments of Yonas, et al. (Reference 2.23) where beams were guided by copper pipes with a radius of the order of the beam radius are an example of channeling. The image forces guided the early portion of the beam around the circles when the skin depth was larger than or equal to the pipe radius. Then, when the skin depth was smaller than or equal to the pipe radius after breakdown, the plasma frozen-in magnetic field "memory" guided subsequent beam particles.

Yonas and Spence also attempted unsuccessfully to inject a beam head into a plasma channel, as indicated in Figure 2.30.

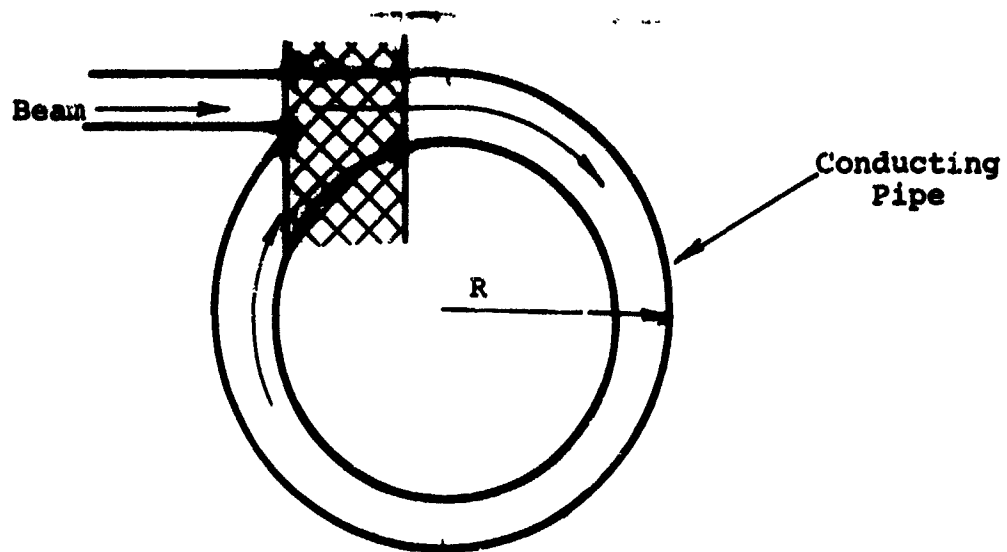


Figure 2.30 The experimental geometry for injection into a plasma channel.

An explanation of the failure is that the transit time of the beam front around the ring was too long, i.e., the gas had broken down, when the beam head reached the cross-hatched region and the highly conducting plasma reflected the beam head to the pipe wall. With the experimental parameters of  $v/\gamma \sim 1$ , current risetime  $\approx 20$  nsec, pressure 0.5 to 0.75 torr, the breakdown time was approximately 5 nsec. With a longitudinal front velocity  $\approx 0.5$  (250 keV electrons), the transit time of the front around the ring would be  $\approx 7$  nsec.

These relatively crude physical arguments would suggest that merging of the beams should be best achieved when transit time of one beam to a merger point,  $t_{tr}$ , satisfies

$$\tau_N < t_{tr} < t_B \quad (\text{beam merger criterion})$$

where  $\tau_N$  and  $t_B$  refer to the electrical neutralization time and breakdown time of the second beam at the merger point. Recall from Section 2.2 that only  $f_e > 1 - \beta_L$ , is required for magnetic interstream forces (attractive for currents flowing in the same direction) to exceed the radial electric space charge repulsion. Our merger criterion is thus conservative. Pressure in the 10 torr range would satisfy the criterion, since then  $\tau_N \approx 0$ , and the gas is not highly conducting ( $t_d \lesssim t_r$ ).

## 2.10 SUMMARY OF BEAM TRANSPORT PHENOMENOLOGY

In this section, we shall try to "pull together" the material of preceding sections and, in particular, look at conditions for high beam transport efficiency in a qualitative, but coupled fashion. Generally speaking, efficient beam transport requires:

1. The beam generated EM fields to be minimized (charge and current neutralization),
2. The beam transverse momentum to be contained to prevent particle loss to the walls (beam self magnetic fields or external fields),
3. Stable modes (velocity spreads in beam and appropriate plasma parameters).

The EM fields are minimized with neutral gas injection by breaking the gas down early in the beam pulse to obtain good current neutralization. This process is lossy for  $v/\gamma \gtrsim 1$  beams because a high degree of current neutralization implies a low net  $B_\theta$  field,

which is usually unable to efficiently contain the transverse momentum of the peak beam current. Injection of a beam into a preformed, highly conducting plasma is the obvious way to minimize the EM fields, but requires an externally applied field to contain the transverse momentum since the net current is now even lower. Benford, et al., (Reference 2.56) have demonstrated that injection of a high  $v/\gamma$  pinched beam into a pre-ionized plasma results in very low transport efficiency. Most of the beam is lost to the walls near the anode window. A cold beam  $\langle \beta_t^2 \rangle / \langle \beta_L^2 \rangle \ll 1$ , should be able to propagate efficiently in a pre-ionized media, however. Thus, if we use a diode geometry to keep the peak current below the critical current (recall  $I_c \approx 8500 \sqrt{\gamma^2 - 1} r_c/d$ ), propagation efficiency should be high in a plasma or a neutral gas at rapid breakdown pressures. As discussed in Section 2.1, high  $v/\gamma$ , cold beams have low current density ( $\approx$  few kA/cm<sup>2</sup>), so if we want to attain current densities of  $10^4$ - $10^5$  A/cm<sup>2</sup> at the downstream end of the transport system, the beam must be compressed. Beam compression is currently an active field of research.

The most straightforward way to transport high current density, high  $v/\gamma$ , (hot) beams, then, is to use external fields in plasmas. Two such configurations have been extensively studied over the past two years:  $B_\theta$ , or linear pinch, transport, and  $B_z$  systems. We discuss neutral gas transport both with and without external fields in this section.

#### 2.10.1 Neutral Gas Transport Without External Fields.

Transport modes in neutral gas-filled drift chambers can be conveniently classified in terms of the gas pressure, as indicated in Table 2.4.

TABLE 2.4

NEUTRAL GAS TRANSPORT MODES

|                       | <u>Beam, Gas Parameters</u>  | <u>Characteristics of Transport</u>  |
|-----------------------|--|--|
| Low pressure          | $\tau_N \gtrsim t_p$   | ion acceleration (large beam energy losses)  |
| Intermediate pressure | $\tau_N < t_B \lesssim t_r$<br>$\sigma_B$ high<br>$v_{net}/\gamma < 1$ | pinched (frozen hose) and drifting beams with high current neutralization (maximum transport efficiency) |
| High pressure         | $\tau_N \sim 0$<br>$t_B \rightarrow \infty$<br>$\sigma$ low            | unstable, pinched beam propagation   |

- 
- $\tau_N$  = electrical neutralization time
  - $t_B$  = breakdown time
  - $t_r$  = beam current risetime
  - $t_p$  = pulse width
  - $\sigma_B$  = conductivity at breakdown

Low Pressure Transport. When  $\tau_N \gtrsim t_p$ , space charge fields dominate the beam behavior and finite geometry (endplates) effects are important. Perhaps the most interesting aspect of this pressure regime is collective ion acceleration, which is discussed in detail in Section 4. We discuss some general features of low pressure transport at pressures outside of ion acceleration conditions.

The electrostatic potential well depth,  $\phi$ , is sketched in Figure 2.31. We can estimate  $\phi$  from Equation 2.20 as:

$$\phi \text{ (volts)} \approx \frac{60 I \text{ (amps)}}{\beta_L} (1/2 + \ln R/a) (1 - e^{-2.4 z_c/R})$$

$$z_c \lesssim 2(R/2.4) \quad (2.119)$$

$$l \lesssim R \lesssim 10 \text{ length units}$$

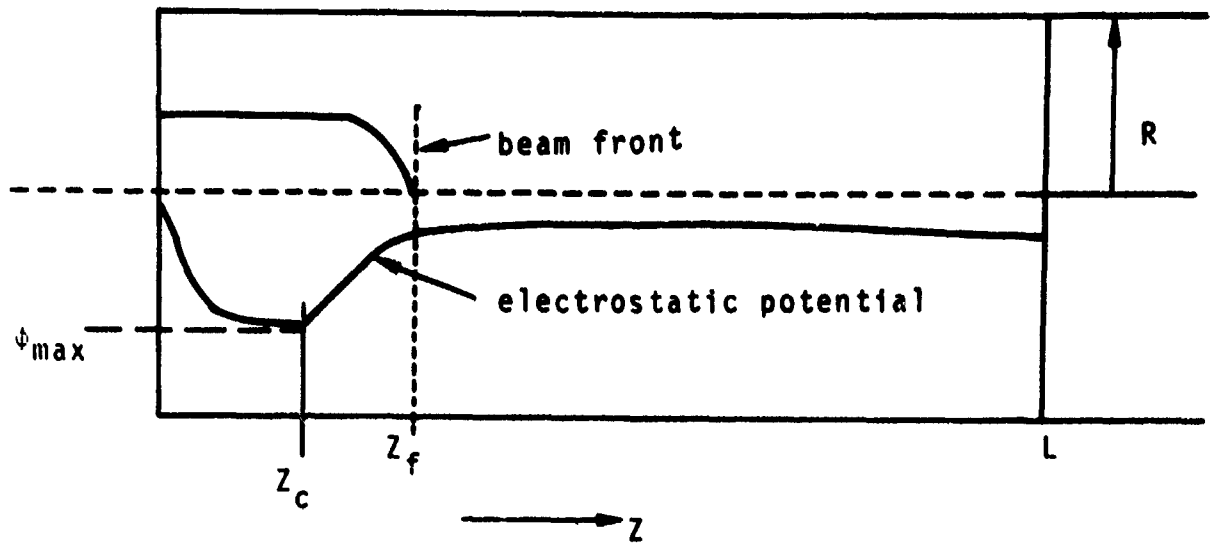
$$z_c = \text{crossover distance for } E_z \text{ (Equation 2.29)}$$

If  $\phi(z_c) \ll$  beam kinetic energy, the beam propagation will not be limited by the longitudinal electrical field, although space charge effects on radial motion must still be considered. If, however,  $\phi(z_c) >$  beam kinetic energy, a length,  $\bar{z}_c$ , is defined by  $\phi(\bar{z}_c) =$  kinetic energy and if the exponential factor in Equation (2.119) is approximated by a straight line,

$$\bar{z}_c \text{ (cm)} \approx \frac{3.4 \times 10^4}{I^P \text{ (amps)}} \left( \frac{t_r}{t_v} \right) \frac{\sqrt{1 + V^P} \sqrt{V^P}}{(1 + 2V^P)} \quad (2.120)$$

$$\cdot R/2.4 \left( \frac{1}{1/2 + \ln R/a} \right), \bar{z}_c \lesssim 2 (R/2.4)$$

where  $V^P =$  peak electron kinetic energy in MeV,  $t_r$  is the current risetime,  $t_v$  is the electron kinetic energy risetime, and  $I^P$  is the peak beam current. The voltage and current rise have been taken as linear, and  $\beta_L \cong \beta$ . If  $I^P \cong 30$  kA,  $t_r/t_v \cong 2$ ,  $V^P \cong 1$  MeV,  $R \cong 6$  cm, and  $a = 1$ , then  $z_c \approx 1.2$  cm. One can



$z_f$  = beam front

$z_c$  = position where  $E_z$  reverses direction

Propagation requires  $\phi_{\max} <$  beam kinetic energy

$$\text{or } v/\gamma - 1 \ll \left[ (1 + 2 \ln R/a) (1 - f_e) \right]^{-1}$$

Figure 2.31 Electrostatic potential in drift chamber ( $t < \tau_N$ ).

estimate a front velocity  $(\beta_f c)^{ES}$  by assuming that the front travels a distance,  $\bar{z}_c$ , over a time scale of  $\tau_N$ :

$$\beta_f^{ES} \cong \frac{\bar{z}_c}{c\tau_N}, \quad \bar{z}_c < \frac{2R}{2.4} \quad (2.121)$$

This velocity is very slow even for low  $v/\gamma$  beams and places a severe constraint on high  $v/\gamma$  beam propagation efficiency at low pressures. If  $\bar{z}_c$  from Equation (2.120)  $\gtrsim (2R/2.4)$  propagation would occur at a velocity determined by the "interior" beam kinetic energy; i.e., the kinetic energy minus the potential evaluated at  $z = 2R/2.4$ .

The discussion of the longitudinal ES field suggests a qualitative picture of the beam-front velocity behavior at low pressures above the ion acceleration cutoff. According to Equation (2.121) the beam front moves slowly until the charge neutralization front has passed  $z \approx 2(R/2.4)$ . Then the end plate effect and the front velocity should increase. The front velocity, however, will still be less than  $\beta c$  and will now depend on the "sharpness" of both the beam front and the space-charge neutralization front. As the beam approaches the downstream end plate, an increase in front velocity is again to be expected since the field will reverse direction as ES force lines start to terminate on the surface charges of the end plate.

Intermediate Pressure Transport. As the pressure increases and  $\tau_N < t_B < t_r$ , beam transport efficiency goes up as current neutralization occurs early in the pulse. We now estimate some limits on transport efficiency in neutral gases. The two conditions we need for efficient transport are

$$(1) \quad \frac{v_{net}}{\gamma} \lesssim 1 \quad (\text{EM requirement})$$

$$(2) \frac{(B_{\theta}^{\text{net}})^2}{8\pi} \gtrsim \langle n kT \rangle_p + \langle n kT \rangle_b \quad (\text{transverse energy containment})$$

where  $\langle n kT \rangle_p$  is the transverse energy/volume of the beam-generated plasma, and  $\langle n kT \rangle_b$  is the average transverse energy/volume of the beam, here expressed in terms of an equivalent temperature. The above conditions can be rewritten as

$$I(t_B) \gtrsim 17,000 \beta_L \gamma \quad (2.122)$$

$$I^2(t_B) \gtrsim 10^{-9} a^2 \left[ \langle n kT \rangle_p + \frac{2 \times 10^8 I^P}{\beta_L \pi a^2} \langle kT \rangle_b \right] \quad (2.123)$$

where  $I(t_B)$  is beam current (amperes) at gas breakdown,  $I^P$  is peak beam current (amperes),  $a$  is the beam radius,  $\langle n kT \rangle_p$  is in  $\text{eV/cm}^3$ , and  $kT$  units are electron volts. The transverse energy of the plasma cannot always be neglected. Equations (2.122) and (2.123) can be combined, yielding

$$\langle kT \rangle_b I^P < 4.4 \times 10^9 \beta_L^3 \gamma^2 \delta^2 - 1.6 \times 10^{-8} a^2 \beta_L \langle n kT \rangle_p \quad (2.124)$$

where  $I_b(t_B) = 17,000 \beta_L \gamma \delta$ . The value of  $\delta$  has to be determined from the length of the desired transport system, subject to the restriction of a maximum value unity.  $\langle kT \rangle_b$  is the equivalent peak average transverse beam temperature (eV) generated in the diode and anode window.

We can follow the arguments of Section 2.7.4 to determine  $\delta$ . The magnetic field energy in the system should be less than the total beam kinetic energy:

$$(\gamma - 1) m_0 c^2 N L_p > \left( \frac{I_b(t_B)^2 (\text{amps}) LF}{100} \right) \quad (2.125)$$

- N = number of beam particles/length  
 L<sub>P</sub> = beam pulse length defined such that the peak N times L<sub>P</sub> = total number of beam particles  
 L = length of transport system  
 F = dimensionless form factor of order unity

$$= \frac{1}{4} \left( \frac{a^2 + b^2}{a^2 - b^2} \right) - \frac{b^2}{a^2 - b^2} - \frac{b^2}{a^2 - b^2} \ln \frac{a}{b} + \ln \frac{R}{b},$$

for a uniform current distribution of outer radius a, inner radius b, the chamber radius is R. Rewriting Equation (2.125) we determine  $\delta$  for a 10 percent maximum energy loss:

$$\delta \approx 3.2 \times 10^{-2} \left[ \frac{v_b^P (\gamma - 1)}{\beta_L^2 \gamma^2} \frac{1}{F} \frac{L_P}{L} \right]^{\frac{1}{2}} \quad (2.126)$$

and, substituting in Equation (2.124), we finally obtain

$$\langle kT \rangle_b I^P \lesssim 2.6 \times 10^4 \left( \frac{L_P}{L} \right) \frac{1}{F} (\gamma - 1) I^P - 1.5 \times 10^{-8} a^2 \beta_L \langle n kT \rangle_p \quad (2.127)$$

If the plasma transverse energy can be neglected, Equation (2.124) gives a criterion independent of  $I^P$ ,

$$\langle kT \rangle_b \lesssim 2.6 \times 10^4 \frac{L_P}{L} \frac{(\gamma - 1)}{F}, \quad (2.128)$$

$$\langle kT \rangle_b < \text{total electron energy}$$

In reality,  $\langle kT \rangle_b$  is coupled to  $I^P$  by diode dynamics. As an example of Equation (2.128), we determine the maximum average transverse beam temperature for efficient transport ( $\sim 90$  percent)

over a 1 meter distance with a 1 MeV beam, 40 nsec peak current-weighted pulse width. With  $P = 1$ ,

$$\langle kT \rangle_b \approx 624 \text{ keV} \quad (2.129)$$

The diode configuration must be such that Equation (2.129) is satisfied, and, since diode "temperature" depends on current density, efficient transport translates in the final analysis to a current density criterion.\*

When hot beams which violate criterion (2.128) are injected into neutral gas chambers, one might expect that the higher transverse momentum electrons would be lost near the anode, and that the now effectively lower temperature beam would transport efficiently thereafter. This is indeed the case, as demonstrated by the experiments of Yonas, et al. (Reference 2.23). Table 2.5 shows their reported energy losses of a 250 keV mean energy electron beam, propagating in a 1-1/4-inch-diameter air-filled pipe. Injected beam energy was  $\sim 300$  calories.

TABLE 2.5  
RELATION BETWEEN NET CURRENT AND BEAM ENERGY LOSS

| Pressure<br>(torr) | Beam energy (cal)<br>10 cm downstream | Net current<br>(kA) at 10 cm | Beam energy<br>(cal) at 100 cm |
|--------------------|---------------------------------------|------------------------------|--------------------------------|
| 0.3                | 282                                   | 43                           | 66                             |
| 0.5                | 249                                   | 32                           | 106                            |
| 0.75               | 143                                   | 13                           | 103                            |
| 1.0                | 196                                   | 15                           | 108                            |

The results show that the highest net current ( $P = 0.3$  torr) mode is the most inefficient, indicating that EM energy loss

\* The transverse energy containment criterion may be expressed in terms of a dimensionless ratio:  $\beta \equiv \langle n kT \rangle_b / (B_0^{\text{net}})^2 / 8\pi \ll 1$ . Inasmuch as  $B_0^{\text{net}}$  is not a beam parameter, it is perhaps more convenient to use the beam current density for beam characterization.

probably dominates at this pressure ( $v_{\text{net}}/\gamma > 1.8$ ). A noteworthy characteristic of hot beam transport after initial energy loss within a few centimeters of the anode is that transport energy decays exponentially. The e-folding decay length varies from 1 to 3 meters depending on the beam temperature and ratio of pipe to beam radius. This phenomenon is not understood at present, but probably represents particle loss--electric field losses would most likely result in a linear decay.

At intermediate pressures, beam front velocity is dominated by the inductive longitudinal field before breakdown, and we can make an estimate of the front velocity in a fashion similar to that used for  $\beta_f^{\text{ES}}$ . We denote the front velocity in this case by  $\beta_f^{\text{Ic}}$ , and

$$\beta_f^{\text{I}} \approx \frac{\text{kinetic energy of beam electrons}}{(ec) E_z (\text{inductive}) t_B} \quad (2.130)$$

or

$$\beta_f^{\text{I}} \approx \frac{(\gamma-1)}{2v^{\text{P}} \beta_L} \frac{1}{(1/2 + \ln R/a)} \left( \frac{t_r}{t_B} \right)$$

where  $v^{\text{P}}$  is  $v$  for the peak current and a linear current rise is assumed. We require that  $z_f > R/2.4$ ,  $\tau_N \ll t_B \lesssim t_r$ , in order to use Equation (2.130). The beam front velocity is the lesser of  $\beta_f^{\text{Ic}}$ ,  $\beta_f^{\text{Tc}}$ , where the transverse energy limitation on the streaming velocity for a neutralized beam is  $\beta_f^{\text{Tc}}$ :

$$\langle (\beta_f^{\text{T}})^2 \rangle \approx \frac{\beta^2}{(1 + v/\gamma)} \quad (2.131)$$

The Lawson model has been used to obtain Equation (2.131). A 1 MeV, 50 kA peak current beam with  $t_r = 2 t_B$  gives  $\beta_f^{\text{I}} \cong 2/3$ , and since  $\beta_f^{\text{T}} \sim 0.67$ , the front velocity should not be limited by inductive fields in the example.

### 2.10.2 Beam Transport in External Field Plasmas.

$B_0$ -Linear Pinch Transport. The first experimental work investigating beam transport in a preformed linear pinch plasma was performed by Roberts and Bennett (Reference 2.57). They transported relatively cold beams ( $v/\gamma \approx 0.2$ ) efficiently, and even transported the beam around a curved ( $\sim 90$  degree total bending) pinch system. Benford and Ecker (Reference 2.58) have investigated linear pinch transport in more detail, correlating transport properties with measurements of the pinch  $B_0$  field as a function of radius at time of beam injection. Most importantly, they have demonstrated efficient transport ( $\approx 90$  percent) of hot beams ( $v/\gamma \approx 7$ ) over distances of two feet. This result is to be compared with a maximum transport efficiency of 30 to 40 percent over such distances with neutral gases and  $v/\gamma \sim 4$  to 5. Figure 2.32 is a schematic of their apparatus.

The previous discussion of neutral gas transport covers much of the phenomenology of transport with a linear pinch system. The important distinction between neutral gas transport at rapid breakdown pressures and linear pinch transport is that the radial profile of the  $B_0$  field that the beam "sees" in the linear pinch system is independently variable and depends on the pinch configuration at the time of beam injection. Recall that the time scale of pinch dynamics is in the microsecond range; i.e., very long compared to the beam pulse width.

Linear pinches break the gas down at the chamber walls, forming a current sheath, which "snowplows" the plasma inward until the plasma has collapsed to the center, and the current is "cored" with a radial profile similar to the Bennett distribution. The pinch then bounces and may recollapse. [See, e.g., Glasstone and Lovberg, (Reference 2.59)]. Some magnetic field profiles of a

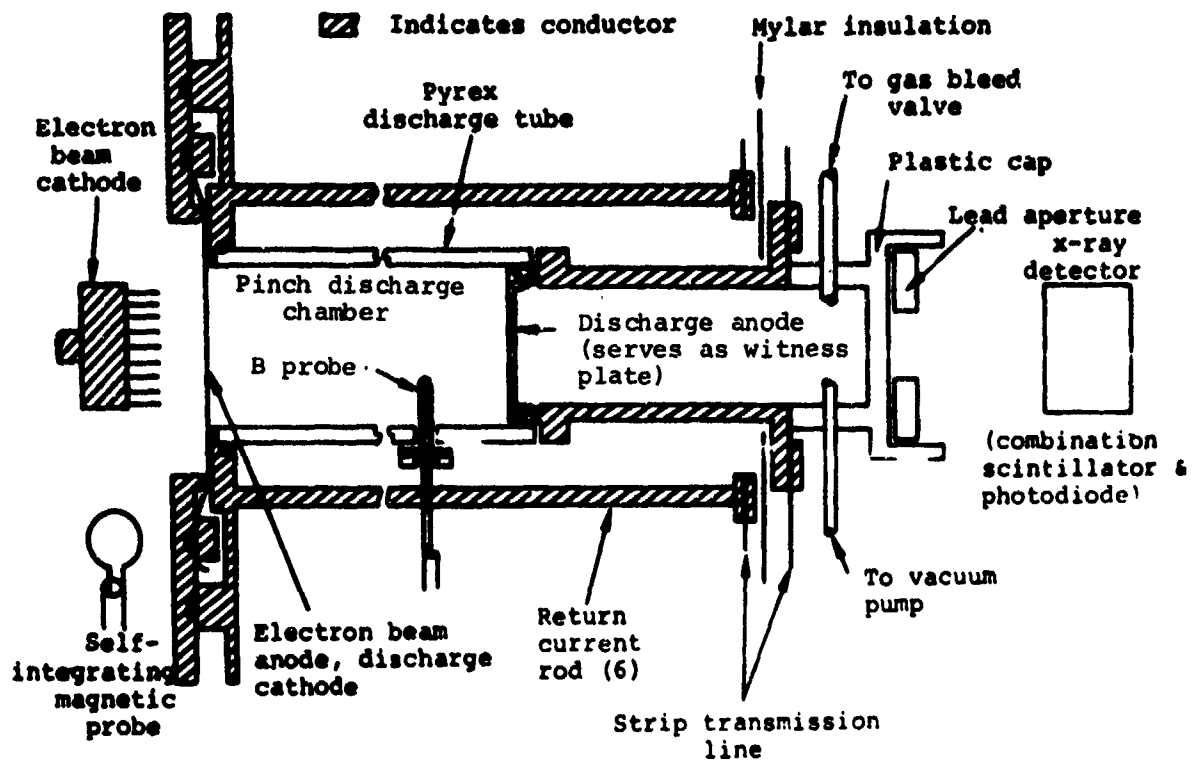


Figure 2.32 Experimental configuration of 2-pinch apparatus and beam-generating diode.

linear pinch system used by Benford and Ecker are shown in Figure 2.33. Thus, depending upon injection time, the beam enters a "hollow," sheathed current,  $B_0$  field or a pinched profile. In the figure, times in the pinch history up to  $\sim 3 \mu\text{sec}$  are sheathed.

Beam-Pinch Interaction Phenomenology. A single particle orbit theory of beam transport has been proposed by Benford and Ecker; the beam propagation is a superposition of single particle orbits of beam electrons in the (undistorted) magnetic field configuration of the pinch at injection time, with initial conditions determined by diode flow.

We assert that three conditions must be satisfied to use single particle orbit theory in the above context:\*

$$1. \quad t_d \approx \frac{4\pi\sigma_1 a^2}{c^2} \gg t_p \quad (\text{beam current neutralization})$$

$$2. \quad \frac{B_0^2}{8\pi} + \frac{n_p m_i v_r^2}{2} \gtrsim \langle nkT \rangle_p + \langle nkT \rangle_b \quad (\text{transverse energy containment})$$

$v_r$  = radial collapse velocity of pinch current sheath

$n_p$  = pinch sheath plasma density

3. Negligible longitudinal plasma penetration when single particle orbit theory predicts longitudinal reflection of beam particles (see Figure 2.38).

---

\*The last two conditions have not been experimentally confirmed.

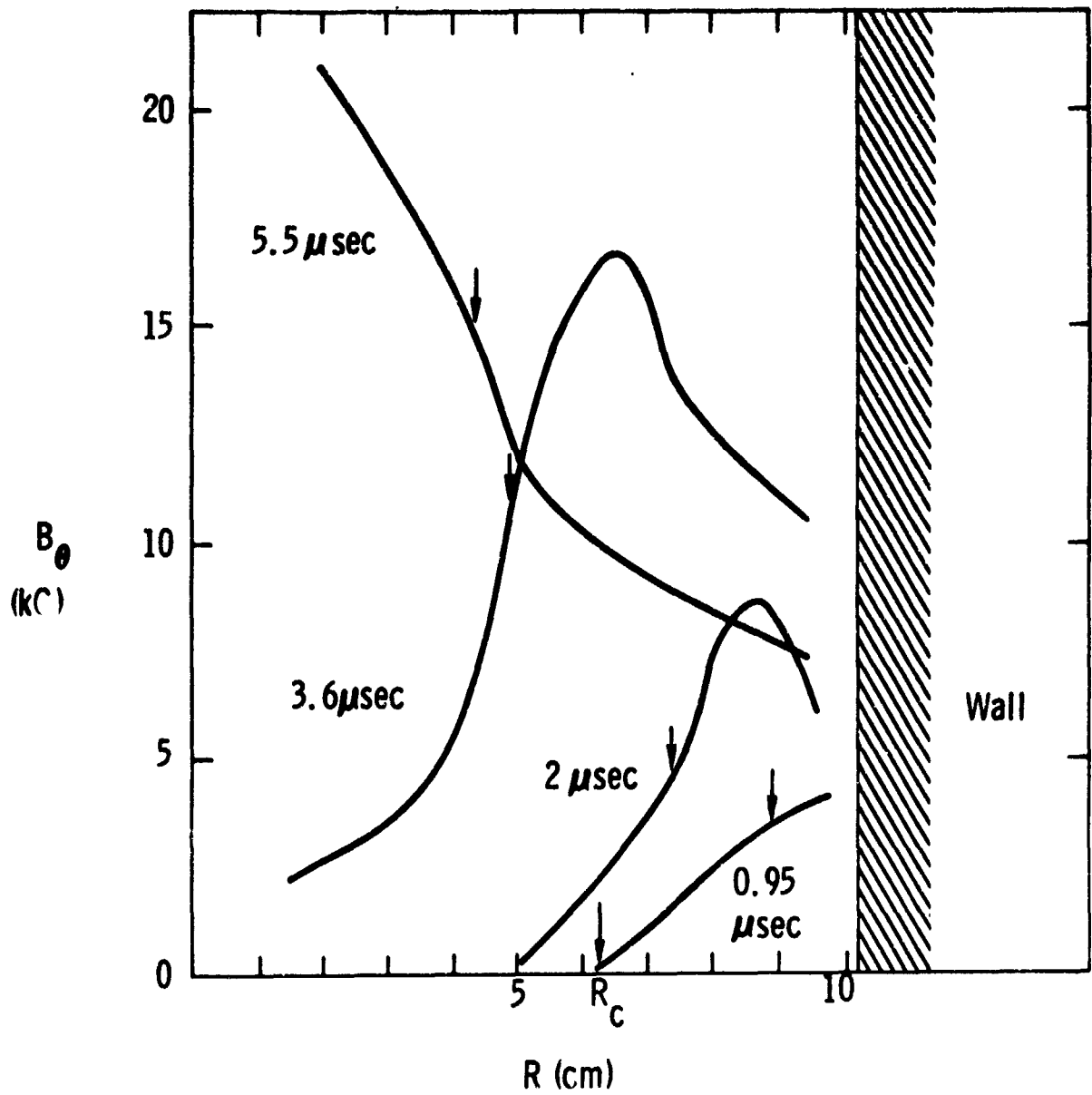


Figure 2.33 Magnetic field profiles at times of beam injection.  $R_C$  is beam cathode radius, arrows indicate damage radii of transported beams.

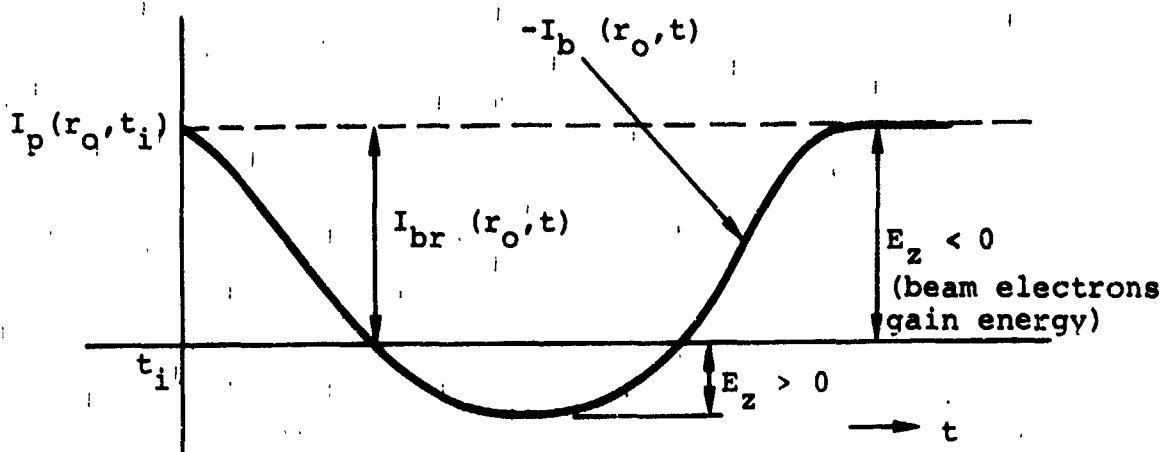
The last two features essentially mean that the  $B_0$  field frozen in the plasma has to be sufficiently strong so that the beam particle kinetic pressure, both transversely (2), and longitudinally when orbit theory predicts negative drift (3), is negligible compared to the existing plasma kinetic pressure. In other words, the beam cannot "pierce its way" through the plasma.

The diffusion time,  $t_d$ , in a linear pinch plasma would typically be approximately a microsecond, assuming a few volt, fully ionized plasma, so the first condition is usually fulfilled. Figure 2.34 shows the beam return current,  $I_{br}$ , at a radius  $r_0$  under this assumption of constant  $B_0(r)$ . The total plasma current does not flow oppositely to the beam or "return" unless  $I_b(r_0, t)$  exceeds  $I_p(r_0, t_i)$ . We see from the diagram that the beam will actually gain energy (albeit only a few keV) from the pinch until  $I_b(r_0, t)$  exceeds  $I_p(r_0, t_i)$ . The departure of  $E_z$  from values at injection and its radial variation are maintained, of course, by the very small changes in the net enclosed flux. The change in current flowing in the external pinch circuitry is also very small.

Let us explore beam propagation for two representative cases.

#### 1. Sheathed Pinch Current-Collapsing Phase

We assume that the conductivity interior to the pinch sheath is high; there is always some current flowing in the interior of the sheath, and the beam would rapidly break the gas down in this region, in any case. Transverse beam energy containment (condition 2) is attained in this phase because the pinch is in a state of pressure unbalance and accelerating inward (snowplowing) and also, when  $R_s > a_0$ , (Figure 2.35) the beam effectively "cools."



$t_i$  = injection time

$I_p(r_0, t_i)$  = pinch current enclosed at radius  $r_0$  at  $t_i$

Figure 2.34 The beam return current in a pinch where  $t_d \gg t_p$

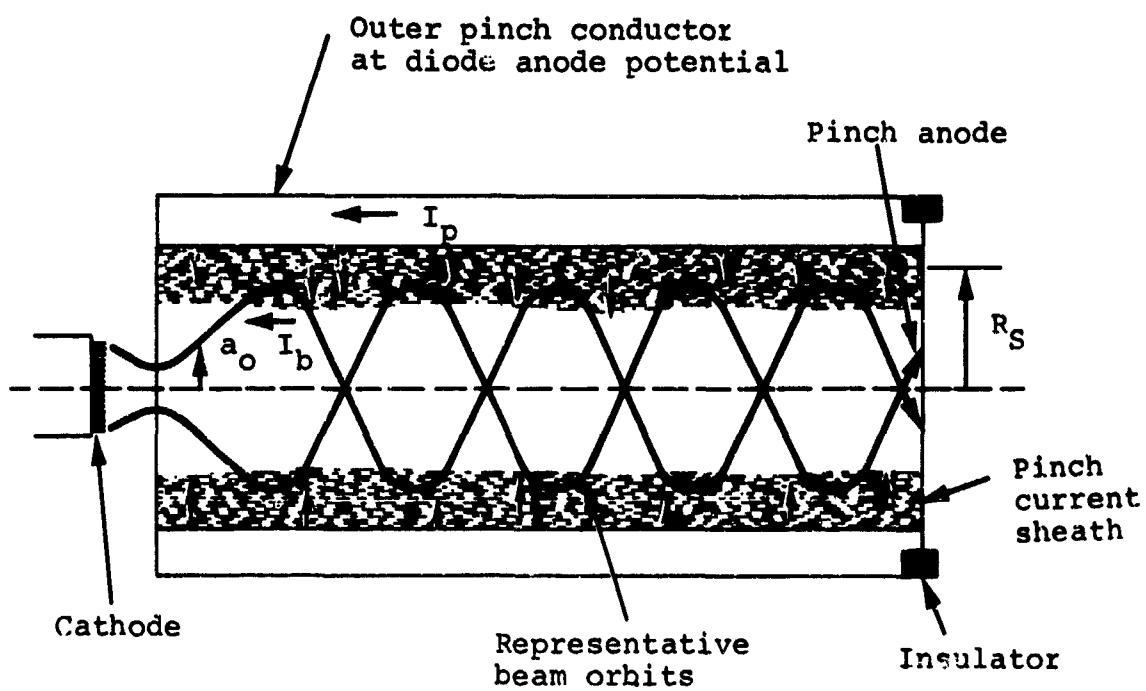


Figure 2.35 Sketch of beam propagation in collapsing pinch

(The transverse energy/cm<sup>3</sup>  $\propto a_0^2/a^2$  in the uniform current density case, for example.) Beam cooling implies that pinch currents much lower than the beam current can contain the beam in the collapsing phase when  $R_s > a_0$ . Benford and Ecker have demonstrated control of beam current density by varying  $R_s$  at  $t_i$ .

## 2. Partially Pinched Phase at Injection

In this phase the single particle model of Benford and Ecker would predict positive  $z$  drift (propagation) or negative  $z$  drift (reflection) depending on the detailed shape of  $B_\theta(r, t_i)$ . Figure 2.36 shows these regions for a nearly pinched plasma. The radius  $R_c$  is the radius within which one would expect the core of the beam to propagate. If  $B_\theta \sim r$ ,  $r \lesssim R_c$  (uniform current density), we can determine  $R_c$  from the Alfvén condition,  $I_A = 17,000 \beta_L \gamma$  amperes, or  $5 R_c B_\theta^c = I_A$ ,  $R_c$  in centimeters,  $B_\theta^c$  in gauss.  $I_A$  refers to the pinch current and  $\beta_L \gamma$  to the beam parameters. If the Larmor radius of the beam electrons is less than  $R_c$ , we can use  $\nabla B$  drift formulas for  $r > R_c$ .

Conditions 2 and 3, which are really coupled, may not be satisfied at pinched or near-pinched injection. If the pinch were steady state, e.g., the pinch field pressure would exactly balance the plasma transverse kinetic pressure, and the additional beam transverse pressure would not be contained without field distortion. We illustrate these remarks in more detail through example.

Let us assume that a beam is injected into an approximately uniform current density region of a nearly steady state pinch, that the beam radius at injection is equal to the Alfvén radius,

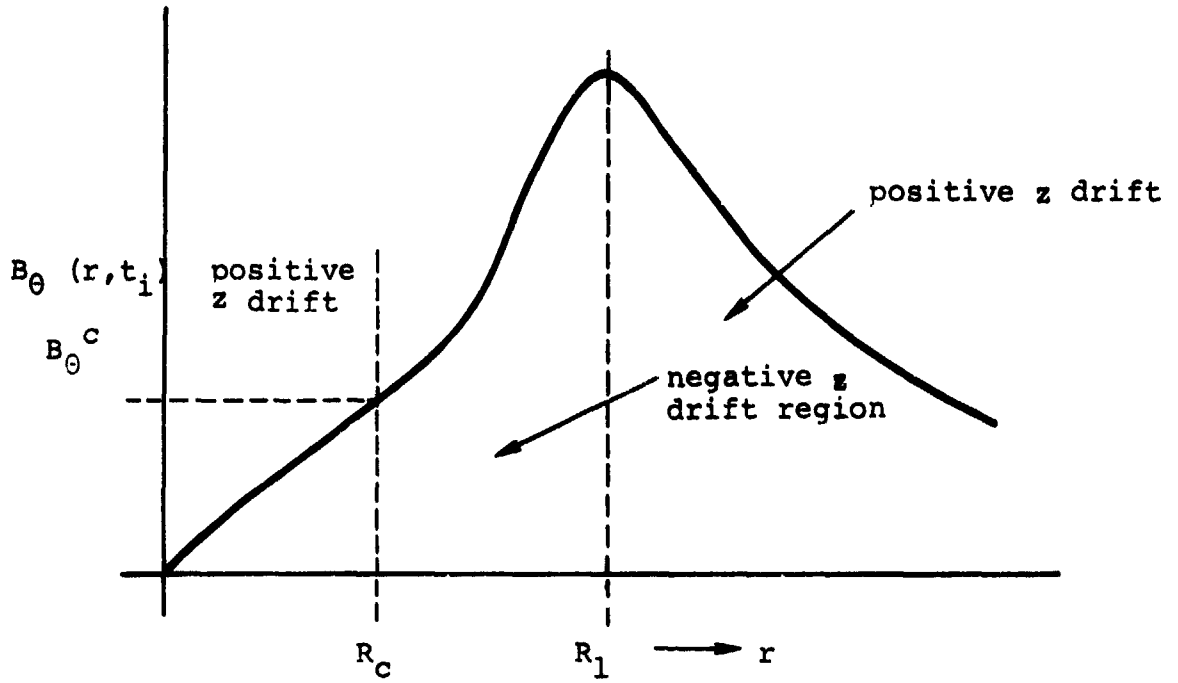


Figure 2.36 Pinched phase beam injection

$R_A$ , and the beam current equals  $I_A$ . Moreover, we take the beam to be zero temperature (cold) at injection.\* The beam moving in the pinch field now becomes hot; i.e.,  $\langle \beta_t^2 \rangle / \langle \beta_L^2 \rangle \sim 1$ . The beam average transverse energy/volume is  $\langle n_b kT \rangle_b \approx n_b W_T / 2$ , where  $W_T$  is the total electron energy. If this transverse kinetic beam "pressure" is negligible compared to the plasma pressure at plasma pressure balance (steady state injection), or, is small compared to the (magnetic-kinetic) pressure imbalance of a radially contracting plasma, we would expect single particle orbit theory in undistorted fields to apply. In the steady state plasma case we require

$$n_b \frac{W_T}{2} = \frac{2 \times 10^8 I_b}{\pi R_A^2 \beta_L} = \frac{2 \times 10^8 (I_A) W_T}{\beta_L \pi (R_A^2) 2} \ll \langle nkT \rangle_p \quad \text{(steady state pinch)}$$

or

$$R_A^2 \geq 5.4 \times 10^{11} \frac{W_T}{\langle nkT \rangle_p} \quad (2.132)$$

with  $W_T$ ,  $\langle kT \rangle_p$  in eV,  $n_b$  in  $\text{cm}^{-3}$ , and  $R_A$  in centimeters. If the plasma density is  $10^{16} / \text{cm}^3$ ,  $\langle kT \rangle_p \sim 10$  eV,  $W_T = 1$  MeV, Equation (2.132) gives  $R_A > 2.3$  cm.

Let us continue and suppose that condition (2.132) is violated at injection. If  $R_A \approx 1$  cm, = pinch radius, e.g.,  $n_b W_T / 2 \sim 10^{18}$  eV/cm<sup>3</sup>, compared with the plasma energy density of  $10^{17}$  eV/cm<sup>3</sup>. We expect, according to our model, that the pinch field will now be distorted, and that this distortion will proceed by motion of the plasma particles with field lines "tied" to plasma motion. Recall that in MHD theory with space charge neutralization

---

\* These restrictions are for analytical convenience.

$$\frac{\partial \vec{B}}{\partial t} = \nabla \times (\vec{v} \times \vec{B}) \times \frac{c^2}{4\pi\sigma} \nabla^2 \vec{B} \quad (2.133)$$

where we have used the expression  $\vec{j}_p = \sigma[\vec{E} + \vec{v} \times \vec{B}/c]$  for the plasma current density. The conductivity has been shown to be high enough that the change in  $B_\theta$  due to the last term in Equation (2.133) is negligible. The time scale of the radially outward plasma fluid motion will critically depend on how many ions have to be "dragged along" with the plasma electrons; i.e., to what extent the fluid is an electron or an electron-ion fluid. Snowplow pinch collapse theory assumes that all ions are pulled along (by an electrostatic charge separation field). The ion pickup in our case will depend on the plasma density outside the main discharge.

We develop a model for the expansion velocity assuming the expansion proceeds in a way to maintain electrical neutrality with uniform charge density in radius. Ions move to maintain neutrality as the pinch discharge region is "pushed" outward by the transverse kinetic pressure of the beam. Let  $dR/dt$  be the velocity of the outer radius,  $R$ , of the pinch discharge (and beam). [See Figure 2.37.] The velocity of the expansion is controlled by ion motion. We estimate  $dR/dt$  in sort of a "reverse snowplow" fashion:

$$2\pi R \left\{ \frac{\gamma m_o n_b^o}{2} \left[ \langle \beta_t^2 \rangle c^2 - \left( \frac{dR}{dt} \right)^2 \right] + n_p^o kT_p - \frac{(B_\theta^o)^2}{8\pi} \right\} \left( \frac{R_o}{R} \right)^2 \\ \approx \frac{d}{dt} \left[ m_i n_i^o \left( \frac{R_o}{R} \right)^2 \int_0^R dr' 2\pi r' v_i(r', R) \right] \quad (2.134)$$

where  $B_0^0$  = magnetic field at injection ( $r = R_0$ )

$n_b^0$  = initial beam number density

$n_i^0$  = initial plasma ion number density

$m_i$  = ion mass

$n_p^0$  = initial plasma number density

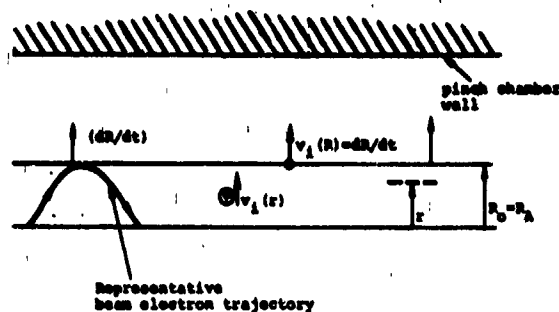
$T_p$  = plasma temperature

$\langle \beta_t^2 \rangle c^2$  = average transverse beam velocity squared

$v_i(r, R)$  = ion radial expansion velocity at radius  $r$  for discharge radius  $R$ .

The electron plasma mass has been neglected on the RHS of Equation (2.134). With uniform density expansion,

$$v_i(r, R) = \frac{r}{R} \frac{dR}{dt}$$



$R_0 = R_h$  - pinch, beam radius at injection time  
 $v_i(r)$  - ion radial velocity

Figure 2.37 The expanding pinch model.

and, if we neglect the last two terms on the LHS of Equation (2.134) [they balance at injection in steady state], we obtain after integration

$$\begin{aligned} \left(\frac{dR}{dt}\right)^2 &\approx \frac{3}{2} \gamma \frac{m_o}{m_i} \frac{n_b^o}{n_i} \beta^2 c^2 \ln \left(\frac{R}{R_o}\right) \\ &\approx 8.2 \times 10^{-4} \left(\frac{\gamma m_p}{m_i}\right) \left(\frac{n_b^o}{n_i}\right) \beta^2 c^2 \ln \left(\frac{R}{R_o}\right) \end{aligned} \quad (2.135)$$

with  $m_p$  = proton mass. If we let  $R = R_o + \Delta$ , Equation (2.135) can be integrated for  $\Delta/R_o < 1$ :

$$\Delta \approx 3.3 \times 10^{-3} \beta^2 c^2 t^2 \left(\frac{\gamma m_p}{m_i} \frac{n_b^o}{n_i}\right) \frac{1}{R_o} \quad (2.136)$$

In our example,  $\gamma = 3$ ,  $n_i^o \approx 10^{16}/\text{cm}^3$ ,  $n_b^o \approx 3 \times 10^{12}/\text{cm}^3$ ,  $R_o = 1$  cm, and with a beam pulse width of 80 nsec, Equation (2.136) gives  $\Delta \approx 20 (m_p/m_i)$  cm over the duration of the beam pulse, corresponding to an average velocity of  $\approx 2.5 \times 10^{-1} (m_p/m_i)$  cm/nsec. We emphasize that this velocity estimate is a lower limit because of our assumption that the ion velocity controls the expansion.

The external circuitry of the pinch system will also affect the beam penetration rate. Our model basically assumed that the discharge chamber was connected to the external (lumped) inductance and capacitance via a resistive impedance transmission line with electrical length long compared to the field distortion time. The longitudinal electric field in the laboratory frame is

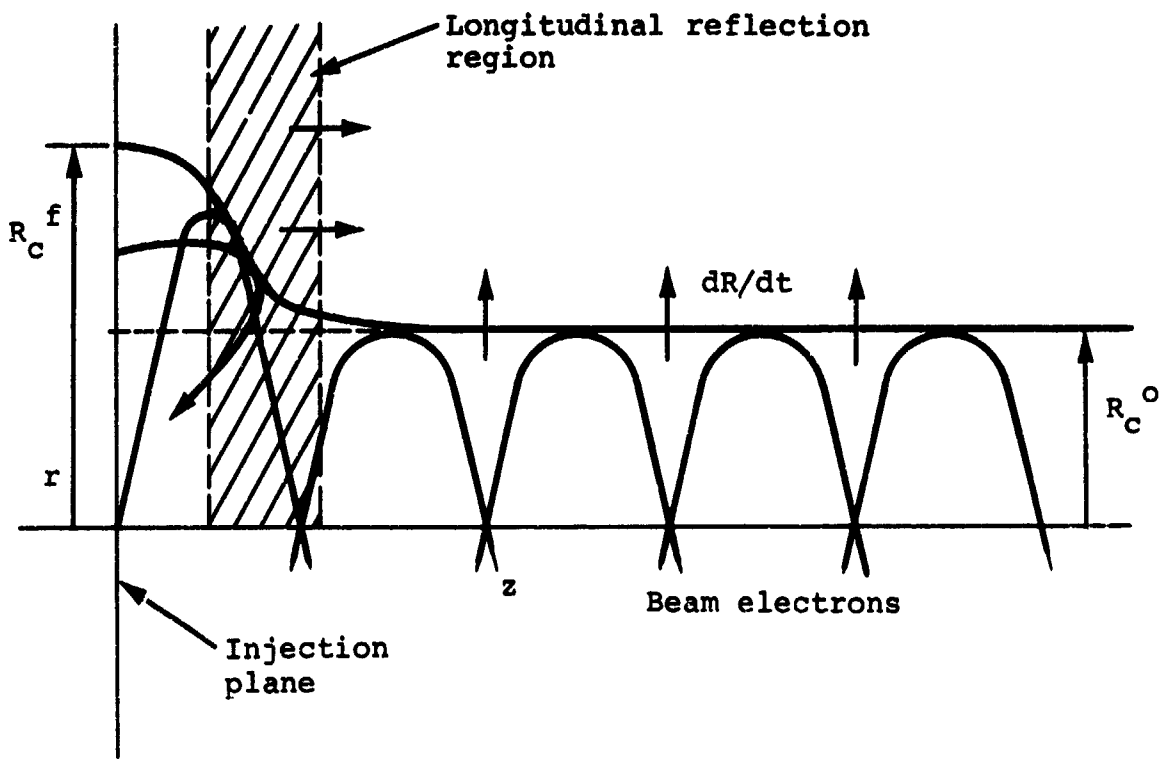
$$E_z \text{ (V/cm)} \sim - (300) \left( \frac{dR}{dt}/c \right) B_0 \quad (2.137)$$

maximally  $\sim 2 \times 10^3$  V/cm in the example. As is well known from linear pinch theory, this field may produce a large voltage spike across the pinch chamber if the external inductance is large compared to the chamber inductance,  $L$ . On the other hand, if the external inductance is small, the voltage across the pinch chamber will essentially remain constant, and the total discharge current will change so that  $L \, dI/dt \approx - I dL/dt$ .<sup>\*</sup> Experimental verification of the model must therefore be performed with a carefully defined system. Most importantly, the beam and pinch parameters should be designed as in the model; motion of the plasma as a whole is desirable, not merely an inner core where the effects of its motion may be shielded from the outer pinch radius-chamber electrode flux region.

The actual penetration process is undoubtedly much more complicated than our simple model where plasma and beam currents were assumed uniform and coextensive, and the pinch expanded outward while maintaining a uniform density. More generally, one might expect an  $(r, z)$  or two-dimensional, penetration process, and certainly not necessarily one that maintains a uniform current density. Figure 2.38 illustrates the two dimensional penetration where beam current is also initially injected at radii outside the critical radius. The longitudinal beam "pressure" is generated by reflection of beam electrons.

---

\* We expect in this case that the pinch distortion time will be somewhat increased if the signal double transit time in the transmission line is short compared to the pinch expansion time scale.



$R_c^o$  = radius of core propagation  $\approx R_A^o$   
in uniform current density case

$R_c^f$  = radius after plasma motion allowing  
complete beam penetration

Figure 2.38 Two-dimensional penetration of  
pinch field by beam

We now compare our remarks with the experimental results and discussions of Benford and Ecker. They report target damage radii and enclosed pinch currents at various injection times using a 160 kA, 500 keV beam. The transport efficiency was reported high (~100 percent), so we assume that all the beam propagated within the damage radii. Moreover, although the  $B_{\theta}(r)$  variation was not exactly linear within damage radii, we will assume it linear. The Alfvén current for their parameters is  $34 \beta_L$  kA. Table 2.6 summarizes the data.  $R_d^{calc}$  is obtained from an estimate from experiment field profiles for the product of the radius and magnetic field to give  $I_A$ , and the beam transverse pressure column corresponds to the maximum pressure (peak current) within the calculated Alfvén radius. The last column is an estimate of the ion plasma inward-streaming energy density for an argon plasma ( $n_i m_i v_i^2 / 2$ ) with initial pressure of 300  $\mu$ m. (All their data referred to the collapsing phase.) This is a rather crude estimate inasmuch as accurate plasma density and collapse velocity parameters are not given. Our calculation assumed collapse velocity of 1.5 cm/ $\mu$ sec, and a discharge current radius of 3 cm. These parameters are probably low for the 2.9  $\mu$ sec, injection time; the velocity rises sharply as the radius contracts in snowplow theory, and the effective radius of the discharge is probably < 3 centimeters.

TABLE 2.6  
BENFORD-ECKER DATA COMPARISON

| $t_i$<br>( $\mu\text{sec}$ ) | $R_d^{\text{exp}}$<br>(cm) | $R_d^{\text{calc}}$<br>(cm) | $n_b \langle kT \rangle_b$<br>(eV/cm <sup>3</sup> ) | $\frac{n_p m_i v_i^2}{2}$<br>(eV/cm <sup>3</sup> ) |
|------------------------------|----------------------------|-----------------------------|---|--|
| 2.9                          | 1.5                        | 1.2                         | $3 \times 10^{18}$                                  | $> 10^{18}$  |
| 2.4                          | 2.0                        | 1.8                         | $1 \times 10^{18}$                                  | $\sim 10^{18}$                                     |
| 1.7                          | 2.8                        | 2.8                         | $5 \times 10^{17}$                                  | $10^{18}$  |

The conclusions indicated by Table 2.6 are that single particle orbit theory is a good approximation since the sheath momentum can contain the beam and that the current should essentially flow within their damage radii. The discrepancies between the calculated and experimental radii at later times are too small to be significant in view of the inaccuracy in the damage radii estimates, and also because of the calculational assumption of a cold beam upon injection. An experimental test of the beam penetration model is therefore not included in the Benford-Ecker data.\*

As a final example of the model, we design a pinch injection profile for transport of a 1 MeV, 2 MA beam at a current density of  $10^5$  A/cm<sup>2</sup>. A magnetic field configuration should rise linearly from the origin to about 3 kG at 2.52 cm. The maximum transverse beam energy density is then  $\sim 2 \times 10^{19}$  eV/cm<sup>3</sup> which implies an argon plasma with  $n_i v_r^2 \gtrsim 10^{30}$  eV/cm. A collapse velocity of  $10^7$  cm/sec and density greater than  $10^{15}$ /cm<sup>3</sup> should be adequate to contain the beam. If the plasma conductivity  $\sim 10^{14}$  sec<sup>-1</sup>

\*Recent data of beam compression in a tapered pinch suggests beam penetration in violation of single particle orbit theory.

(100 mhos/cm), the beam would lose about 100 keV energy/meter of transport. Figure 2.39 shows a sketch of this field profile. This example illustrates a basic feature of hot beam transport in linear pinches; namely the high transverse beam pressure can be advantageously contained by the collapsing pinch at much lower pinch currents than the beam current. In a sense, we are utilizing the kinetic streaming energy of the ions, gained over a much longer time scale than the beam pulse width, to maintain a confining field configuration.

We conclude the linear pinch phenomenology by mentioning two recent experiments to investigate other applications of linear pinch transport (Reference 2.59). In one experiment, two beams from magnetically isolated cathodes were injected into a pinch to look at beam mixing (Reference 2.59). As expected, when injection was interior to the pinch current sheath the beams did mix. Beam compression has also been investigated in a tapered pinch configuration and preliminary experiments have not indicated any current density enhancement. Moreover, the beam appeared to penetrate the more highly pinched downstream field region in violation of single particle orbit theory (Reference 2.60).

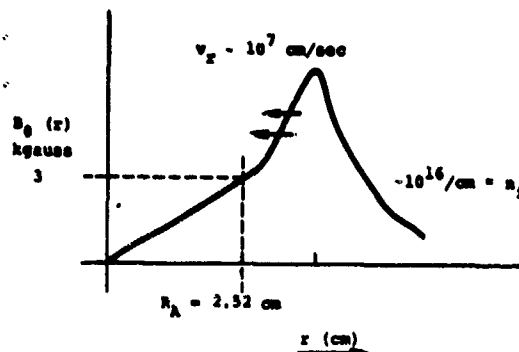


Figure 2.39 A magnetic field profile for transport of a 1 MeV, 2 megampere beam at  $10^5$  A/cm<sup>2</sup>.

2.10.3 Solenoidal Field Transport. Beam transport in solenoidal, or  $B_z$ , external fields has been experimentally studied over the past two years. The first work was performed at Cornell University using  $v/\gamma \sim 2$  to 3 beams at current densities of a few  $\text{kA/cm}^2$  (Reference 2.37). A beam transport efficiency of 24 percent at 15  $\mu\text{m}$  pressure was reported using a 10 kG field, compared to a 6 percent efficiency without the field. At 435 m pressure the 10 kG field gave the same transport efficiency as no field; the field apparently prevented space charge beam blowup at the low pressure. This early work has been extended at Cornell and NRL and efficiencies of 85 percent have been attained over 2 meters using similar beams (Reference 2.61). Hammer and Levine have reported high transport efficiency with higher  $v/\gamma$  beams ( $\sim 10$ ) (Reference 2.62). More recently, Stallings at PI (Reference 2.52) has looked at  $B_z$  transport efficiencies with a  $v/\gamma > 10$  beam over a wide range of magnetic field values (up to  $\sim 30$  kG) and has discovered a substantial dropoff in transport efficiency above about 9 kG.

The requirements for efficient transport in  $B_z$  systems are, as might be expected from our previous discussions, that the EM fields of the beam be rapidly shorted out by charge and current neutralization (preionization or rapid gas breakdown), and that transverse beam momentum be contained by the field. We have already discussed charge neutralization and the role of current neutralization in the  $z$  direction to keep  $B_\theta^{\text{net}}$  low. So, as without  $B_z$  fields, we want  $v_{\text{net}}/\gamma \leq 1$  strictly from EM limitations. The  $B_z$  systems have another dimension to consider, however. Effects of theta currents and diamagnetism or paramagnetism have to be evaluated. The remainder of this section is largely devoted to an exploration of theta currents.

Diode Flow. As already mentioned (Section 2.1), no self-consistent theory for diode flow with longitudinal electric fields exists, so we are uncertain about the theta motion in the diode, and consequently also about the beam injection conditions into the transport system. We first briefly discuss electron motion in the diode qualitatively. When electrons are emitted from the cathode in the presence of the field (which must fringe into the diode to avoid mirroring of high transverse momentum electrons), the guiding center of the electron orbit is accelerated azimuthally about the system axis by forces due to the presence of a radial electric field and the  $B_\theta$  self field. This guiding center motion gives rise to a macroscopic volume theta current that appears as a rotation of the cathode emission pattern at the anode window. The radial electric field contribution is diamagnetic, whereas the rotation due to the self field giving rise to twisted magnetic field lines is paramagnetic. Experimental evidence shows that the paramagnetic volume theta current dominates with present high-current diode configurations.\* If one believes that the guiding center motion in the diode approximately follows field lines and, recalling that the pitch angle will increase with radius and with current density due to the self field ( $B_\theta$ ), we expect rotation to increase with radius and current density. Hammer has measured the twist of a strip cathode pattern and found an approximately linear dependence of the angle (up to  $\sim 50$  degrees) upon  $I/\gamma B_z$ . At a few hundred kiloampere beam currents, current densities  $\sim 10$  to  $30 \text{ kA/cm}^2$ , and  $B_z$  in the few kilogauss range,  $v_\theta$  and  $v_z$  of beam electrons appear to be comparable.

---

\*The radial electric field is shorted out by the electrodes in high current, larger aspect ratio ( $r_c/d$ ) diodes.

The general trajectory of an electron in the diode is a superposition of motion of a guiding center rotation about the system axis and a gyrofrequency rotation about the guiding center. The gyro-rotation gives rise to a magnetization or surface current, type of diamagnetic theta current, and is experimentally manifested by a "smearing" of the projected cathode emission surfaces over cyclotron radii. Stallings has shown that the cyclotron radii may be of the order of those expected for electrons with nearly total energy transverse to  $B_z$ .\*

We can quantitatively estimate the relative importance of the theta current contributions of rotation about the axis and gyro-rotation with a simple model. The model is given to allow a practical working description of diode flow and transport phenomenology, and we proceed recognizing the perils of crude estimates. Let us assume that the radial electric field contribution to rotation about the axis is negligible compared to  $B_\theta$  self-field effect (large aspect ratio diodes), that the current density is uniform in radius, and that the guiding centers approximately follow field lines. This latter assumption is equivalent to restricting the model to cases where the curvature drift velocity is small compared to rotational velocity about the axis. Referring to Figure 2.40, we obtain

$$\begin{aligned} v_{\perp c} &= v_z \sin \alpha (r) \\ v_{\perp r} &= v_z \tan \alpha (r) \\ \tan \alpha (r) &= \frac{B_\theta (r)}{B_z} \end{aligned} \quad (2.138)$$

with

$$\begin{aligned} v_{\perp c} &= \text{perpendicular cyclotron or gyro velocity} \\ v_{\perp r} &= \text{perpendicular rotational velocity about system axis} \end{aligned}$$

---

\* These measurements were made a few centimeters beyond the anode window.

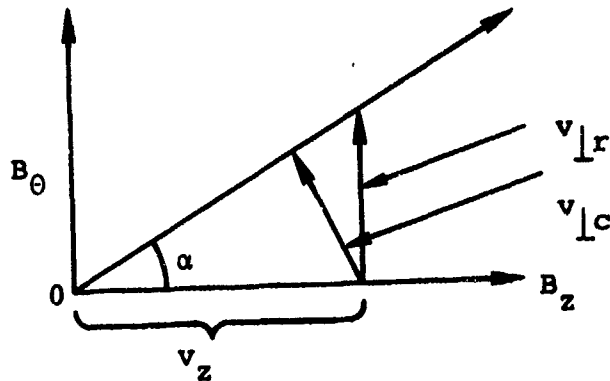


Figure 2.40 Perpendicular velocity components in combined  $B_\theta$  and  $B_z$  magnetic fields.

The longitudinal electron velocity as a function of radius,  $\beta_L c$ , is given by

$$\beta_L(r) \approx \frac{\beta}{\sqrt{1 + \sin^2 \alpha + \tan^2 \alpha}} \quad (2.139)$$

where  $\beta$  refers to the total electron velocity. The average longitudinal  $\beta$ ,  $\langle \beta_L \rangle$ , for uniform charge density is then

$$\langle \beta_L \rangle = \frac{2}{a^2} \beta \int_0^a \frac{r'}{(1 + \sin^2(r') + \tan^2(r'))^{1/2}} dr' \quad (2.140)$$

We can define a condition for validity of the assumption of uniform current density from Equation (2.139). Let us require that

$$\frac{\beta - \beta_L(a)}{\beta} < 1/2$$

i.e., current density uniform within 50 percent. This condition translates from Equation (2.139) into requiring  $\alpha(a) < 1$ .

Equation (2.140) becomes

$$\langle \beta_L \rangle \approx \frac{\beta}{a^2 C_1^2} \left[ \left( 1 + 2C_1^2 a^2 \right)^{1/2} - 1 \right] \quad (2.141)$$

$C_1 a < 1$

where

$$C_1 \equiv \frac{I(\text{amps})}{5a^2 B_z}$$

$a$  in centimeters,  $B_z$  in gauss. When  $C_1 a \sim 1$ , Equation (2.141) says that  $\langle \beta_L \rangle \sim 0.7\beta$ , and if  $C_1 a > 1$ , a condition  $C_1 a \lesssim 1$  defines an approximately uniform density core of radius  $a$ . [Recall the data of Stallings (Section 2.1.3) regarding experimental observations of a peaked current density along the axis.]

Assuming that  $C_1 a \lesssim 1$ , we proceed with the uniform beam model. The rotational angular velocity about the axis,  $\omega$ , is from Reference 2.37, e.g.,

$$\begin{aligned} \omega &\approx \left( \frac{\langle \beta_L \rangle c B_\theta}{r B_z} - \frac{c E_r}{r B_z} \right) \quad (2.142) \\ &= - \frac{|I(\text{amps})| c}{5a^2 B_z \langle \beta_L \rangle} \left( f_e - \frac{1}{\gamma_L^2} \right) \end{aligned}$$

and with  $f_e \approx 1$ ,  $C_1 a < 1$ ,  $\omega$  is approximately constant:

$$\omega \approx - \frac{|I(\text{amps})|}{5a^2 B_z} \langle \beta_L \rangle c \quad (2.143)$$

The paramagnetic change of  $B_z$  along the axis,  $\Delta B_z^p$ , due to rotation about the system axis, can now be estimated with a rigid rotor model, assuming  $\partial B_r / \partial z$  negligible compared to  $4\pi/c j_b$ ,

$$\left. \begin{aligned} \Delta B_z^p &\approx \frac{4\pi}{c} n_b e \omega a^2 / 2 \\ &\approx \frac{\pi a^2}{25} \frac{j_b^2}{B_z} \end{aligned} \right\} \quad (2.144)$$

with  $j_b$  the beam z-current in A/cm<sup>2</sup>. Similarly, we estimate the diamagnetic gyrorotation contribution to  $B_z$  at  $r = a$ ,  $\Delta B_z^d$ :

$$\Delta B_z^d \left( 2B_z^i - \Delta B_z^d \right) \approx 8\pi n_b W_\perp(a) \quad (2.145)$$

where  $B_z^i$  is the applied field,  $n_b$  is the beam particle density, and  $W_\perp$  is the perpendicular gyrorotational energy at the beam edge. Combining Equations (2.138), (2.144), and (2.145), we obtain an equation of comparison, evaluating  $\Delta B_z^d$  at  $r = a$  and  $\Delta B_z^p$  at  $r = 0$ :

$$\frac{\Delta B_z^d \left( 2B_z^i - \Delta B_z^d \right)}{\left( \Delta B_z^p \right)^2} \approx \frac{\gamma}{v} \cos^2 \alpha(a) \quad (2.146)$$

and since the maximum,  $\Delta B_z^d$  occurs when  $B_z^d \approx \Delta B_z^i$ ,

$$\left( \frac{\Delta B_z^d}{\Delta B_z^p} \right) \lesssim \sqrt{\frac{\gamma}{v}} \cos \alpha(a) \quad (2.147)$$

Thus, if  $v/\gamma > 1$ , and rotational effects due to the radial electric field are negligible, the model predicts a net paramagnetic beam. Although we have restricted the model to

$$C_1 a \approx \frac{B_\theta(a)}{B_z} < 1$$

the geometry of Figure 2.40 suggests that the conclusion of Equation (2.147) is probably valid for  $C_1 a \gtrsim 1$ .

Transport System Phenomenology. The first question which arises in discussing transport phenomenology is the influence of the anode foil upon injected beam orbits. If the foil essentially remains intact at solid densities during the beam pulse and  $(\omega_c/v) \ll 1$ , the beam electrons enter the transport region with a multiple scattering velocity distribution about their incident velocity vector at the anode. If  $\delta$  is the angle the velocity vector makes with the  $\vec{B}$  vector after scattering, similar considerations as in Figure 2.40 give

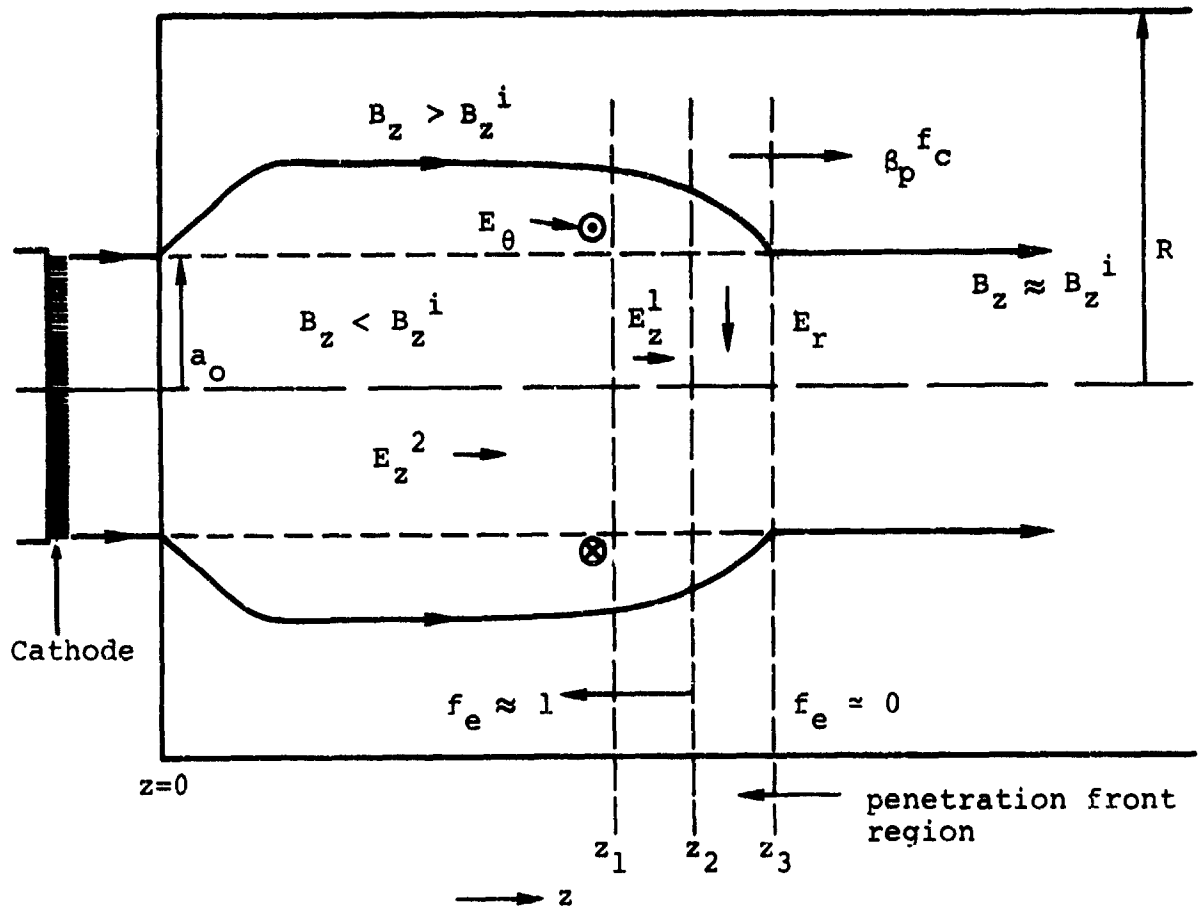
$$\left. \begin{aligned} v_{lc} &\approx v \sin \delta \\ v_{lr} &\approx v \cos \delta \sin \alpha \\ v_z &\approx v \cos \delta \cos \alpha \end{aligned} \right\} \quad (2.148)$$

and  $\tan \alpha = |B_\theta^{\text{net}}|/B_z$  to allow for current neutralization. Another important question regarding the transition region from the diode to the transport system is whether the particle motion is adiabatic as  $B_\theta$  is reduced by current neutralization. A non-adiabatic transition will partially convert diode rotational transverse energy to transport system gyrorotation, as can be seen from Equations (2.148), e.g., with  $\delta$  replaced by

the diode  $\alpha$  value. If the transition is adiabatic, Equation (2.138) indicates that the transverse energy in the transport system will decrease, since  $\alpha$  is diminished from the diode value. Finally, it is necessary to determine whether  $B_z$  field lines are "tied" at the anode window, or, in other words, whether the field diffusion time in the anode over distances of the order of the beam radius is large compared to the beam pulse width.

A sketch of a beam penetrating a neutral gas is shown in Figure 2.41 for the case of a net diamagnetic beam channel, and with field lines assumed tied at the anode window. The field line intersecting the outer cathode emitter is indicated. The configuration is an asymmetric double mirror geometry with the downstream end moving at velocity  $\beta_p^f c$ , which we anticipate to generally be  $\ll \beta c$  of beam electrons. Aside from the theta electric field, the electric fields in the penetration front region are as previously discussed without an external  $B_z$  field. In the region  $z_2 \lesssim z \lesssim z_3$  the electrostatic field is primarily radial, from  $z_1 \lesssim z \lesssim z_2$ ,  $E_z^1 \propto L \, dI/dt$ , and for  $z < z_1$ ,  $E_z^2 \approx [I(t) - I(t_B)] / \pi \sigma_B a^2$ , where  $I(t_B)$  is the z-directed current at the breakdown time  $t_B$ , and  $\sigma_B$  is the conductivity at breakdown along field lines. The  $E_\theta$  field is, of course, in a direction to drive plasma currents to counteract beam theta currents.

In neutral gas propagation without  $B_z$  fields the beam electrons in the penetration front are lost radially to the chamber walls when  $f_e < 1/\gamma^2$ . If  $B_z^i$  is sufficiently large, however, the longitudinal space charge field can prevent beam electron escape to the wall. In other words, beam electron motion is primarily azimuthal and longitudinal for large enough  $B_z$ .



$z_1$  = distance where gas breakdown occurs

$z_2$  = distance at which electrical neutralization is achieved

$z_3$  = furthest penetration length of beam into neutral gas

Figure 2.41 Beam penetrating a neutral gas with  $B_z$ .

The space charge limitation on propagation in the z direction is, from Section 2.10.1,

$$v/(\gamma - 1) < \frac{1}{(1 + 2 \ln R/a)} \frac{1}{(1-f_e)} \quad (2.149)$$

On the other hand, sinusoidal or radially contained beam particle motion in the uniform beam approximation requires for  $f_e \cong 0$

$$v/\gamma \lesssim 4 \times 10^{-8} B_z^2 a \quad (2.150)$$

with  $B_z$  in gauss and  $a$  in centimeters. With no space charge neutralization, a 10 kilogauss field, e.g., could contain a 500 keV beam of radius 2.5 cm with currents up to about 300 kiloamperes ( $v/\gamma \sim 10$ ). The electrostatic field at the penetration front can therefore cause substantial reflection of beam electrons back to the diode.

We can express the criterion for particle reflection generally using Hamiltonian formalism and conservation of canonical angular momentum for axially symmetric systems. Non-relativistically, reflection will at least occur for all particles satisfying

$$\left( \frac{p_\theta^0}{r} + \frac{e}{c} A_\theta \right)^2 > 2m_0 (E_0 - \Delta E - e |V(r,z)|) > 0, \quad (2.151)$$

$z > z_1$

with  $p_\theta^0 = m_0 r_0^2 \dot{\theta}_0 - (e/c) r_0 A_\theta =$  electron canonical angular momentum at  $z = 0$   
 $r_0 =$  radius of electron at  $z = z_0$   
 $A_\theta =$  theta component of vector potential  
 $E_0 =$  electron kinetic energy at  $z = z_0$

$\Delta E$  is the energy loss in transport up to  $z = z_1$  and  $V(r, z)$  is the electrostatic potential for  $z > z_2$ . Let us rewrite Equation (2.151) for a simple case where  $B_z(r, z) \approx B_z^i(r)f(z)$ . Moreover, if we assume no collisions in the anode window,  $P_\theta^0$  can be related back to emission at the cathode. We obtain

$$P_\theta^0 = -\frac{e}{2e} r_c^2 B_z^i (< 0)$$

where  $r_c$  = emission radius at cathode, and  $\dot{\theta}$  is taken zero at the cathode. Such a  $P_\theta^0$  corresponds to electrons which do not encircle the system axis (Reference 2.63). Equation (2.151) becomes

$$\left[ f(z)r - \frac{r_c^2}{r} \right]^2 > \left( \frac{2c}{eB_z^i} \right)^2 2m_0 (E_0 - \Delta E - eV) .$$

$$> 0.47 \frac{[(E_0 - \Delta E - eV)(eV)]}{[B_z^i (\text{gauss})]^2} \quad (2.152)$$

This equation is, of course, valid both for adiabatic and non-adiabatic motion.

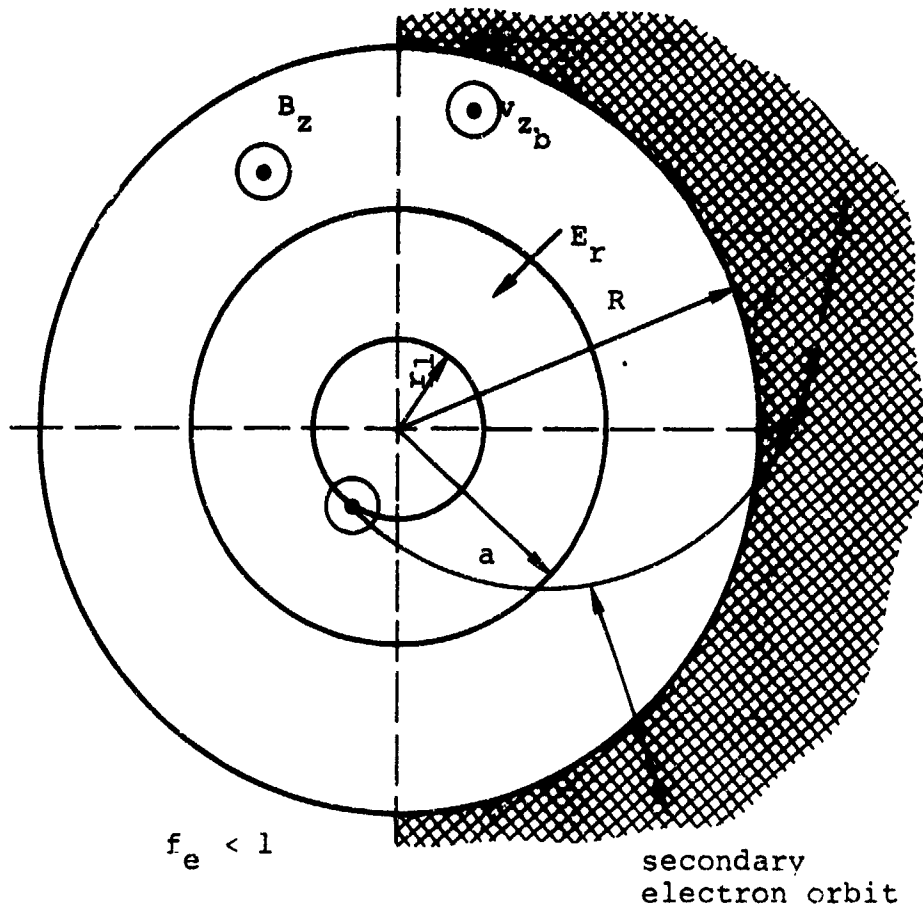
If electrons enter the penetration front into the region where  $f_e < 1/\gamma_L^2$  the rotational volume beam theta currents shift from paramagnetic to diamagnetic rotation [see Equation (2.142)] and electrons are displaced radially outward as they reflect. Upon returning to the diode, the rotation due to  $B_\theta (z < z_2)$  is now diamagnetic. If electrons are also electrostatically plugged at the diode, particle loss occurs when diode voltage begins to drop. Even if the beam front has reached the end of the transport system and  $V \approx 0$  throughout the channel, the mirror geometry resulting from tied field lines at the end of the transport system with a net diamagnetic channel will reflect

electrons because of energy loss  $\Delta E$ . (An energy loss of  $\sim 100$  keV/m would occur with a  $10^5$  A/cm<sup>2</sup> beam with  $\sigma \approx 100$  mhos/cm, corresponding to a fully ionized plasma of a few volts temperature.) When a substantial fraction of beam electrons are reflected near the penetration front, the front velocity  $B_f^P c$ , is more appropriately calculated by a pressure balance argument similar to the linear pinch penetration process:

$$\frac{(\Delta B_z)^2}{8\pi} \approx \frac{\eta_e}{2} m_o \left[ \langle \beta_{Lc} - (\beta_{fc}^P) \rangle \right]^2 \quad (2.153)$$

where  $\eta_e$  is the average reflected electron density and  $\beta_{Lc}$  is the average incident electron velocity.

Plasma Theta Currents. Beam-induced plasma theta currents will be diamagnetic with the exceptions of (1) those induced by  $E_\theta$  when the beam is diamagnetic and (2), under appropriate conditions, those due to axial rotation of electrons reflected from the diode by electrostatic plugging. We neglect the latter plasma theta currents in our discussion; they would only be important in low density plasmas or with very high  $B_z$  fields. The characterization of the volume plasma theta current before electrical neutralization for neutral gas injection may be quite different than without  $B_z$  fields. Our previous assumption (Section 2.4) that secondary electrons escape "instantaneously" from the beam channel to the chamber wall until  $f_e = 1$  is not a good approximation with high  $B_z$  fields. We use a simple model to determine limits on  $B_z$  for escape of secondaries to the chamber wall at radius  $R$ . The turning radius,  $r_t$ , must be larger than the chamber radius,  $R$ . Referring to Figure 2.42, and assuming negligible diamagnetism, Busch's theorem (Equation 2.92) states



$r_1$  = radius at which secondary is created by collisional ionization  
 $a$  = beam radius

Figure 2.42 Cross section of beam chamber showing secondary electron orbits when  $r_t \geq R$

$$\dot{\theta} \equiv \omega(r) = \frac{\omega_L}{\gamma(r)} \left[ 1 - \left( \frac{r_1}{r} \right)^2 \right] \quad (2.154)$$

$$\omega_L \equiv \frac{eB_z}{2 m_0 c}$$

when  $\dot{\theta} = v_r = v_z = 0$  at  $r = r_1$  (electron birth). If we further assume that the space charge field is primarily radial and due to a beam of uniform charge density,

$$\gamma(r) = 1 + 2v_b (1-f_e) \left[ \frac{a^2 - r_1^2}{2a^2} + \ln \frac{r}{a} \right], \quad r > a \quad (2.155)$$

$v_b$  = primary beam  $v$

Combining Equations (2.154) and (2.155), and taking  $\beta \approx \beta_\theta$  at  $r = r_t$ ,

$$\frac{\omega_L^2}{c^2} = \frac{[\gamma(r_1, r_t)]^{2-1}}{G(r_1, r_t)} \quad (2.156)$$

$$G \equiv r_t^2 \left[ 1 - \left( \frac{r_1}{r_t} \right)^2 \right]^2$$

We use  $r_1 \approx 0$  in Equation (2.156) for a representative secondary electron orbit; we could insure that all secondary electrons escape, e.g., by evaluating  $G$  at  $r_1 = 0$  and  $\gamma$  at  $r_1 = a$ . Equation (2.156) gives

$$\frac{\omega_L^2 R^2}{c^2} \lesssim \left[ 1 + 2v_b (1-f_e) \left( \frac{1}{2} + \ln R/a \right) \right]^2 - 1 \quad (2.157)$$

or

$$B_z \text{ (gauss)} \lesssim \frac{17,000 \text{ (amps)}}{5R} \left\{ \left[ 1 + 2v_b (1-f_e) \left( \frac{1}{2} + \ln R/a \right) \right]^2 - 1 \right\}^{\frac{1}{2}}$$

$r_t \geq R$

This equation can be expressed in a form more appropriate for neutral gas penetration, where  $f_e$  is increasing behind the front. Electrical neutralization will occur via secondary electron escape to the wall until

$$v_b (1-f_e) \lesssim \frac{1}{(1 + 2 \ln R/a)} \left[ \left( \frac{\omega_L^2 R^2}{c^2} + 1 \right)^{\frac{1}{2}} - 1 \right]$$

$r_t \geq R$  (2.158)

If the beam current in the penetration front is space charge limited (Equation 2.149),

$$(\gamma - 1) \lesssim \left( \omega_L^2 \frac{R^2}{c^2} + 1 \right)^{\frac{1}{2}} - 1$$

} (2.159)

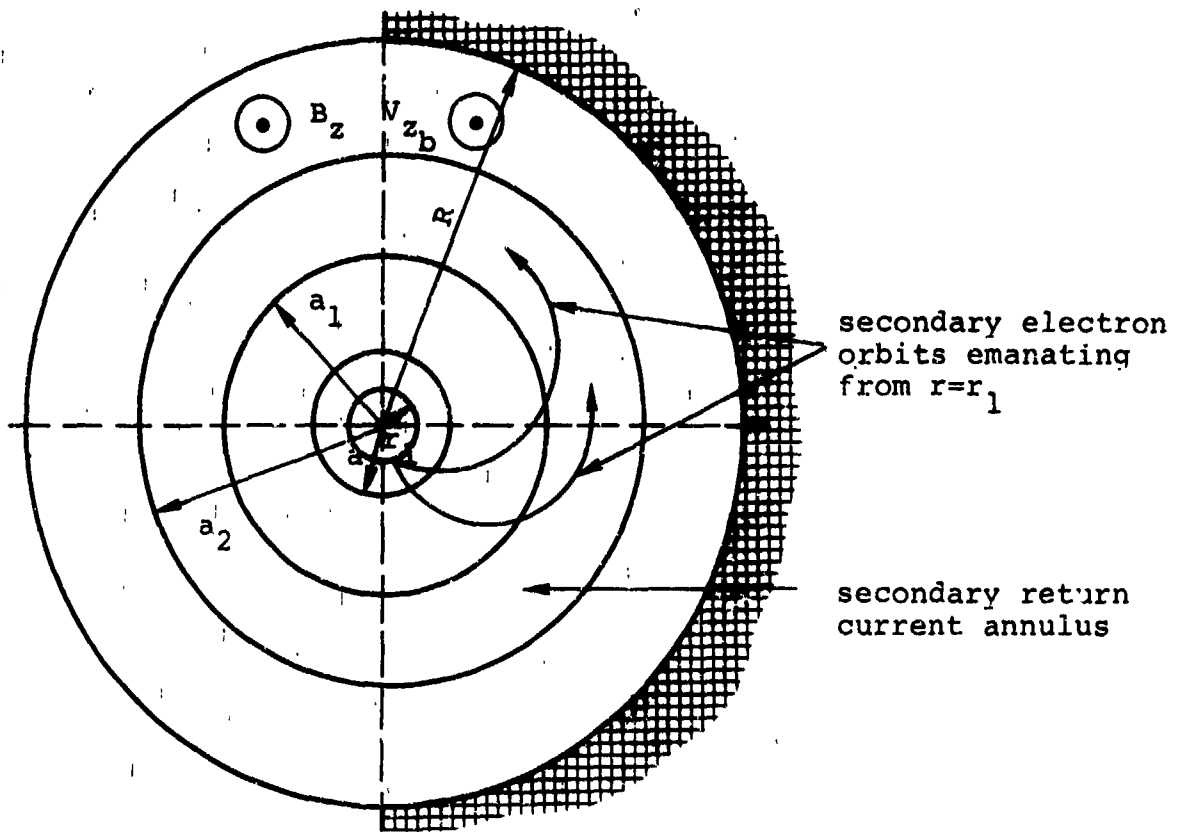
or

$$B_z \text{ (gauss)} \lesssim \frac{17,000 \text{ (amps)}}{5R} \sqrt{\gamma^2 - 1}$$

When  $B_z$  exceeds the limit of Equations (2.157) or (2.159), or if  $v_b (1-f_e)$  satisfies (2.158), secondary electrons will no longer escape to the wall. In a similar fashion we can then determine upper  $B_z$  or lower  $v_b (1-f_e)$  limits such that  $a \leq r_t \leq R$ , as depicted in Figure 2.43:

$$B_z \text{ (gauss)} \lesssim \frac{17,000 \text{ (amps)}}{5a} \left\{ [1 + v_b (1-f_e)]^2 - 1 \right\}^{\frac{1}{2}}$$

$a \leq r_t \leq R$  (2.160)



$a_1$  = inner radius of secondary electron beam  $\geq a$   
 $a_2$  = outer radius of secondary electron beam  $\leq R$   
 $a$  = beam radius

Figure 2.43 Cross section of beam chamber showing secondary electron orbits when  $a \lesssim r_t \lesssim R$ .

or in other words, an annular secondary electron "beam" with inner radius  $> a$  is formed until

$$\begin{aligned} v_b (1-f_e) &\lesssim \left( \frac{\omega_L^2 a^2}{c^2} + 1 \right)^{\frac{1}{2}} - 1 \\ &= \left[ \left( \frac{5aB_z}{17,000} \right)^2 + 1 \right]^{\frac{1}{2}} - 1 \end{aligned} \quad (2.161)$$

As an example of the above equations, let us take  $B_z = 3$  kG,  $a = 2.5$  cm, and  $R = 10$  cm. Equations (2.158) and (2.161) give

$$\begin{aligned} r_t &\geq R, & v_b (1-f_e) &\gtrsim 2.6 \\ a \leq r_t &\leq R, & 2.4 \leq v_b (1-f_e) &\lesssim 2.6 \end{aligned}$$

When an annular return current "beam" is formed, the secondaries in turn ionize the background gas, creating additional secondaries which are then expelled outward to the wall unless  $B_z$  exceeds a value of the order  $17,000/5 (R-a_2)$ , where  $a_2$  is the outer radius of the annular return current beam. The neutralization process for this range of  $v_b (1-f_e)$  and lower values is thus of a cascade type. At still higher  $B_z$  levels, or as  $f_e$  continues to increase, not all secondaries will leave the beam channel, and we expect the radial electric field to increase again if the beam current is still increasing.\* Therefore, at lower gas pressures where breakdown does not occur early in the pulse, or, if the perpendicular conductivity after breakdown is low and the beam current continues to rise substantially

\* Even if  $f_e \approx 1$ , at some point during the beam current rise, a space charge field may still be generated until the current reaches its peak value.

after breakdown, the net  $z$  current may exhibit oscillation due to the re-establishment and neutralization of space charge fields. (Recall that the  $E_z$  space charge field opposes the inductive field during the beam current rise.) A summary sketch of the radial motion of secondary electron currents generated by space charge fields is shown in Figure 2.44.

Finally, we come to the case when  $B_z$  is sufficiently large that  $r_t < \text{skin depth} \approx c/\omega_p$ ,  $\omega_p$  the plasma frequency. We see from Equation 2.156 that  $(\omega_L/\omega_p)^2 \gg$  terms of order unity to entirely prevent space charge neutralization. Lee and Sudan (Reference 2.64) have considered the current neutralization problem for an undistorted, non-rotating beam penetrating an infinite plasma with a frozen-in  $B_z$  field. Their criterion for destruction of current neutralization is  $\omega_L^2/\omega_p^2 \gg 1$ ; the physical basis of this criterion is apparent from our model. Whether in fact current neutralization may be completely eliminated in a finite system is not clear. The EM cavity model (Section 2.2) showed that in a long tube away from the endplate,  $E_z$  is indeed in a direction to accelerate beam electrons when  $f_e \lesssim 1/2 \gamma^2$ . In a finite system, however, the chamber endplate would cause generation of a large  $E_z$  field to drive a return current even when  $f_e \approx 0$ . So it appears that substantial current neutralization might occur in a finite system without charge neutralization if  $B_z$  is large enough. In fact, one expects that the space charge limit of Eq. (2.149), with  $v$  replaced by  $v_{\text{net}}$ , would give an upper bound on the net current.

We can now estimate the plasma volume theta currents,  $j_{p\theta}$ , induced by space charge fields. To do this we need the secondary electron charge density,  $\rho_p$ , as a function of radius and  $\omega(r)$ :  $j_{p\theta} = \rho_p(r) r\omega(r)$ . The charge density can be evaluated explicitly from radial force balance and Poisson's equation. The first case we consider is a  $\leq r_t \leq R$  for all secondary electrons.

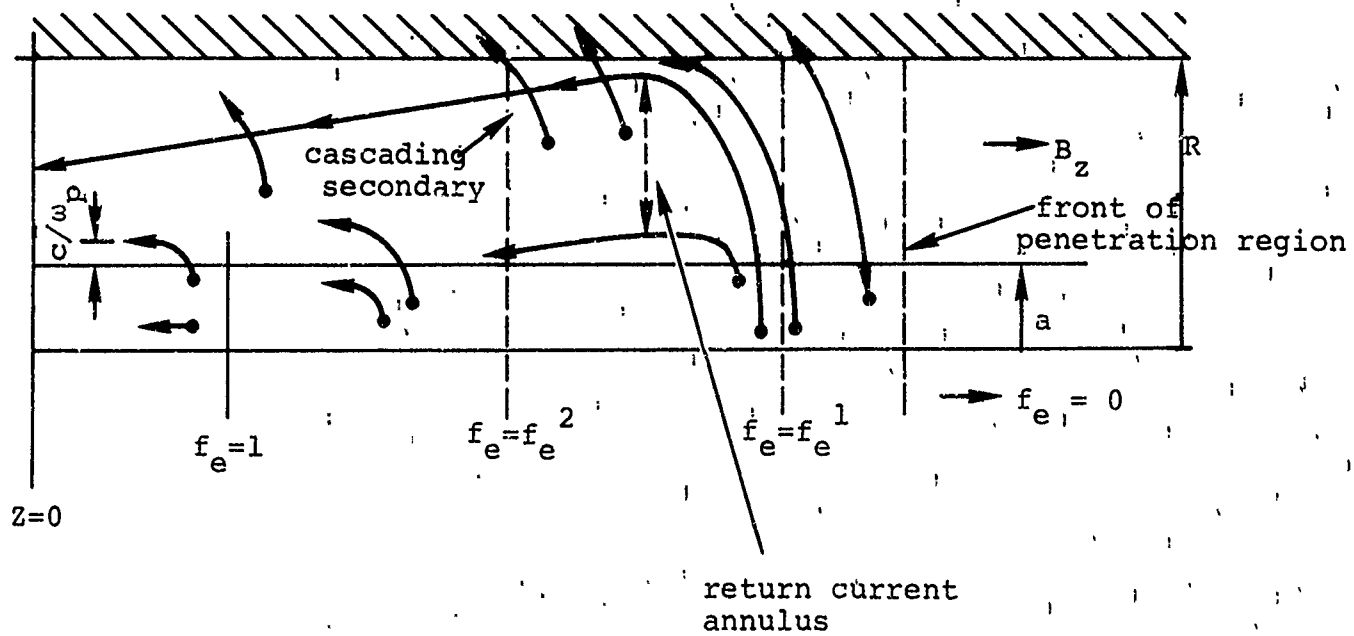


Figure 2.44 Secondary electron return currents at various stages of electrical neutralization with  $B_z$  fields

$$\begin{array}{ll}
 v_b (1-f_e^1) & \rightarrow \quad r_t \geq R \\
 v_b (1-f_e^2) & \rightarrow \quad a \leq r_t \leq R
 \end{array}$$

$$\rho_p(r, r_1) \approx -\delta/4\pi \left[ \frac{2m_0}{e} \omega_L^2 \left( 1 + \left( \frac{r_1}{r} \right)^4 \right) \right]$$

$\delta$  = normalization factor

The determination of  $\delta$  can be obtained from

$$\int_{a_1}^{a_2} dr' \cdot \left\{ \underbrace{\int_0^a \rho_p(r', r_1) dr_1}_{\rho_p(r')} \cdot 2\pi r_1 \right\} = f_e \lambda_b$$

$\lambda_b$  = beam charge/length.

Equation (2.154) determines  $\omega(r)$ . Rather than proceeding with this straightforward, but tedious, evaluation, we shall estimate  $j_{p\theta}$  assuming negligible radial variation in  $\rho_p(r')$ :

$$\rho_p \approx \frac{f_e \lambda_b}{\pi(a_2^2 - a_1^2)}$$

an approximate expression for  $\omega(r)$  can be obtained from Equation (2.154) by averaging  $r_1$  over the beam radius. The field exclusion interior to the plasma return current,  $\Delta B_z$ , is then

$$\Delta B_z \approx \frac{4\pi}{c} \gamma \int_{a_1}^{a_2} \frac{f_e \lambda_b}{\pi(a_2^2 - a_1^2)} \omega_L \left( 1 - \frac{a^2}{3r^2} \right) r dr$$

$$a < a_1, a_2 < R$$

Rewriting the above equation, we obtain

$$\frac{\Delta B_z}{B_z} \approx 2 f_e \frac{(v_b)}{\gamma} \left[ 1 - \frac{2}{3} \frac{a^2}{\pi(a_2^2 - a_1^2)} \ln a_2/a_1 \right]$$

$$a < a_1, a_2 < R \quad (2.162)$$

The upper limit on  $f_e$  in Equation (2.162) is given by Equation (2.161), and  $a_2$  is determined by (2.156). The equation is strictly valid only if  $\Delta B_z/B_z \lesssim 0.1$ , since we have assumed a constant  $B_z$  field in its derivation. The space charge limit on  $v_b$  in Equation (2.162) is

$$\frac{v_b}{\gamma-1} < [F(f_e, f_{er}, a, a_2, R)]^{-1} \quad (2.163)$$

where

$$F \equiv (1-f_e)(1 + 2 \ln R/a) + 2f_e (1-f_{er}) \ln R/a_2$$

$$+ f_e (1-f_{er})$$

$f_{er}$  = fractional electrical neutralization of the return current channel.

When  $f_e$  exceeds the limit of Equation (2.161) and  $r_t \ll a$  for most secondary electrons, plasma theta currents can be estimated by assuming that the plasma return current channel is nearly coextensive with the beam channel, but displaced by a skin depth,  $c/\omega_p$ . In this case, secondaries created by further ionizing collisions essentially form a hollow Brillouin-type annular beam with the beam edge as a cathode and with radial thickness inversely proportional to  $B^2$  and  $(\gamma - 1/2)^{1/2}$ . Classical

space charge flow theory for hollow Brillouin beams shows that their diamagnetism is at most a few percent (Reference 2.1).

We have argued above that the radial electric field of partially compensated beams can generate substantial diamagnetic plasma currents and that return current electrons in general may have energies comparable to the primary beam. The space charge diamagnetism may greatly exceed classical space charge flow diamagnetism because of partial charge compensation behind the penetration front. In order to achieve efficient beam transport, the space charge fields must, of course, be rapidly shorted out ( $\tau_N \ll t_r$ , the beam risetime). At pressures such that  $\tau_N \lesssim 2\pi/\omega_C$ , the plasma electrons non-adiabatically pass through the space charge front and it seems reasonable to assume that their diamagnetic volume theta currents are essentially determined by  $B_\theta^{\text{net}}$ . If  $\tau_N \gg 2\pi/\omega_C$  the transition will be adiabatic and the volume theta currents will also be determined by  $B_\theta^{\text{net}}$  beyond  $f_e \approx 1$ .

The diode flow model which we have previously given, together with similar arguments for plasma currents, allow us to determine the net  $\Delta B_z$ ,  $\Delta B_z^T$ , of the beam channel for  $\tau_N \lesssim t \lesssim t_B$ . The only paramagnetic contribution to  $\Delta B_z$  in general is the volume beam theta current after  $f_e > 1/\gamma_L^2$ .

We obtain

$$\begin{aligned} \Delta B_z^T(r) &\equiv B_z(r) - B_z^i \\ &\approx \frac{2\pi n_b}{c} e\omega_b (a^2 - r^2) - \frac{2\pi n_p}{c} e\omega_p (a^2 - r^2) \\ &+ \left\{ (B_z^i)^2 - 8\pi \left[ n_b W_{\perp cb}(r) + n_p W_{\perp cp}(r) \right] \right\}^{\frac{1}{2}} - B_z^i \end{aligned} \quad (2.164)$$

where the b(p) subscripts refer to beam (plasma) quantities and  $W_{\perp c}$  is the perpendicular gyrotational energy. We rewrite Equation (2.164):

$$\begin{aligned} \Delta B_z^T(r) &\approx \frac{\pi^2}{25} \frac{j_b^2}{B_z^2} (1 - f_m)^2 (a^2 - r^2) + \left\{ (B_z^i)^2 - 10^3 \langle \beta_L \rangle j_b [\gamma_b g(r) \right. \\ &\quad \left. + \gamma_p \left( \frac{n_b}{n_p} \right) f_m \sin^2 \alpha(r)] \right\}^{\frac{1}{2}} - B_z^i, \\ &\tau_N \leq t < t_B \end{aligned} \quad (2.165)$$

with

$f_m$  = fractional magnetic neutralization

$\langle \beta_L c \rangle$  = average longitudinal beam velocity

$g \equiv \frac{\tan^2 \langle \delta \rangle}{\cos^2 \alpha(r)}$  for a non-adiabatic anode transition

$\equiv \tan^2 \alpha(r)$  for an adiabatic transition

$\langle \delta \rangle$  is the average scattering angle with respect to  $\vec{B}^{\text{net}}$

$$\tan \alpha(r) = \frac{B_{\theta}^{\text{net}}(r)}{B_z}$$

$$\gamma_p = (1 - \langle \beta_p \rangle^2)^{-\frac{1}{2}}$$

$$\langle \beta_p \rangle \approx \beta_L \left( \frac{n_b}{n_p} \right) f_m$$

The beam current density  $j_b$  is in A/cm<sup>2</sup>,  $B_z$  in gauss. A "strong" sensitivity to the current density and degree of magnetic neutralization is exhibited by Equation (2.165). As an example of the equation, let us take  $f_m \approx 0.1$ ,  $B_z^i \approx 5$  kilogauss,  $j_b = 5 \times 10^3$  A/cm<sup>2</sup> and  $g = 0.25$ . Then Equation (2.165) gives  $\Delta B_z(r=0) = 1.6$  kilogauss and the beam channel is net paramagnetic. On the other hand, if we inject the same beam into a preionized highly conducting plasma so that  $f_m \approx 1$ , Equation (2.165) states that the channel will be diamagnetic with  $\Delta B_z(r \approx a) \cong (-) 200$  gauss. Our estimates have, of course, neglected space charge induced diamagnetism under the assumption that  $\tau_N \lesssim 2\pi/\omega_c$ . Finally, we note that when  $f_m \rightarrow 1$ , the anode window transition may be important in determining the nature of the channel  $\Delta B_z$ .

A rough criterion to ensure a net diamagnetic channel may be obtained following arguments used in the derivation of Equation (2.146). A more general version of this equation appropriate for a non-adiabatic transition at the anode window is

$$\frac{\Delta B_z^d (2B_z^i - \Delta B_z^d)}{(\Delta B_z^p)^2} \approx \left( \frac{v_{lc}}{v_{lr}} \right)^2 \left( \frac{\gamma}{v} \right) \approx \left( \frac{\gamma}{v} \right) \frac{\tan^2 \delta}{\sin^2 \alpha} \quad (2.166)$$

Thus, a sufficient criterion for dominant channel diamagnetism under the assumption that guiding centers follow field lines is

$$\tan \delta \gg \sqrt{\frac{\gamma}{v}} \sin \alpha(a) \quad (2.167)$$

The remaining task for completion of our discussion of  $B_z$  transport phenomenology is to couple  $\Delta B_z$  to beam energy loss. The method is analogous to the  $B_\theta$  discussion with z-currents, only now we additionally include  $E_\theta$  and  $dB_z/dt$ . We explicitly consider only one case; namely, when  $\Delta B^T \approx B_z$  is diamagnetic and dominated by the surface currents associated with gyrorotation. The theta electric field is then:

$$E_\theta \text{ (V/cm)} \approx - \frac{5r\Delta B_z}{\Delta t \text{ (nsec)}} \quad (2.168)$$

A rough criterion for the validity of previous calculations of  $\Delta B_z$  where  $E_\theta$  was neglected is

$$E_\theta \text{ (2}\pi a) \ll \frac{(\gamma-1)}{2} (10^6) \quad (2.169)$$

or

$$\Delta B_z \text{ (gauss)} \ll \frac{10^4 (\gamma-1)}{a^2} \Delta t \text{ (nsec)}$$

and  $\tau_N \lesssim \Delta t \leq t_B$ , the breakdown time, for diamagnetism near the beam penetration front. After breakdown the plasma currents are collisionally dominated and in a direction to oppose further changes in  $B_z$ . Then  $E_\theta$  may be estimated from

$$E_\theta \approx \frac{j_{b\theta}(t) - j_{b\theta}(t_B)}{\sigma_l} \quad (t > t_B) \quad (2.170)$$

The radial drift velocity of the beam-plasma system across  $B_z$  lines for the case of a highly ionized plasma after breakdown is approximately:

$$v_r \text{ (cm/nsec)} \approx \frac{E_\theta \text{ (V/cm)}}{10 B_z \text{ (gauss)}} \quad (2.171)$$

Conditions for Efficient Transport with  $B_z$  Fields. Our discussion has related beam and plasma induced changes in  $B_z$  to space charge fields ( $f_e$ ) and the self-magnetic fields ( $f_m$ ), and indicated the coupling between these parameters and energy loss due to  $\Delta B_z$ . The models showed that when  $f_e < 1/\gamma_L^2$  the beam channel will be net diamagnetic (low pressure propagation) and when  $f_e \sim 1$ , the channel will be paramagnetic unless  $f_m \approx 1$ . The complications of the general transport problem with  $B_z$  can be largely circumvented in outlining conditions for efficient transport in neutral gases. The arguments are very like those regarding current neutralization without  $B_z$ , except that we additionally require the transverse conductivity after breakdown to be high. Then  $\Delta B_z$  is small and losses due to  $E_\theta$  are minimized, and space charge relaxation of the beam may proceed after breakdown with increasing beam current. The model essentially defines conditions for validity of single particle beam orbit theory.

Recall from Section 2.5 that the perpendicular conductivity for a Lorentz plasma (electron/neutral collisions or negligible ion motion) is

$$\sigma_\perp \approx \sigma_\parallel \left[ \frac{1}{1 + (\bar{\omega}_c/v)^2} \right] \quad (2.172)$$

where  $\sigma_\parallel$  is the parallel conductivity,  $v$  is the effective collision frequency, and  $\bar{\omega}_c$  is the cyclotron frequency associated with the  $B_z$  field at breakdown. To minimize net theta currents, we desire  $\sigma_\perp$  large ( $\approx \sigma_\parallel$ ) in the sense that

$$t_{d_\perp} \approx \frac{4\pi\sigma_\perp a^2}{c^2} \gg t_p \quad (2.173)$$

where  $t_p$  is the beam pulse width. This condition translates to:

1.  $\sigma_{\parallel}$  large at breakdown (or injection with preformed plasmas)
2.  $\bar{\omega}_c/\nu < 1$

If we assume the plasma nearly fully ionized ( $\nu = \nu_{e,i}$ ) the requirements  $\bar{\omega}_c/\nu < 1$  is

$$\bar{B}_z \lesssim 3 \times 10^{-12} \frac{n_p}{T_e^{3/2}} \quad (2.174)$$

where  $\bar{B}_z$  is the  $B_z$  field value at breakdown. Thus, if we assume a fully ionized plasma at 1 torr,  $T_e \sim 5$  volts,  $\bar{B}_z \lesssim 9$  kG, a value close to the level above which Stallings observes a decrease in transport efficiency (Figure 2.45). Whether or not this criterion is in fact relevant to his data depends, of course, on the plasma parameters. Our guess above appears reasonable in view of the minimum requirements on  $\sigma_{\parallel}$  for the high transport efficiency at the optimum transport field. Equation (2.174) is in general a more severe constraint on the maximum  $B_z$  field than the Lee and Sudan result,  $(\omega_c/\omega_p)^2 < 1$ . Also, the condition is independent of whether the channel is net diamagnetic or paramagnetic.

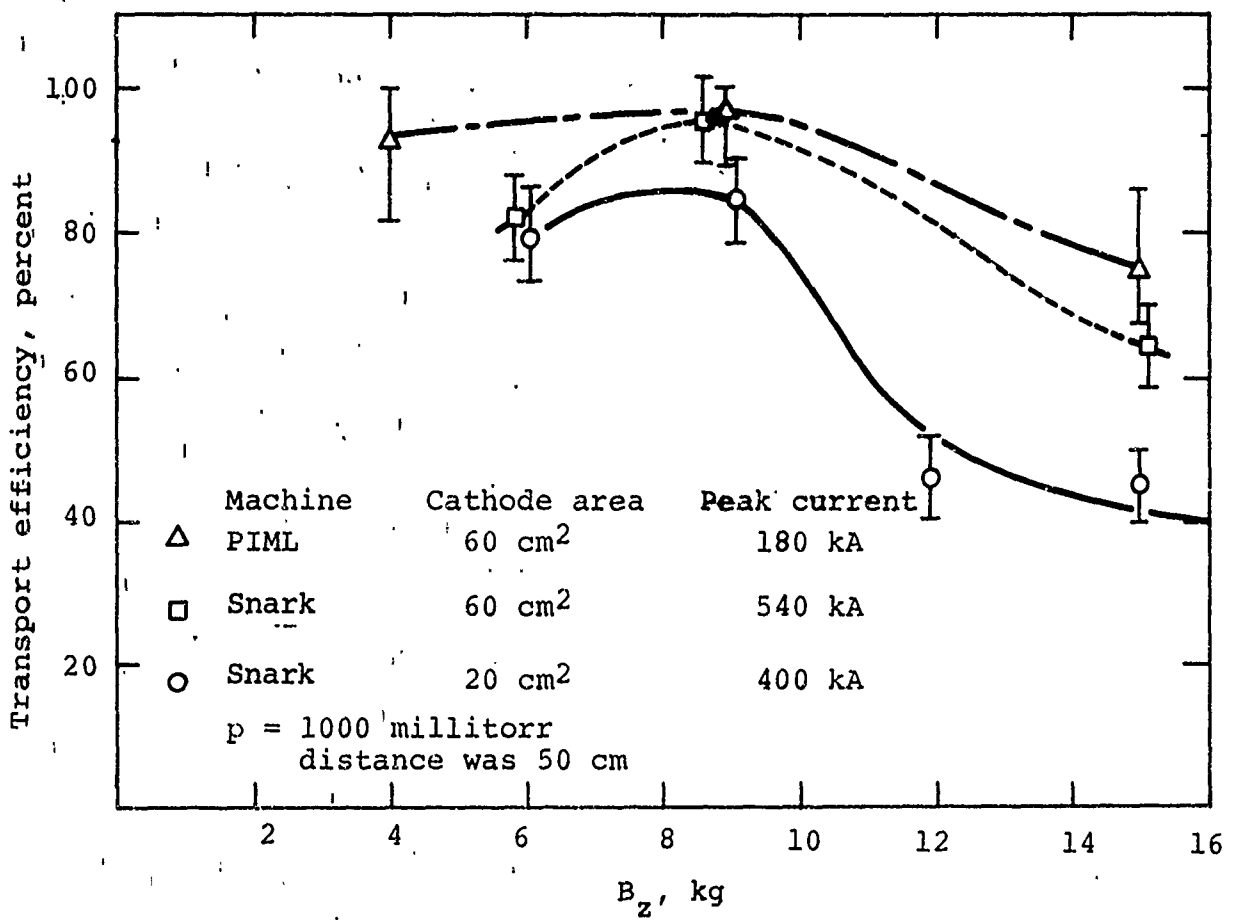


Figure 2.45 Charge transport efficiency at 1/2 meter for three current densities.

## 2.11 PLASMA HEATING

Plasma heating and/or confinement using intense relativistic electron beams and their associated electric and magnetic fields is a relatively new interest of the plasma physics community and both the experimental and theoretical work to date in this area is rather preliminary. The major direction of intense beam technology in the past has been in the areas of efficient transport of beams of controlled energy density; beams have merely provided an energy source for X-ray production or material response studies with rapid energy deposition. Substantial plasma heating would correspond to poor beam transport and has therefore not been of interest.

Electron beam accelerator technology has advanced to the point where beams exist or are within the state of the art with total energies from kilojoules to several megajoules and with electron energies from tens of kilovolts to 20 MeV. Thus beams represent an interesting energy source for direct or supplemental heating of plasmas. Also, these beams may be used to collectively accelerate ions (deuterons) giving several kilojoules of ion energy plasma heating. Another application has recently been suggested by Yoshikawa (Reference 2.35). He proposes using a force-free beam equilibrium distribution to generate strong magnetic fields for plasma confinement--analogously to use of superconducting rings.

There are, of course, several aspects of potential plasma heating schemes which affect the nature of the optimum beam and the problem areas with respect to present day technology. For example, if we desire to heat a confined plasma for controlled thermonuclear reactor (CTR) application, the question arises

whether the beam is to be internally or externally generated. An externally generated beam immediately confronts us with an injection problem, whereas an internally generated beam is probably more severely energy limited than an external beam, assuming inductive acceleration. (Use of electrodes in a low density CTR confinement system would present plasma contamination problems.) The injection problem appears difficult but feasible. The Astron field configuration, e.g., is designed to accept and trap a relativistic beam of relatively low current (kiloampere) from our point of view. An intense, pulsed beam must necessarily extract an equal plasma return current from the confinement system to avoid buildup of large space charge fields, and although the net current may be very small, injection could result in a serious distortion of the magnetic field configuration simply to allow the return current to flow out the beam channel.

The problem areas are quite different for heating high  $\beta$ , high density plasmas with limited or no confinement. Such plasmas would be of more interest as intense radiation and neutron sources than for power production. [Recent calculations by Eden and Saunders (Reference 2.65) have estimated  $\sim 10^9$  joules trigger energy to give useful energy return.] Since plasmas with densities in the  $10^{19}$  to  $10^{20}/\text{cm}^3$  range and temperatures of 1 to 10 keV require (pulsed) megagauss fields for even partial containment, and therefore are limited to times at most of the order of 100 nsec, beam energy deposition rate is a dominant consideration. The dense plasma focus (DPF), e.g., is a plasma with limited confinement (50 to 100 nsec) and Mather and Rostoker (Reference 2.66) and Friewald, et al. (Reference 2.67) have recently performed initial studies on electron beam enhancement of DPF plasma heating. Beam injection into the large magnetic fields of the DPF is also a major problem here. D-T pellet

ignition with electron beam triggering and with no external confinement fields has been proposed by Winterberg (Reference 2.68) and further studied recently by Babykin, et al. (Reference 2.69). The major beam problem is achieving the required power densities; current densities of  $10^8$  to  $10^9$  A/cm<sup>2</sup> appear to be necessary. The present state of the art for relativistic beams is  $\sim 10^5 - 10^6$  A/cm<sup>2</sup>.

A beam plasma heating technique currently under study is turbulent heating of low density ( $\sim 10^{14}$ /cm<sup>2</sup>) plasmas. Altyntsev, et al. (Reference 2.70) have injected a 4 MeV, 15 kA, 50 nsec beam into a plasma with a solenoidal field and report electron temperatures from 10 to 100 keV at densities from  $10^{11}$  to  $10^{14}$ /cm<sup>3</sup>. We consider turbulent heating in detail in the next section.

2.11.1 Turbulent Plasma Heating. A considerable effort has been devoted to the study of turbulent heating and anomalous resistance effects in discharge plasmas (Reference 2.71). Recently several investigators have looked at turbulent heating using relativistic electron beams (Reference 2.72). Basically, all these efforts are directed toward enhancing the energy deposition rate over the Coulomb collisional transfer rate. The importance of doing so can be seen by looking at the single electron stopping power,  $dE/dx$ , in a plasma. For electrons (test particles) moving at velocities in excess of the plasma electron thermal velocity,

$$dE/dx = \frac{Z^2 \omega_p^2 e^2}{2\pi\beta^2 c^2} L \quad (2.175)$$

where  $\omega_p$  is the plasma frequency,  $\beta c$  is the incident electron velocity,  $L$  is the Coulomb logarithm (Reference 2.73), and  $Z$  is the charge state of the plasma ions.

Prentice (Reference 2.74) has evaluated  $L$  numerically for relativistic electrons (and relativistic plasmas) including effects due to excitation of longitudinal and transverse plasma waves. Taking  $Z = 1$ ,  $T_e \cong 5$  keV,  $n_p = 10^{19}$  cm<sup>3</sup>, he obtains  $dE/dx \sim 15$  eV/cm for a 1 MeV electron. At  $n_p \sim 10^{15}$ /cm<sup>3</sup>, (CTR plasma density),  $dE/dx \cong 1.5 \times 10^{-3}$  eV/cm so the 1 MeV electron range would be  $\sim 10^9$  cm.\* If we consider many electrons or a beam, this range is reduced many orders of magnitude by collective effects. The longitudinal electric field driving the plasma return current after gas breakdown is in the 100 V/cm range, depending on the plasma conductivity and current density, and 1 MeV electrons are now stopped over  $10^4$  cm with a Coulomb conductivity ( $\nu = \nu_{e,i}$ ). If one injects into appropriate plasma densities, we may reduce this collective range orders of magnitude further by inducing longitudinal electrostatic instabilities. The plasma conductivity is now lowered by an effectively higher collision frequency due to instability wave-particle scattering.

As discussed in Section 2.8.1, the beam may generate electron-ion modes (plasma return currents) or electron-electron modes (beam and plasma electrons); i.e., plasma electrons may scatter off plasma electron-plasma ion waves or plasma electron-beam electron waves, or both. Let us consider a possible heating sequence in a beam-plasma system with return current equal to the beam current.

For simplicity assume a hydrogen plasma, fully ionized at injection, with an electron temperature  $T_e \cong 1$  volt. The heating process will start with the Buneman mode if  $v_d \gtrsim v_{te}$ . (We use the same notation as in Section 2.8.1). This requirement is satisfied if

$$T_e \lesssim 10^{22} (j_p/n_p)^2 \quad (\text{Buneman mode}) \quad (2.176)$$

\* The classical electron range amounts to energy transfer to plasmas well within the Lawson fusion feasibility criterion:  $n_p \tau \gtrsim 10^{14}$  cm<sup>-3</sup> sec.

with  $j_p$  = plasma return current density (A/cm<sup>2</sup>),  $n_p$  = plasma density (cm<sup>-3</sup>), and  $T_e$  in eV. The heating rate/volume, ( $j_p^2/\sigma$ ) may be determined from

$$\frac{d}{dt} \left[ \frac{n_p m_e v_d^2}{2} + \frac{n_p 3kT_e}{2} \right] \approx j_p^2 / \sigma_{\text{eff}} \quad (2.177)$$

where  $\sigma_{\text{eff}}$  is the anomalous conductivity equaling  $\omega_p^2 / 4\pi I / \nu_{\text{eff}}$  (sec<sup>-1</sup>), and  $\nu_{\text{eff}}$  is the 90 degree scattering time for electrons off ES instability waves. Equation (2.177) assumes that the plasma electrons are thermalized "instantaneously."\* The Buneman mode corresponds to  $v_d \gtrsim v_{te}$  so we assume that the streaming and thermal energies are approximately equal, giving

$$\frac{d}{dt} T_e \text{ (eV)} \approx 7.4 \times 10^{21} \left( \frac{j_p}{n_p} \right)^2 \nu_{\text{eff}}^B \text{ (Buneman)} \quad (2.178)$$

where  $j_p$  = plasma current density (A/cm<sup>2</sup>)

$n_p$  = plasma density (cm<sup>-3</sup>)

$\nu_{\text{eff}}^B$  = Buneman mode collision frequency

$$\approx \frac{\omega_p}{2\pi} \left( \frac{m_e}{m_i} \right)^{1/3}$$

For a hydrogen plasma,  $\nu_{\text{eff}}^B \approx 500 \sqrt{n_p}$ . Substituting in Equation (2.178), we obtain

$$\begin{aligned} T_e(t) &\approx 7.4 \times 10^{21} \left( \nu_{\text{eff}}^B / n_p^2 \right) \int_{t_0}^t j_p^2(t') dt' \\ &\approx \frac{3.7 \times 10^{24}}{n_p^{3/2}} \int_{t_0}^t j_p^2(t') dt' \end{aligned} \quad (2.179)$$

\* Recall that the electron-electron collision frequency is  $1836 \nu_{e,i}$ .

until  $T_e(t) = (j_p/n_p)^2 \times 10^{22}$ .

The heating rate will slow down when Equation (2.176) is no longer satisfied as the ion-acoustic transition occurs when  $C_s < v_d < v_{te}$ . The ion sound speed is denoted by  $C_s \approx \sqrt{kT_e/m_i}$ . In a hydrogen plasma, we now require  $T_e \lesssim (43) 10^{22} (j_p/n_p)^2$ . We neglect the drifting energy to obtain a heating rate for the ion-acoustic mode:

$$\frac{dT_e(\text{eV})}{dt} \approx 1.5 \times 10^{22} (j_p/n_p)^2 v_{\text{eff}}^{\text{IA}} \quad (2.180)$$

The units are the same as for Equation (2.159) and  $v_{\text{eff}}^{\text{IA}}$  is the effective collision frequency for ion-acoustic wave scattering.

The form of  $v_{\text{eff}}^{\text{IA}}$  suggested by Sagdeev is (Reference 2.75)

$$v_{\text{eff}}^{\text{IA}} \approx 10^{-2} \frac{T_e}{T_i} \left( \frac{v_d}{v_{te}} \right) \omega_p, \quad T_e > T_i \quad (2.181)$$

$$v_d < v_{te}$$

Other authors propose different forms and some experimental data appear to agree with all of these various forms (Reference 2.76). Guillory and Benford (Reference 2.42) have looked at the transition region between Buneman and ion-acoustic modes using a Lorentzian plasma electron velocity distribution and use an "optimistic" value for hydrogen:

$$v_{\text{eff}} \approx \frac{(0.055)}{1 + 5.9 v_{te}/v_d} \omega_p \quad (2.182)$$

They obtain Equation (2.182) by assuming  $v_{\text{eff}} \approx$  maximum instability growth rate.

A lower limit on the plasma density for return current anomalous heating follows from our assumption that  $j_p \approx -j_b$ , which requires the magnetic diffusion time,  $t_d$ , be long compared to the beam pulse width,  $t_p$ . If we take  $t_d \gtrsim 2t_p$ ,

$$\sigma (\text{sec}^{-1}) > \frac{4.5 \times 10^{11} t_p}{\pi a^2} \quad (2.183)$$

with  $t_p$  in nsec and the beam radius,  $a$ , in centimeters. Equations (2.178) and (2.181) indicate that  $v_{\text{eff}} \propto \omega_p$ , so  $\sigma \propto \sqrt{n_p}$ . The Buneman mode, for example, requires

$$n_p \gtrsim 1.75 \times 10^{12} \left( \frac{t_p}{\pi a^2} \right)^2 \quad (2.184)$$

A final constraint on return current heating is that the driving electron field be low enough to allow the beam to traverse the system length,  $L$ :

$$eE_z L = e \left( \frac{j_p}{\sigma} \right) L \lesssim \text{beam electron kinetic energy} \quad (2.185)$$

We illustrate the above discussion with an example. Let  $|j_b| \approx j_p \approx j_b^p t/t_r$  where  $j_b^p$  is the peak beam current density,  $\approx 10^4 \text{ A/cm}^2$ , and assume a linear current rise with  $t_r = 50 \text{ nsec}$ . Take a cross-sectional area of  $10 \text{ cm}^2$  for the beam-plasma channel and a hydrogen plasma with density of  $10^{14}/\text{cm}^3$ , fully ionized with an initial temperature of one volt. From Equation (2.176) we see that if  $j_p = |j_b^p|$ , the Buneman mode would cut off at  $T_e = 100 \text{ volts}$ , and we see from Equation (2.179) that we are essentially in the ion-acoustic mode throughout the beam pulse. Equation (2.180) has an I-A mode cutoff temperature of  $4.3 \text{ keV}$ . In view of the uncertainties in  $v_{\text{eff}}^{\text{IA}}$ , we shall estimate the

heating rate conservatively, i.e., use the smallest collision frequency in Equation (2.182), obtained by taking  $(v_{te}/v_d)$  at the IA cutoff ( $\sim 43$ ). Equation (2.183) gives the lower bound on  $\sigma: \sigma \gtrsim 2.2 \times 10^{12}/\text{sec}$  for  $t_e \approx t_r = 50$  nsec. Substituting for  $v_{\text{eff}}^{\text{IA}}$  in  $\sigma$  gives  $2.4 \times 10^{14}/\text{sec}$ , so we are well above the lower bound. From Equation (2.180)

$$T_e(t_r) \sim 1.6 \times 10^9 \left( \frac{1}{t_r^2} \right) \int_0^{t_r} t^{3/3} dt \approx 27 \text{ volts}$$

This temperature is, of course, not interesting for CTR applications. If we use an optimistic collision frequency,  $(v_{te}/v_d \sim 1$  [Equation (2.182)]),  $\sigma \approx 5.6 \times 10^{12}/\text{sec}$ , and we only marginally satisfy the lower  $\sigma$  bound criterion. In this case,  $T_e(t_r) \approx 1.1$  keV. The sensitivity of the temperature estimate to the effective collision frequency is apparent. For a given  $v_{\text{eff}}$ , the temperature is optimized by decreasing the plasma density to the lower bound.

The remarks up to this point have been directed toward return current heating. Simultaneous e-e mode heating may occur, or even dominate the heating process, provided the beam velocity spread is not too large (Reference 2.77). The Singhaus criterion (Section 2.8.1) requires for e-e instability growth

$$\left( \frac{v_b}{v_o} \right)^2 \ll \left[ 0.7 \frac{\omega_p}{v} \frac{n_b}{\gamma n_p} \right] \quad (2.186)$$

where

- $n_b$  = beam number density.
- $v_b$  = rms beam longitudinal velocity spread
- $v_o$  = average longitudinal beam velocity

Equation (2.186) further indicates that the e-e mode may be initiated by return current heating if not originally present. Both  $\nu_{e,i}$  and  $\nu_{\text{eff}}^{\text{IA}}$  are decreased by increasing temperature. Assuming  $(v_b/v_o) \sim 1$ , Equation (2.186) gives

$$\nu < 4 \times 10^4 \frac{n_b}{\gamma \sqrt{n_p}} (v_b/v_o \sim 1) \quad (2.187)$$

with the densities in  $\text{cm}^{-3}$ . Taking  $n_b \sim 2 \times 10^{12} \text{ cm}^3$  from the example above and  $\gamma \approx 2$ ,  $\nu < 4 \times 10^9/\text{sec}$ . If we determine  $\nu_{\text{eff}}^{\text{IA}}$  from Equation (2.182) with  $\nu_{\text{te}}/v_d \sim 1$ , Equation (2.187) is satisfied for both  $\nu_{e,i}$  and  $\nu_{\text{eff}}^{\text{B}}$ .\* The heating rate is

$$\frac{dT_e(\text{eV})}{dt} = 1.5 \times 10^{22} \left(\frac{j_p}{n_p}\right)^2 \nu_{\text{eff}}^{\text{e-e}} \quad (2.188)$$

where

$$\nu_{\text{eff}}^{\text{e-e}} \approx 0.3 \left(\frac{n_b}{\gamma n_p}\right) \left(\frac{v_o}{v_b}\right)^2 \omega_p - \nu/2$$

a maximum value. The parameters of the example give

$$\nu_{\text{eff}}^{\text{ee}} \approx 1.7 \times 10^9/\text{sec} - \nu/2$$

and, taking the minimum value of  $\nu_{\text{eff}}^{\text{IA}}$ ,  $\nu_{\text{eff}}^{\text{ee}} \approx 1.7 \times 10^9/\text{sec}$ . The additional e-e heating then gives  $T_e^{(\text{ee})} = 4.2 \text{ keV}$  and the e-e mode is dominant over the I-A heating in this example.

If we consider a confined system where plasma return currents have decayed, estimation of the e-e mode heating requires

\* We are assuming a linear superposition of e-e and e-i modes.

a knowledge of the level of turbulence; i.e., the amplitude of the ES waves. Lewis (Reference 2.44) discusses the heating in the linear limit.

2.11.2 A Plasma Heating Technique Using Collectively Accelerated Ions.\* Recent generator and diode development work has shown the feasibility of constructing electron beam accelerators with several hundred kilojoules of beam energy (Reference 2.78). One such design would employ a large annular cathode, a design particularly convenient for collective accelerations of ions. We describe a technique for plasma heating using collectively accelerated deuterium ions. An important aspect of the scheme is that it utilizes only reported experimental results both for ion production efficiency and plasma parameters. Any optimization of ion fluxes generated by the electron beams would, of course, increase the efficiency of the system. In view of the small effort in this area to date, it is reasonable to assume that further experimental investigations directed toward understanding the collective ion acceleration process will lead to higher efficiencies. This plasma heating technique must ultimately be compared, for practical purposes, with efficiencies of plasma heating using high power CO<sub>2</sub> lasers or the electrons themselves.

A 300 kJ electron beam accelerator, for example, can be used in a low pressure neutral gas mode to accelerate deuterons to energies of 2 MeV. With many small copper pipes emanating from magnetically isolated cathodes, evenly spaced around an annular ring, we can assume generation of  $10^{14}$  deuterons/76 kA with 500 keV electrons or  $10^{14}$  deuterons/100 kA for 1 MeV electrons. These numbers are obtained from published data for ion

---

\* This material has been reported in S. Putnam, An Intense Pulsed Neutron and Kilovolt X-ray Source, PIIR-33-71, Physics International Company, San Leandro, Ca., July 1971.

production using  $v/\gamma \cong 2$  as the criterion for reproducible deuteron energy from each pipe accelerating channel (Reference 2.79). Thus, a 1 MeV machine could be expected to produce 1.92 kJ of deuteron energy and a 500 keV machine could produce 5.06 kJ.

We can argue the above experimentally reported deuteron numbers from simple physics, somewhat independently of the acceleration mechanism (see Section 4). The number of acceleration ions,  $N_i$ , can be estimated from

$$N_i = n_b \bar{F}_e \pi a_o^2 L \quad (2.189)$$

where

$n_b$  = electron beam density

$\bar{F}_e$  = fractional electrical neutralization of the ion bunch

$a_o$  = average beam radius

$L$  = bunch length at the start of acceleration

For 2 MeV deuterons,  $\beta_L^{\text{ion}}$ , the maximum ion velocity/c is  $\approx 4.6 \times 10^{-2}$ . During acceleration (in the case where the beam front and ion bunch are coincident),  $\beta_L^e \lesssim \beta_L^{\text{ion}}$ , where  $\beta_L^e$  refers to the electron streaming velocity. From Equation (2.189),

$$N_{\text{ion}} > 4.5 \times 10^9 \bar{F}_e L I_b \text{ (A)} \quad (2.190)$$

where

$I_b$  = beam current

If  $I_b = 7.8 \times 10^4$ ,  $N_{\text{ion}} > 3.5 \times 10^{14} \bar{F}_e L$ . We know that  $\bar{F}_e$  exceeds  $1/\gamma^2$ , let us take  $\bar{F}_e \approx 2/\gamma^2$ . Then for 500 keV electrons,

$$N_{\text{ion}} \gtrsim 1.8 \times 10^{14} L \quad (2.191)$$

The bunch length,  $L$ , should be of the order of the beam radius ( $\sim 1$  cm). The ion number could be doubled if the beam pulse were long enough to accelerate two ion bunches. These simple arguments imply the perhaps obvious conclusion that higher ion numbers are obtainable from higher-current, lower-energy electron beams. Also, the estimate suggests that if desired ion energies are not too high, we can use higher currents per accelerating pipe (and therefore fewer pipes) without degrading the number of accelerated ions. The current value per pipe above was chosen to stay within experimentally verified parameters.

The individual pipes are to be geometrically focused toward the heated plasma region with or without an intermediate transport system such as a linear pinch. The ion bunches and electron beamlets would be transported at first within the pipes until the pipes converged to contact and then would be transported simply in a large tapered drift chamber. A tapered linear pinch could be used for additional focusing as a final stage before plasma injection.

As an example of an application for this intense ion source to plasma heating and neutron production, we consider a readily obtainable plasma which possesses many desirable features for ion injection--the dense plasma focus (DPF). The magnetic field configuration of the DPF increases the ion aperture up to several centimeters, and contains a  $10^{19}$  to  $10^{20}/\text{cm}^3$  density plasma at a few kiloelectron volts over containment times from 50 to 100 nsec. Some experiments are already underway using electrons to heat the focus plasma, (Reference 2.66), but there are two serious problems in using electrons rather than ions. Perhaps the main difficulty with electrons is injection. The 2 MG or so magnetic field containing the plasma reflects all but a small fraction of the

electrons along the axis if the electrons are directed toward the anode from the exterior. If the electrons are injected through a hole in the anode, the field defocuses the electrons. Secondly, the electron energy deposition range at 1 MeV is  $\approx 10$  meters, and collective enhancement of energy deposition does not appear to be significant with these plasma parameters unless the beam has a very small velocity spread. The velocity spread criterion for electron-electron instability modes (the Singhaus criterion) would refer to transported electrons entering the plasma focus at any one time. In view of the defocusing effect of the DPF magnetic field for anode interior injection, it appears difficult to argue a small velocity spread in the plasma, even if a sufficiently cold beam were injected (Reference 2.67).\*

In contrast to electrons, the 2 MeV deuterons have a range of  $\approx 4$  cm in a  $10^{20}/\text{cm}^3$ , 1 to 10 keV plasma, and can be focused by the 2 MG magnetic field if injected through a hole in the anode. (The Larmor radius,  $\sim 1.4$  mm, is the approximate radius of focal plasma.) Thus eight to nine radial oscillations of the deuterons in the (typical)  $\sim 1.5$  cm length of the focal cylinder will deposit all their energy. Both the ion energy and specie can be altered, using this scheme, to achieve complete energy deposition within the plasma region for varying plasma parameters; in fact, the ions themselves can be used as a diagnostic tool to characterize the focal plasma and "tune" the system.

Approximately one-tenth of the injected ion energy, or 190 to 500 joules, will be directly transferred to the plasma

---

\* Collective enhancement of electron energy deposition is suggested as a plausible explanation for observed neutron enhancement with electron beam injection inside the anode.

## REFERENCES

### SECTION 2

- 2.1 P. Kirstein and others; "Space-Charge Flow"; 1967; McGraw-Hill Book Company, New York, N. Y.; Unclassified.
- 2.2 D. C. dePackh; Radiation Project Progress Report No. 5; 1968; Naval Research Laboratory, Washington, D. C.; Unclassified.
- 2.3 F. Friedlander and others; DASA 2173, 1968; Varian Associates.
- 2.4 J. Creedon; "Production of Advanced X-ray Sources Using Intense Relativistic Beams"; Volume 1; September 1971; PIFR-227/294 Draft Report, Physics International Company, San Leandro, California; Unclassified.
- 2.5 J. Clark and others; Report No. LPS 23, 1969; Laboratory for Plasma Studies, Cornell University; Unclassified.
- 2.6 B. Ecker; "Production of Advanced X-ray Sources Using Intense Relativistic Beams"; Volume 1, September 1971; PIFR-227/294 Draft Report, Physics International Company, San Leandro, California; Unclassified.
- 2.7 I. Langmuir; Physical Review, 1929, Vol. 33, Page 954; Unclassified.
- 2.8 M. Friedman and others; Report No. LPS 61, December 1970; Laboratory for Plasma Studies, Cornell University; Unclassified.
- 2.9 G. Loda and others; PIIR-4-71, 1970; Physics International Company, San Leandro, California; Unclassified; Bulletin of the American Physical Society, 1970, Vol. 15, Page 1401; Unclassified.

**Preceding page blank**

## REFERENCES (cont.)

- 2.10 B. Ecker and others; PIIR-27-71, May 1971; Physics International Company, San Leandro, California; Unclassified; Also presented at the Eleventh Symposium on Electron, Ion and Laser Beam Technology, Boulder, Colorado, May 1971; Unclassified.
- 2.11 D. Hammer and others; "Effects of External Magnetic Field on Accelerating High-Current Electron Beams"; April 1970, Internal Report, Naval Research Laboratory, Washington, D.C.; Unclassified.
- 2.12 D. C. dePackh; Radiation Project Internal Report No. 7, April 1968; Naval Research Laboratory, Washington, D. C.; Unclassified.
- 2.13 S. Putnam; PIFR-105-Draft, April 1970; Physics International Company, San Leandro, California; Unclassified.
- 2.14 S. Putnam; PIIR-29-71, June 1971; Physics International Company, San Leandro California; Unclassified; Also presented at the Eleventh Symposium on Electron, Ion and Laser Beam Technology, Boulder, Colorado, May 1971; Unclassified.
- 2.15 G. McClure; Physical Review, 1953, Vol. 90, Page 796; Unclassified; W. Jesse and others; Physical Review, 1955, Vol. 97, Page 1668, Unclassified.
- 2.16 P. Felsenthal and others; Physical Review, 1965, Vol. 139, Page A1796; Unclassified.
- 2.17 J. Creedon; PIIR 17-67, March 1967; Physics International Company, San Leandro, California; Unclassified.
- 2.18 G. Yonas and others; "Record of 10th Symposium on Electron, Ion, and Laser Beam Technology"; 1970; L. Marton, editor; San Francisco Press, Inc., San Francisco, California; Unclassified.
- 2.19 L. Spitzer; "Physics of Fully Ionized Gases"; 1961; Interscience Publishers, New York, N. Y.; Unclassified.
- 2.20 S. Brown; "Basic Data of Plasma Physics"; 1959; MIT Press, Cambridge, Massachusetts; Unclassified.

REFERENCES (cont.)

- 2.21 M. A. Head and others; "Plasma Diagnostics with Microwaves"; 1965; John Wiley and Sons, Inc., New York, N. Y.; Unclassified.
- 2.22 C. L. Chen; Physical Review, 1964, Vol. 135, Page A627; Unclassified.
- 2.23 G. Yonas and others; PIFR-106, October 1968; Unclassified; Also PIFR-106-2 August 1969; Physics International Company, San Leandro, California; Unclassified.
- 2.24 S. Chandrasekhar; "The Electromagnetic Wake Following a Pulse of Charged Particles"; IDA Report, July 1961; Unclassified; S. Yadavalli; Physics of Fluids, 1965, Vol. 8, Page 956; Unclassified; J. Cox and others; Physics of Fluids, 1970, Vol. 13, Page 182; Unclassified; D. Hammer and others; Physics of Fluids, 1970, Vol. 13, Page 1831; Unclassified.
- 2.25 D. Swain; Bulletin of the American Physical Society, 1971, Vol. 16, No. 11, Page 1129; Unclassified; Also submitted to the Journal of Applied Physics.
- 2.26 I. M. Kapchinskij and others; "Proceedings of the International Conference on High Energy Accelerators and Instrumentation"; 1959. CERN, Page 274; Unclassified.
- 2.27 A. Garren; UCRL-19313, August 1969, Lawrence Berkeley Laboratory, Berkeley, California; Unclassified.
- 2.28 W. Link; IEEE Transactions on Nuclear Science, 1967, Vol. NS-14, Page 777; Unclassified.
- 2.29 J. Lawson; Journal of Electronics and Control; 1956, Vol. 5, Page 146; Unclassified.
- 2.30 T. Walsh; Plasma Physics, 1963, Vol. 5, Page 17; Unclassified.
- 2.31 H. Alfven; Physical Review, 1939, Vol. 55, Page 425; Unclassified.
- 2.32 W. Bennett; Physical Review, 1934, Vol. 45, Page 890; Unclassified; and Physical Review, 1955, Vol. 98, Page 6; Unclassified.

## REFERENCES (cont.)

- 2.33 G. Benford and others; Physics of Fluids, 1970, Vol. 13, Page 2621; Unclassified.
- 2.34 D. Hammer and others; Physics of Fluids, 1970, Vol. 13, Page 1831; Unclassified.
- 2.35 S. Yoshikawa; Physical Review Letters, 1971, Vol. 26, Page 295; Unclassified.
- 2.36 W. Neugebauer; IEEE Transaction of Electron Devices, 1967, Vol. ED-14, No. 10, Page 686; Unclassified.
- 2.37 M. Andrews and others; Physics of Fluids, 1970, Vol. 13, Page 1322; Unclassified.
- 2.38 A. Toepfer; Physical Review, 1971, Vol. A-3, Page 1444; Unclassified.
- 2.39 S. Graybill and others; Applied Physics Letters, 1966, Vol. 8, Page 18; Unclassified.
- 2.40 T. E. Stringer; Journal of Nuclear Energy, 1964, Vol. C-6, Page 267; Unclassified.
- 2.41 O. Buneman; Physical Review, 1959, Vol. 115, Page 503; Unclassified.
- 2.42 J. Guillory and others; "Estimates of Dense Plasma Heating by Stable Intense Electron Beams"; to be published in Plasma Physics; Unclassified.
- 2.43 S. Bludman and others; Physics of Fluids, 1960, Vol. 3, Page 747; Unclassified.
- 2.44 H. Lewis; "Stability of a Relativistic Beam in a Plasma"; July 1961, Institute for Defense Analysis Report; Unclassified.
- 2.45 H. Bohmer and others; Physics of Fluids, 1971, Vol. 14, Page 150; Unclassified.
- 2.46 G. Ascoli; Coordinated Science Laboratory Report, R-131, 1961; University of Illinois, Urbana, Illinois; Unclassified.

REFERENCES (cont.)

- 2.47 H. Singhaus; *Physics of Fluids*, 1964, Vol. 7, Page 1535; Unclassified.
- 2.48 G. Budker; *Atomic Energy*, 1956, Vol. 5, Page 9; Unclassified; D. Finkelstein and others; "Plasma Physics"; J. Drummond, editor, 1961; McGraw Hill Book Company, New York, N. Y.; Unclassified.
- 2.49 B. Cherikov; *Journal of Nuclear Energy*, 1956, Vol. C-8, Page 455; Unclassified.
- 2.50 S. Weinberg; *Journal of Mathematical Physics*, 1964, Vol. 5, Page 371; Unclassified; *Journal of Mathematical Physics*, 1967, Vol. 8, Page 614; Unclassified.
- 2.51 D. Hammer; private communication; also to be published in minutes of DNA Simulation Meeting, January 1971, Defense Nuclear Agency; Washington, D. C.; Unclassified.
- 2.52 C. Stallings; "Production of Advanced X-ray Sources Using Intense Relativistic Beams"; Volume 1, PIFR-227/294 Draft Report, September 1971, Physics International Company, San Leandro, California; Unclassified.
- 2.53 C. Longmire; "Elementary Plasma Physics"; 1963, Interscience Publishers, New York, N. Y.; Unclassified.
- 2.54 C. Striffler and others; *Physics of Fluids*, 1970, Vol. 13, Page 1851; Unclassified.
- 2.55 G. Benford; *Bulletin of the American Physical Society*, 1972, Vol. 17 for APS Meeting in San Francisco, California, January 1972; Unclassified.
- 2.56 J. Benford and others; PIIR-10-70, December 1969, Physics International Company, San Leandro, California (to be published in *Physics of Fluids*, February 1972); Unclassified.
- 2.57 T. Roberts and others; *Plasma Physics*, 1968, Vol. 10, Page 381; Unclassified.
- 2.58 J. Benford and others; *Physical Review Letters*, 1971, Vol. 26, Page 1160; Unclassified.

REFERENCES (cont.)

- 2.59 S. Glasstone and others; "Controlled Thermonuclear Reactors"; 1960, Van Nostrand, Princeton, N. J.; Unclassified.
- 2.60 J. Benford; "Production of Advanced X-ray Sources Using Intense Relativistic Beams"; Volume 1, September 1971, PIFR-227/294 Draft Report; Physics International Company, San Leandro, California; Unclassified.
- 2.61 J. Bzura; Bulletin of the American Physical Society, 1970, Vol. 15, Page 1452; Unclassified.
- 2.62 D. Hammer and others; to be published in Proceedings of the DNA Simulation Meeting, January 1971, Defense Nuclear Agency, Washington, D. C.; Unclassified.
- 2.63 G. Schmidt; "Physics of High Temperature Plasmas"; 1966, Academic Press, New York, N. Y.; Unclassified.
- 2.64 R. Lee and others; Physics of Fluids, 1971, Vol. 14, Page 1213; Unclassified.
- 2.65 M. J. Eden and others; Nuclear Fusion, 1971, Vol. 11, Page 37; Unclassified.
- 2.66 J. Mather and N. Rostoker; private communication, January 1971.
- 2.67 D. Friewald and others; "Neutron Enhancement from Relativistic Electron Beam-Dense Plasma Focus Interactions"; submitted to Physics Letters A; Unclassified.
- 2.68 F. Winterberg; Physical Review, 1968, Vol. 174, Page 212; Unclassified.
- 2.69 M. Babykin and others; Conference on Plasma Physics and Controlled Nuclear Fusion Research, Paper IAEA/CN-28/D-10, June 1971, Madison, Wisconsin, sponsored by the International Atomic Energy Agency; Unclassified.
- 2.70 A. Altyntsev and others; JETP Letters, 1971, Vol. 13, Page 139; Unclassified.
- 2.71 S. Hamberger and others; Physical Review Letters, 1968, Vol. 21, Page 674; Unclassified; S. Hamberger and others; Physical Review Letters, 1970, Vol. 25, Page 999; Unclassified.

REFERENCES (cont.)

- 2.72 R. Lovelace and others; Physical Review Letters, 1971, Vol. 27, Page 1256; Unclassified.
- 2.73 D. Sivukhin; "Review of Plasma Physics"; Volume 4, 1966; Consultant's Bureau, New York, N. Y.; Unclassified.
- 2.74 A.J.R. Prentice; Plasma Physics, 1967, Vol. 9, No. 4, Page 433; Unclassified.
- 2.75 R. Sagdeev; "Proceedings of the 18th Symposium in Applied Mathematics"; 1967, Page 281; Unclassified; S. P. Gary; Physical Review Letters, 1971, Vol. 26, Page 1097; Unclassified.
- 2.76 V. Sazonenko and others; Nuclear Fusion, 1970, Vol. 10, Page 155; Unclassified.
- 2.77 J. Guillory; Bulletin of the American Physical Society, 1971, Vol. 16, No. 11, Page 1282; Unclassified.
- 2.78 G. Yonas and others; PIIR-26-61, June 1971, Physics International Company, San Leandro, California; Unclassified; also presented at Eleventh Symposium on Electron, Ion and Laser Beam Technology, May 1971, Boulder, Colorado; Unclassified.
- 2.79 J. Rander and others; PIIR-2-71, July 1971, Physics International Company, San Leandro, California; Unclassified.

## SECTION 3

### ELECTRODYNAMIC CALCULATIONS

#### 3.1 BASIC EQUATIONS

The purpose of this section is to formulate the quadrature of the EM field equations; i.e., to express the fields in terms of integrals over beam-current-source functions. We do not explicitly include external fields, although the external field of a linear-pinch transport system may easily be superimposed upon self fields for analysis of the current-neutralization problem. Several investigators have considered EM fields generated by an undistorted beam pulse passing through an infinite plasma. Chandrasekhar (Reference 3.1) and Yadavilli (Reference 3.2) have evaluated field expressions in the wake of the beam pulse and Zwick (Reference 3.3) has investigated the region behind the space-charge neutralization front. The general formalism used by these authors can be used, of course, to determine fields over all space. Somewhat different techniques have been used more recently by Hammer and Rostoker (Reference 3.4) and Cox and Bennett (Reference 3.5) to look at the same problem. Our work is directed toward geometries more relevant to experiments of beams and drift chambers; in particular, we investigate the effects of finite boundaries and finite beam risetime. The field expressions are derived for the following boundary conditions:

1. Long pipe with no endplates
2. Long pipe with a single endplate
3. Closed cylindrical cavity

In these three cases the plasma conductivity is taken to be constant. We also formally evaluate EM fields for the case of a conductivity varying with distance behind the beam front. CALCOMP plots are included for EM fields of a finite risetime beam in a long pipe filled with constant conductivity plasma (the current neutralization problem) and for a beam entering a long pipe through a conducting plate (anode window), i.e., the beam-injection problem. A summary of the results of these calculations has been given in Section 2.6.

We begin by formulating a gauge useful for problems with azimuthal symmetry and unpolarized beams (no theta component of the current density). The Maxwell's equations are

$$\nabla \times \vec{B} = \frac{4\pi}{c} (\vec{j}_b + \vec{j}_p) + \frac{1}{c} \frac{\partial \vec{E}}{\partial t} \quad (3.1)$$

$$\nabla \cdot \vec{E} = 4\pi (\rho_b + \rho_p) \quad (3.2)$$

$$\nabla \times \vec{E} = - \frac{1}{c} \frac{\partial \vec{B}}{\partial t} \quad (3.3)$$

and 
$$\nabla \cdot \vec{B} = 0 \quad (3.4)$$

The "b" subscript refers to beam quantities and "p" refers to the plasma counterparts. If we assume a scalar conductivity,  $\sigma$ , and take

$$\vec{j}_p = \sigma \vec{E}, \quad \sigma = \sigma(r, z, t),$$

the equations defining  $\vec{E}$  and  $\vec{B}$  are

$$\nabla \times \nabla \times \vec{B} + \frac{1}{c^2} \frac{\partial^2}{\partial t^2} \vec{B} + \frac{4\pi\sigma}{c^2} \frac{\partial \vec{B}}{\partial t} = \frac{4\pi}{c} [\nabla \times \vec{j}_b + \nabla\sigma \times \vec{E}] \quad (3.5)$$

$$\nabla \times \nabla \times \vec{E} + \frac{1}{c^2} \frac{\partial^2}{\partial t^2} \vec{E} + \frac{4\pi}{c^2} \frac{\sigma \partial \vec{E}}{\partial t} + \frac{4\pi}{c^2} \vec{E} \frac{\partial \sigma}{\partial t} = - \frac{4\pi}{c^2} \frac{\partial \vec{j}_b}{\partial t} \quad (3.6)$$

We immediately see that  $\vec{B} = B_\theta \hat{e}_\theta$ ,  $\vec{E} = E_r \hat{e}_r + E_z \hat{e}_z$ , and that if  $\nabla\sigma = 0$ , the equations decouple. However, even if  $\nabla\sigma = 0$ , it is not convenient to solve these equations directly since the  $E_r$  and  $E_z$  equations do not decouple in cylindrical coordinates.

Perhaps the most convenient approach is to use the vector and scalar potentials,  $\vec{A}$  and  $\phi$ , with

$$\begin{aligned}\vec{B} &= \nabla \times \vec{A} \\ \vec{E} &= -\nabla\phi - \frac{1}{c} \frac{\partial \vec{A}}{\partial t}\end{aligned}\quad (3.7)$$

We obtain

$$\begin{aligned}\nabla \times \nabla \times \vec{A} + \frac{4\pi\sigma}{c^2} \frac{\partial \vec{A}}{\partial t} + \frac{1}{c^2} \frac{\partial^2 \vec{A}}{\partial t^2} &= \\ \frac{4\pi}{c} \vec{j}_b - \nabla \left( \frac{4\pi\sigma\phi}{c} + \frac{1}{c} \frac{\partial\phi}{\partial t} \right) + \frac{4\pi\nabla\sigma\phi}{c}\end{aligned}\quad (3.8)$$

The radial component of Equation (3.8) is

$$\begin{aligned}-\frac{\partial^2 A_r}{\partial z^2} + \frac{\partial^2 A_z}{\partial z \partial r} + \left( \frac{4\pi\sigma}{c} + \frac{1}{c} \frac{\partial}{\partial t} \right) \frac{1}{c} \frac{\partial}{\partial t} A_r &= \\ \frac{4\pi}{c} j_{b_r} - \frac{\partial}{\partial r} \left( \frac{4\pi\sigma}{c} + \frac{1}{c} \frac{\partial}{\partial t} \right) \phi + \frac{4\pi}{c} \frac{\partial\sigma}{\partial r} \phi\end{aligned}\quad (3.9)$$

and the z component,

$$\begin{aligned}\frac{1}{r} \frac{\partial}{\partial r} \left( \frac{r \partial A_r}{\partial z} \right) - \frac{1}{r} \frac{\partial}{\partial r} \left( \frac{r \partial A_z}{\partial r} \right) + \left( \frac{4\pi\sigma}{c} + \frac{1}{c} \frac{\partial}{\partial t} \right) \frac{1}{c} \frac{\partial A_z}{\partial t} &= \\ \frac{4\pi}{c} j_{b_z} - \frac{\partial}{\partial z} \left( \frac{4\pi\sigma}{c} + \frac{1}{c} \frac{\partial}{\partial t} \right) \phi + \frac{4\pi}{c} \left( \frac{\partial\sigma}{\partial z} \right) \phi\end{aligned}\quad (3.10)$$

We now choose a gauge:  $A_r = 0$ . Then Equations (3.9) and (3.10) yield

$$\frac{\partial^2 A_z}{\partial z \partial r} = \frac{4\pi}{c} j_{b_r} - \frac{\partial}{\partial r} \left( \frac{4\pi\sigma}{c} + \frac{1}{c} \frac{\partial}{\partial t} \right) \phi + \frac{4\pi}{c} \frac{\partial \sigma}{\partial r} \phi \quad (3.11)$$

$$- \frac{1}{r} \frac{\partial}{\partial r} r \frac{\partial A_z}{\partial r} + \left( \frac{4\pi\sigma}{c} + \frac{1}{c} \frac{\partial}{\partial t} \right) \frac{1}{c} \frac{\partial A_z}{\partial t} = \frac{4\pi}{c} j_{b_z} - \quad (3.12)$$

$$\frac{\partial}{\partial z} \left( \frac{4\pi\sigma}{c} + \frac{1}{c} \frac{\partial}{\partial t} \right) \phi + \frac{4\pi}{c} \left( \frac{\partial \sigma}{\partial z} \right) \phi \quad (3.13)$$

If  $\sigma = \sigma(t)$ ,

$$\left( \frac{4\pi\sigma}{c} + \frac{1}{c} \frac{\partial}{\partial t} \right) \phi = \frac{4\pi}{c} \int j_{b_r} dr' - \frac{\partial A_z}{\partial z} + f(z,t),$$

where  $f(z,t)$  is an arbitrary function. Substituting Equation (3.13) into Equation (3.12) gives

$$- \frac{\partial^2 A_z}{\partial z^2} - \frac{1}{r} \frac{\partial}{\partial r} \left( r \frac{\partial A_z}{\partial r} \right) + \frac{4\pi\sigma}{c^2} \frac{\partial A_z}{\partial t} + \frac{1}{c^2} \frac{\partial^2 A_z}{\partial t^2} = \frac{4\pi}{c} j_{b_z} - \frac{\partial \bar{Q}}{\partial z} \equiv s \quad (3.14)$$

$$\bar{Q} \equiv \frac{4\pi}{c} \int_0^r j_{b_r} dr' - f(z,t)$$

Equations (3-13) and (3-14) are our basic equations; we need only solve for  $A_z = A$ , inasmuch as  $\phi$  is determined from

$$\phi = c e^{-f4\pi\sigma dt'} \left\{ \int dt' e^{4\pi f \sigma dt'} \left[ - \frac{\partial A}{\partial z} + Q \right] + H(r,z) \right\} \quad (3.15)$$

where  $H$  is an arbitrary function. Equation (3.7) now gives

$$\begin{aligned}
 B_{\theta} &= - \frac{\partial A}{\partial r} \\
 E_r &= - \frac{\partial \phi}{\partial r} \\
 E_z &= - \frac{\partial \phi}{\partial z} - \frac{1}{c} \frac{\partial A}{\partial t}
 \end{aligned}
 \tag{3.16}$$

3.1.1 Green's Functions. Equation (3-14) can be solved using Green's function techniques for several interesting beam problems. If the beam travels at constant velocity  $v$  in the positive  $z$  direction we can rewrite Equation (3.14) in terms of the variable  $u = \gamma(vt - z)$ , where  $u$  is the (positive) distance behind the beam front:

$$\left( -\nabla_r^2 - \frac{\partial^2}{\partial u^2} + 2k \frac{\partial}{\partial u} \right) A(u, r) = S(u, r)
 \tag{3.17}$$

$$k \equiv \frac{2\pi\sigma\gamma v}{c^2}, \quad \sigma = \text{constant.}$$

Let  $A = W e^{ku}$ ; then

$$\left( \nabla_r^2 + \frac{\partial^2}{\partial u^2} - k^2 \right) W = -S e^{-ku} \equiv S'(r, u)
 \tag{3.18}$$

The Green's function for Equation (3.18) satisfies

$$\left( \nabla_r^2 + \frac{\partial^2}{\partial u^2} - k^2 \right) G = \frac{\delta(r-r')}{r} \delta(u-u')$$

and

$$W = \int_0^{\infty} r' dr' \int_{-\infty}^{\infty} du' G(r, r', u, u') S'(r', u')$$

The evaluation of  $G$  for a beam in infinite space,  $G^{\infty}$ , is simple using standard techniques:

$$G^{\infty} = -\frac{1}{2} \int_0^{\infty} \frac{\lambda e^{-\sqrt{\lambda^2+k^2} |u-u'|}}{\sqrt{\lambda^2+k^2}} J_0(\lambda r) J_0(\lambda r') d\lambda \quad (3.19)$$

where  $J_0$  is the zero order Bessel function. Another useful case which can be obtained simply is the Green's function for a beam in a long conducting pipe of radius  $R$ , filled with plasma of constant conductivity:

$$G_{\text{long pipe}} = -\left(\frac{1}{R^2}\right) \sum_{n=1}^{\infty} \frac{e^{-\sqrt{\left(\frac{\lambda_n}{R}\right)^2+k^2} |u-u'|}}{\left[J_1(\lambda_n)\right]^2 \sqrt{\left(\frac{\lambda_n}{R}\right)^2+k^2}} J_0\left(\frac{\lambda_n r}{R}\right) J_0\left(\frac{\lambda_n r'}{R}\right) \quad (3.20)$$

$\lambda_n$  is defined by  $J_0(\lambda_n) = 0$ ,  $n = 1, 2, \dots$ . The boundary condition  $E_z = 0$  at  $r = R$  is satisfied by the vector potential defined by Equation (3.20).

The two Green's functions above solve the inhomogeneous vector potential equation [Equation (3.14) when the source function,  $S = S(r, vt - z)$ ]. If the beam charges are accelerated, the problem is more difficult and we use a slightly different technique to solve Equation (3.14) for  $S = S(r, z, t)$ . Again we assume a constant conductivity plasma and take the case of a long conducting pipe. Expand  $A$  and  $S$  in radial modes:

$$\left. \begin{aligned} S(r, z, t) &= \sum_{n=1}^{\infty} S_n(z, t) J_0\left(\frac{\lambda_n r}{R}\right) \\ A(r, z, t) &= \sum_{n=1}^{\infty} A_n(z, t) J_0\left(\frac{\lambda_n r}{R}\right) \end{aligned} \right\} \quad (3.21)$$

where  $J_0(\lambda_n) = 0$ ,  $n = 1, 2, \dots, n$ . If  $j_{b_z}$  or  $\int_0^r j_{b_r} dr'$  are not zero for  $r = R$ , we define  $f(z, t) = f(R, z, t)$  so that  $S(R, z, t) = 0$ .

Equation (3.14) gives

$$\left[ -\frac{\partial^2}{\partial z^2} + \frac{1}{c^2} \frac{\partial^2}{\partial t^2} + \frac{4\pi\sigma}{c^2} \frac{\partial}{\partial t} + \left(\frac{\lambda_n}{R}\right)^2 \right] A_n = S_n(z, t) \quad (3.22)$$

Taking the Laplace transform with respect to  $z \rightarrow s$  and  $t \rightarrow p$ , we obtain

$$A_n(p, s) = - \frac{S(p, s)}{s^2 - \left[ \frac{1}{c^2} (p + 2\pi\sigma)^2 + \left(\frac{\omega_n}{c}\right)^2 \right]} + (\text{homogeneous terms involving initial conditions and boundary conditions at } z = 0), \quad (3.23)$$

$$\omega_n^2 = \left(\frac{\lambda_n}{R}\right)^2 c^2 - (2\pi\sigma)^2$$

We take the homogeneous terms to be zero, since the method presented in the closed pipe problem below (Section 3.3) allows superposition of the proper homogeneous solutions to satisfy the boundary conditions at the cavity end plates and the initial conditions.\* The inverse transform with respect to  $z$  gives

$$A_n(p, z) = (-c) \int_0^z du \frac{S(p, u) \sinh \left[ \frac{1}{c} \sqrt{(p + 2\pi\sigma)^2 + \omega_n^2} (z-u) \right]}{\sqrt{(p + 2\pi\sigma)^2 + \omega_n^2}}$$

\* In other words, by using Equation (3.24) for the solution of the inhomogeneous vector potential equation which is the complete solution for a pipe without endplates, we can obtain the solution for an arbitrary current distribution in a closed cavity by adding homogeneous solutions using the method of Section 3.3.

Finally, taking the inverse transform in  $t$ ,

$$\begin{aligned}
 A_n(t, z) = & \left(\frac{c}{2}\right) \int_0^z du \int_0^t ds S(u, s) e^{-2\pi\sigma(t-s)} \\
 & \cdot \left[ J_0 \left( \omega_n \sqrt{(t-s)^2 - \left(\frac{z-u}{c}\right)^2} \right) H \left[ (t-s) - \left(\frac{z-u}{c}\right) \right] \right. \\
 & \left. - J_0 \left( \omega_n \sqrt{(t-s)^2 - \left(\frac{u-z}{c}\right)^2} \right) H \left[ (t-s) - \left(\frac{u-z}{c}\right) \right] \right], \quad (3.24)
 \end{aligned}$$

where  $H$  is the Heaviside function;

$$H(x) = 1, x > 0$$

$$= 0, x \leq 0$$

If  $\omega^2 < 0$ , Equation (3.24) is changed by replacing  $J_0$  by  $I_0$ , the modified Bessel function.

We complete this discussion of EM quadrature formulations by including for reference the well-known Green's function for a static charge distribution in a closed cylindrical cavity. This static potential is useful for determining the EM fields in a cavity when ions are present before the gas breaks down and current neutralization effects are important. In other words, before breakdown the EM fields can be approximated by a superposition of the beam fields (obtained with  $\sigma = 0$ ) and the electrostatic fields of the ion charge distribution. We desire a solution of

$$\nabla^2 \phi = -4\pi\rho,$$

with B.C.

$$\frac{\partial \phi}{\partial z} (+R, z) = 0 \quad (3.25)$$

$$\frac{\partial \phi}{\partial r} (r, 0) = \frac{\partial \phi}{\partial r} (r, L) = 0,$$

L is the length of the cavity. The Green's function satisfies  $\nabla^2 G = -4\pi[\delta(r-r')/r]\delta(z-z')$  and

$$\phi = \int_0^R r' dr' \int_0^L dz' G(r, r', z, z') \rho(r', z').$$

Using the representation of  $\frac{\delta(r-r')}{r'}$ ,

$$\frac{\delta(r-r')}{r} = \frac{2}{R^2} \sum_{n=1}^{\infty} \frac{1}{[J_1(\lambda_n R)]^2} J_0\left(\frac{\lambda_n r}{R}\right) J_0\left(\frac{\lambda_n r'}{R}\right)$$

we find

$$G(r, r', z, z') = \frac{8\pi}{R} \sum_{n=1}^{\infty} \frac{J_0\left(\frac{\lambda_n r}{R}\right) J_0\left(\frac{\lambda_n r'}{R}\right)}{\lambda_n [J_1(\lambda_n R)]^2 \sinh\left(\frac{\lambda_n L}{R}\right)} \quad (3.26)$$

$$\cdot \begin{cases} \sinh\left(\frac{\lambda_n}{R}\right)z \sinh\frac{\lambda_n}{R}(L-z'), & z < z' \\ \sinh\frac{\lambda_n}{R}(L-z) \sinh\frac{\lambda_n}{R}z', & z > z' \end{cases}$$

### 3.2 EXACT EM FIELDS FOR A BEAM IN A LONG PIPE FILLED WITH CONSTANT CONDUCTIVITY PLASMA--THE CURRENT NEUTRALIZATION PROBLEM\*

We discuss the exact EM fields generated by an undistorted beam passing through a long straight conducting pipe of radius  $R$ , filled with a gas of conductivity  $\sigma$ , and present CALCOMP field plots. These fields are of interest in low temperature beam transport problems with a pre-ionized gas or in multiple-pulse experiments where previous pulses have ionized the gas. We allow a pulse with finite risetime and explicitly evaluate fields for the case of an exponential current rise. The current density profile in radius is taken of the form

$$J_0 \left( \frac{\lambda_1 r}{R} \right)$$

a function which gives closed expressions for the fields.

#### 3.2.1 Assumptions

- a. The gas pressure or plasma density is high enough to justify using the concept of conductivity ( $p \gtrsim 0.5$  to 10 Torr).
- b.  $j_{b\theta} = j_{br} = 0$ ; i.e., the radial and theta beam current density components are negligible.
- c. Azimuthal symmetry.

---

\*The material of this section was reported in S. Putnam, Theoretical Electron Beam Studies, PIQR-105-3, Feb. 1969, Physics International Company (submitted to DNA).

$$\begin{aligned}
 \text{d. } j_{b_z} &= -C_1 J_0 \left( \frac{\lambda_1}{R} r \right) g(u); \\
 g(u) &= \left. \begin{aligned} &(1 - e^{-\alpha u}), \quad u > 0; \\ &= 0, \quad u < 0; \end{aligned} \right\} \quad (3.27)
 \end{aligned}$$

where  $u$  is the distance behind beam fronts (positive)  $= \gamma(vt - z)$ ,  $C_1$  is the current normalization constant,  $\lambda_1$  is the first zero of  $J_0$ , the zero order Bessel function  $\approx 2.4$ . Figure 3.1 shows the radial and  $u$ -dependence of  $j_{b_z}$ .

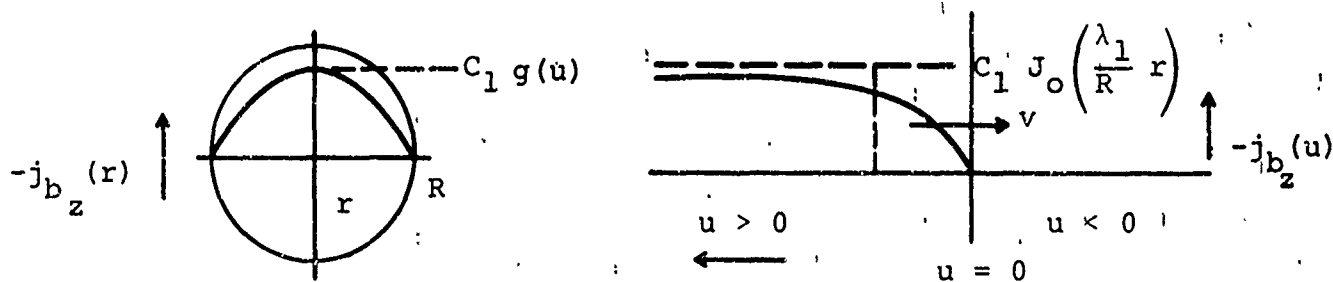


Figure 3.1 The radial and longitudinal profiles for  $j_{b_z}$ .

The radial form dependence of  $j_{b_z}$  is chosen for mathematical simplicity, and because it has the appealing properties of a maximum current density at  $r = 0$  and zero at the pipe radius. Also, this zero order mode will usually dominate the EM field expressions with more general radial profiles.

3.2.2 Basic Equations and Discussion of Model. The equations that the EM fields satisfy with the above assumptions, are

$$\left( -\frac{1}{r} \frac{\partial}{\partial r} \left( r \frac{\partial}{\partial r} \right) - \frac{\partial^2}{\partial z^2} + \frac{1}{c^2} \frac{\partial^2}{\partial t^2} + \frac{4\pi\sigma}{c^2} \frac{\partial}{\partial t} \right) A = \frac{4\pi}{c} j_{b_z} \quad (3.28)$$

$$\left( \frac{4\pi\sigma}{c} + \frac{1}{c} \frac{\partial}{\partial t} \right) \phi = -\frac{\partial A}{\partial z} \quad (3.29)$$

$$\left. \begin{aligned} E_r &= -\frac{\partial \phi}{\partial r} \\ E_z &= -\frac{\partial \phi}{\partial z} - \frac{1}{c} \frac{\partial A}{\partial t} \\ B_\theta &= -\frac{\partial A}{\partial r} \end{aligned} \right\} \quad (3.30)$$

where A is the z-component of the vector potential  
 $\phi$  is the scalar potential  
 $\sigma$  is the conductivity (a constant).

Rewriting Equations (3.28), (3.29), and (3.30) in terms of the variable u gives

$$\left( -\frac{1}{r} \frac{\partial}{\partial r} \left( r \frac{\partial}{\partial r} \right) - \frac{\partial^2}{\partial u^2} + 2k \frac{\partial}{\partial u} \right) A = \frac{4\pi}{c} j_{b_z} \quad (3.31)$$

$$k \equiv \frac{2\pi\sigma\gamma v}{c^2}$$

$$\phi = \frac{e^{-\epsilon u}}{\beta} \int_{-\infty}^u e^{\epsilon s} \frac{\partial A}{\partial s} ds, \quad \epsilon \equiv \frac{2k}{\gamma^2 \beta^2} \quad (3.32)$$

$$E_z = \gamma \left[ \frac{\partial \phi}{\partial u} - \beta \frac{\partial A}{\partial u} \right] \quad (3.33)$$

We now take

$$\left. \begin{aligned} A &= J_0 \left( \frac{\lambda_1}{R} r \right) A(u) \\ \phi &= J_0 \left( \frac{\lambda_1}{R} r \right) \phi(u) \end{aligned} \right\} \quad (3.34)$$

and Equation (3.31) reduces to

$$\left[ -\frac{\partial^2}{\partial u^2} + 2k \frac{\partial}{\partial u} + \left( \frac{\lambda_1}{R} \right)^2 \right] A(u) = \left( -\frac{4\pi}{c} \right) C_1 g(u) = S(u) \quad (3.35)$$

The solution of Equation (3.35) is

$$A(u) = \frac{1}{2\sqrt{\xi}} \left\{ e^{-(\sqrt{\xi}-k)u} \int_{-\infty}^u e^{(\sqrt{\xi}-k)s} S(s) ds \right. \\ \left. - e^{+(\sqrt{\xi}+k)u} \int_{+\infty}^u e^{-(\sqrt{\xi}+k)s} S(s) ds \right\} \quad (3.36)$$

with  $\xi = k^2 + \left( \frac{\lambda_1}{R} \right)^2$ .

Substituting in Equation (3.35) for S(u) and referring to Equations (3.30) and (3.34) gives

$$\begin{aligned}
B_{\theta} &= \left( \frac{4\pi}{c} \right) C_1 \left( \frac{\lambda_1}{R} \right) J_1 \left( \frac{\lambda_1}{R} r \right) \left( \frac{1}{2\sqrt{\xi}} \frac{\alpha}{\eta_2(\eta_2+\alpha)} e^{\eta_2 u}, u < 0 ; \right) \\
&= - \frac{4\pi}{c} C_1 \left( \frac{\lambda_1}{R} \right) J_1 \left( \frac{\lambda_1}{R} r \right) \left\{ \begin{array}{l} \frac{1}{2\sqrt{\xi}} \left[ \frac{1}{\eta_2} + \frac{1}{\eta_1} (1 - e^{-\eta_1 u}) \right] \\ - \left[ \frac{e^{-\alpha u} - e^{-\eta_1 u}}{\eta_1 - \alpha} - \frac{e^{-\alpha u}}{\eta_2 + \alpha} \right], u > 0 \end{array} \right. \quad (3.37)
\end{aligned}$$

where  $\eta_1 = \sqrt{\xi} - k$  , ( $>0$ )

$$\eta_2 = \sqrt{\xi} + k$$

Similarly, using Equations (3.30), (3.32), and (3.33),

$$\begin{aligned}
E_r &= \left( - \frac{4\pi}{c} \right) C_1 \left( \frac{\lambda_1}{R} \right) J_1 \left( \frac{\lambda_1}{R} r \right) \left[ \frac{\alpha}{2\beta\sqrt{\xi}} \frac{e^{\eta_2 u}}{(\epsilon + \eta_2)(\eta_2 + \alpha)} \right] u < 0 \\
&= \left( - \frac{4\pi}{c} \right) C_1 \left( \frac{\lambda_1}{R} \right) J_1 \left( \frac{\lambda_1}{R} r \right) \frac{\alpha}{2\beta\sqrt{\xi}} \left[ \frac{e^{-\epsilon u}}{(\eta_2 + \alpha)(\epsilon + \eta_2)} + \underbrace{\frac{(-1)}{(\eta_1 - \alpha)} \frac{(e^{-\eta_1 u} - e^{-\epsilon u})}{\epsilon - \eta_1}}_{(1)} \right. \\
&\quad \left. + \underbrace{\frac{(\eta_1 + \eta_2)}{(\eta_1 - \alpha)(\eta_2 + \alpha)} \frac{(e^{-\alpha u} - e^{-\epsilon u})}{(\epsilon - \alpha)}}_{(2)} \right], u > 0 \quad (3.38)
\end{aligned}$$

and finally,

$$\begin{aligned}
 E_z &= -\gamma J_0 \left( \frac{\lambda_1}{R} r \right) \frac{4\pi}{c} \frac{C_1}{2\sqrt{\xi}} \left( \frac{\alpha}{\eta_2 + \alpha} \right) e^{\eta_2(u)} \left[ \frac{1}{\beta} \frac{\eta_2}{\epsilon + \eta_2} - \beta \right], \quad u < 0 \\
 &= -\gamma J_0 \left( \frac{\lambda_1}{R} r \right) \frac{4\pi}{c} \frac{C_1}{2\sqrt{\xi}} \left\{ \frac{\alpha}{\beta} \left[ \frac{1}{\eta_1 - \alpha} \frac{\left( \eta_1 e^{-\eta_1 u} - \epsilon e^{-\epsilon u} \right)}{\epsilon - \eta_1} \right] - \frac{\epsilon e^{-\epsilon u}}{(\eta_2 + \alpha)(\epsilon + \eta_2)} \right. \\
 &\quad \left. + \frac{(-1)(\eta_1 + \eta_2)}{(\eta_1 - \alpha)(\eta_2 + \alpha)} \frac{1}{\epsilon - \alpha} \left( \alpha e^{-\alpha u} - \epsilon e^{-\epsilon u} \right) \right] \\
 &\quad \left. - \beta \left[ e^{-\eta_1 u} + \frac{\alpha e^{-\alpha u} - \eta_1 e^{-\eta_1 u}}{\eta_1 - \alpha} + \frac{\alpha}{\eta_2 + \alpha} e^{-\alpha u} \right] \right\}, \quad u > 0
 \end{aligned}
 \tag{3.39}$$

At this point, we remark about several properties of the above field expressions. As expected,  $E_r$  vanishes at  $r = 0$ ,  $E_z$  is a maximum at  $r = 0$  and vanishes at the pipe radius, and  $B_\theta = 0$  for  $r = 0$  and increases out to  $r = R$ . The electric fields decay exponentially to zero behind the beam front,\* whereas  $B_\theta$  approaches the value from the beam current only. The fields extend in front of the actual beam head, and are attenuated in front of the beam. The e-folding length in front is  $L = 1/\gamma (\sqrt{k^2 + (\lambda_1/R)^2} + k)^{-1}$ , indicating the effects of both the plasma relaxation length ( $1/k$ ) and the geometrical factor,  $R/\lambda_1$ . If  $\sigma = k \cong 0$  in the medium, as would be the case near the head of a beam propagating in a neutral gas,  $L = 1/\gamma R/\lambda_1$ .

\* When  $\sigma = k = 0$ ,  $E_r$  does not vanish far behind the beam front.

The field configuration moves with velocity  $v$ , the beam velocity, and the penetration ahead of the beam is compressed or expanded about the beam front depending on  $\gamma$ . As  $\gamma$  increases, the fields compress about the head, and in the limit  $\gamma \rightarrow \infty$ , the leading edge is "blunt."

The field expressions for  $u > 0$  change form when the beam drives the tube plasma at resonances; i.e., when any of the denominators in the equations vanish.\* For example, if  $\eta_1 = \alpha$ , Equation (3.37) for  $B_\theta$  with  $u > 0$  becomes

$$B_\theta|_{\eta_1 = \alpha} = \left(\frac{-4\pi}{c}\right) C_1 \left(\frac{\lambda_1}{R}\right) J_1\left(\frac{\lambda_1}{R} r\right) \frac{1}{2\sqrt{\xi}} \left\{ \frac{1}{\eta_2} + \frac{1}{\alpha_1} \left(1 - e^{-\alpha_1 u}\right) - ue^{-\alpha u} - \frac{e^{-\alpha u}}{\eta_2 + \alpha} \right\}, \quad u > 0. \quad (3.40)$$

The resonant forms for  $E_r$ ,  $u > 0$  are given in Table 3.1. Refer to the numbered terms in Equation (3.38).

---

\* All expressions in Equations (3.37), (3.38), and (3.39), are finite as given. We merely rewrite the equations in a more convenient form at resonant conditions for use in computer evaluation of the field expressions. The term resonance is used because the beam current drives the plasma tube system at eigenmodes of the homogeneous vector potential equation.

TABLE 3.1  
 $E_r$  RESONANT TERM REPLACEMENTS

| Resonance                                   | Replace | By   |
|---|---------|--|
| $\eta_1 = \alpha$<br>$\epsilon \neq \alpha$ | 1 + 2   | $\frac{e^{-\alpha u} - e^{-\epsilon u}}{(\eta_2 + \alpha)(\epsilon + \alpha)}$ |
| $\eta_1 = \alpha = \epsilon$                | 1 + 2   | $\frac{u e^{-\alpha u}}{\eta_2 + \alpha}$                                      |
| $\eta_1 \neq \alpha$<br>$\epsilon = \eta_1$ | 1       | $-\frac{1}{\eta_1 - \alpha} u e^{-\eta_2 u}$                                   |
| $\eta_1 \neq \alpha$<br>$\epsilon = \alpha$ | (2)     | $\frac{\eta_1 + \eta_2}{(\eta_1 - \alpha)(\eta_2 + \alpha)} u e^{-\alpha u}$   |

Finally, we look at the resonant forms for  $E_z$  with  $u > 0$ , Equation (3.39). Again referring to the numbered terms and using Table 3.2, the  $E_z$  equation changes may be obtained for the various resonances.

TABLE 3.2

$E_z$  RESONANT TERM REPLACEMENTS

| Resonance                                   | Replace   | With   |
|---|-----------|--|
| $\eta_1 = \alpha$<br>$\epsilon \neq \alpha$ | (1) + (2) | $\left(\frac{1}{\epsilon - \alpha}\right) \frac{\alpha e^{-\alpha u} - \epsilon e^{-\epsilon u}}{\eta_2 + \alpha}$ |
|   | (3)       | $e^{-\alpha u} (\alpha u - \beta)$   |
| $\eta_1 = \alpha$<br>$\epsilon = \alpha$    | (1) + (2) | $\left(\frac{1}{\eta_2 + \alpha}\right) e^{-\alpha u} (\alpha u - 1)$  |
|   | (3)       | $e^{-\alpha u} (+\alpha u - \beta)$  |
| $\eta_1 \neq \alpha$<br>$\epsilon = \eta_1$ | (1)       | $\left(\frac{1}{\eta_1 - \alpha}\right) e^{-\eta_1 u} (\eta_1 u - 1)$  |
| $\eta_1 \neq \alpha$<br>$\epsilon = \alpha$ | (2)       | $-\frac{(\eta_1 + \eta_2)}{(\eta_1 - \alpha)(\eta_2 + \alpha)} e^{-\alpha u} (\alpha u - 1)$                       |

The above equations have been programmed to obtain CALCOMP plots of  $B_\theta$ ,  $E_r$ , and  $E_z$  for a given set of  $\alpha$ ,  $k$ ,  $\beta$ ,  $\lambda_1/R$  parameters, including all resonant conditions. Several plots are given below. To obtain field values use

$$\begin{aligned}
 B_\theta &= (-) \text{ B THETA } \left(\frac{4\pi}{c}\right) C_1 \left(\frac{\lambda_1}{R}\right) J_1 \left(\frac{\lambda_1}{R} r\right) \text{ (gauss)} \\
 E_r &= (-) \text{ ER } \frac{4\pi}{c} C_1 \left(\frac{\lambda_1}{R}\right) J_1 \left(\frac{\lambda_1}{R} r\right) \times 300 \text{ V/cm} \\
 E_z &= (-) \text{ EZ } \frac{4\pi}{c} C_1 J_0 \left(\frac{\lambda_1}{R} r\right) \times 300 \text{ V/cm}
 \end{aligned} \tag{3.41}$$

where B THETA, etc., are the ordinates of the plots, and

$$C_1 = \frac{I_b^{\text{peak}} \text{ (amps)}}{20\pi} \left(\frac{\lambda_1 c}{R^2}\right) \frac{1}{J_1(\lambda_1)} \tag{3.42}$$

and 
$$\frac{4\pi C_1}{c} \cong 0.923 I_b^p / R^2, \quad R \text{ in cm.}$$

If  $I_b^{\text{peak}} = 5 \times 10^4$  amps,  $4\pi C_1/c = 4.6 \times 10^4 / R^2$ , and, e.g.,

$$E_z = 1.4 \times 10^7 \frac{\lambda_1}{R^2} J_0 \left(\frac{\lambda_1}{R} r\right) \text{ EZ V/cm.}$$

We also plot a function that indicates whether the assumed beam profile function is constrictive or divergent; i.e., whether the radial force on the beam electrons is inward or outward.

The radial force on a beam electron for constant z directed beam velocity,  $F_r$ , is

$$F_r = -e [E_r - \beta B_\theta] \quad (3.43)$$

Thus, if  $E_r - \beta B_\theta > 0$  the beam electrons experience a pinching force. We have

$$\text{Constriction: } E_r - \beta B_\theta > 0 \text{ or } (ER - \beta B \text{ THETA}) < 0$$

$$\text{Divergence: } E_r - \beta B_\theta < 0 \text{ or } (ER - \beta B \text{ THETA}) > 0$$

A plot of  $(ER - \beta B \text{ THETA}) \equiv ERBT$  accompanies the field plots for each case below. Table 3.3 gives the parameters for the graphs.

TABLE 3.3

| Case | $\alpha$  | $\beta$ | k               | $\lambda_1/R$ |
|------|-----------|---------|-----------------|---------------|
| 1    | $10^{-2}$ | 0.7     | 6               | 1             |
| 2    | $10^{-2}$ | 0.7     | 0               | 1             |
| 3    | $10^{-2}$ | 0.7     | 49.995          | 1             |
| 4    | $10^{-2}$ | 0.99498 | 49.995          | 1             |
| 5    | $10^{-2}$ | 0.7     | $6 \times 10^4$ | 1             |

The  $\alpha$  value  $10^{-2}$  corresponds approximately to a current two e-folding time of 7 nsec. We have taken two  $\beta$  values corresponding to  $\sim 200$  keV and 5 MeV electrons. The three k values correspond to conductivities of

| k               | $\sigma$                |  |
|-----------------|-------------------------|--|
| 0               | 0                       | (vacuum)   |
| 6               | $3 \times 10^{10}$ /sec | (weakly ionized gas)                                   |
| 50              | $2.4 \times 10^{11}$    | (intermediate conductivity)                            |
| $6 \times 10^4$ | $10^{14} = 100$ mhos/cm | (fully ionized plasma<br>of $\sim$ few eV temperature) |

The graphs exhibit many interesting features with physical application. First of all we note that  $E_z$  is small and negative for  $u < 0$ , and reverses sign when  $\sigma \neq 0$  just behind the beam front. Recalling from Equation (3.41) that the graph EZ values scale directly with  $E_z$  at the center of the pipe ( $r = 0$ ) where  $J_0 = 1$ , the field peak for case 4 (5 MeV electrons) with  $I^{\text{peak}} = 5 \times 10^4$  amps, e.g., is  $\approx 9 \times 10^4$  V/cm. Such an  $E_z$  field would, of course, bunch electrons near the center of the beam, with the maximum bunching determined by the electron kinetic energy. Near the pipe wall where  $E_z$  is zero, the electrons would precede the center electrons, suggesting the formation of a current sheath near the pipe wall in front of the beam core.\* Beam electrons would be bunched near the center until  $E_r$  rises to overcome the  $\bar{V} \times \bar{B}$  force ( $ERBT > 0$ ), when electrons would be lost to the pipe. In other words, we see the crude outline of the beam penetration process and a possible ion acceleration mechanism near the beam front. The actual ion energies attainable may be considerably higher than the primary electron kinetic energy, depending on the duration of the fields or the trapping time. The duration depends on the effective penetration velocity in the medium and, for the cases where the beam ionizes the gas, the breakdown distance. We consider these questions in more detail in Section 4.

\*This variation in  $E_z$  with radius points out an essential distinction between beams in large cavities and in pipes with radius nearly equal to the beam radius. The current sheath effect in pipes has many interesting implications for stability and beam bending.

The  $B_\theta$  plots indicate the time or distance behind the beam front over which partial current neutralization decays and thus where the  $B_\theta$  values approach those of the beam only. As  $B_\theta$  approaches  $(\eta_1 \eta_2)^{-1}$ , plasma currents become negligible.

A finite beam length as well as multiple pulse fields, or any other desired superposition of currents may easily be calculated for the assumed radial current function of the model. The results given by the model may be experimentally verified by low pre-ionization of the gas. We can ensure that electron avalanching will not occur, and therefore that the conductivity remains roughly constant, by keeping the E-fields below determined levels for a given gas pressure. Equations (3.37), (3.38), and (3.39) then directly give the required conductivity to achieve this criterion. The wall currents, plasma neutralization, etc., are given by this theory.

Case 1. Weakly Conducting Gas

Parameters:

$$\sigma \approx 3 \times 10^{10} / \text{sec} \approx 3 \times 10^{-2} \text{ mhos/cm}$$

$$E = \text{electron energy} = 200 \text{ keV}$$

$$R = 2.4 \text{ cm}$$

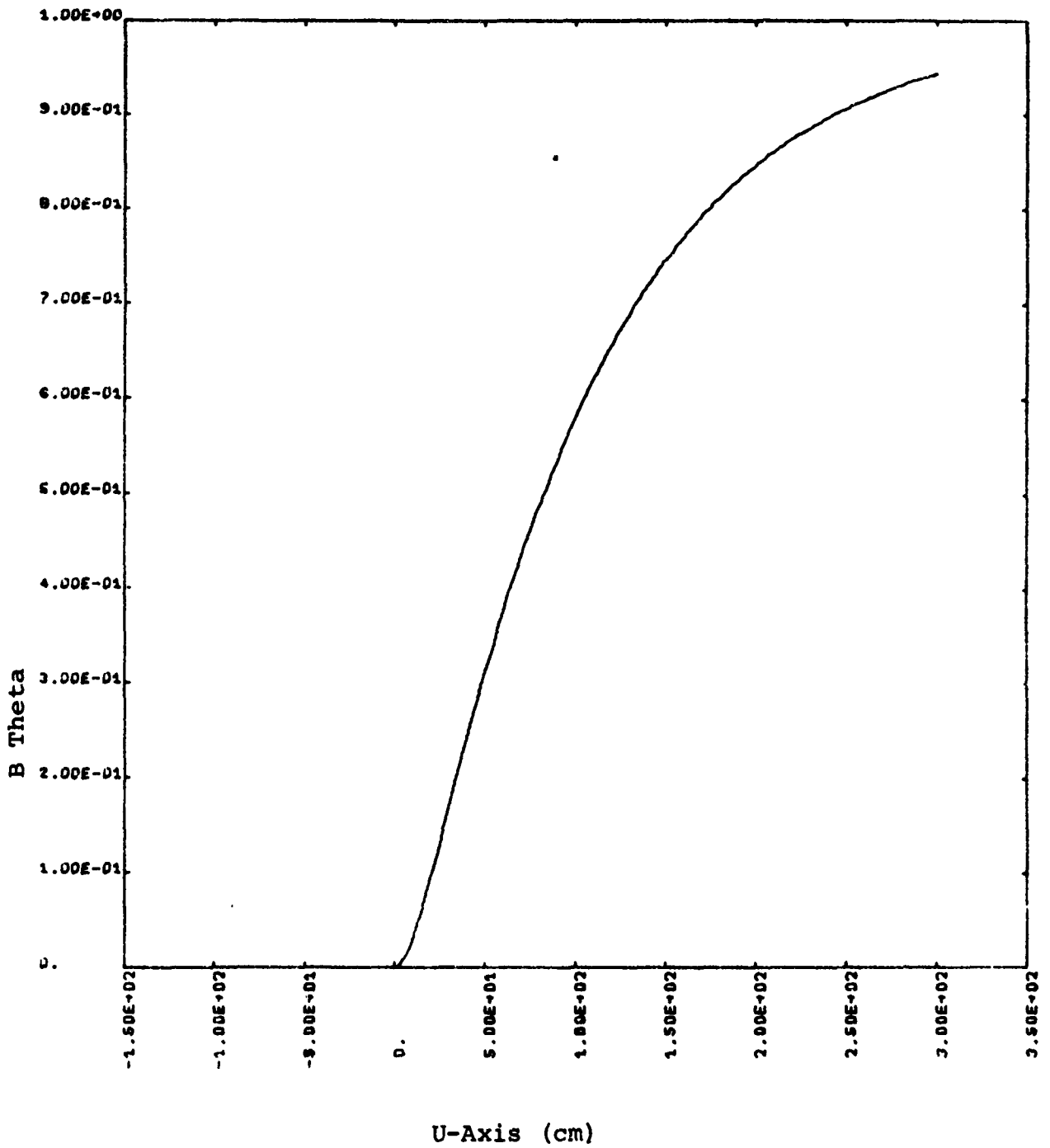
$$t_r \approx 7 \text{ nsec}$$

$$I_b^P = 5 \times 10^4 \text{ amps}$$

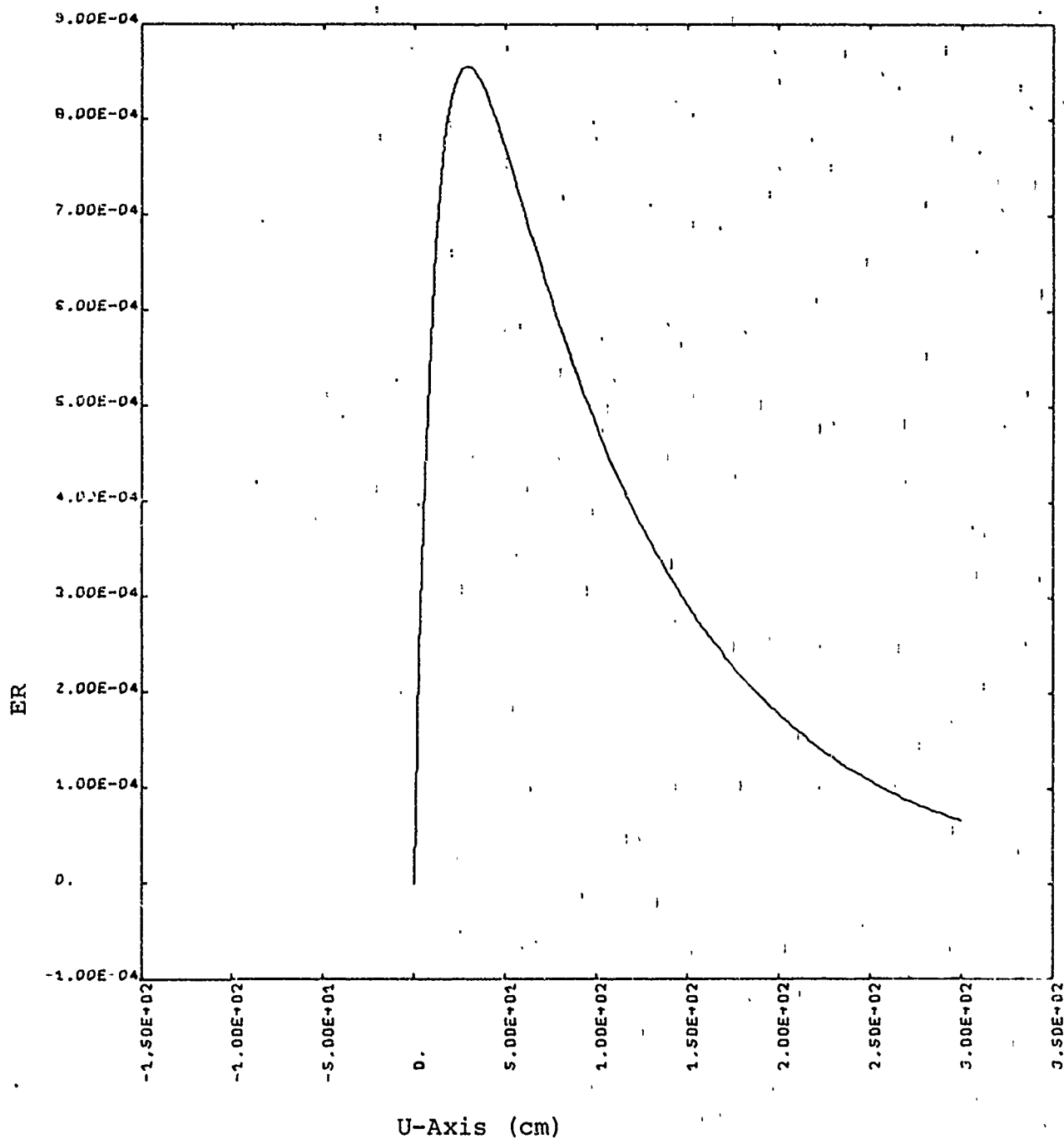
$$B_\theta(r, u) = -8 \times 10^3 J_1(r) B \text{ THETA (gauss)}$$

$$E_r(r, u) = -2.4 \times 10^6 J_1(r) ER \text{ (V/cm)}$$

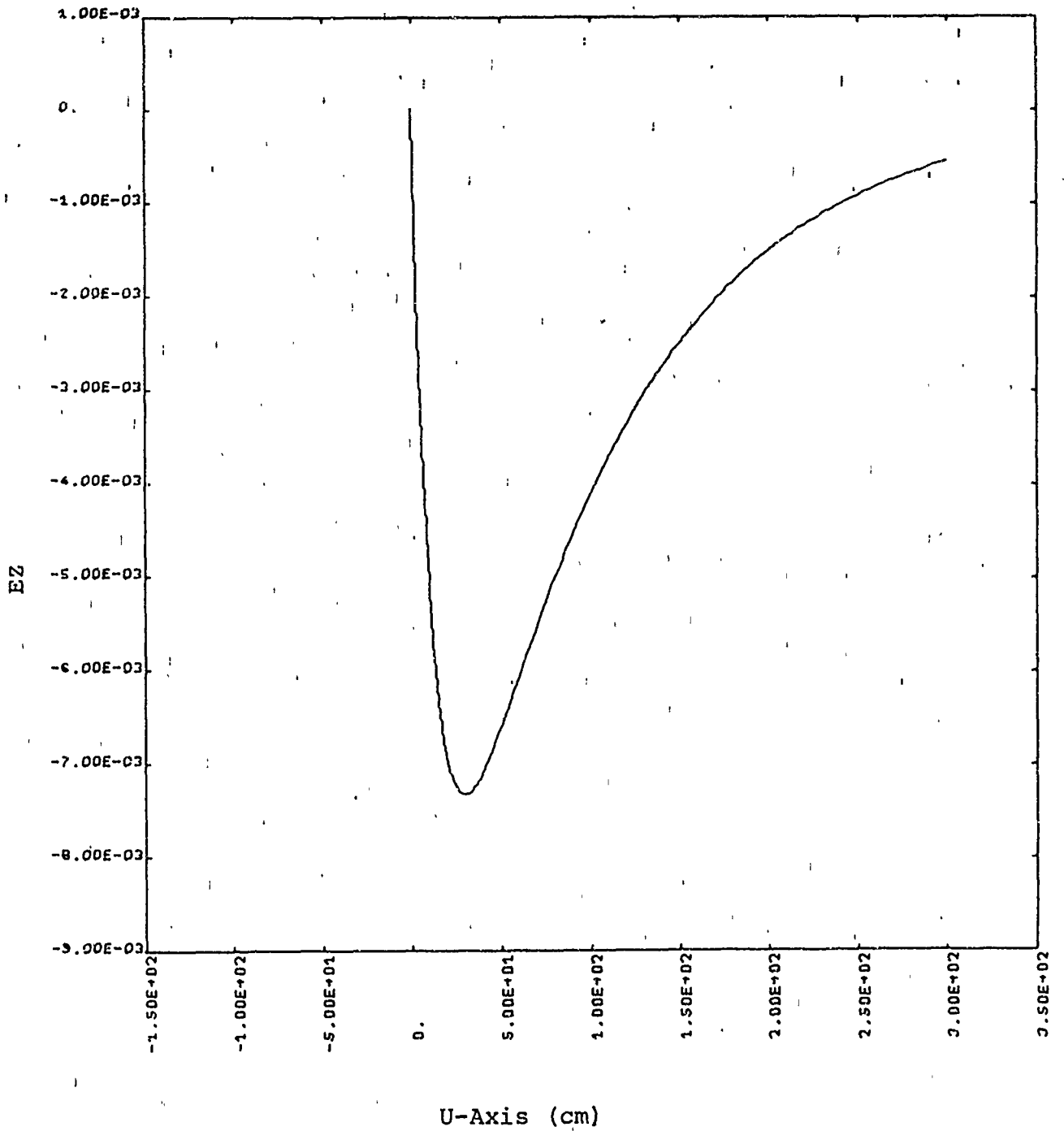
$$E_z(r, u) = -2.4 \times 10^6 J_0(r) EZ \text{ (V/cm)}$$



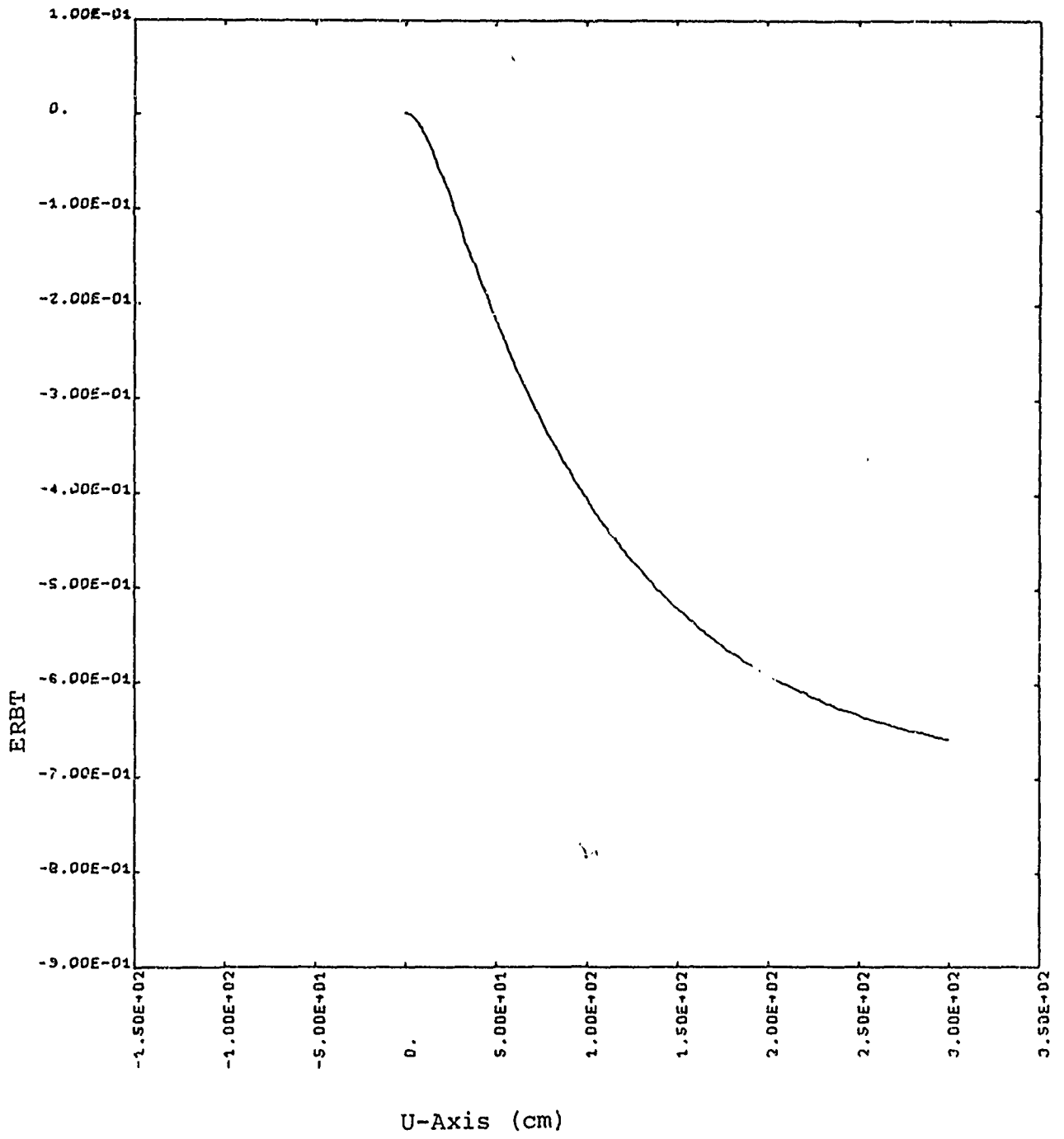
Case 1. B Theta (u)



Case 1. ER



Case 1. EZ



Case 1. ERBT

Case 2. Vacuum Propagation

Parameters:

$$\sigma = 0$$

$$E \approx 200 \text{ keV}$$

$$R = 2.4$$

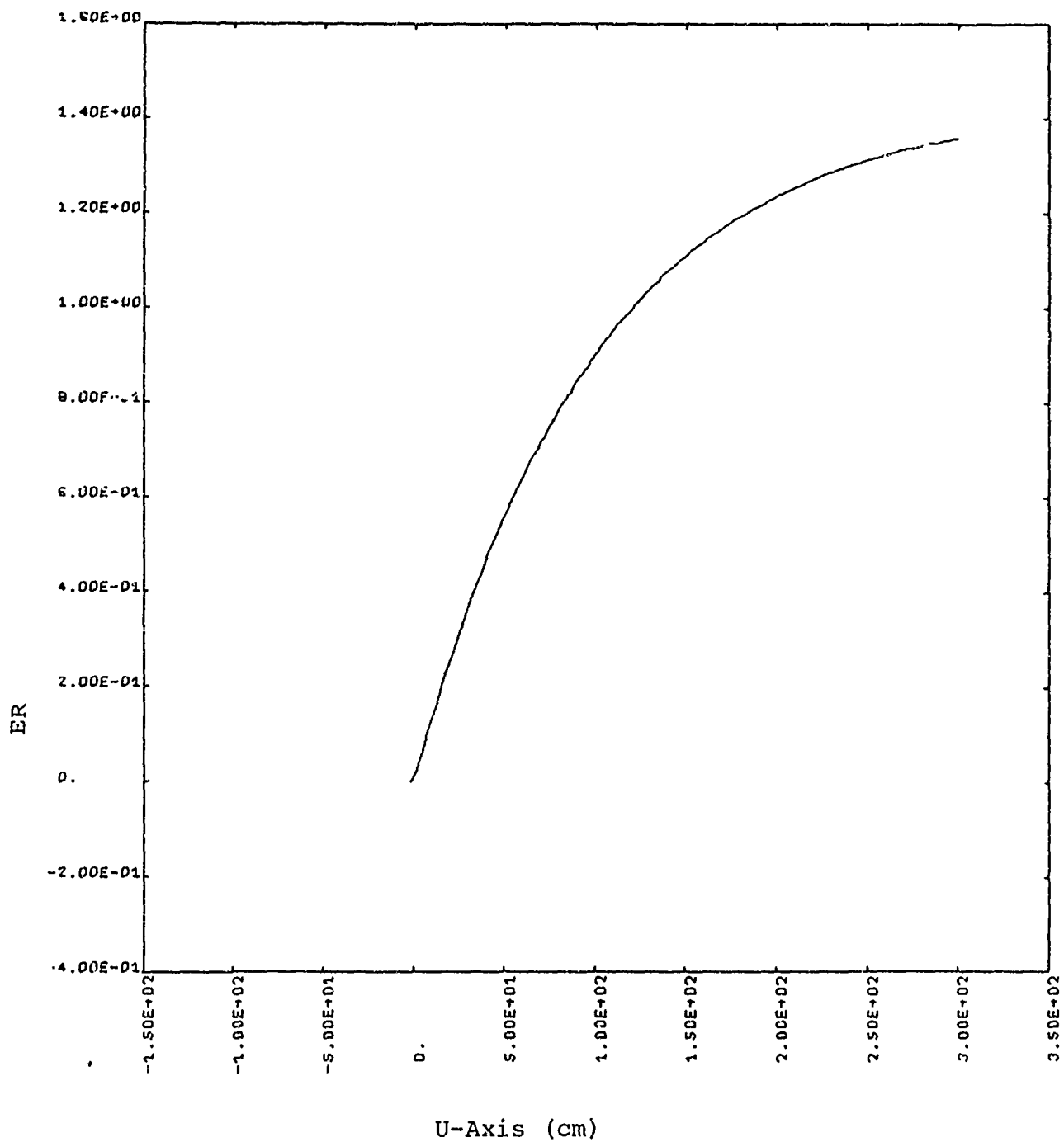
$$t_r = 7 \text{ nsec}$$

$$I_b^P = 5 \times 10^4 \text{ amperes}$$

$$B_\theta(r,u) = - 8 \times 10^3 J_1(r) \text{ BTETA (gauss)}$$

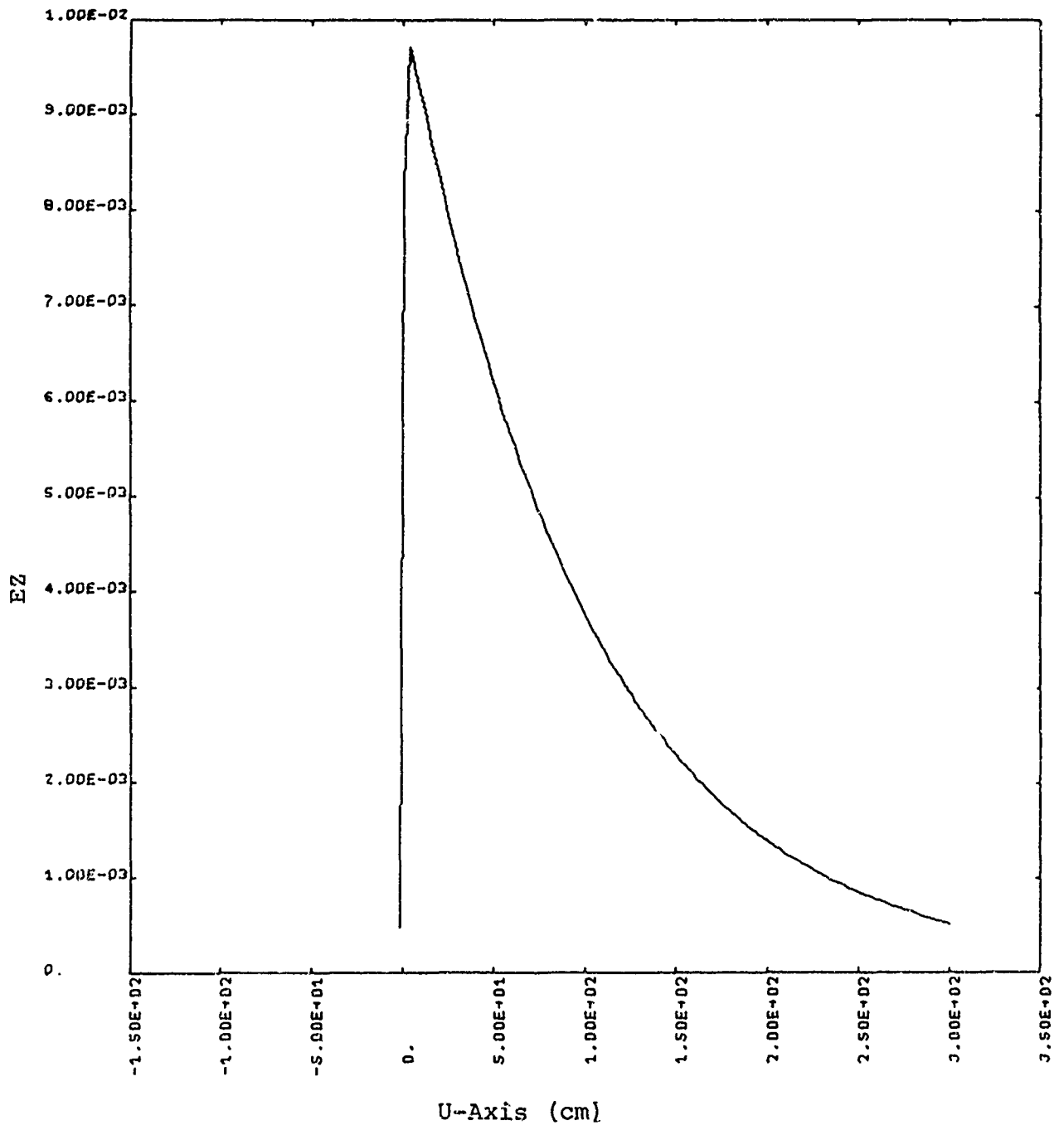
$$E_r(r,u) = - 2.4 \times 10^6 J_1(r) \text{ ER (V/cm)}$$

$$E_z(r,u) = - 2.4 \times 10^6 J_0(r) \text{ EZ (V/cm)}$$

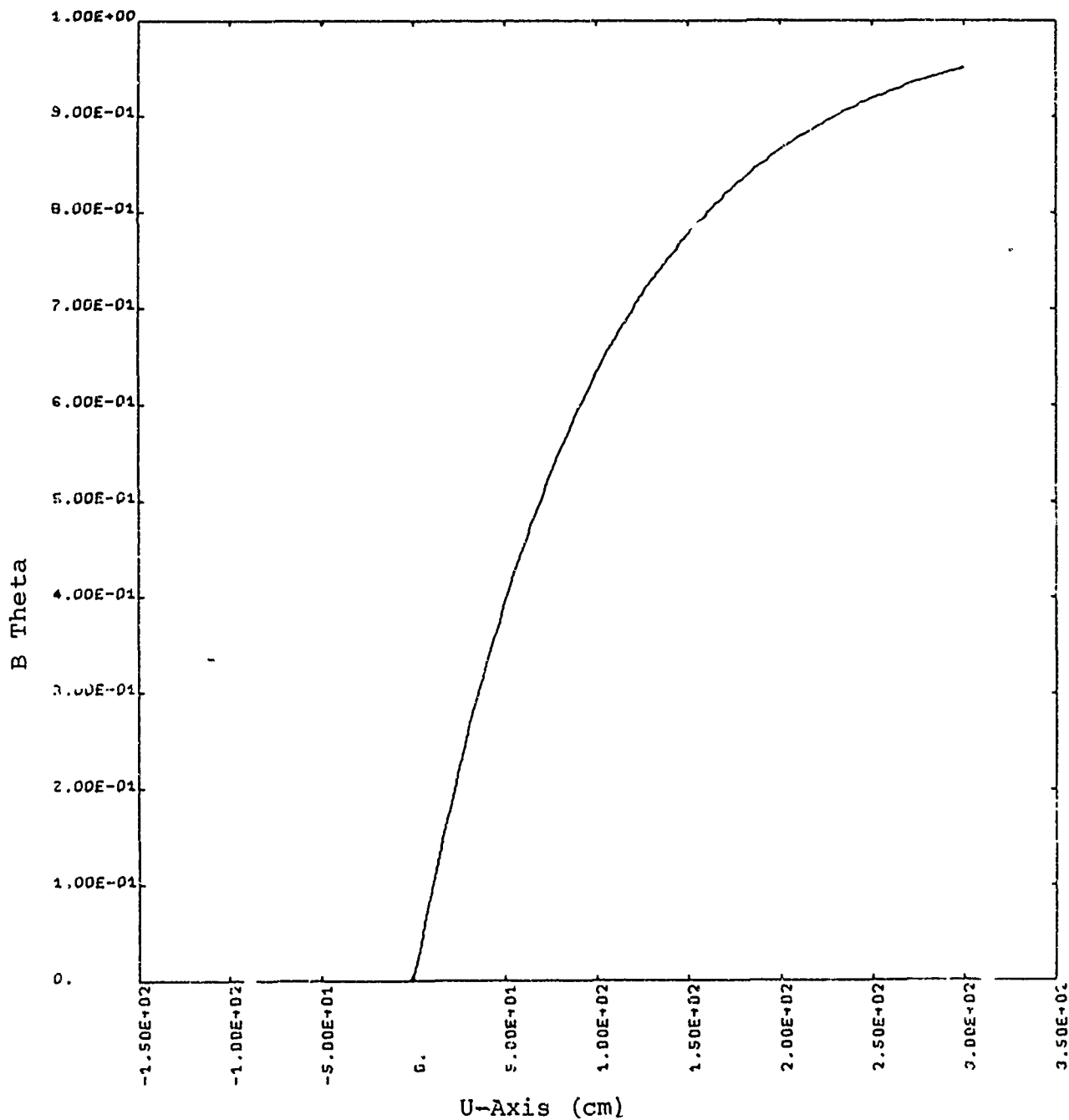


Case 2. ER

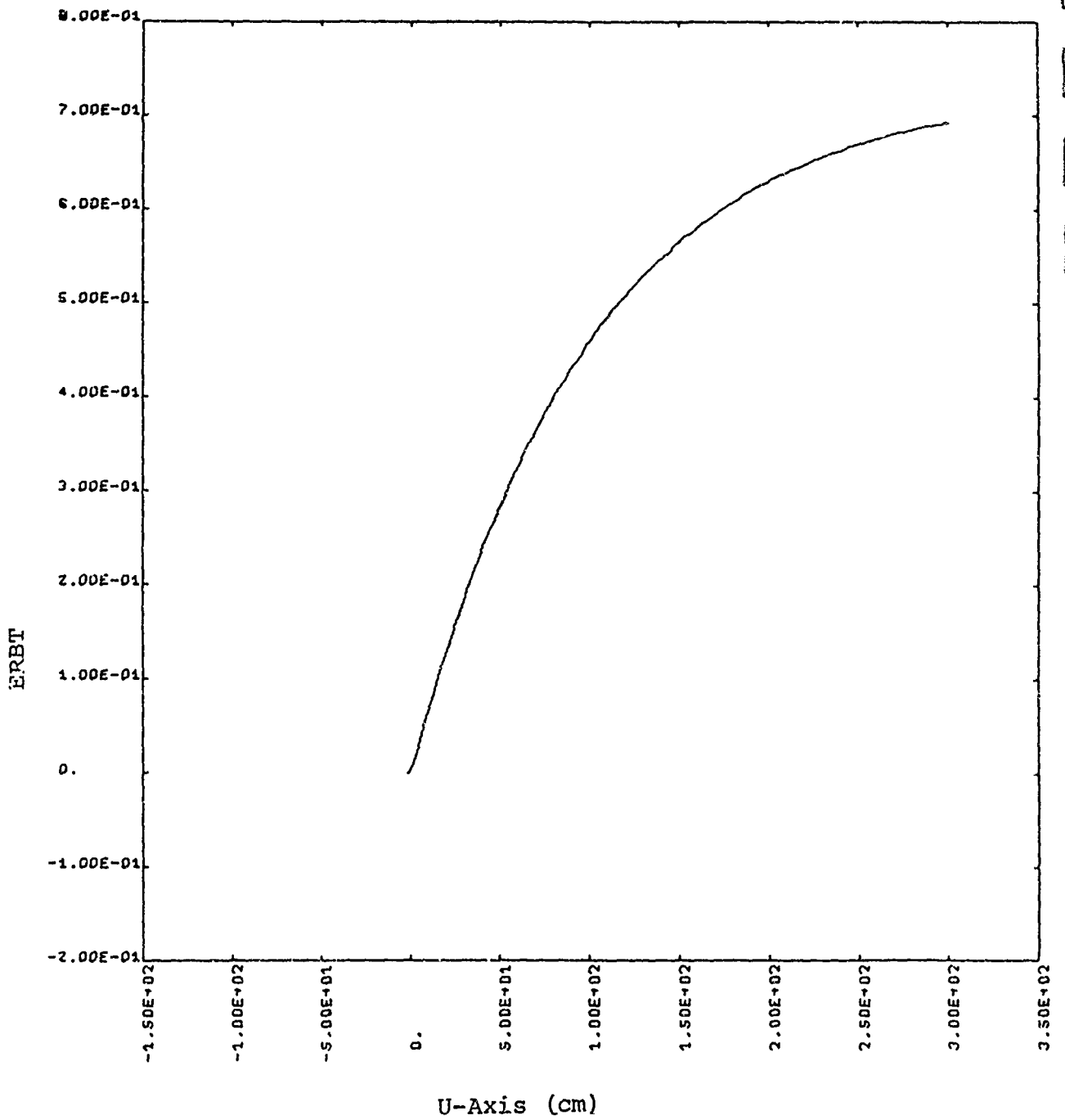
Note that  $E_z$  is in direction to accelerate beam electrons.  
Space charge field dominates inductive component.



Case 2.  $E_z$



Case 2. B Theta (u)



Case 2. ERBT

Case 3. Intermediate Conductivity, Low Energy Electrons

Parameters:

$$\sigma \approx 2.4 \times 10^{11} / \text{sec} \approx 0.24 \text{ mhos/cm}$$

$$E = 200 \text{ keV}$$

$$R = 2.4 \text{ cm}$$

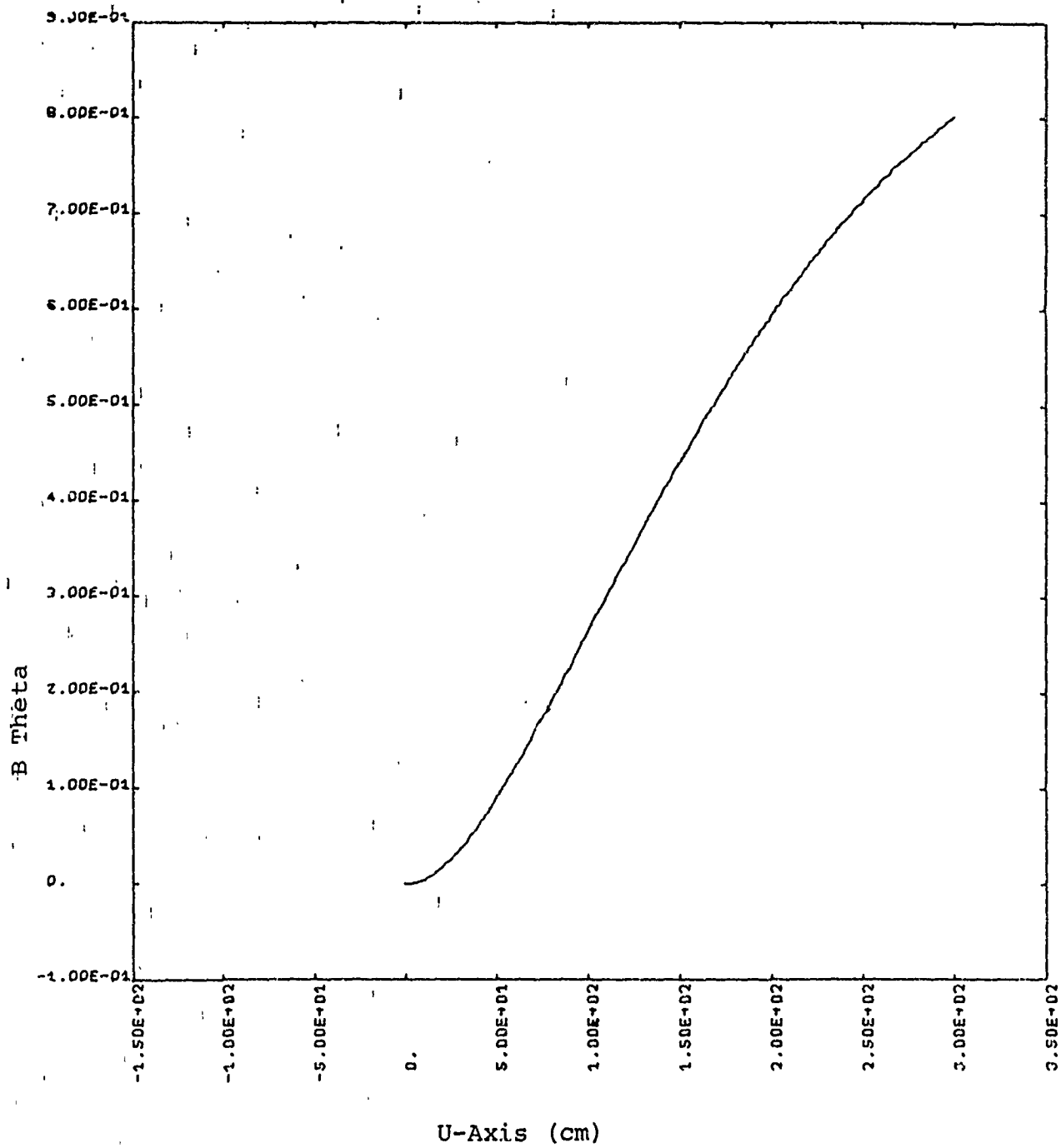
$$t_r = 7 \text{ nsec}$$

$$I_b^P = 5 \times 10^4 \text{ amps}$$

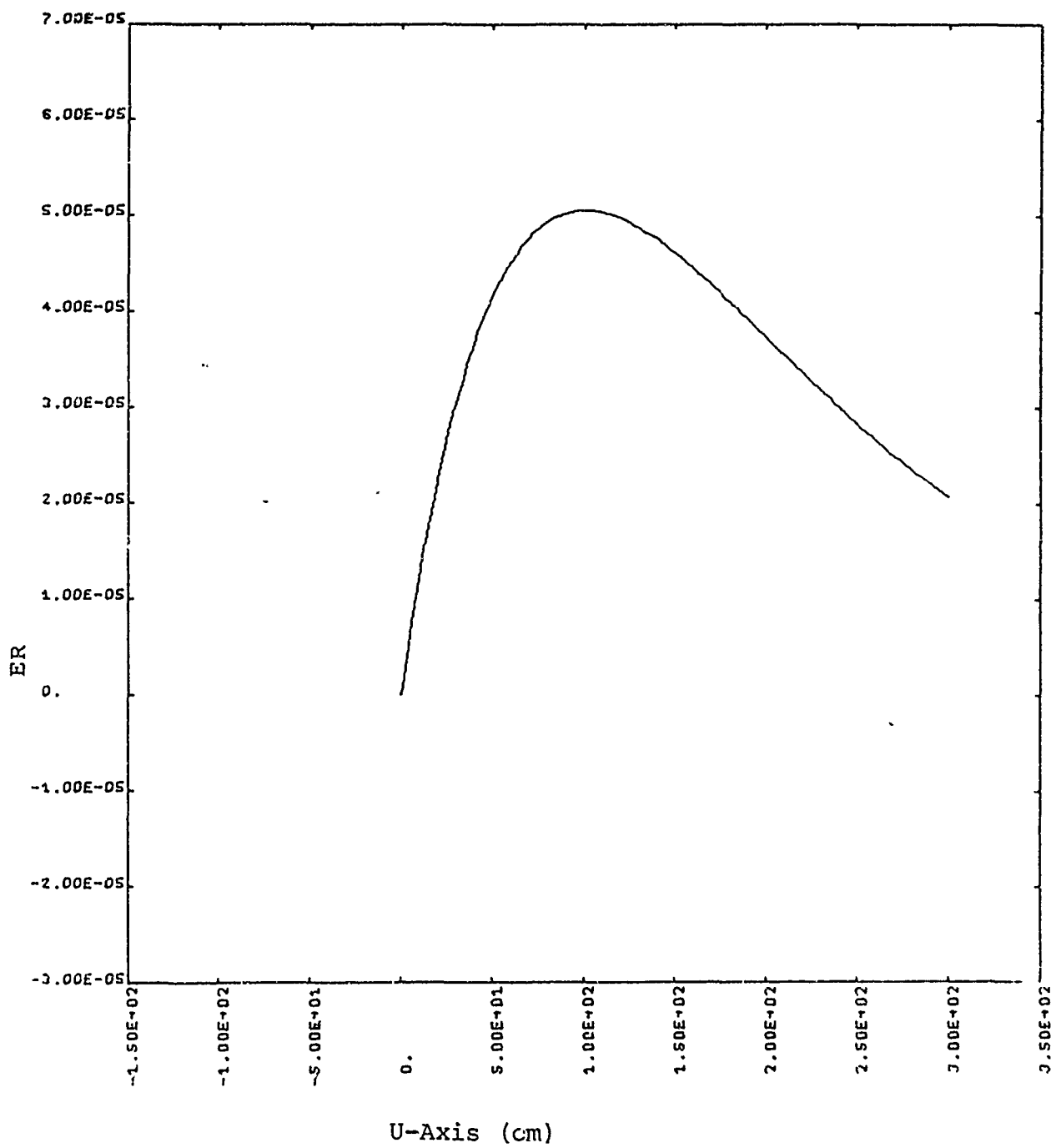
$$B_\theta(r, u) = -8 \times 10^3 J_1(r) B \text{ THETA (gauss)}$$

$$E_r(r, u) = -2.4 \times 10^6 J_1(r) ER \text{ (V/cm)}$$

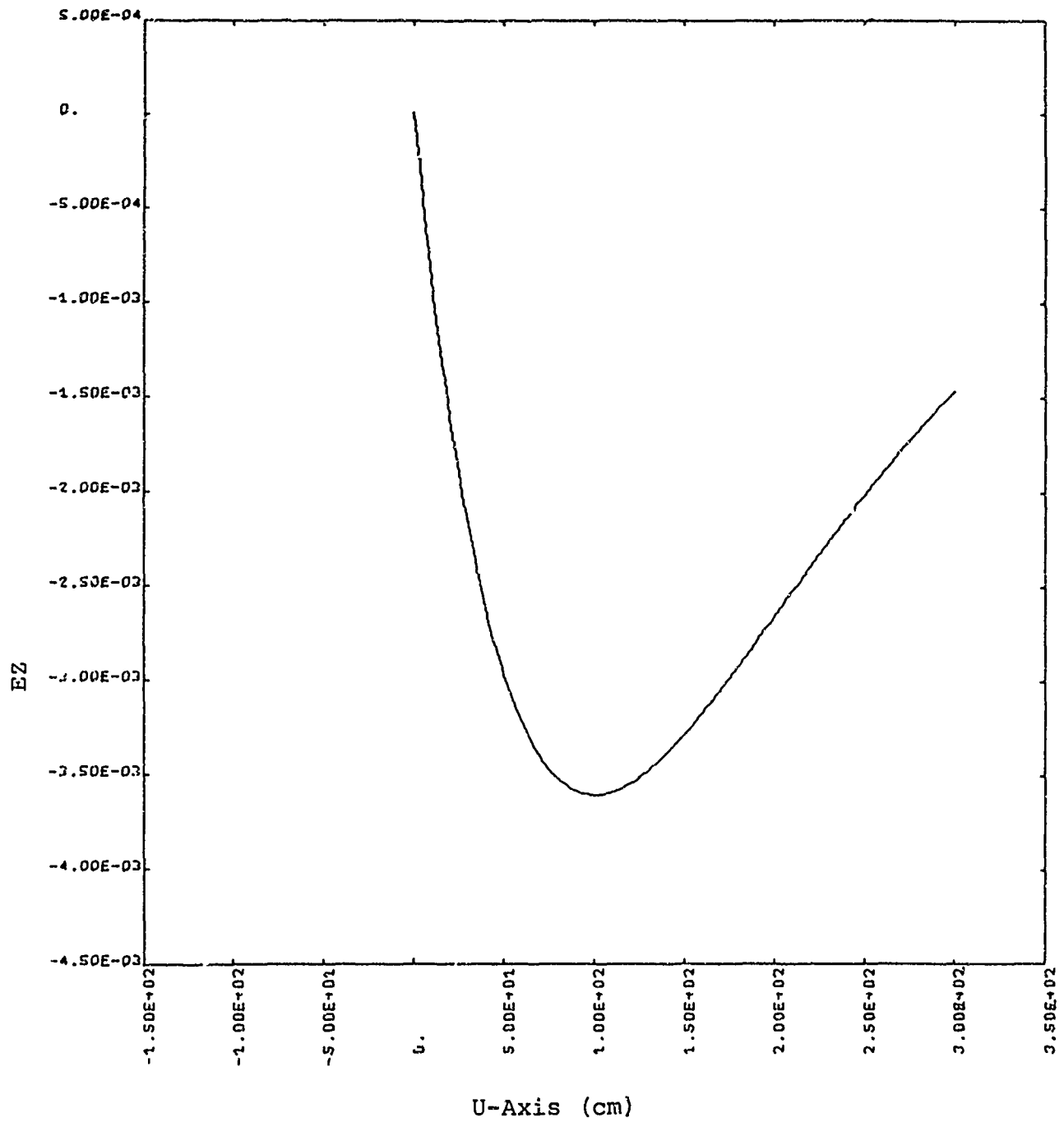
$$E_z(r, u) = -2.4 \times 10^6 J_0(r) EZ \text{ (V/cm)}$$



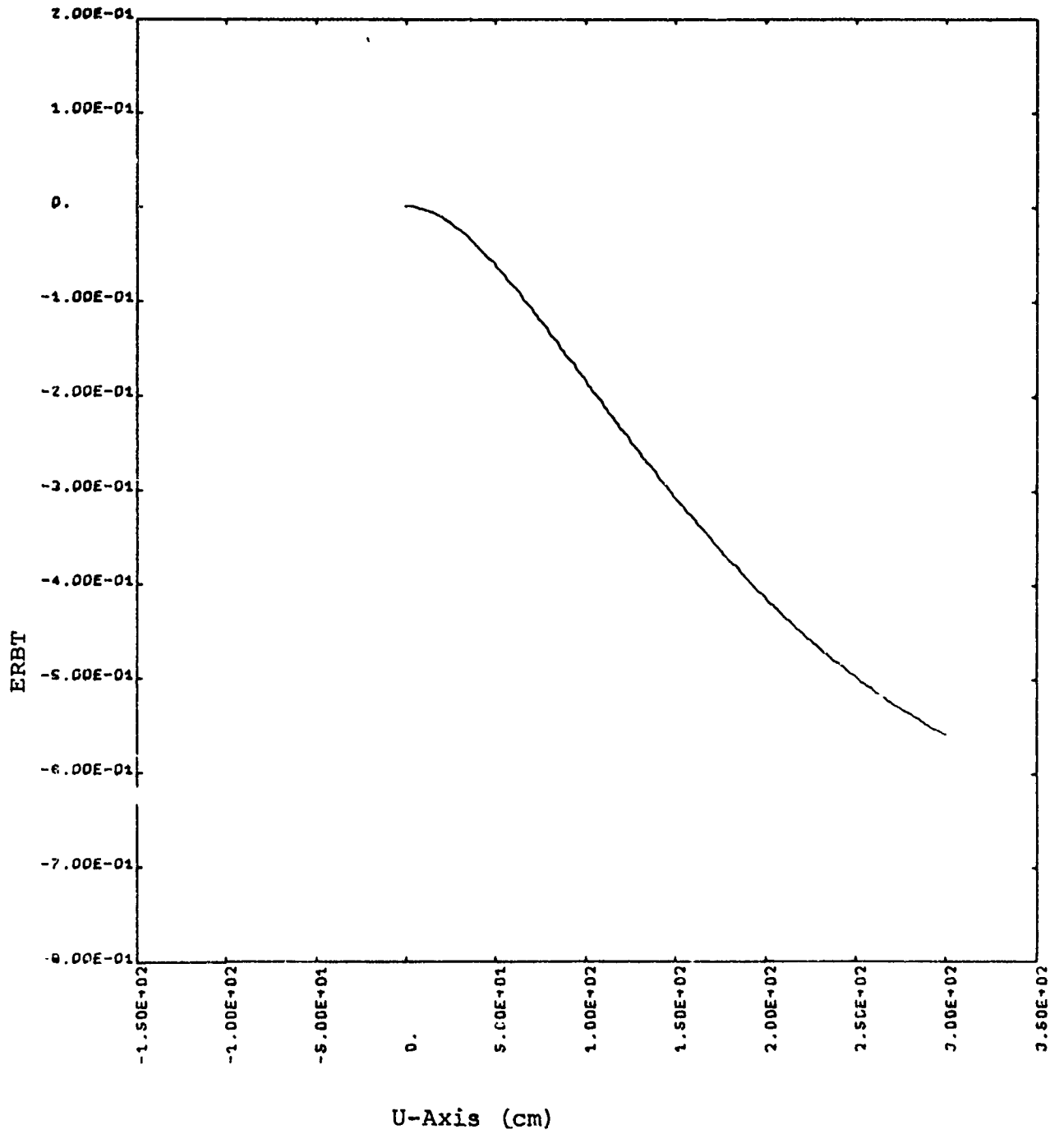
Case 3. B Theta (u)



Case 3. ER



Case 3. EZ



Case 3. ERBT

Case 4. Intermediate Conductivity, High Energy Electrons

Parameters:

$$\sigma = 2.4 \times 10^{11} / \text{sec} \approx 0.24 \text{ mhos/cm}$$

$$E = 5 \text{ MeV}$$

$$R = 2.4 \text{ cm}$$

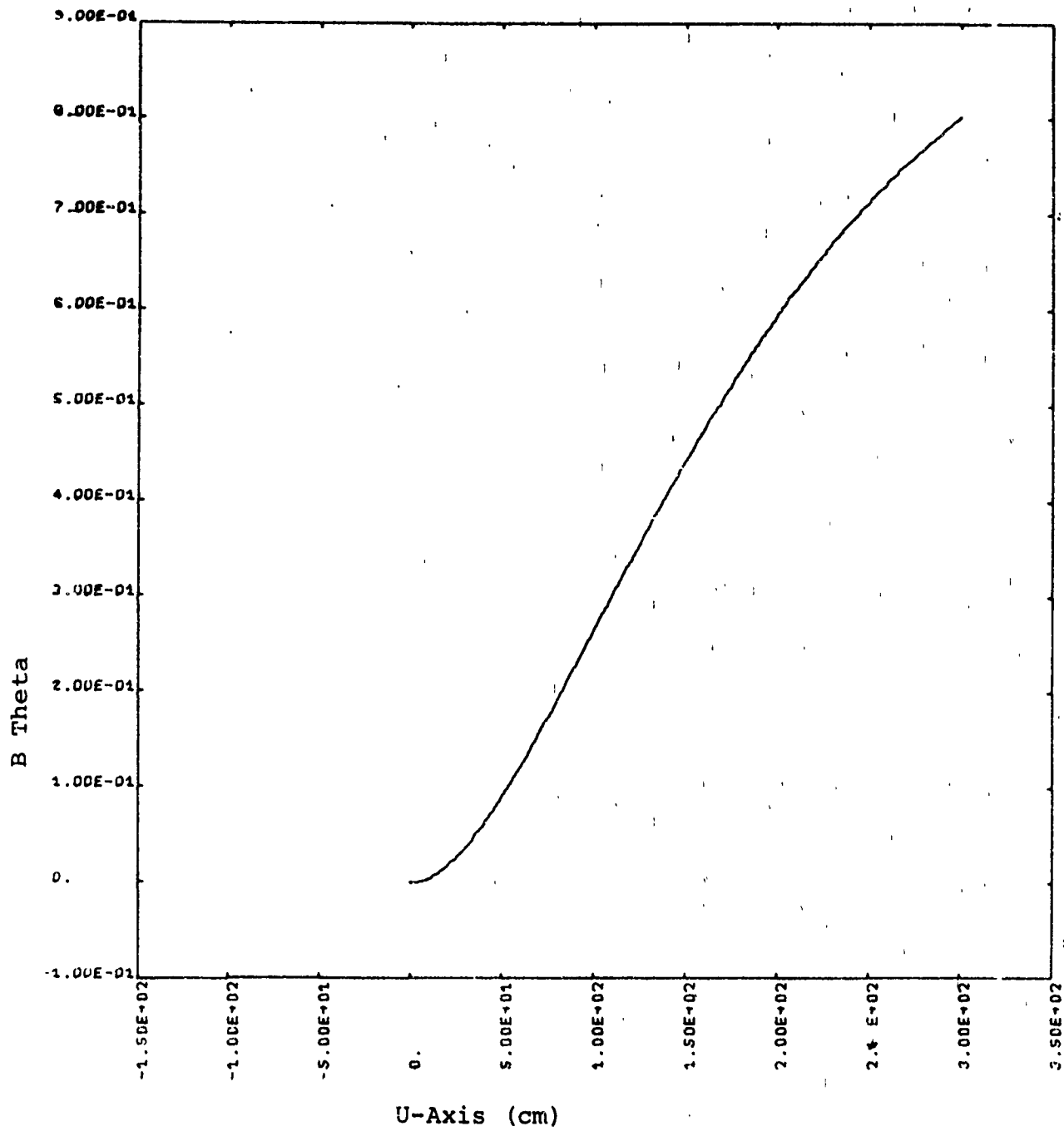
$$t_r = 7 \text{ nsec}$$

$$I_b^p = 5 \times 10^4 \text{ amperes}$$

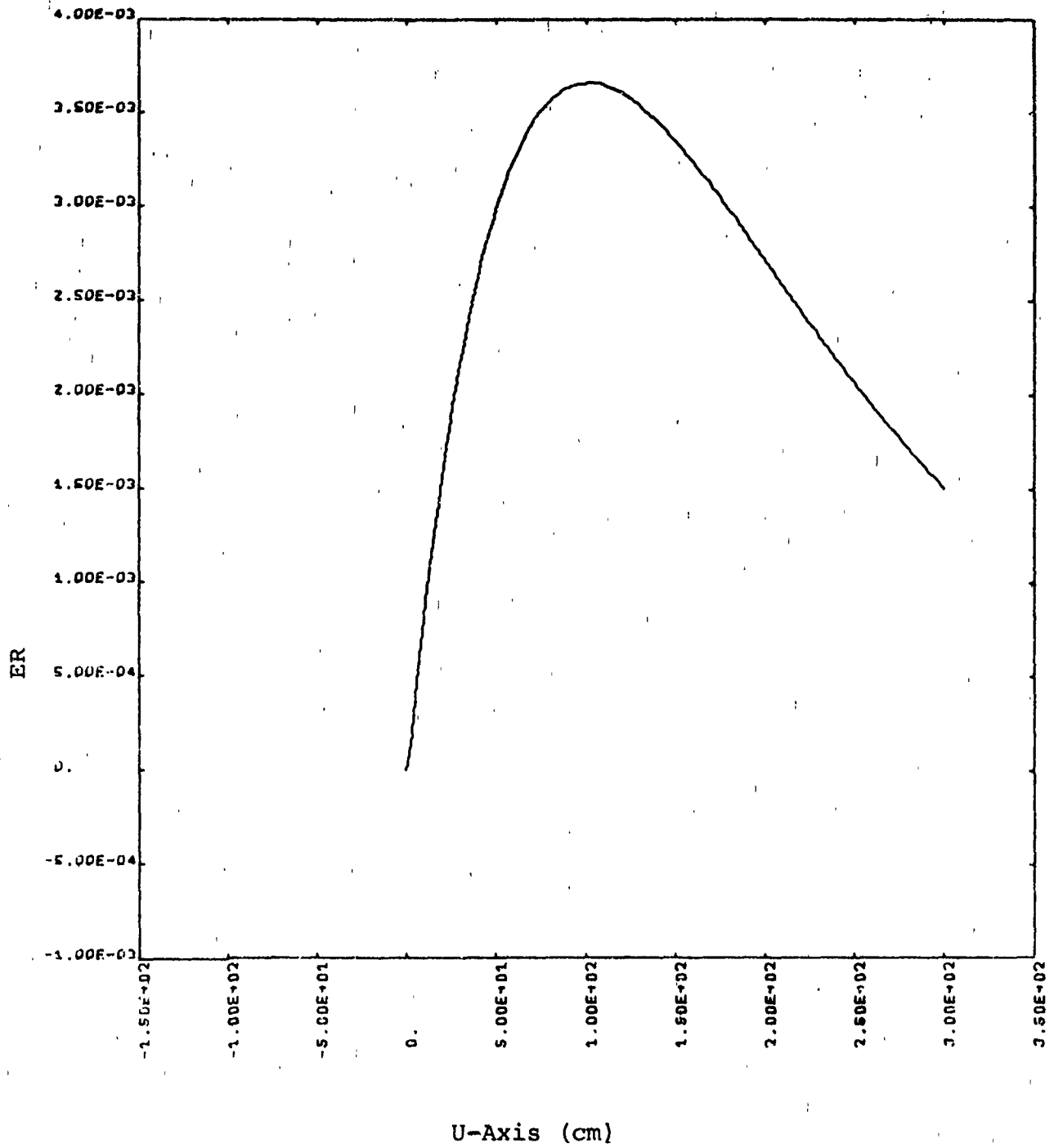
$$B_\theta(r, u) = -8 \times 10^3 J_1(r) \text{ B THETA (gauss)}$$

$$E_r(r, u) = -2.4 \times 10^6 J_1(r) \text{ ER (V/cm)}$$

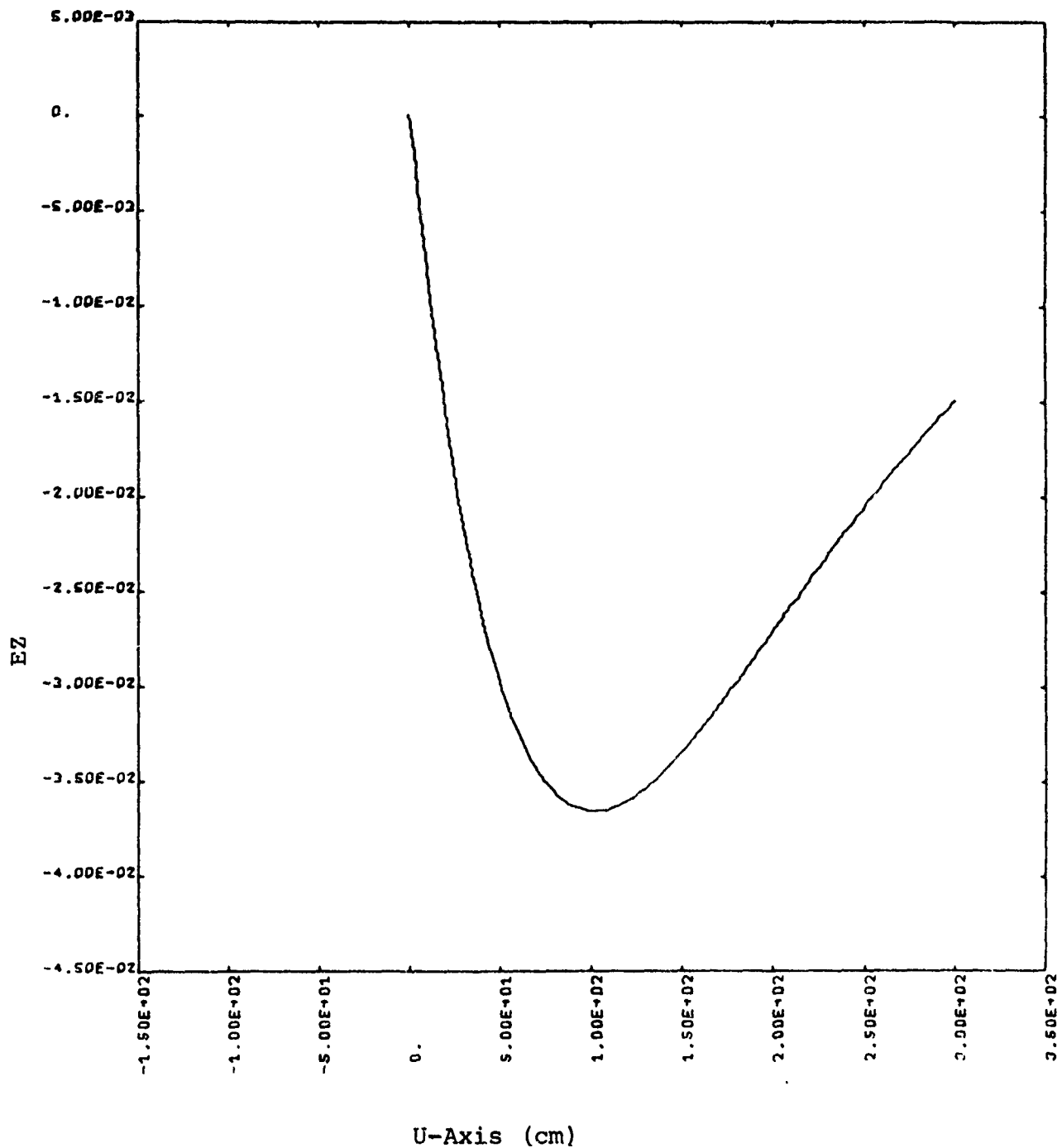
$$E_z(r, u) = -2.4 \times 10^6 J_0(r) \text{ EZ (V/cm)}$$



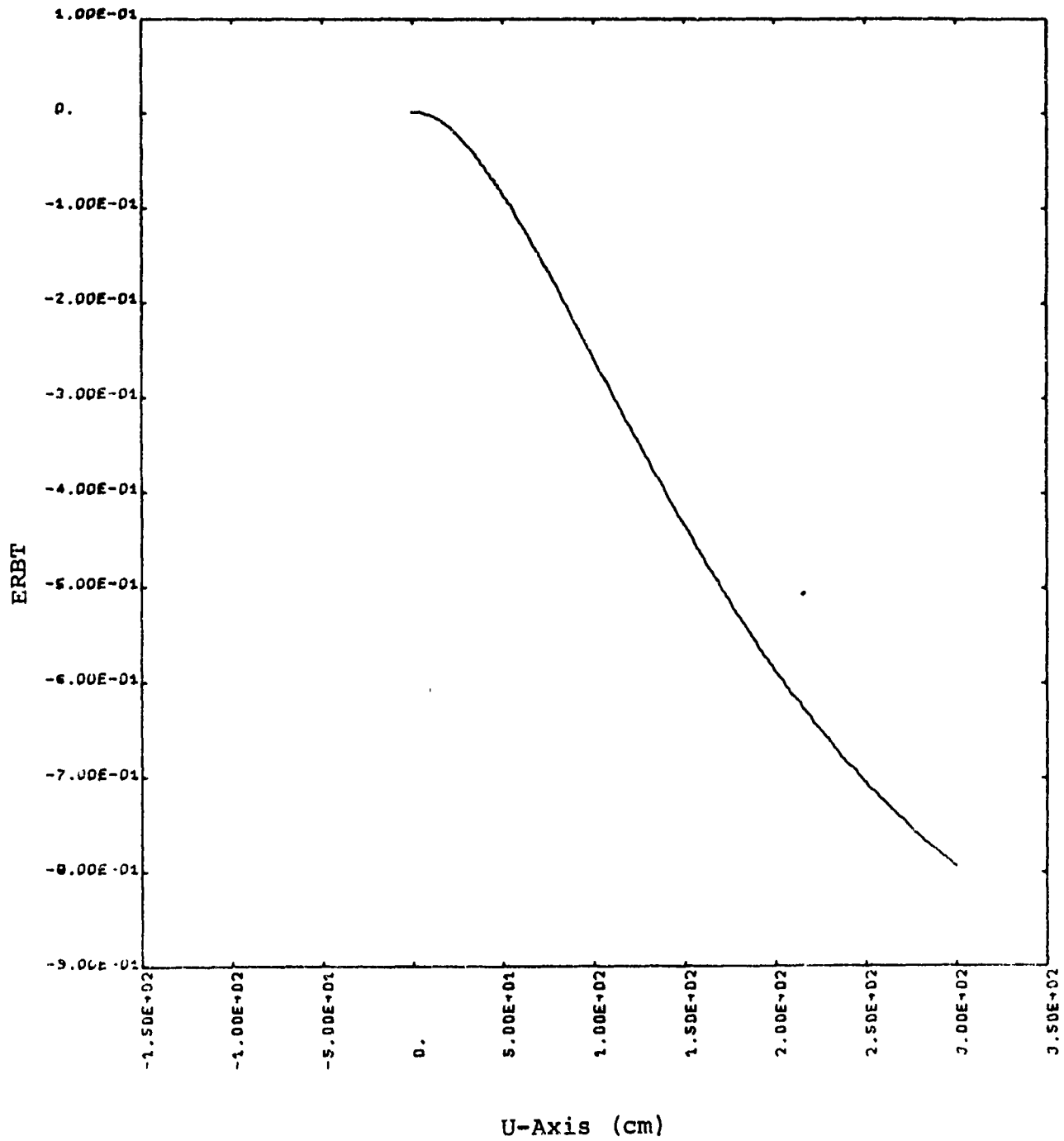
Case 4. B Theta (u)



Case 4. ER



Case 4. EZ



Case 4. ERBT

Case 5. High Conductivity

Parameters:

$$\sigma = 10^{14}/\text{sec} \approx 100 \text{ mhos/cm}$$

$$E = 200 \text{ keV}$$

$$R = 2.4 \text{ cm}$$

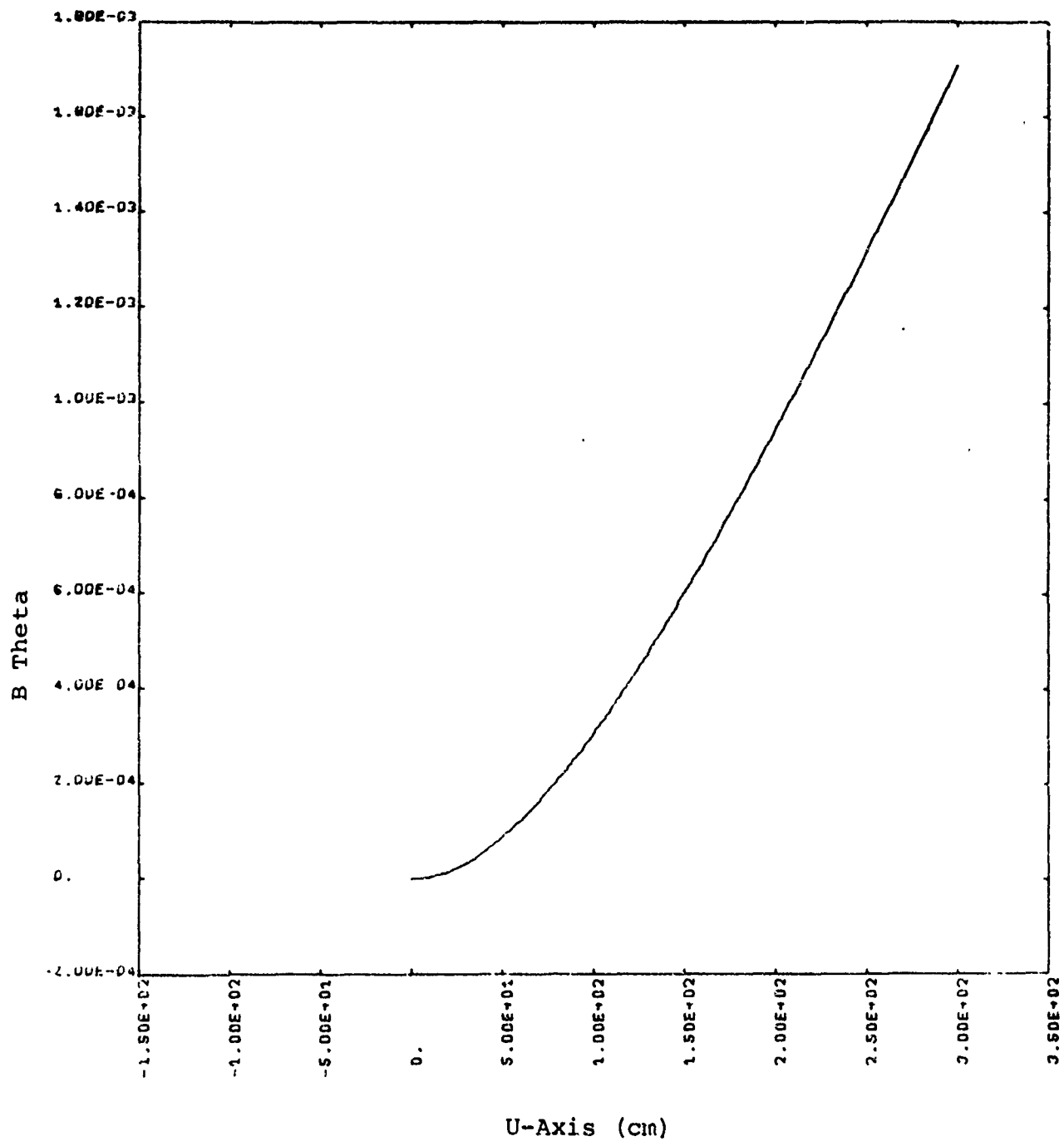
$$t_r = 7 \text{ nsec}$$

$$I_b^P = 5 \times 10^4 \text{ amps}$$

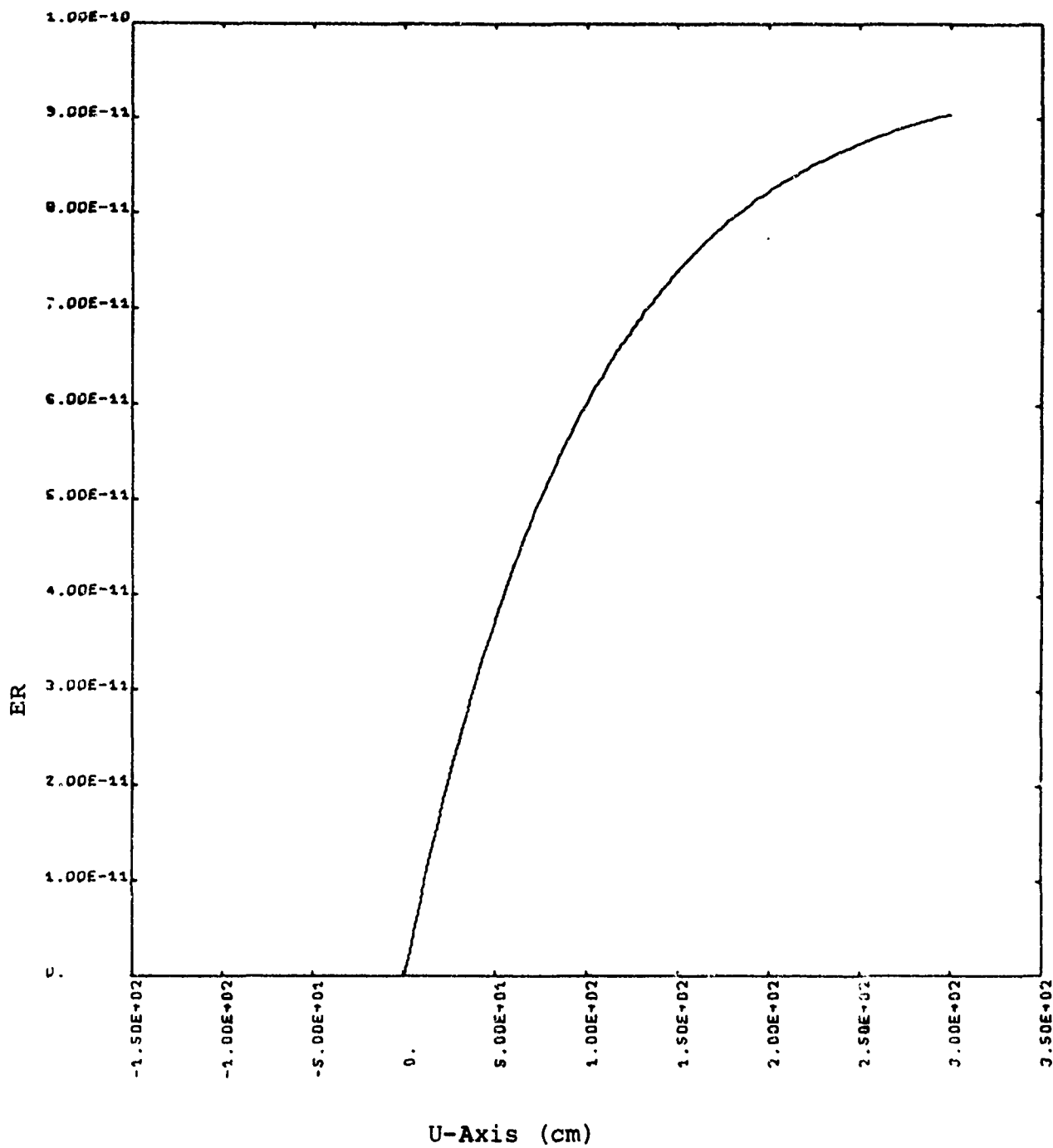
$$B_\theta(r,u) = -8 \times 10^3 J_1(r) B \text{ THETA (gauss)}$$

$$E_r(r,u) = -2.4 \times 10^6 J_1(r) ER \text{ (V/cm)}$$

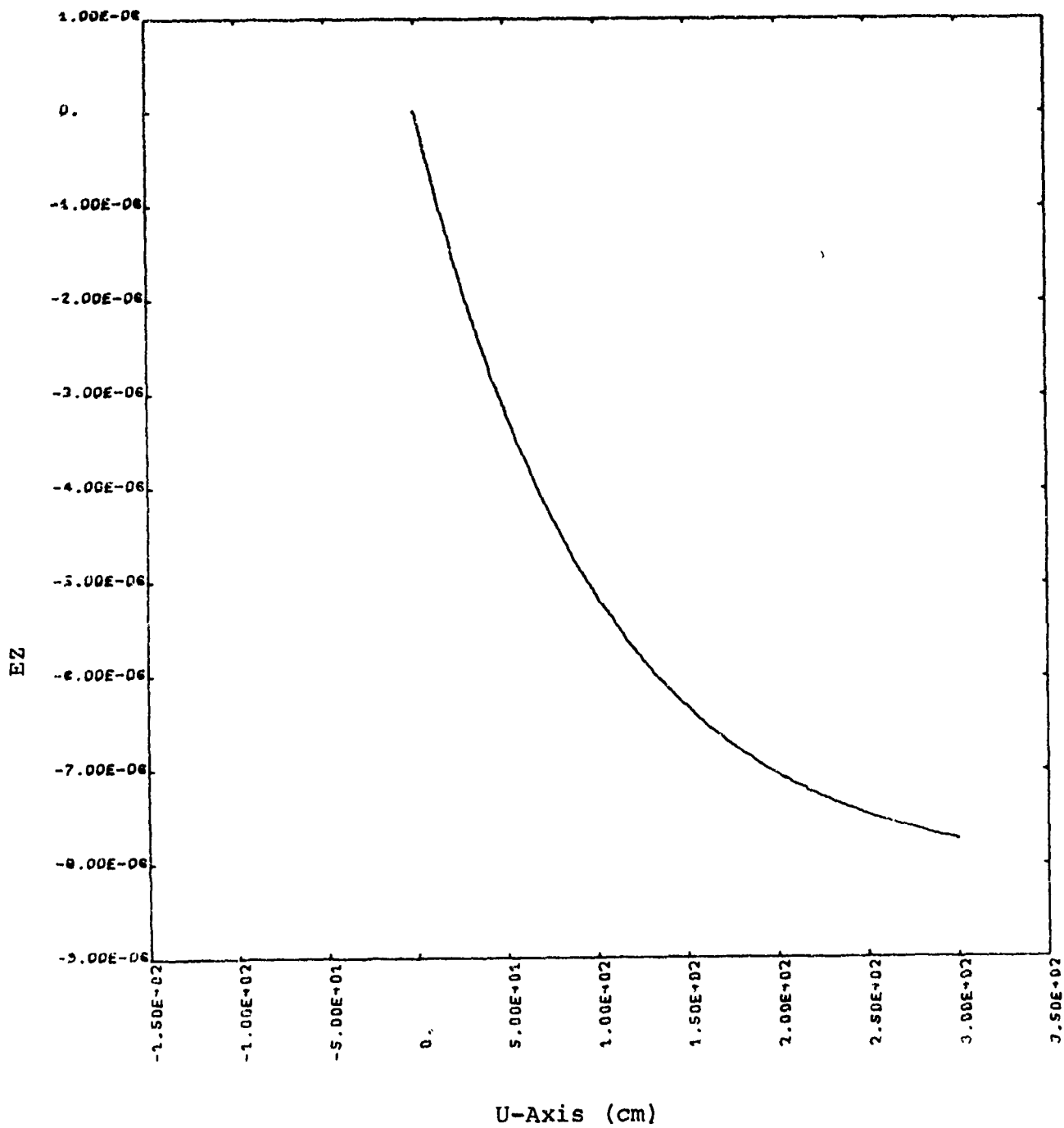
$$E_z(r,u) = -2.4 \times 10^6 J_0(r) EZ \text{ (V/cm)}$$



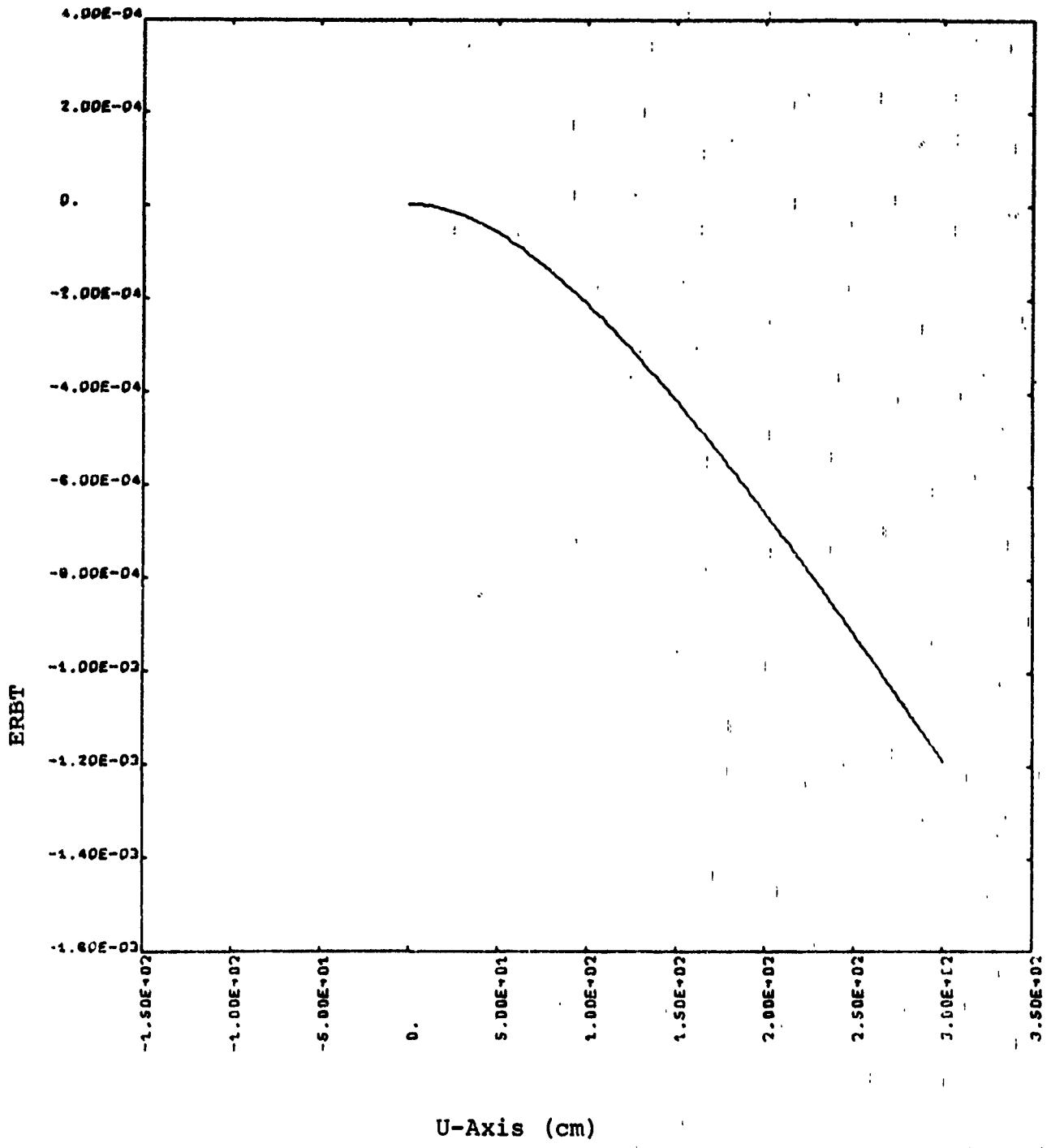
Case 5. B Theta (u)



Case 5. ER



Case 5. EZ



Case 5. ERBT

### 3.3 THE CLOSED CAVITY PROBLEM\*

3.3.1 Introduction. The solution of the exact electromagnetic (EM) equations for a 3 parameter beam (finite rise time, pulse width, and decay time) crossing a drift chamber of finite radius and length is presented. The chamber is filled with a plasma of constant conductivity and the walls are assumed perfectly conducting. Two beam current density radial profiles are considered: a uniform current density out to the beam radius, and a Gaussian profile typical of pinched beams. The problem is set up to handle any ordering of beam and chamber lengths.

The solution is obtained in terms of a single infinite sum of radial modes; each mode contains a translationally invariant part which gives the fields for a long tube without endplates, and a finite integral which derives from the radiative fields of the surface charges accelerated by the beam fields as the beam passes through the cavity.

The endplates considerably complicate the mathematics but, of course, must be included in any theory which attempts to compare with experimental geometries. The endplates have a major effect on the electric fields when the fractional electrical neutralization,  $f_e < 1$ ; the perfectly conducting endplates "short out" the radial electric field near the plates, and the magnitude and, indeed, the direction, of the longitudinal electric field are changed by the existence of endplates.

---

\*This material has been reported in S. Putnam, Theoretical Electron Beam Studies, PIQR-105-4, Aug. 1969, Physics International Company, (submitted to DNA).

3.3.2 Mathematical Development. The basic EM field equations for azimuthal symmetry that we need are

$$\left( -\frac{1}{r} \frac{\partial}{\partial r} \left( r \frac{\partial}{\partial r} \right) - \frac{\partial^2}{\partial z^2} + \frac{1}{c^2} \frac{\partial^2}{\partial t^2} + \frac{4\pi\sigma}{c^2} \frac{\partial}{\partial t} \right) A = S \quad (3.44)$$

$$S = \text{source function} = \frac{4\pi}{c} j_{b_z} - \frac{\partial \bar{Q}}{\partial z} \quad (3.45)$$

$$\bar{Q} \equiv \frac{4\pi}{c} \int_0^r j_{b_r} dr' - f(z,t) \quad (3.46)$$

$$\left( \frac{4\pi\sigma}{c} + \frac{1}{c} \frac{\partial}{\partial t} \right) \phi = -\frac{\partial A}{\partial z} + Q \quad (3.47)$$

$$\left. \begin{aligned} E_r &= -\frac{\partial \phi}{\partial r} \\ E_z &= -\frac{\partial \phi}{\partial z} - \frac{1}{c} \frac{\partial A}{\partial t} \\ B_\theta &= -\frac{\partial A}{\partial r} \end{aligned} \right\} \quad (3.48)$$

where  $A$  is the  $z$ -component of the vector potential  
 $\phi$  is the scalar potential  
 $\sigma$  is the conductivity (a constant).

$f(z,t)$  is an arbitrary function which is useful for specifying boundary conditions at  $r = R$ . This function derives from the choice of gauge and will be taken zero below.

We transform variables above for mathematical convenience. Let  $u = \gamma(vt-z)$  = distance in the beam frame, which we assume moves with constant velocity  $v$ . Let

$$\left. \begin{aligned} u_0 &= \gamma vt \\ u_1 &= -\gamma z \end{aligned} \right\} u = u_0 + u_1$$

In these variables the equations above become

$$\left[ -\frac{1}{r} \frac{\partial}{\partial r} \left( r \frac{\partial}{\partial r} \right) - \gamma^2 \frac{\partial^2}{\partial u_1^2} + \gamma^2 \beta^2 \frac{\partial^2}{\partial u_0^2} + 2k \frac{\partial}{\partial u_0} \right] A = \frac{4\pi}{c} j_{bz} \quad (3.49)$$

$$\left( \frac{\partial}{\partial u_0} + \epsilon \right) \phi = \frac{1}{\beta} \frac{\partial A}{\partial u_1} \quad (3.50)$$

$$k = \frac{2\pi\sigma\gamma v}{c^2}, \quad \epsilon = \frac{2k}{\beta^2 \gamma^2} \quad (3.51)$$

$$\left. \begin{aligned} E_r &= -\frac{\partial \phi}{\partial r} \\ E_z &= \gamma \left[ \frac{\partial \phi}{\partial u_1} - \beta \frac{\partial A}{\partial u_0} \right] \\ B_\theta &= -\frac{\partial A}{\partial r} \end{aligned} \right\} \quad (3.52)$$

We have taken  $j_{br} = 0$ , or  $Q = 0$ , in these equations for mathematical simplicity. The radial beam current component can easily be handled in the methods developed below, but since the main point here is an exposition of boundary effects, we take  $j_{br} = 0$  in our beam model.

The boundary effects (surface currents and charges) give homogeneous contributions to A; i.e., Equation (3.44) with  $S = 0$ , and since they are not translationally invariant, we must keep  $u_0$  and  $u_1$  as independent variables. However, the particular, or inhomogeneous part of the vector potential,  $A^p$ , deriving from the beam current, is translationally symmetric under the assumption of constant beam velocity, and we write Equation (3.49) as

$$\left[ -\frac{1}{r} \frac{\partial}{\partial r} \left( r \frac{\partial}{\partial r} \right) - \frac{\partial^2}{\partial u^2} + 2k \frac{\partial}{\partial u} \right] A^p = \frac{4\pi}{c} j_{b_z}(r, u) \quad (3.53)$$

The vector potential, A,  $\phi$ , and S are now expanded in radial modes:

$$\left. \begin{aligned} A &= \sum_{n=1}^{\infty} A_n J_0 \left( \frac{\lambda_n}{R} r \right) \\ S &= \sum_{n=1}^{\infty} S_n J_0 \left( \frac{\lambda_n}{R} r \right) \\ \phi &= \sum_{n=1}^{\infty} \phi_n J_0 \left( \frac{\lambda_n}{R} r \right) \end{aligned} \right\} \quad (3.54)$$

where  $\lambda_n$  are the zeros of  $J_0$ , the zero order Bessel function. The Equations (3.53) are appropriate for a conducting wall or  $E_z = 0$  at  $r = R$ . Substituting Equation (3.54) into Equations (3.49), (3.50), and (3.53),

$$\left[ -\frac{\partial^2}{\partial u^2} + 2k \frac{\partial}{\partial u} + \left( \frac{\lambda_n}{R} \right)^2 \right] A_n^p = S_n \quad (3.55a)$$

$$\left[ -\gamma^2 \frac{\partial^2}{\partial u_1^2} + \gamma^2 \beta^2 \frac{\partial^2}{\partial u_0^2} + 2k \frac{\partial}{\partial u_0} + \left( \frac{\lambda_n}{R} \right)^2 \right] A_n^h = 0 \quad (3.55b)$$

$$\left( \frac{\partial}{\partial u_0} + \epsilon \right) \phi_n = \frac{1}{\beta} \frac{\partial A_n}{\partial u_1} \quad (3.56)$$

where

$$A_n = A_n^P + A_n^h$$

$$A_n^P = A_n^P(u), \text{ the particular modal component}$$

$$A_n^h = A_n^h(u_0, u_1), \text{ the homogeneous modal component}$$

If we consider a finite perfectly conducting cylindrical cavity (see Figure 3.2) the boundary conditions are

$$E_r = 0 \quad |_{u_1=0, -\gamma L} \quad (3.57)$$

or, if  $A_n^P = A_n^P(u) = f_1(u_0) f_2(u_1)$ , the factorability implies that Equation (3.57) may be satisfied by taking

$$\frac{\partial A_n}{\partial u_1} = 0 \quad |_{u_1=0, -\gamma L} \quad (3.58)$$

This is obvious if we integrate Equation (3.56):

$$\phi_n = \frac{e^{-\epsilon u_0}}{\beta} \int_{-\infty}^{u_0} e^{\epsilon s} \frac{\partial A_n}{\partial u_1} ds \quad (3.59)$$

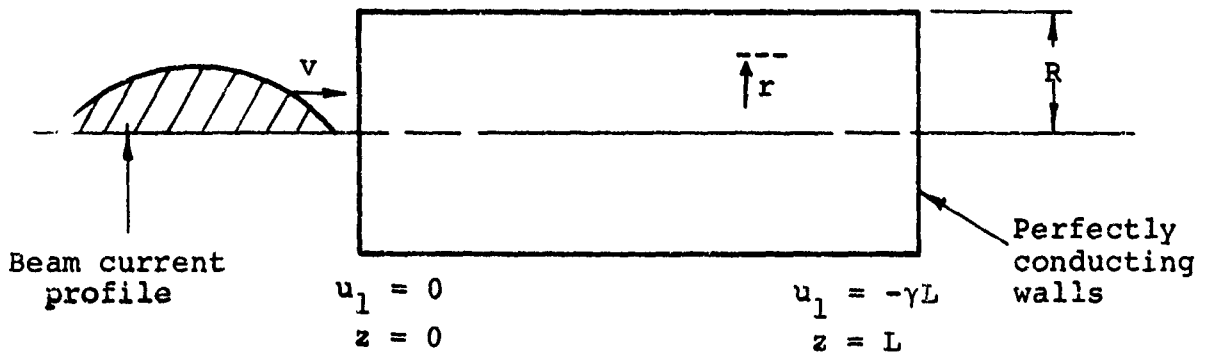


Figure 3.2 Cavity geometry.

The initial values of  $E_r$ ,  $E_z$  and  $B_\theta$  must also be specified for all  $0 \leq z \leq L$  at  $t = u_0 = 0$  to define the problem. If we assume the beam front to be at  $z = 0$  for  $t = 0$ ,  $A_n$  and  $\partial A_n / \partial u_0$  must equal zero at  $t = 0$  for all  $u_1$  inside the cavity if the end plates are perfectly conducting, as we assume.

We now proceed to determine  $A_n^P$  for a beam with finite rise and decay times. We assume a beam profile

$$j_{bz} = f(r)g(u)$$

with

$$\begin{aligned} f(r) &= CH(a-r) = C, \quad 0 \leq r \leq a \\ &= 0, \quad r > a \end{aligned}$$

and

$$\begin{aligned} g(u) &= 0, \quad u \leq 0 \\ &= (1 - e^{-\alpha_1 u}), \quad 0 \leq u \leq \tau_p \\ &= \frac{1 - e^{-\alpha_1 u}}{1 - e^{-\alpha_2(\Delta - \tau_p)}} \left( 1 - e^{-\alpha_2(\Delta - u)} \right) \\ &\quad \tau_p \leq u \leq \Delta \\ &= 0, \quad u \geq \Delta \end{aligned}$$

(3.60)

Figure 3.3 shows the function  $g(u)$ . Note that the square wave pulse limit is obtained from Equation (3.60) by letting  $\alpha_1 \rightarrow \infty$ ,  $\alpha_2 \rightarrow \infty$ ,  $\Delta \rightarrow 0$ , with  $\alpha_2(\Delta - \tau_p)$  remaining constant as the limit is taken.

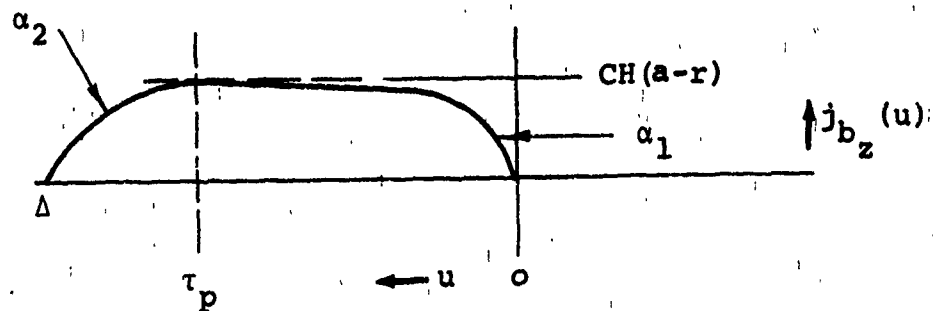


Figure 3.3 The  $u$  dependence for  $j_{b_z}$

We obtain the source function for the  $n^{\text{th}}$  radial mode,  $S_n$ , from

$$\begin{aligned}
 S_n &\equiv \frac{4\pi}{c} j_{b_z n} = \frac{4\pi}{c} g(u) \left[ \frac{2}{R^2} \frac{1}{[J_1(\lambda_n)]^2} \int_0^R r' f(r') J_0\left(\frac{\lambda_n r'}{R}\right) dr' \right] \\
 &= \frac{4\pi}{c} \left( \frac{2}{\lambda_n} \right) \frac{c}{[J_1(\lambda_n)]^2} \left( \frac{a}{R} \right) J_1\left(\frac{\lambda_n}{R} a\right) g(u) \quad (3.61) \\
 &\equiv F_n g(u)
 \end{aligned}$$

and Equation (3.55) becomes

$$\left[ -\frac{\partial^2}{\partial u^2} + 2k \frac{\partial}{\partial u} + \left( \frac{\lambda_n}{R} \right)^2 \right] A_n^P = F_n g(u) \quad (3.62)$$

The quadrature for Equation (3.62) is

$$A_n^P = \frac{F_n}{2\sqrt{\xi}} \left\{ e^{-\eta_1 u} \int_{-\infty}^u e^{\eta_1 s} g(s) ds - e^{\eta_2 u} \int_{+\infty}^u e^{-\eta_2 s} g(s) ds \right\} \quad (3.63)$$

with

$$\xi = k^2 + \left( \frac{\lambda_n}{R} \right)^2$$

$$\eta_1 = \sqrt{\xi} - k$$

$$\eta_2 = \sqrt{\xi} + k$$

Although each of the constants defined in Equation (3.63) is  $n$  dependent, we will not explicitly denote them as such. Using  $g(u)$  from Equation (3.60) in Equation (3.63) we obtain after straightforward integration:

$$A_n^P = \frac{F_n}{2\sqrt{\xi}} \left\{ \begin{array}{l} \Gamma_1 e^{\eta_2 u}, u \leq 0 \\ \frac{1}{\eta_1} + \frac{1}{\eta_2} + \Gamma_2 e^{-\eta_1 u} - \Gamma_3 e^{-\alpha_1 u} + \Gamma_4 e^{\eta_2 u}, 0 \leq u \leq \tau_p \\ e^{-\eta_1 u} \Gamma_5 + \Gamma_6 + e^{\eta_2 u} \Gamma_7 - \Gamma_8 e^{\alpha_2 u}, \tau_p \leq u \leq \Delta \\ \Gamma_9 e^{-\eta_1 u}, u \geq \Delta \end{array} \right\} \quad (3.64)$$

The constants defining the longitudinal beam profile are

$$\Gamma_1 \equiv \hat{Q} \left\{ \frac{e^{-\alpha_2 \Delta}}{\alpha_2 - \eta_2} \left( e^{(\alpha_2 - \eta_2) \tau_p} - e^{(\alpha_2 - \eta_2) \Delta} \right) + \frac{e^{-\eta_2 \tau_p} - e^{-\eta_2 \Delta}}{\eta_2} \right\} \quad (3.65)$$

$$+ \frac{\left( 1 - e^{-\eta_2 \tau_p} \right)}{\eta_2} - \frac{1 - e^{-(\eta_2 + \alpha_1) \tau_p}}{\eta_2 + \alpha_1} ,$$

$$\hat{Q} \equiv \frac{1 - e^{-\alpha_1 \tau_p}}{1 - e^{-\alpha_2 (\Delta - \tau_p)}}$$

$$\Gamma_2 \equiv \frac{\alpha_1}{\eta_1 (\eta_1 - \alpha_1)}$$

$$\Gamma_3 \equiv \frac{1}{\eta_2 + \alpha_1} + \frac{1}{\eta_1 - \alpha_1}$$

$$\Gamma_4 \equiv \Gamma_1 - \frac{1}{\eta_2} + \frac{1}{\eta_2 + \alpha_1}$$

$$\Gamma_5 \equiv \hat{Q} \left\{ \frac{e^{-\alpha_2 \Delta + (\eta_1 + \alpha_2) \tau_p}}{\eta_1 + \alpha_2} - \frac{e^{\eta_1 \tau_p}}{\eta_1} \right\}$$

$$- \frac{\left( e^{(\eta_1 - \alpha_1) \tau_p} - 1 \right)}{\eta_1 - \alpha_1} + \frac{\left( e^{\eta_1 \tau_p} - 1 \right)}{\eta_1}$$

$$\Gamma_6 \equiv \hat{Q} \left( \frac{1}{\eta_1} + \frac{1}{\eta_2} \right)$$

$$\begin{aligned}
\Gamma_7 & \equiv \hat{Q} e^{-\eta_2 \Delta} \left( \frac{1}{\eta_2 - \alpha_2} - \frac{1}{\eta_2} \right) \\
\Gamma_8 & \equiv \hat{Q} e^{-\alpha_2 \Delta} \left( \frac{1}{\eta_1 + \alpha_2} + \frac{1}{\eta_2 - \alpha_2} \right) \\
\Gamma_9 & \equiv \frac{\left( e^{\eta_1 \tau_p} - 1 \right)}{\eta_1} - \frac{\left( e^{(\eta_1 - \alpha_1) \tau_p} - 1 \right)}{\eta_1 - \alpha_1} \\
& + \hat{Q} \left\{ \frac{e^{\eta_1 \Delta} - e^{\eta_1 \tau_p}}{\eta_1} - \frac{e^{-\alpha_2 \Delta}}{\eta_1 + \alpha_2} \cdot \right. \\
& \quad \left. \left( e^{(\eta_1 + \alpha_2) \Delta} - e^{(\eta_1 + \alpha_2) \tau_p} \right) \right\}
\end{aligned}$$

The above equations for  $A_n^P$  satisfy continuity of the functions and their derivatives with respect to  $u$  at  $u = 0$ ,  $\tau_p$ , and  $\Delta$ , as required by EM field continuity.

We digress briefly to remark that we have now obtained the vector potential for the case of a finite pulse with current profile given by Equation (3.60) traveling through a long conducting pipe of radius  $R$ , filled with a medium of conductivity  $\sigma$ :

$$A(r, u) \underset{\text{(long pipe)}}{=} \sum_{n=0}^{\infty} A_n^P(u) J_0 \left( \frac{\lambda_n r}{R} \right)$$

with  $A_n^P(u)$  given by Equations (3.64) and (3.65). This result is a generalization of the problem discussed in Section 3.2, where a semi-infinite beam filling the pipe [radial current variation

$\propto J_0(\lambda_{1r}/R)$  was considered. We have directly obtained the wake fields in the pipe from Equations (3.64) and (3.65) ( $u \gg \Delta$ ), and could easily continue the calculation for a second pulse in this wake.

We return to the finite length cavity problem and determine the homogeneous vector potential terms to be added to Equation (3.64) in order that the boundary conditions, Equation (3.57), be satisfied. The equation for  $A_n^h$  is

$$\left[ -\gamma^2 \frac{\partial^2}{\partial u_1^2} + \gamma^2 \beta^2 \frac{\partial^2}{\partial u_0^2} + 2k \frac{\partial}{\partial u_0} + \left( \frac{\lambda_n}{R} \right)^2 \right] A_n^h = 0 \quad (3.55b)$$

with  $\frac{\partial A_n}{\partial u_1} = \frac{\partial A_n^p}{\partial u_1} + \frac{\partial A_n^h}{\partial u_1} = 0$ ,  $u_1 = 0$ ,  $-\gamma L$  (3.66)

Let us define a function  $W_n(u_0, u_1)$ :

$$W_n \equiv A_n^h \exp\left(\frac{k}{\beta^2 \gamma^2} u_0\right) \quad (3.67)$$

which satisfies

$$\left[ -\frac{1}{\beta^2} \frac{\partial^2}{\partial u_1^2} + \frac{\partial^2}{\partial u_0^2} + Q \right] W_n = 0$$

$$W_n(0, u_1) = A_n^h(0, u_1) \quad (3.68)$$

$$\frac{\partial W_n}{\partial u_0}(0, u_1) = \frac{\partial A_n^h}{\partial u_0}(0, u_1) + \frac{k}{\beta^2 \gamma^2} A_n^h(0, u_1)$$

$$\frac{\partial W}{\partial u_1}(u_0, u_1) = e^{(k/\beta^2 \gamma^2) u_0} \frac{\partial A_n^h}{\partial u_1}$$

$$Q \equiv \frac{1}{\beta^2 \gamma^2} \left( \frac{\lambda_n}{R} \right)^2 - \left( \frac{k}{\beta^2 \gamma^2} \right)^2$$

It is convenient to take the beam head ( $u = 0$ ) at  $u_1 = 0$  when  $u_0 = 0$ . The initial conditions are then that all fields in the cavity be zero before the beam enters the cavity, or  $A_n, \partial A_n / \partial u_0 = 0$  for  $u_0 = 0$ . We can easily make  $A_n^P$  and  $\partial A_n^P / \partial u_0 = 0$  at  $u = 0$  by subtracting  $A_n^P$  for  $u \leq 0$  from  $A_n^P$  of Equation (3.64). Define a new  $A_n^P$  for the cavity problem,  $\bar{A}_n^P$ :

$$\bar{A}_n^P = \frac{F_n}{2\sqrt{\xi}} \left\{ \begin{array}{ll} 0, & u \leq 0 \\ \frac{1}{\eta_1} + \frac{1}{\eta_2} + \Gamma_2 e^{-\eta_1 u} - \Gamma_3 e^{-\alpha_1 u} + (\Gamma_4 - \Gamma_1) e^{\eta_2 u}, & 0 \leq u \leq \tau_p \\ \Gamma_5 e^{-\eta_1 u} + \Gamma_6 + (\Gamma_7 - \Gamma_1) e^{\eta_2 u} - \Gamma_8 e^{\alpha_2 u}; & \tau_p \leq u \leq \Delta \\ \Gamma_9 e^{-\eta_1 u} - \Gamma_1 e^{\eta_2 u}, & u \geq \Delta \end{array} \right. \quad (3.69)$$

For the moment let us not worry about the form of  $\bar{A}_n^p$  when  $u \geq \Delta$ ; the homogeneous function will remove the divergent  $e^{\eta_2 u}$  term. The initial conditions for  $W_n$  are now

$$W_n(0, u_1) = \frac{\partial W_n}{\partial u_0}(0, u_1) = 0$$

In order to solve Equations (3.68) we use the Laplace transform technique and transform with respect to  $u_0$ :

$$\left[ -\frac{\partial^2}{\partial u_1^2} + \beta^2(p^2 + Q) \right] W_n(p, u_1) = \beta^2 \left[ p W_n(0, u_1) + \frac{\partial W_n}{\partial u_0}(0, u_1) \right] = 0 \quad (3.70)$$

The boundary conditions therefore enter only in the homogeneous solutions of Equation (3.70) which we write in the form

$$W_n(p, u_1) = f_1(p) \frac{\cosh \beta \sqrt{p^2 + Q} (u_1 + \gamma L)}{\beta \sqrt{p^2 + Q} \sinh \beta \sqrt{p^2 + Q} \gamma L} + \frac{f_2(p) \cosh \beta \sqrt{p^2 + Q} u_1}{\beta \sqrt{p^2 + Q} \sinh \beta \sqrt{p^2 + Q} \gamma L} \quad (3.71)$$

where  $f_1$  and  $f_2$  are functions of  $p$  chosen to satisfy

$$\frac{\partial \bar{A}_n^p}{\partial u_1} + e^{-k/\beta^2 \gamma^2 u_0} \frac{\partial W_n}{\partial u_1} = 0, \quad u_1 = 0, \quad -\gamma L \quad (3.72)$$



Similarly, when  $u_1 = -\gamma L$ ,

$$\begin{aligned} \frac{\partial \bar{A}_n^p}{\partial u_1} (u_0, -\gamma L) &= \frac{F_n}{2\sqrt{\xi}} \left\{ \left[ \eta_1 \Gamma_2 e^{-\eta_1 u_0} e^{\eta_1 \gamma L} + \alpha_1 \Gamma_3 e^{-\alpha_1 u_0} e^{\alpha_1 \gamma L} \right. \right. \\ &+ \left. \left. \eta_2 (\Gamma_4 - \Gamma_1) e^{\eta_2 u_0} e^{-\eta_2 \gamma L} \right] H[u_0 - \gamma L] H[\gamma L + \tau_p - u_0] \right. \\ &+ \left[ -\eta_1 \Gamma_5 e^{-\eta_1 u_0} e^{\eta_1 \gamma L} + \eta_2 (\Gamma_7 - \Gamma_1) e^{\eta_2 u_0} e^{-\eta_2 \gamma L} \right. \\ &- \left. \left. \alpha_2 \Gamma_8 e^{\alpha_2 u_0} e^{-\alpha_2 \gamma L} \right] H[u_0 - \gamma L - \tau_p] H(\gamma L + \Delta - u_0) \right. \\ &+ \left. \left[ -\eta_1 \Gamma_9 e^{-\eta_1 u_0} e^{\eta_1 \gamma L} - \eta_2 \Gamma_{10} e^{\eta_2 u_0} e^{-\eta_2 \gamma L} \right] H(u_0 - \gamma L - \Delta) \right\} \quad (3.75) \end{aligned}$$

We are now in a position to determine the  $f_1(p)$  and  $f_2(p)$  of Equation (3.71). Inspection of Equations (3.74) and (3.75) reveals that we need the Laplace transform (L) of the function  $e^{-\nu u_0} H(u_0 - \delta) H(\Psi - u_0)$ . Elementary integration gives

$$L \left[ e^{-\nu u_0} H(u_0 - \delta) H(\Psi - u_0) \right] = \frac{1}{p + \nu} \left\{ e^{-\delta(\nu + p)} - e^{-\Psi(\nu + p)} \right\} \quad (3.76)$$

Equations (3.71), (3.72), (3.74), and (3.76) give:

$$\begin{aligned}
\frac{\partial W}{\partial u_1}(p,0) &= -f_1(p) = -\frac{F_n}{2\sqrt{\epsilon}} \left\{ \frac{-\eta_1 \Gamma_2 \left(1 - e^{-\tau_p(\eta_1 - k/\beta^2 \gamma^2 + p)}\right)}{p + (\eta_1 - k/\beta^2 \gamma^2)} \right. \\
&+ \frac{\alpha_1 \Gamma_3 \left(1 - e^{-\tau_p(\alpha_1 - k/\beta^2 \gamma^2 + p)}\right)}{p + (\alpha_1 - k/\beta^2 \gamma^2)} + \frac{\eta_2 (\Gamma_4 - \Gamma_1) \left(1 - e^{-\tau_p(p - \eta_2 - k/\beta^2 \gamma^2)}\right)}{p - (\eta_2 + k/\beta^2 \gamma^2)} \\
&+ \frac{-\eta_1 \Gamma_5 \left(e^{-\tau_p(\eta_1 - k/\beta^2 \gamma^2 + p)} - e^{-\Delta(\eta_1 - k/\beta^2 \gamma^2 + p)}\right)}{p + (\eta_1 - k/\beta^2 \gamma^2)} \\
&+ \frac{\eta_2 (\Gamma_7 - \Gamma_1)}{p - (\eta_2 + k/\beta^2 \gamma^2)} \left( e^{-\tau_p(p - \eta_2 - k/\beta^2 \gamma^2)} - e^{-\Delta(p - \eta_2 - k/\beta^2 \gamma^2)} \right) \\
&- \frac{\alpha_2 \Gamma_8}{p - (\alpha_2 + k/\beta^2 \gamma^2)} \left( e^{-\tau_p(p - \alpha_2 - k/\beta^2 \gamma^2)} - e^{-\Delta(p - \alpha_2 - k/\beta^2 \gamma^2)} \right) \quad (3.77) \\
&- \left. \frac{\eta_1 \Gamma_9}{p + (\eta_1 - k/\beta^2 \gamma^2)} e^{-\Delta(\eta_1 - k/\beta^2 \gamma^2 + p)} - \frac{\eta_2 \Gamma_1}{p - (\eta_2 + k/\beta^2 \gamma^2)} e^{-\Delta(p - \eta_2 - k/\beta^2 \gamma^2)} \right\}
\end{aligned}$$

Similarly, using Equation (3.75),

$$\begin{aligned}
\frac{\partial W}{\partial u_1}(p, -\gamma L) &= -f_2(p) = -\frac{F_n}{2\sqrt{\xi}} \left\{ \frac{-\eta_1 \Gamma_2 e^{\eta_1 \gamma L}}{p + (\eta_1 - k/\beta^2 \gamma^2)} \left( e^{-\gamma L(\eta_1 - k/\beta^2 \gamma^2 + p) - (\tau_p + \gamma L)} \right. \right. \\
&\quad \left. \left. - e^{-(\gamma L + \tau_p)(\eta_1 - k/\beta^2 \gamma^2 + p)} \right) + \frac{\alpha_1 \Gamma_3 e^{\alpha_1 \gamma L}}{p + (\alpha_1 - k/\beta^2 \gamma^2)} \left( e^{-\gamma L(\alpha_1 - k/\beta^2 \gamma^2 + p)} \right. \right. \\
&\quad \left. \left. - e^{-(\gamma L + \tau_p)(\alpha_1 - k/\beta^2 \gamma^2 + p)} \right) \right\} \\
&+ \frac{\eta_2 (\Gamma_4 - \Gamma_1) e^{-\eta_2 \gamma L}}{p - (\eta_2 + k/\beta^2 \gamma^2)} \left( e^{-\gamma L(p - \eta_2 - k/\beta^2 \gamma^2)} - e^{-(\gamma L + \tau_p)(p - \eta_2 - k/\beta^2 \gamma^2)} \right) \\
&- \frac{\eta_1 \Gamma_5 e^{\eta_1 \gamma L}}{p + (\eta_1 - k/\beta^2 \gamma^2)} \left( e^{-(\gamma L + \tau_p)(\eta_1 - k/\beta^2 \gamma^2 + p)} - e^{-(\gamma L + \Delta)(\eta_1 - k/\beta^2 \gamma^2 + p)} \right) \\
&+ \frac{\eta_2 (\Gamma_7 - \Gamma_1) e^{-\eta_2 \gamma L}}{p - (\eta_2 + k/\beta^2 \gamma^2)} \left( e^{-(\gamma L + \tau_p)(p - \eta_2 - k/\beta^2 \gamma^2)} - e^{-(\gamma L + \Delta)(p - \eta_2 - k/\beta^2 \gamma^2)} \right) \\
&- \frac{\alpha_2 \Gamma_8 e^{-\alpha_2 \gamma L}}{p - (\alpha_2 + k/\beta^2 \gamma^2)} \left( e^{-(\gamma L + \tau_p)(p - \alpha_2 + k/\beta^2 \gamma^2)} - e^{-(\gamma L + \Delta)(p - \alpha_2 - k/\beta^2 \gamma^2)} \right) \\
&- \left. \frac{\eta_1 \Gamma_9 e^{\eta_1 \gamma L}}{p + (\eta_1 - k/\beta^2 \gamma^2)} \left( e^{-(\gamma L + \Delta)(\eta_1 - k/\beta^2 \gamma^2 + p)} \right) - \frac{\eta_2 \Gamma_1 e^{-\eta_2 \gamma L}}{p - (\eta_2 + k/\beta^2 \gamma^2)} e^{-(\gamma L + \Delta)(p - \eta_2 - k/\beta^2 \gamma^2)} \right\}
\end{aligned}$$

(3.78)

We have now completely defined  $W_n(p, u_1)$ . The terms of  $f_1$  and  $f_2$  are of the same form and we need to invert to  $(u_0, u_1)$  space functions of the form

$$\frac{C \cdot \cosh \beta \sqrt{p^2 + Q} (u_1 + b_1)}{\beta \sqrt{p^2 + Q} \sinh \beta \sqrt{p^2 + Q} \gamma L} \frac{1}{p + b_2} e^{-b_3 p} \quad (3.79)$$

where  $C$ ,  $b_1$ ,  $b_2$ , and  $b_3$  are constants. Denoting the inverse transform by  $L^{-1}$  we have,

$$L^{-1} [(36)] = \int_0^{u_0} ds h_1(u) h_2(u_0 - u) \quad (3.80)$$

$$\text{with } h_1(u_0) = \left(\frac{C}{\beta}\right) L^{-1} \left[ \frac{\cosh \beta \sqrt{p^2 + Q} (u_1 + b_1)}{\beta \sqrt{p^2 + Q} \sinh \beta \sqrt{p^2 + Q} \gamma L} \right]$$

$$h_2(u_0) = L^{-1} \left[ \frac{1}{p + b_2} e^{-b_3 p} \right] = e^{-b_2(u_0 - b_3)} H(u_0 - b_3)$$

We can write  $h_1(u_0)$  as

$$h_1(u_0) = \frac{C}{\beta} \int_0^{u_0} J_0 \left( \sqrt{Q(u_0^2 - v^2)} \right) f_3(v) dv \quad (3.81)$$

$$\text{with } f_3(u_0) = L^{-1} \left[ \frac{\cosh \beta p (u_1 + b_1)}{\sinh \beta p \gamma L} \right]$$

In order to evaluate  $f_3(u_0)$ , we write

$$\frac{\cosh \beta p(u_1 + b_1)}{\sinh \beta p \gamma L} = \frac{e^{-\beta p(\gamma L - u_1 - b_1)} + e^{-\beta p(\gamma L + u_1 + b_1)}}{1 - e^{-2\beta p \gamma L}}$$

and obtain

$$f_3(u_0) = \sum_{0 \leq m \leq u_0/2\beta\gamma L} \left[ \delta(u_0 - \beta(\gamma L - u_1 - b_1) - 2\beta\gamma L m) + \delta(u_0 - \beta(\gamma L + u_1 + b_1) - 2\beta\gamma L m) \right] \quad (3.82)$$

where  $m$  is an integer and  $\delta$  is the delta function. Returning to Equation (3.81), we have

$$h_1(u_0) = \frac{C}{\beta} \sum_{0 \leq m \leq u_0/2\beta\gamma L} \left\{ J_0 \left\{ Q \left[ u_0^2 - [\beta(\gamma L - u_1 - b_1) + 2\beta\gamma L m]^2 \right] \right\}^{\frac{1}{2}} \cdot H \left[ u_0 - \beta(\gamma L - u_1 - b_1) - 2\beta\gamma L m \right] + J_0 \left\{ Q \left[ u_0^2 - [\beta(\gamma L + u_1 + b_1) + 2\beta\gamma L m]^2 \right] \right\}^{\frac{1}{2}} \cdot H \left[ u_0 - \beta(\gamma L + u_1 + b_1) - 2\beta\gamma L m \right] \right\} \quad (3.83)$$

We are now in a position to explicitly write out  $A_n = \bar{A}_n^p + A_n^n$ ,  
for notational convenience let us define a function G:

$$G(k, v, \kappa, \psi) = G_1 - G_2$$

$$G_1(h, v, \kappa, \psi) = \frac{e^{-v u_0}}{\beta} \int_0^{u_0} ds e^{(v - \kappa / \beta^2 \gamma^2) s} H(u_0 - s - \kappa)$$

$$\cdot H[\psi - (u_0 - s)] \left\{ \sum_{0 \leq m \leq s / 2\beta\gamma L} \left[ J_0 \left( \sqrt{Q[s^2 - \beta^2 (u_1 - 2\gamma L m)^2]} \right) \right. \right.$$

$$\cdot H[s + \beta u_1 - 2\beta\gamma L m] + J_0 \left( \sqrt{Q[s^2 - \beta^2 (2\gamma L + u_1 + 2\gamma L m)^2]} \right)$$

$$\left. \left. \cdot H[s - \beta(2\gamma L + u_1) - 2\beta\gamma L m] \right] \right\}, \quad (3.84)$$

$$G_2(k, v, \kappa, \psi) = \frac{e^{-v(u_0 - \gamma L)}}{\beta} \int_0^{u_0} ds e^{(v - \kappa / \beta^2 \gamma^2) s} H[u_0 - s - (\kappa + \gamma L)]$$

$$\cdot H[\psi + \gamma L - (u_0 - s)] \left\{ \sum_{0 \leq m \leq s / 2\beta\gamma L} \left[ J_0 \left( \sqrt{Q[s^2 - \beta^2 (\gamma L - u_1 + 2\gamma L m)^2]} \right) \right. \right.$$

$$\cdot H[s - \beta(\gamma L - u_1) - 2\beta\gamma L m] + J_0 \left( \sqrt{Q[s^2 - \beta^2 (\gamma L + u_1 + 2\gamma L m)^2]} \right)$$

$$\left. \left. \cdot H[s - \beta(\gamma L + u_1) - 2\beta\gamma L m] \right] \right\}. \quad (3.85)$$

We obtain for the complete vector potential of the  $n^{\text{th}}$  radial mode:

$$\begin{aligned}
 A_n = & \frac{F_n}{2\sqrt{\xi}} \left\{ \left( \frac{1}{\eta_1} + \frac{1}{\eta_2} \right) H(\tau_p - u) H(u) + \Gamma_2 \left[ e^{-\eta_1 u} + H(\tau_p - u) H(u) + \eta_1 G(k, \eta_1, 0, \tau_p) \right] \right. \\
 & - \Gamma_3 \left[ e^{-\alpha_1 u} H(\tau_p - u) H(u) + \alpha_1 G(k, \alpha_1, 0, \tau_p) \right] + (\Gamma_4 - \Gamma_1) \left[ e^{\eta_2 u} H(\tau_p - u) H(u) \right. \\
 & - \eta_2 G(k, -\eta_2, 0, \tau_p) \left. \right] + \Gamma_5 \left[ e^{-\eta_1 u} H(u - \tau_p) H(\Delta - u) \right. \\
 & + \eta_1 G(k, \eta_1, \tau_p, \Delta) \left. \right] + \Gamma_6 H(u - \tau_p) H(\Delta - u) \\
 & + (\Gamma_7 - \Gamma_1) \left[ e^{\eta_2 u} H(u - \tau_p) H(\Delta - u) - \eta_2 G(k, -\eta_2, \tau_p, \Delta) \right] \\
 & - \Gamma_8 \left[ e^{\alpha_2 u} H(u - \tau_p) H(\Delta - u) - \alpha_2 G(k, -\alpha_2, \tau_p, \Delta) \right] \\
 & + \Gamma_9 \left[ e^{-\eta_1 u} H(u - \Delta) + \eta_1 G(k, \eta_1, \Delta, \infty) \right] \\
 & \left. - \Gamma_{10} \left[ e^{\eta_2 u} H(u - \Delta) - \eta_2 G(k, -\eta_2, \Delta, \infty) \right] \right\}. \tag{3.86}
 \end{aligned}$$

In order to verify that  $A_n$  satisfies the boundary and initial conditions we note some properties of the G functions:

$$\begin{aligned} \frac{\partial G_1}{\partial u_1} &= e^{-vu_0} H(u_0 - \kappa) H[\Psi - u_0], \quad u_1 = 0 \\ &= 0, \quad u_1 = -\gamma L \end{aligned} \tag{3.87}$$

$$\begin{aligned} \frac{\partial G_2}{\partial u_1} &= 0, \quad u_1 = 0 \\ &= e^{-v(u_0 - \gamma L)} H[u_0 - (\kappa + \gamma L)] H[\Psi + \gamma L - u_0], \quad u_1 = -\gamma L \end{aligned} \tag{3.88}$$

$$\left. \begin{aligned} G_1(0, u_1) &= G_2(0, u_1) = 0 \\ \frac{\partial G_1}{\partial u_0}(0, u_1) &= \frac{\partial G_2}{\partial u_0}(0, u_1) = 0 \end{aligned} \right\} \tag{3.89}$$

Equations (3.87), (3.88), and (3.89) show that  $A_n$  of Equation (3.86) does indeed satisfy the necessary conditions for fields in a closed cavity.

Let us consider the properties of the solution to Equation (3.86) when  $\gamma L \rightarrow \infty$ . Referring to Equations (3.84) and (3.85) we see that  $m = 0$  and

$$\begin{aligned} \lim_{\gamma L \rightarrow \infty} G_1 &\rightarrow \frac{e^{-vu_0}}{\beta} \int_0^{u_0} ds e^{(v-k/\beta^2\gamma^2)s} H(u_0 - s - \kappa) H[\Psi - (u_0 - s)] \\ &\quad \cdot J_0 \left( \sqrt{Q(s^2 - \beta^2 u_1^2)} \right) H(s + \beta u_1) \end{aligned} \tag{3.90}$$

and

$$\lim_{\gamma L \rightarrow \infty} G_2 \rightarrow 0.$$

Equation (3.86) should reduce to Equation (3.64) when  $\gamma L \rightarrow \infty$ ;  $u_0 \rightarrow \infty$ ; i.e.,  $A_n \rightarrow A_n^P$ , the translationally invariant form for no end plates. To recover this form we require that

$$\lim_{\substack{\gamma L \rightarrow \infty \\ u_0 \rightarrow \infty}} \left\{ \begin{array}{l} G(k, -\eta_2, \Delta, \infty) \rightarrow \frac{1}{\eta_2} e^{\eta_2 u} \\ G(k, -\eta_2, \tau_p, \Delta) \rightarrow 0 \\ G(h, -\eta_2, 0, \tau_p) \rightarrow 0 \end{array} \right. \quad (3.91)$$

and all other G functions to approach 0. Equation (3.90) gives

$$\lim_{\gamma L \rightarrow \infty} G_1(k, -\eta_2, \Delta, \infty) = \frac{e^{\eta_2 u_0}}{\beta} \int_{-\beta u_1}^{u_0 - \Delta} e^{-(\eta_2 + k/\beta^2 \gamma^2) s} J_0 \left( \sqrt{Q(s^2 - 2u_1^2)} \right) ds$$

or, letting

$$w = \sqrt{s^2 - \beta^2 u_1^2},$$

$$\lim_{\gamma L \rightarrow \infty} G_1(k, -\eta_2, \Delta, \infty) = \frac{e^{\eta_2 u_0}}{\beta} \int_0^{\sqrt{(u_0 - \Delta)^2 - \beta^2 u_1^2}} \frac{w J_0(\sqrt{Q} w)}{\sqrt{w^2 + \beta^2 u_1^2}} \cdot e^{-(\eta_2 + k/\beta^2 \gamma^2) \sqrt{w^2 + \beta^2 u_1^2}} dw$$

Then

$$\lim_{\substack{\gamma L \rightarrow \infty \\ u_0 \rightarrow \infty}} G_1(k, -\eta_2, \Delta, \infty) \rightarrow \frac{e^{\eta_2 u_0}}{\beta} \int_0^{u_0} \frac{w \cdot e^{-(\eta_2 + k/\beta^2 \gamma^2) \sqrt{w^2 + \beta^2 u_1^2}}}{\sqrt{w^2 + \beta^2 u_1^2}} J_0(\sqrt{Q}w) dw$$

$$= e^{\eta_2 u_0} \cdot \frac{e^{\eta_2 u_1}}{\eta_2} \quad (3.92)$$

where we have used the known integral

$$\int_0^{\infty} \frac{e^{-a\sqrt{x^2+y^2}}}{\sqrt{x^2+y^2}} J_0(bx) x dx = \frac{e^{-y\sqrt{a^2+b^2}}}{\sqrt{a^2+b^2}},$$

with  $y > 0$ .

Now let us look at the case of a semi-infinite beam ( $\Delta, \tau_p \rightarrow \infty$ ) in the limit as  $\gamma L \rightarrow \infty$ . We address ourselves to the question of whether  $A_n$  of Equation (3.86) reduces to the form for a semi-infinite beam in a long pipe with no end plates as  $u_0 \rightarrow \infty$ . We want

$$\lim_{\substack{\gamma L \rightarrow \infty \\ u_0 \rightarrow \infty}} A_n \rightarrow \frac{F_n}{2\sqrt{\xi}} \begin{cases} \Gamma_1 e^{\eta_2 u}, & u \leq 0 \\ \frac{1}{\eta_1} + \frac{1}{\eta_2} + \Gamma_2 e^{-\eta_1 u} - \Gamma_3 e^{-\alpha_1 u}, & u \geq 0 \end{cases}$$

with

$$\begin{aligned}
\bar{\Gamma}_1 &= \lim_{\tau_p, \Delta \rightarrow \infty} \Gamma_1 = \frac{\alpha_1}{\eta_2(\eta_2 + \alpha_1)} \\
\bar{\Gamma}_2 &= \lim_{\tau_p, \Delta \rightarrow \infty} \Gamma_2 = \frac{\alpha_1}{\eta_1(\eta_1 - \alpha_1)} = \Gamma_2 \\
\bar{\Gamma}_3 &= \lim_{\tau_p, \Delta \rightarrow \infty} \Gamma_3 = \frac{\eta_1 + \eta_2}{(\eta_1 - \alpha_1)(\eta_2 + \alpha_1)} = \Gamma_3
\end{aligned} \tag{3.93}$$

( $\Gamma_4 \rightarrow 0$  as  $\tau_p, \Delta \rightarrow \infty$ .)

In terms of Equation (3.86) for  $A_n$  we require

$$\lim_{\substack{\gamma L \rightarrow \infty \\ u_0 \rightarrow \infty}} \left\{ \begin{aligned} G(k, \eta_1, 0, \infty) &\rightarrow 0 \\ G(k, \alpha_1, 0, \infty) &\rightarrow 0 \\ G(k, -\eta_2, 0, \infty) &= \frac{e}{\eta_2} \eta_2^u \end{aligned} \right. \tag{3.94}$$

In a similar fashion as above we can verify that Equations (3.94) are indeed satisfied. We summarize the above discussion:

(i) If  $u_0 < \beta\gamma L$ , then end plate at  $u_1 = -\gamma L$  can be neglected

(ii) If (i) is satisfied and

$$(u_0 - \Delta)^2 - \beta^2 u_1^2 \gg 0 \quad (\text{finite beam of length } \Delta/\gamma v)$$

$$u_0^2 - \beta^2 u_1^2 \gg 0 \quad (\text{semi-infinite beam})$$

then the end plate at  $u_1 = 0$  can be neglected. These comments, of course, are relevant to the vector potential  $A$  and are correct for  $B_\theta$ . The electric field components involve a time integral of  $A$  through  $\phi$ . They do not reduce to the no-endplate case when  $\sigma = 0$  unless  $-\beta u_1 \rightarrow \infty$ .

We complete this discussion with an observation about the effects of a finite conductivity ( $k \neq 0$ ). We have tacitly assumed that

$$Q = \frac{1}{\beta^2 \gamma^2} \left( \frac{\lambda n}{R} \right)^2 - \left( \frac{k}{\beta^2 \gamma^2} \right)^2 > 0.$$

If  $k = \sigma = 0$ , or, if for a given  $k$  the mode number is large enough this is always so. When

$$\frac{k^2}{\beta^2 \gamma^2} > \left( \frac{\lambda n}{R} \right)^2, \quad Q < 0,$$

and the above formalism carries through with the replacement of  $J_0$  by  $I_0$  in Equations (3.83), (3.84), and (3.85). If  $Q = 0$ , the  $G$  functions then become simple exponentials. We can draw an analogy with respect to the nature of the various  $Q$  orderings above by relating the cavity eigenmodes to a harmonic oscillator with viscous damping:

$Q > 0 \rightarrow$  underdamped

$Q = 0 \rightarrow$  critically damped

$Q < 0 \rightarrow$  overdamped

**3.3.3 Discussion.** The mathematical presentation above is complicated by the rather general form of the assumed beam profile and the allowed arbitrary ordering of beam and chamber lengths. It is a simple matter to reduce the formalism for any of several interesting beam transport problems. The reduction of the G functions for a single endplate has already been discussed and is explicitly considered in Section 3.4. Such a case would be relevant to beam injection into a very long pipe for times before the beam nears the end of the tube. The precursor signal which travels ahead of the beam at velocity  $c$  and which could cause precursor ionization effects, can then be easily obtained. We also point out that a less general beam profile (we have a 3 parameter profile) substantially reduces the number of terms in each radial mode.

The number of important radial modes depends on the beam radial profile. We have derived the formulas for the Heaviside radial function which would be applicable, for example, to problems where

the beam uniformly fills the conducting pipe. Another case of interest is a Gaussian radial profile, corresponding to experimental profiles for pinched beams where  $R$  is much greater than the effective beam radius. Then we have

$$j_{b_z} = f(r)g(u)$$

with 
$$f(r) \approx C e^{-b^2 r^2} \quad (R \gg \frac{1}{b}) \quad (3.95)$$

and 
$$S_n \equiv \frac{4\pi}{c} j_{b_z} = \frac{4\pi}{c} g(u) \left\{ \frac{2}{R^2} \frac{C}{[J_1(\lambda_n)]^2} \int_0^R r' e^{-b^2 r'^2} J_0\left(\frac{\lambda_n r'}{R}\right) dr' \right.$$

$$\left. \equiv F_n g(u) ,$$

or, if we approximate  $\int_0^R dr' ( )$  by  $\int_0^\infty dr' ( )$ ,

$$F_n = \frac{4\pi C}{c} \frac{e^{-(\lambda_n/2Rb)^2}}{R^2 b^2} \frac{1}{[J_1(\lambda_n)]^2} \quad (3.96)$$

The formulation follows through by replacing  $F_n$  from Equation (3.61) by Equation (3.96). The radial mode convergence is now very rapid. For example, if  $Rb = 10$ , corresponding to approximately a ten to one ratio of chamber radius to beam radius, a few terms of the infinite radial sum, up to about  $\lambda_n \approx 20$ , are adequate.

If one is interested in times before gas breakdown when  $\sigma$  is small and current neutralization is negligible, an approximation for the EM fields may be obtained by taking  $\sigma$  such that the charge relaxation time,  $\tau_e$ , calculated for a conducting medium is equal to the electrical neutralization time calculated from secondary ion-electron production due to collisional ionization by the beam electrons:

$$\tau_N \text{ (nsec)} = \frac{10^9}{4\pi\sigma} \frac{0.7}{\beta P \text{ (Torr)}} , \quad (3.97)$$

where  $\sigma$  is in gaussian units ( $\text{sec}^{-1}$ ) and the air collision cross section has been used [Equation (2.37)]. This procedure gives the same time scale for the decay of the radial electric field in the two cases. The algebra of the formalism is simplified if  $\sigma = k = 0$ , corresponding to vacuum or very low pressure beam injection. The large electric fields generated by typical high intensity beams when  $\sigma = 0$  ( $\sim 10^6$  V/cm) would restrict the validity of the calculation to low  $v/\gamma$  beams where beam distortion would not be severe.

The actual evaluation of the EM fields from the above formulas is best accomplished numerically. The fields can be plotted for given beam and geometry parameters at specified  $r$  and  $z$  as a function of time over a specified time interval. Although the expression for  $A_n$  are tedious in the general case, they

involve only two types of functions. The particular component  $A_n^p$  contains only algebraic sums of exponentials, and the homogeneous component  $A_n^h$  has only sums of terms of the form

$$e^{-a u_0} \int_{b_1}^{b_2} ds e^{a_2 s} J_0 \left( \sqrt{Q(s^2 - a_3^2)} \right)$$

Standard computer packages exist for the  $J_0$  and  $J_1$  functions and for the roots of these functions. In many cases of practical interest an asymptotic evaluation of the above integral will be entirely adequate, and this can be done analytically.

### 3.4 SINGLE ENDPLATE, ZERO CONDUCTIVITY PROBLEM-- THE INJECTION PROBLEM

We now reduce the formalism of the closed cavity problem explicitly for the case of a beam entering a long conducting pipe through a single endplate. We shall take the plasma conductivity to be zero, which implies that the EM fields are relevant to the initial penetration of the beam into the drift chamber before the gas is appreciably ionized. The radiative fields of the accelerated surface charges are included in the formulation; i.e., the precursor fields which travel ahead of the beam front at velocity  $c$ . The problem therefore complements the cavity model EM fields of Section 2.2 where we estimated the fields in the quasi-static case with the beam across the entire chamber length. By superposition of the fields calculated here with the approximately static fields due to ions, very good estimates of the EM fields can be obtained for times before gas breakdown or for  $t \lesssim 2(L-z)/c$  (see Figure 3.4).

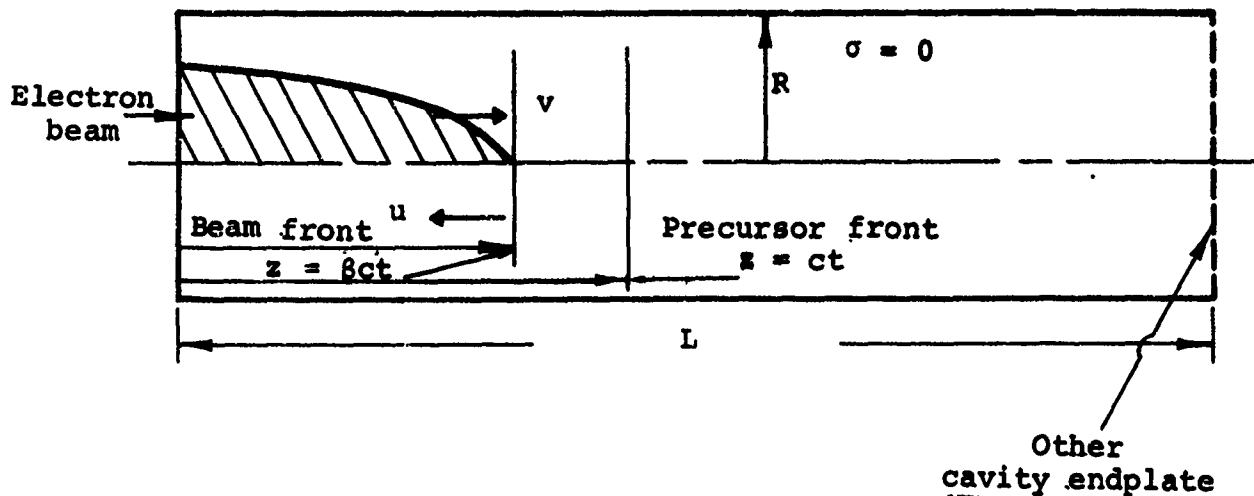


Figure 3.4 Open-ended pipe geometry.

We assume

- (i)  $j_{b_z} = f(r)g(u)$  ,  $u = \gamma(vt - z)$
- (ii)  $j_{b_r} = j_{b_\theta} \approx 0$
- (iii)  $f(r) = C e^{-b^2 r^2}$  ,  $(R \gg \frac{1}{b})$  (gaussian radial profile)
- (iv)  $g(u) = (1 - e^{-\alpha u})$  ,  $u \geq 0$   
 $= 0$  ,  $u < 0$  } finite risetime

From Equation (3.96),

$$\begin{aligned}
 F_n &= \frac{4\pi C}{c} \frac{e^{-\left(\frac{\lambda_n}{2Rb}\right)^2}}{R^2 b^2} \frac{1}{\left[J_1(\lambda_n)\right]^2} \\
 &= 2/5 \frac{I^P}{R^2} \frac{e^{-\left(\frac{\lambda_n}{2Rb}\right)^2}}{\left[J_1(\lambda_n)\right]^2} \quad (3.98)
 \end{aligned}$$

where  $I^P$  is the peak current in amperes. We define  $E_R$ ,  $E_Z$ , and  $B$  THETA:

$$E_R = (-E_r) = \frac{1}{5} \frac{I^P}{R^2} \sum_{n=1}^{\infty} \bar{\phi}_n \frac{e^{-\left(\frac{\lambda_n}{2Rb}\right)^2}}{\left[J_1(\lambda_n)\right]^2} J_1\left(\frac{\lambda_n}{R} r\right)$$

$$E_Z = E_z = \frac{1}{5} \frac{I^P}{R} \sum_{n=1}^{\infty} \bar{E}_{zn} \frac{e^{-\left(\frac{\lambda_n}{2Rb}\right)^2}}{\left[J_1(\lambda_n)\right]^2} \frac{1}{\lambda_n} J_0\left(\frac{\lambda_n}{R} r\right) \quad (3.99)$$

$$B \text{ THETA} = (-B_\theta) = \frac{1}{5} \frac{I^P}{R^2} \sum_{n=1}^{\infty} \bar{A}_n \frac{e^{-\left(\frac{\lambda_n}{2Rb}\right)^2}}{\left[J_1(\lambda_n)\right]^2} J_1\left(\frac{\lambda_n}{R} r\right)$$

with  $\bar{\phi}_n$ ,  $\bar{E}_{zn}$ , and  $\bar{A}_n$  functions of  $u_0 = \gamma vt$  and  $u_1 = -\gamma z$ . Equations (3.86), (3.90), and (3.93) give with  $\sigma = 0$

$$\bar{A}_n = \bar{A}_n^p + \bar{A}_n^h,$$

$$\bar{A}_n^p = \Gamma_1^n e^{\frac{\lambda_n}{R} u} H(-u) + \left[ \frac{2R}{\lambda_n} + \Gamma_2^n e^{-\frac{\lambda_n}{R} u} - \Gamma_3 e^{-\alpha u} \right] \cdot H(u) \quad (3.100)$$

$$\bar{A}_n^h = \left( -\frac{\lambda_n}{R} \right) \frac{\Gamma_1^n}{\beta} \int_{\left\{ \begin{array}{l} 0, u_0 > -\beta u_1 \\ -\beta u_1 - u_0, u_0 < -\beta u_1 \end{array} \right\}}^{\infty} ds e^{-\frac{\lambda_n}{R} s} J_0 \left[ \sqrt{Q \left[ (u_0 + s)^2 - \beta^2 u_1^2 \right]} \right]$$

$$+ \left\{ \begin{array}{l} \frac{\lambda_n}{R} \frac{\Gamma_2^n}{\beta} \int_{\delta}^{u_0 + \beta u_1} e^{-\frac{\lambda_n}{R} s} J_0 \left[ \sqrt{Q \left[ (u_0 - s)^2 - \beta^2 u_1^2 \right]} \right] ds \\ - \frac{\Gamma_3^n \alpha}{\beta} \int_0^{u_0 + \beta u_1} e^{-\alpha s} J_0 \left[ \sqrt{Q \left[ (u_0 - s)^2 - \beta^2 u_1^2 \right]} \right] ds \end{array} \right\} H(u_0 + \beta u_1) \quad (3.101)$$

and

$$\begin{aligned}\Gamma_1^n &= \frac{\alpha R^2}{\lambda_n (\lambda_n + \alpha R)} \\ \Gamma_2^n &= \frac{\alpha R^2}{\lambda_n (\lambda_n - \alpha R)} \\ \Gamma_3^n &= \frac{2\lambda_n R}{(\lambda_n - \alpha R)(\lambda_n + \alpha R)}, \quad Q = \frac{1}{\beta^2 \gamma^2} \left(\frac{\lambda_n}{R}\right)^2\end{aligned}\tag{3.102}$$

Similarly,

$$\begin{aligned}\bar{E}_z^n &= \bar{E}_{zn}^p + E_{zn}^h, \quad \bar{E}_{zn}^p = \frac{1}{\gamma\beta} \frac{\partial \bar{A}_n^p}{\partial u}, \quad \text{and} \\ \bar{E}_{zn}^h &= \frac{1}{\gamma\beta} \left(\frac{\lambda_n}{R}\right)^2 \int_0^{u_0} ds \bar{A}_n^h(u_1, s).\end{aligned}$$

Substituting from Equations (3.57) and (3.58),

$$\begin{aligned}\bar{E}_{zn}^p &= \frac{1}{\gamma\beta} \left\{ \frac{\lambda_n}{R} \Gamma_1^n e^{\frac{\lambda_n}{R} u} H(-u) + \left[ \left(-\frac{\lambda_n}{R}\right) \Gamma_2^n e^{-\frac{\lambda_n}{R} u} \right. \right. \\ &\quad \left. \left. + \alpha \Gamma_3^n e^{-\alpha u} \right] H(u) \right\},\end{aligned}\tag{3.103}$$

and

$$\begin{aligned}
 E_{zn}^h &= \frac{1}{\beta \gamma} \left( \frac{\lambda_n}{R} \right)^2 \left\{ (-) \frac{\Gamma_1^n}{\beta} \int_{\substack{0, u_0 > -\beta u_1 \\ -\beta u_1 - u_0, u_0 < -\beta u_1}}^{\infty} e^{-\frac{\lambda_n}{R} s} J_0 \left[ \sqrt{Q \left[ (u_0 + s)^2 - \beta^2 u_1^2 \right]} \right] ds \right. \\
 &+ \left[ -\frac{\Gamma_2^n}{\beta} \int_0^{u_0 + \beta u_1} e^{-\frac{\lambda_n}{R} s} J_0 \left[ \sqrt{Q \left[ (u_0 - s)^2 - \beta^2 u_1^2 \right]} \right] ds \right. \\
 &+ \frac{\Gamma_3^n}{\beta} \int_0^{u_0 + \beta u_1} e^{-\alpha s} J_0 \left[ \sqrt{Q \left[ (u_0 - s)^2 - \beta^2 u_1^2 \right]} \right] ds \\
 &\left. - \frac{2}{\beta} \left( \frac{R}{\lambda_n} \right) \int_{-\beta u_1}^{u_0} J_0 \left( \sqrt{Q(s^2 - \beta^2 u_1^2)} \right) ds \right] H(u_0 + \beta u_1) \left. \right\} \quad (3.104)
 \end{aligned}$$

We verify the convergence of the last term of Equation (3.104) as  $u_0 \rightarrow \infty$ . Let  $\omega^2 = s^2 - \beta^2 u_1^2$ , then we can rewrite the term as

$$\lim_{u_0 \rightarrow \infty} \int_0^{\sqrt{u_0^2 - \beta^2 u_1^2}} \frac{\omega J_0(\sqrt{Q} \omega)}{\sqrt{\omega^2 + \beta^2 u_1^2}} d\omega^* = \frac{\beta u_1 \sqrt{Q}}{\sqrt{Q}}$$

\* See, for example, Lebedev, Special Functions and Their Applications, (Prentice-Hall, 1965), p. 133.

Finally, we write out the expression for  $\bar{\phi}_n$  of ER:

$$\bar{\phi}_n = \bar{\phi}_n^p + \bar{\phi}_n^h,$$

$$\bar{\phi}_n^p = \bar{A}_n^p / \beta \quad (3.105)$$

$$\begin{aligned} \bar{\phi}_n^h &= \frac{1}{\beta} \frac{\partial}{\partial u_1} \int_0^{u_0} ds \bar{A}_n^h(u_1, s) = \frac{1}{\gamma} \left( \frac{R}{\lambda_n} \right)^2 \frac{\partial \bar{E}_{zn}^h}{\partial u_1} \\ &= \frac{1}{\beta} \left\{ -\Gamma_1 e^{\lambda_n/R u_1}, u_0 + \beta u_1 < 0 \right. \\ &+ H(u_0 + \beta u_1) \left[ -\frac{\Gamma_1 e^{(\lambda_n/R)u_0}}{\beta} \int_{u_0}^{\infty} e^{-(\lambda_n/R)s} \frac{\partial J_0}{\partial u_1} \left( \sqrt{Q(s^2 - \beta^2 u_1^2)} \right) ds \right. \\ &- \Gamma_2 e^{-(\lambda_n/R)(u_0 + \beta u_1)} - \frac{\Gamma_2 e^{-(\lambda_n/R)u_0}}{\beta} \int_{-\beta u_1}^{u_0} ds e^{(\lambda_n/R)s} \frac{\partial J_0}{\partial u_1} \left( \sqrt{Q(s^2 - u_1^2)} \right) \\ &+ \Gamma_3 e^{-\alpha(u_0 + \beta u_1)} + \frac{\Gamma_3 e^{-\alpha u_0}}{\beta} \int_{\beta u_1}^{u_0} ds e^{\alpha s} \frac{\partial J_0}{\partial u_1} \left( \sqrt{Q(s^2 - u_1^2)} \right) \\ &\left. \left. - \frac{2R}{\lambda_n} - \frac{2r}{\lambda_n \beta} \int_{-\beta u_1}^{u_0} \frac{\partial J_0}{\partial u_1} \left( \sqrt{Q(s^2 - \beta^2 u_1^2)} \right) ds \right] \right\} \quad (3.106) \end{aligned}$$

### 3.4.1 Numerical Evaluation of EM Fields for Injection

Problem. The equations above have been programmed to calculate the EM fields and draw CALCOMP plots at specified  $r$  and  $z$  as a function of time, or at specified  $r$  and  $t$  as a function of  $z$ . To avoid convergence problems in the numerical integrations involving the zero-order Bessel function, the integrals have been taken from root to root of  $J_0(x) = 0$ . The radial sum of the Gaussian profile has been cut off when the term falls below 1/150 of the first term. The parameters for Figures 3.5a through 3.5k, which show  $E_z$  versus  $t$  at various distances from the endplate, are

$$\begin{aligned}I^P &= 5 \times 10^4 \text{ A} \\ \gamma &= 3 \text{ (1 MeV electrons)} \\ r &= 0 \\ R &= 6 \text{ cm} \\ t_r &= \text{risetime} = 20 \text{ nsec} \\ b &= 1 \text{ (cm)}^{-1} \approx \text{(beam radius)}^{-1} \\ \alpha &= \frac{2}{\gamma\beta ct_r}\end{aligned}$$

$z$  in centimeters is indicated on the curves.

$E_z$  is plotted for a positive current; therefore, for an electron beam,  $E_z$  is the negative of  $EZ$  in volts/centimeter. All times are in nanoseconds.

Figure 3.6 is calculated at  $z = 50$  cm for the same parameters as Figures 3.5a through 3.5k, except that  $\gamma = 1.2$  and  $r = 1$ . Figure 3.6 is presented to show by comparison with Figure 3.5k the effect of a different  $\gamma$  upon the influence of the endplate.

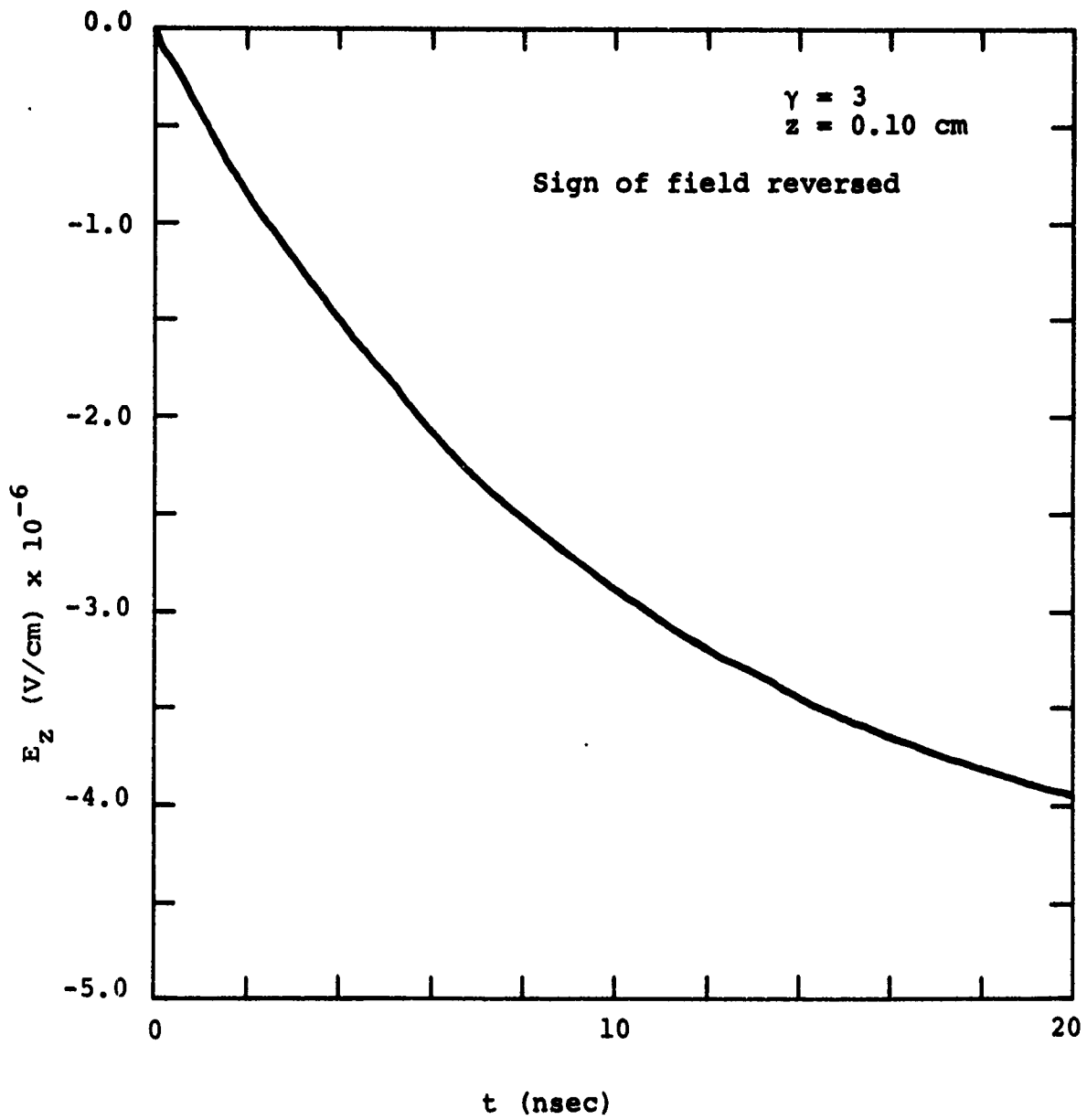


Figure 3.5a

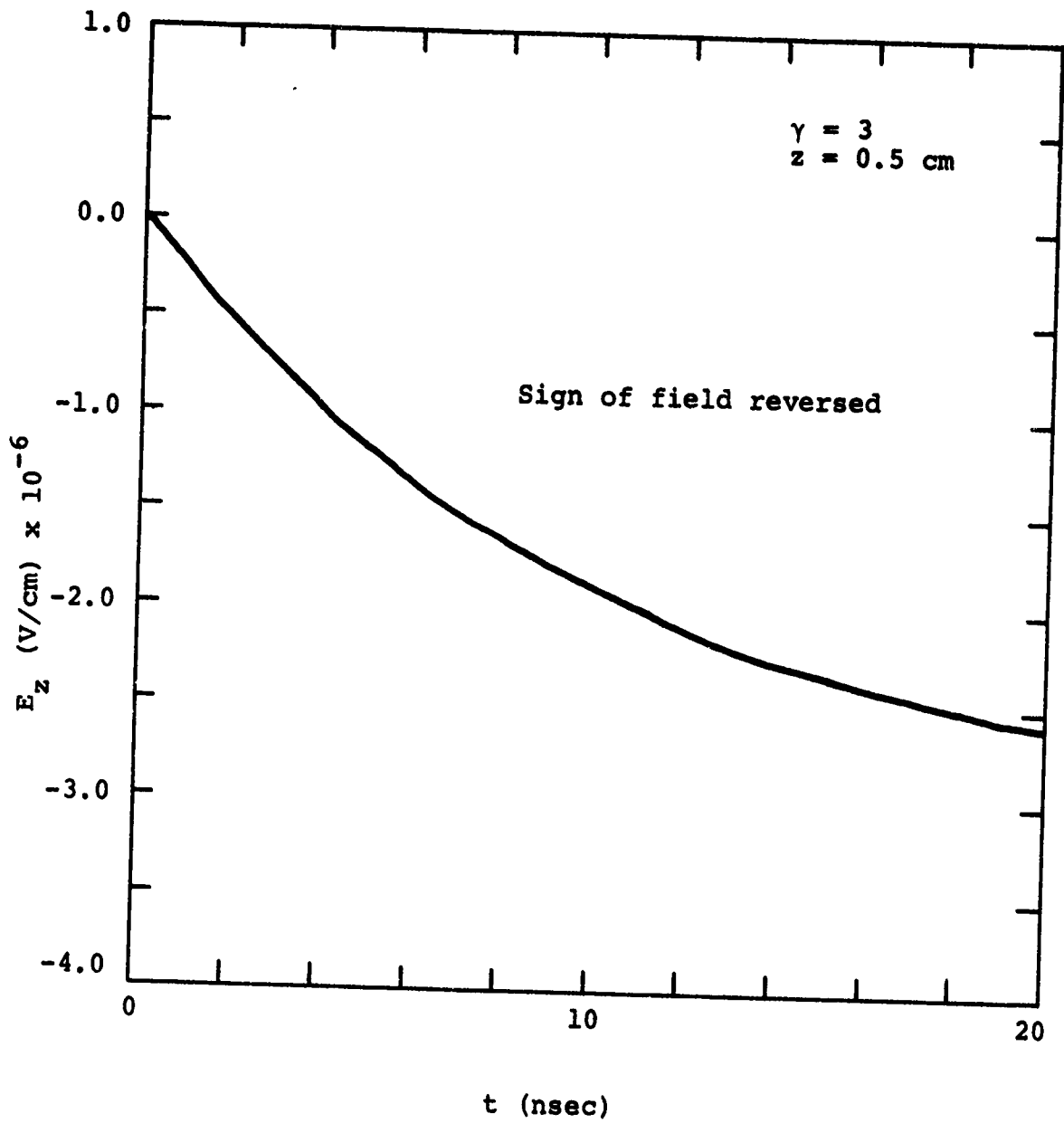


Figure 3.5b

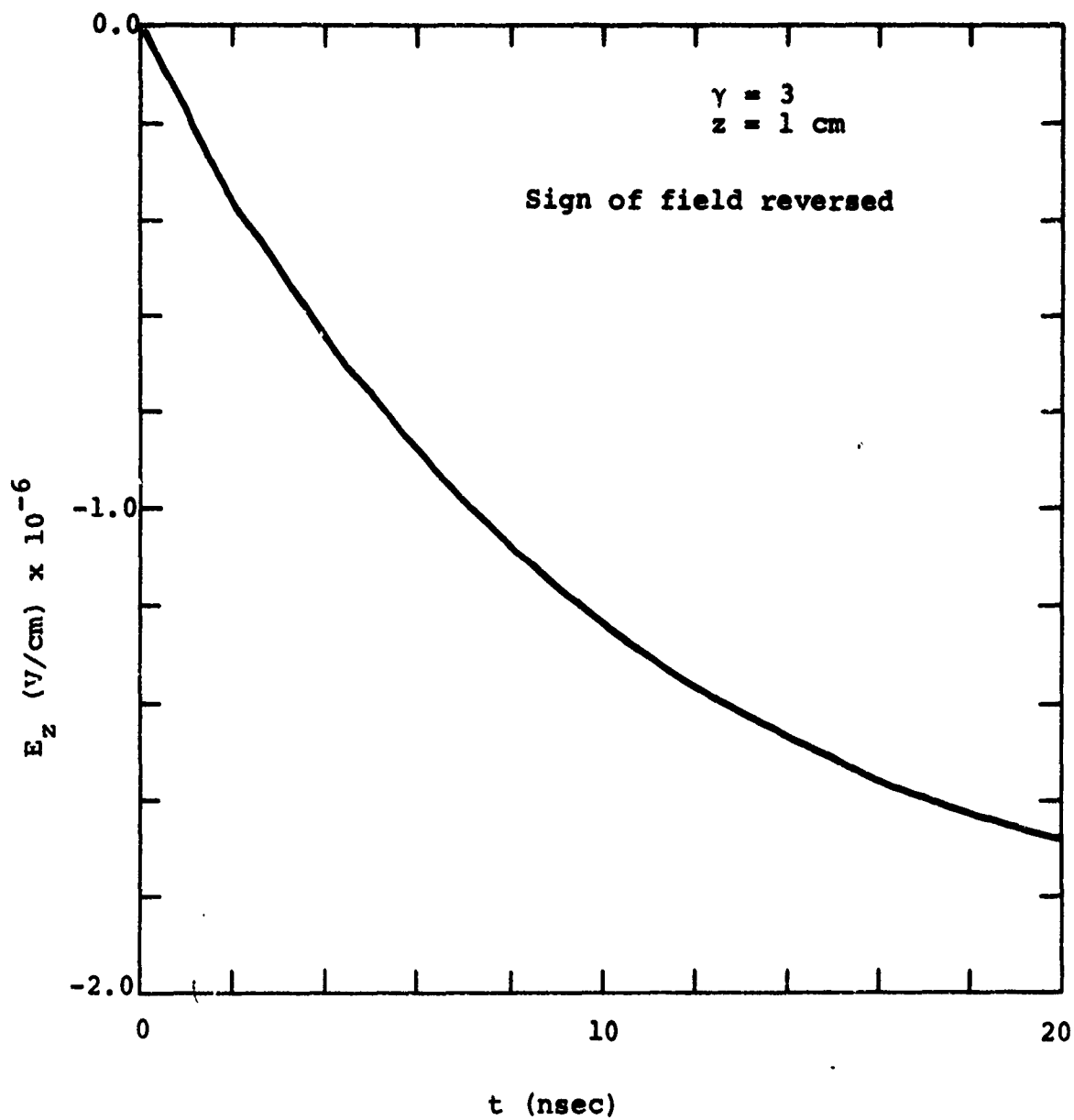


Figure 3.5c

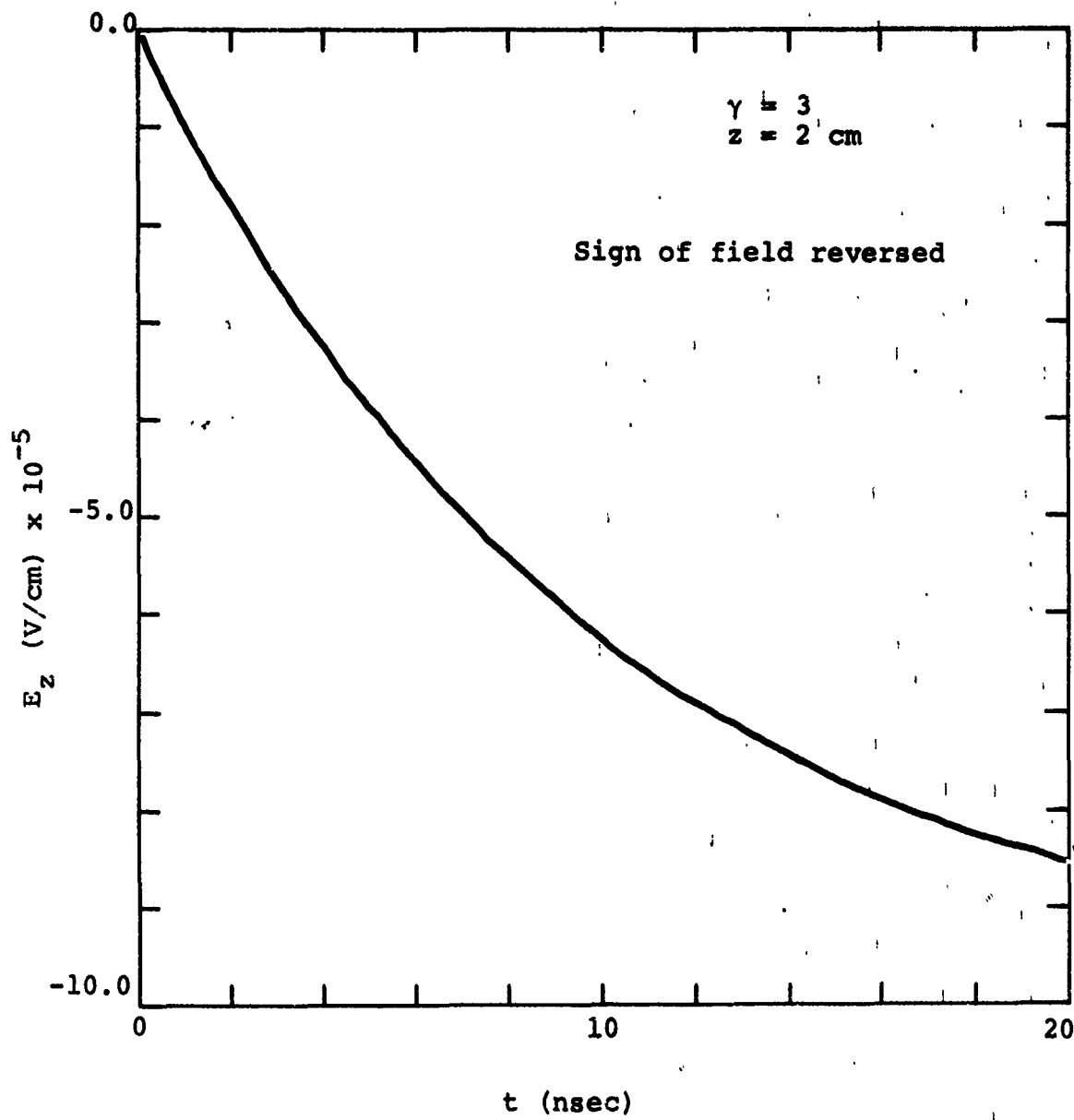


Figure 3.5d

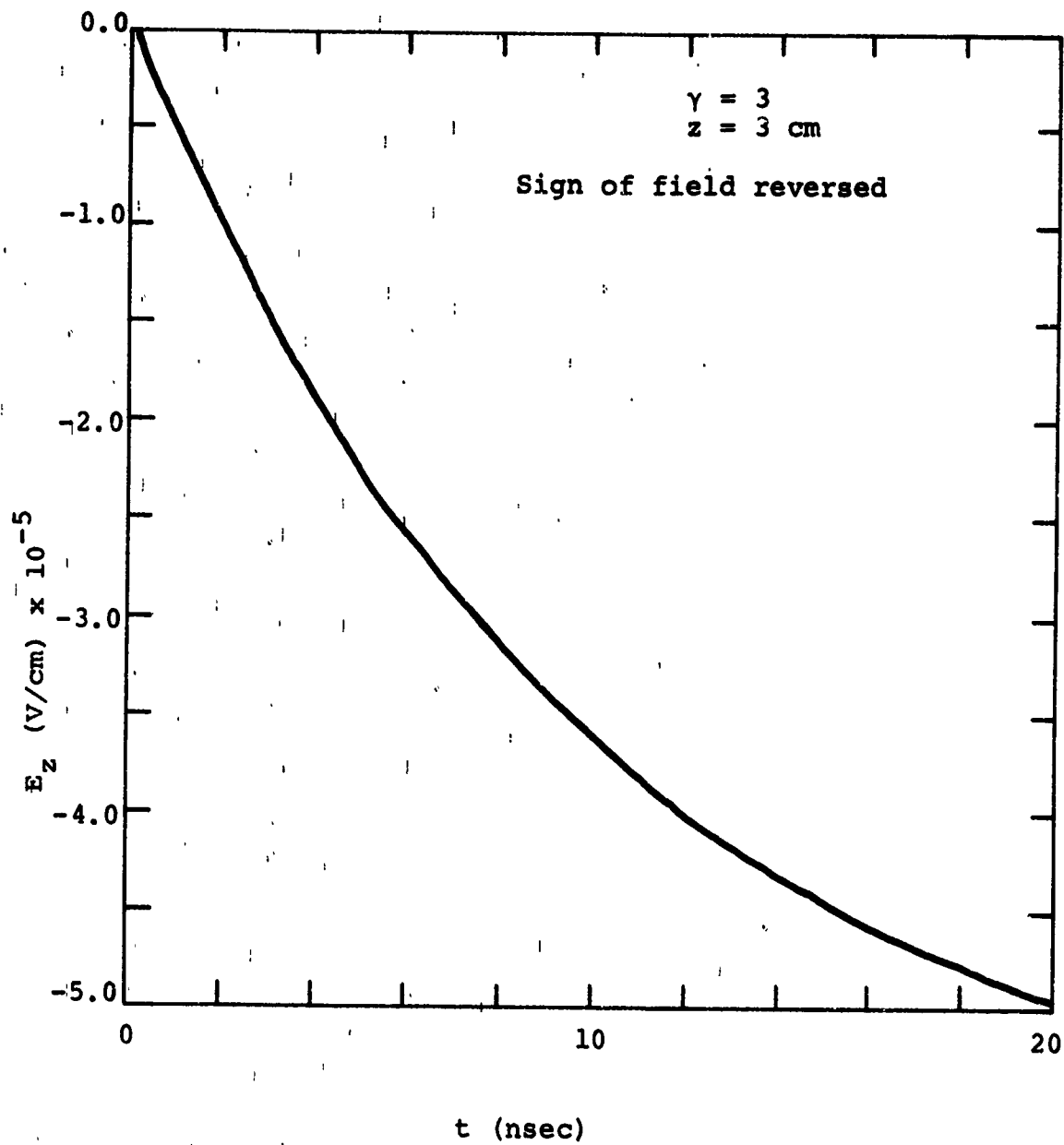


Figure 3.5e

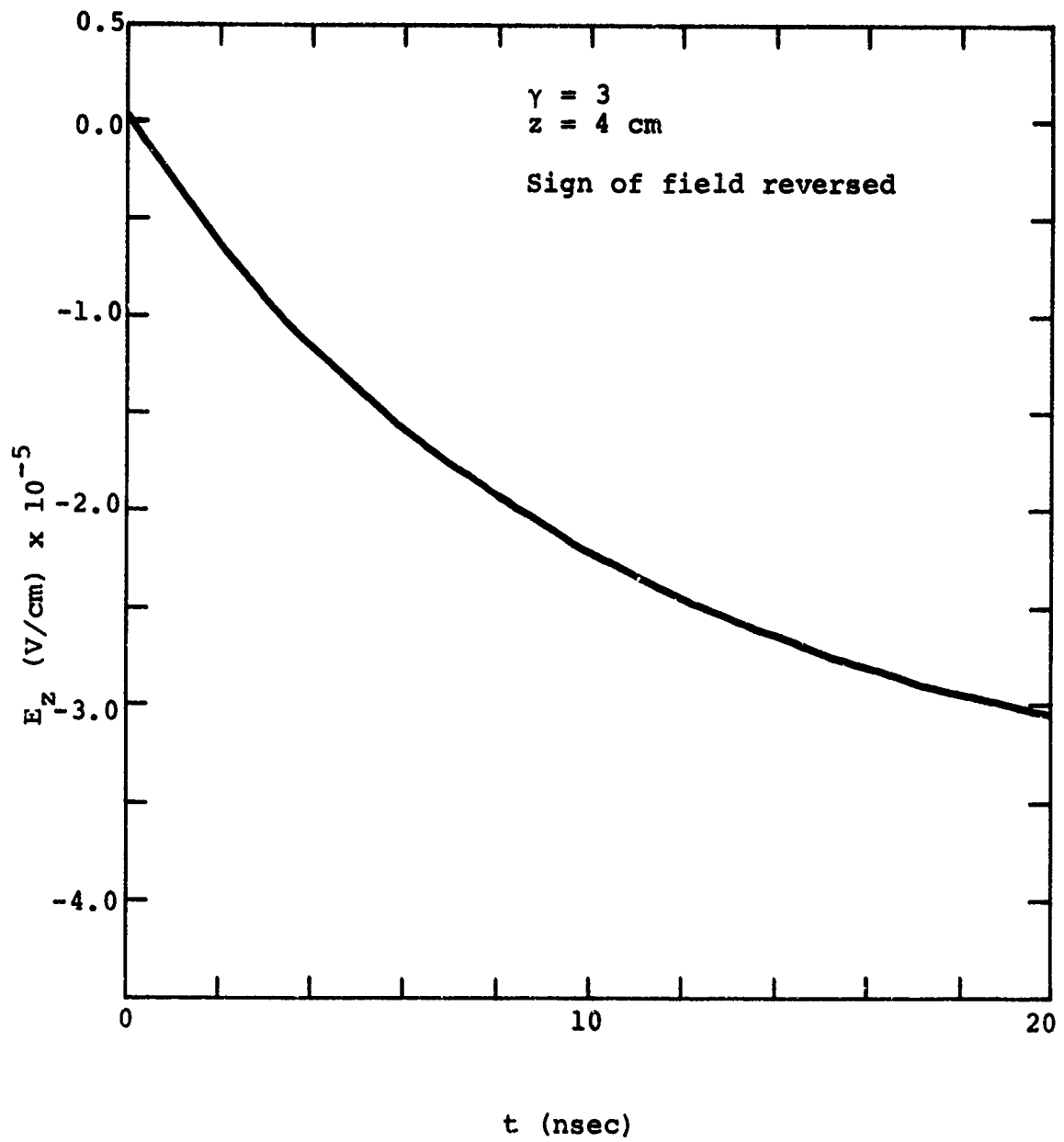


Figure 3.5f

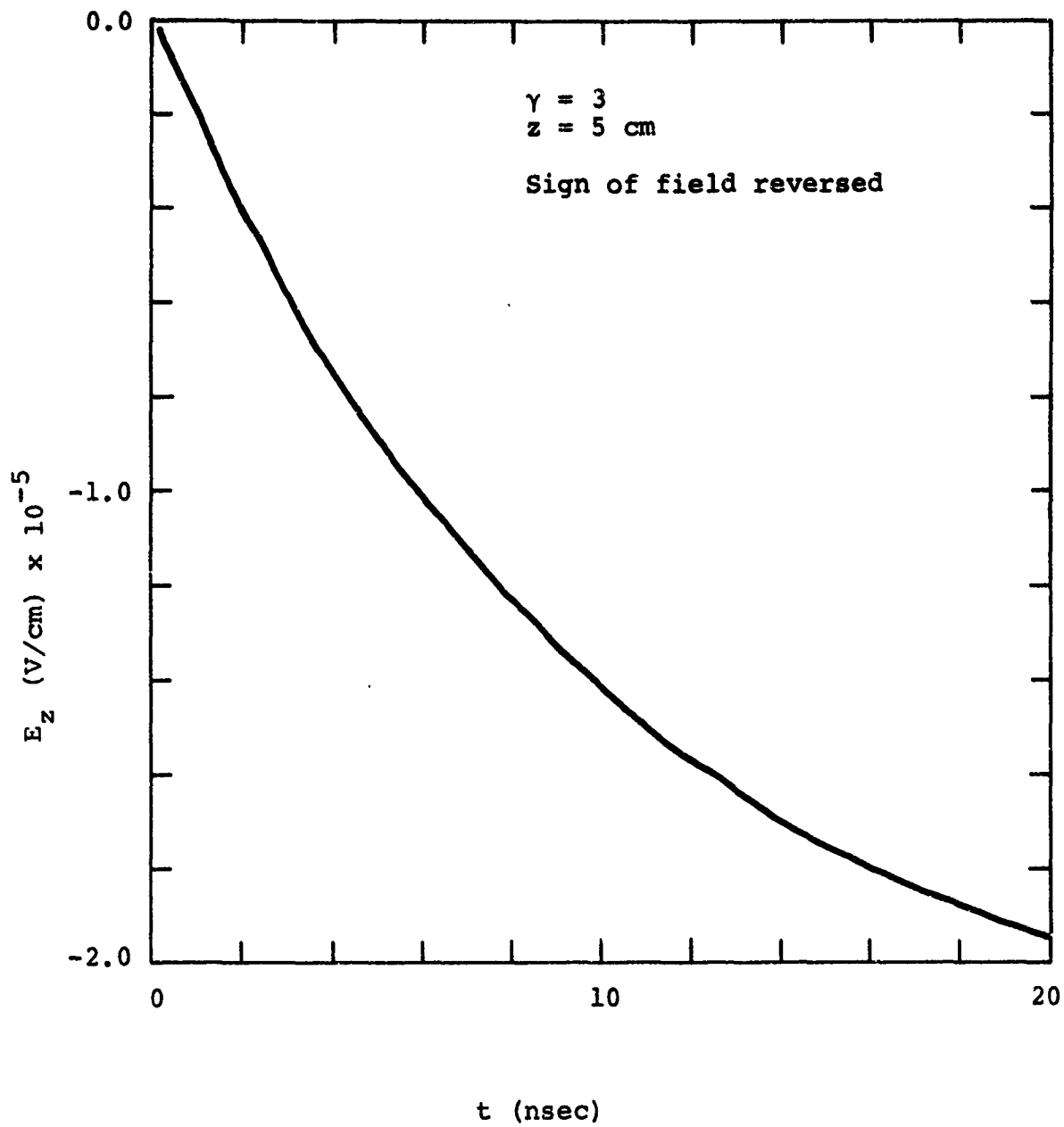


Figure 3.5g

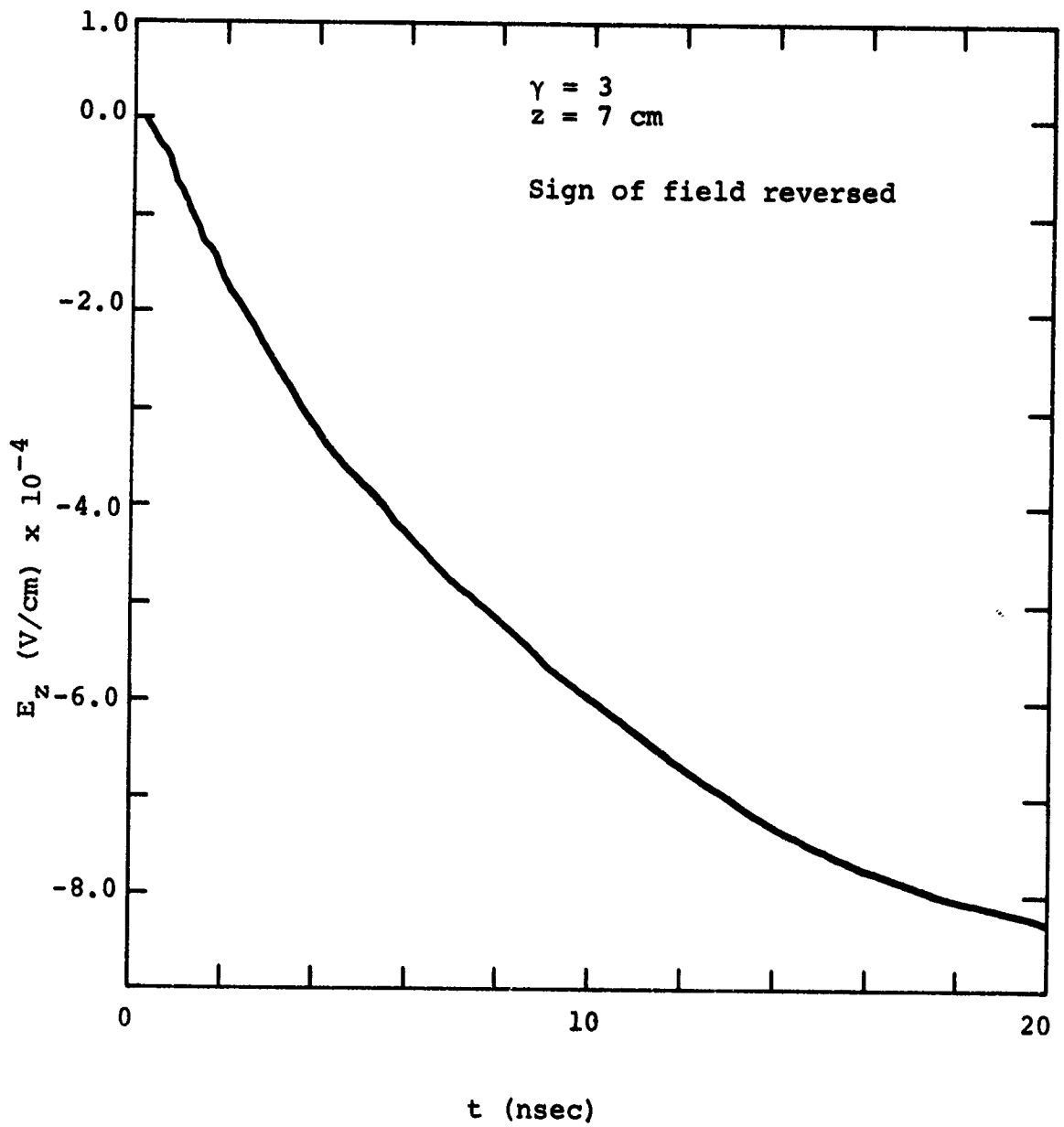


Figure 3.5h

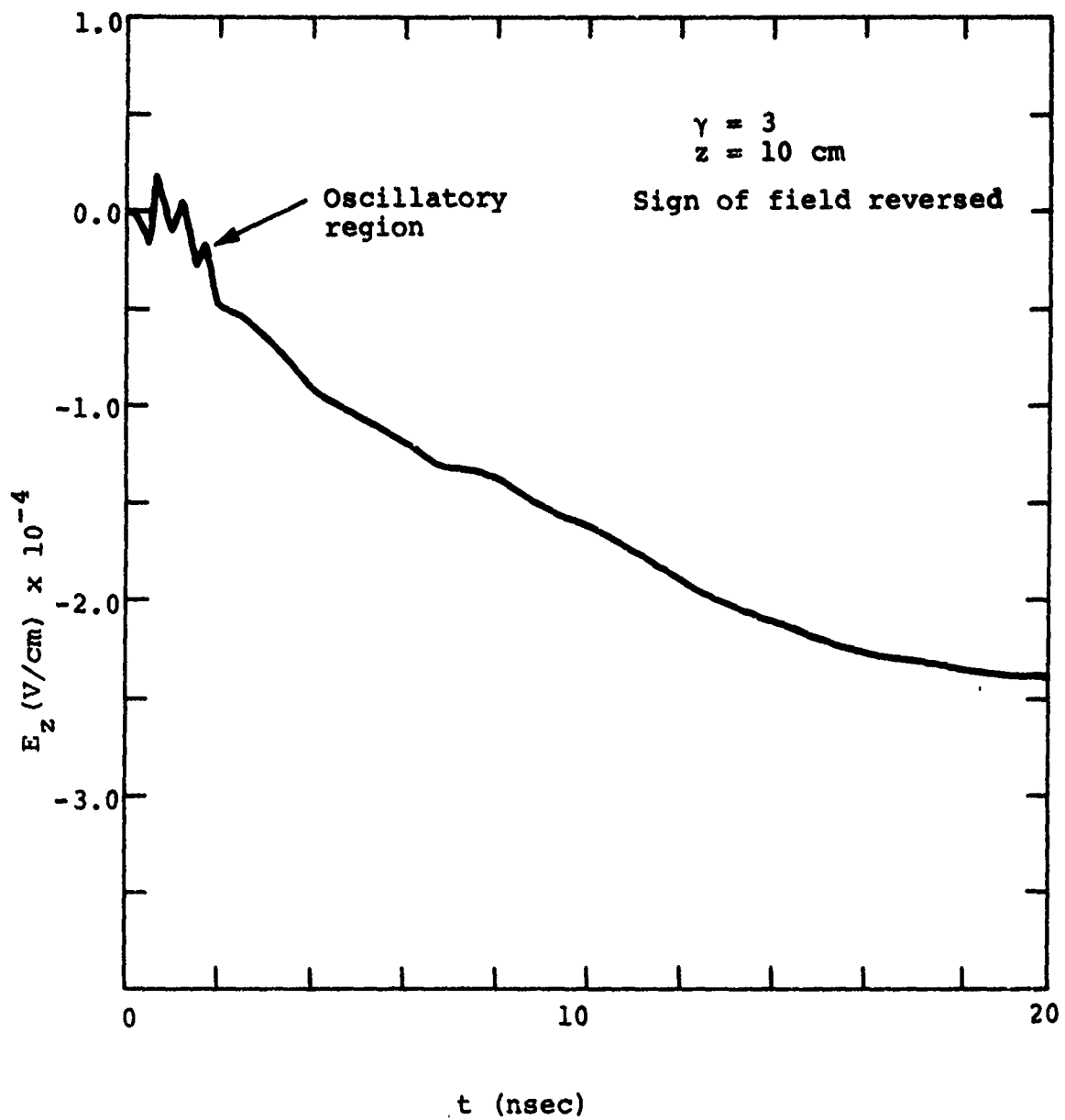


Figure 3.5i

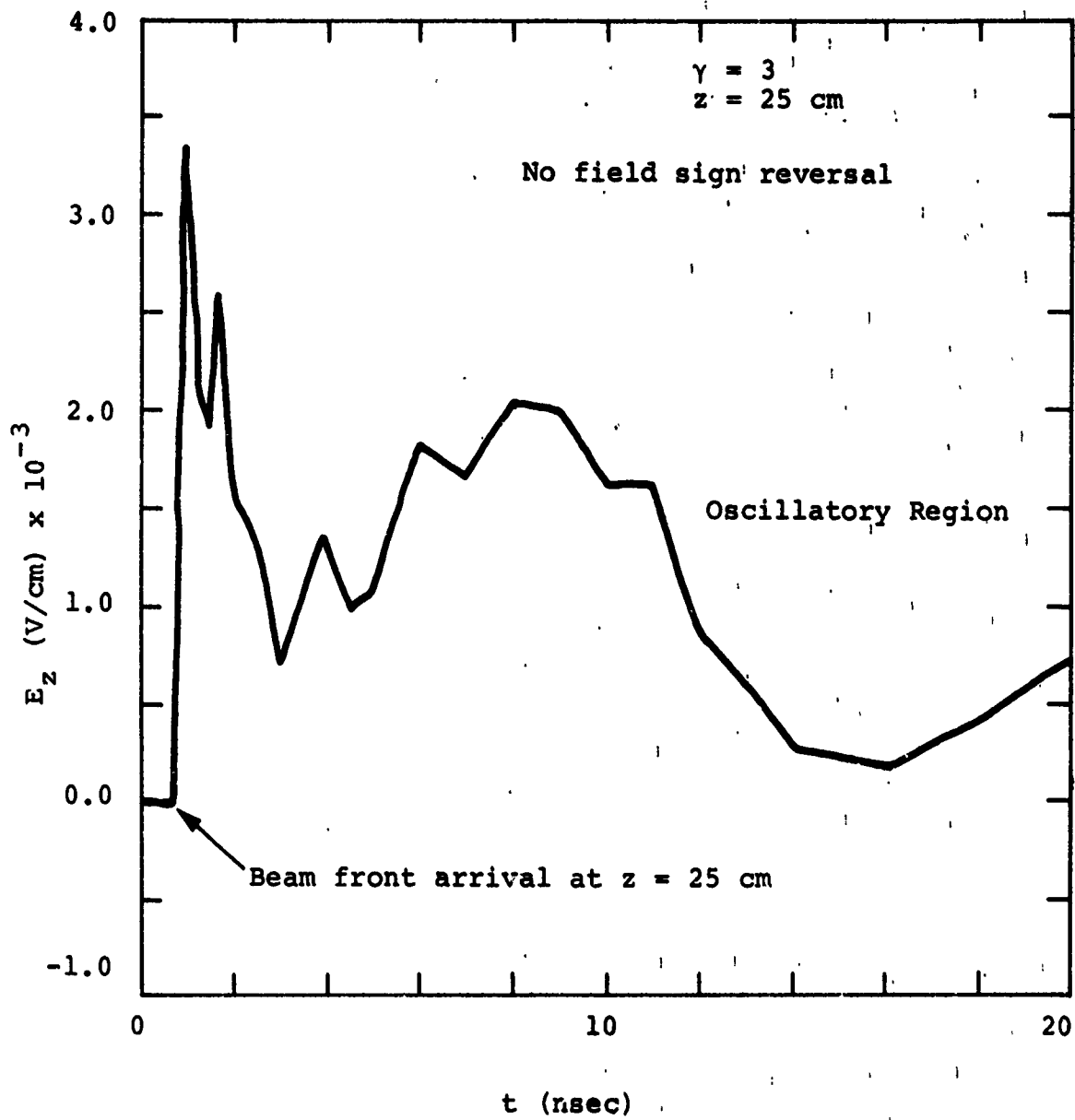


Figure 3.5j

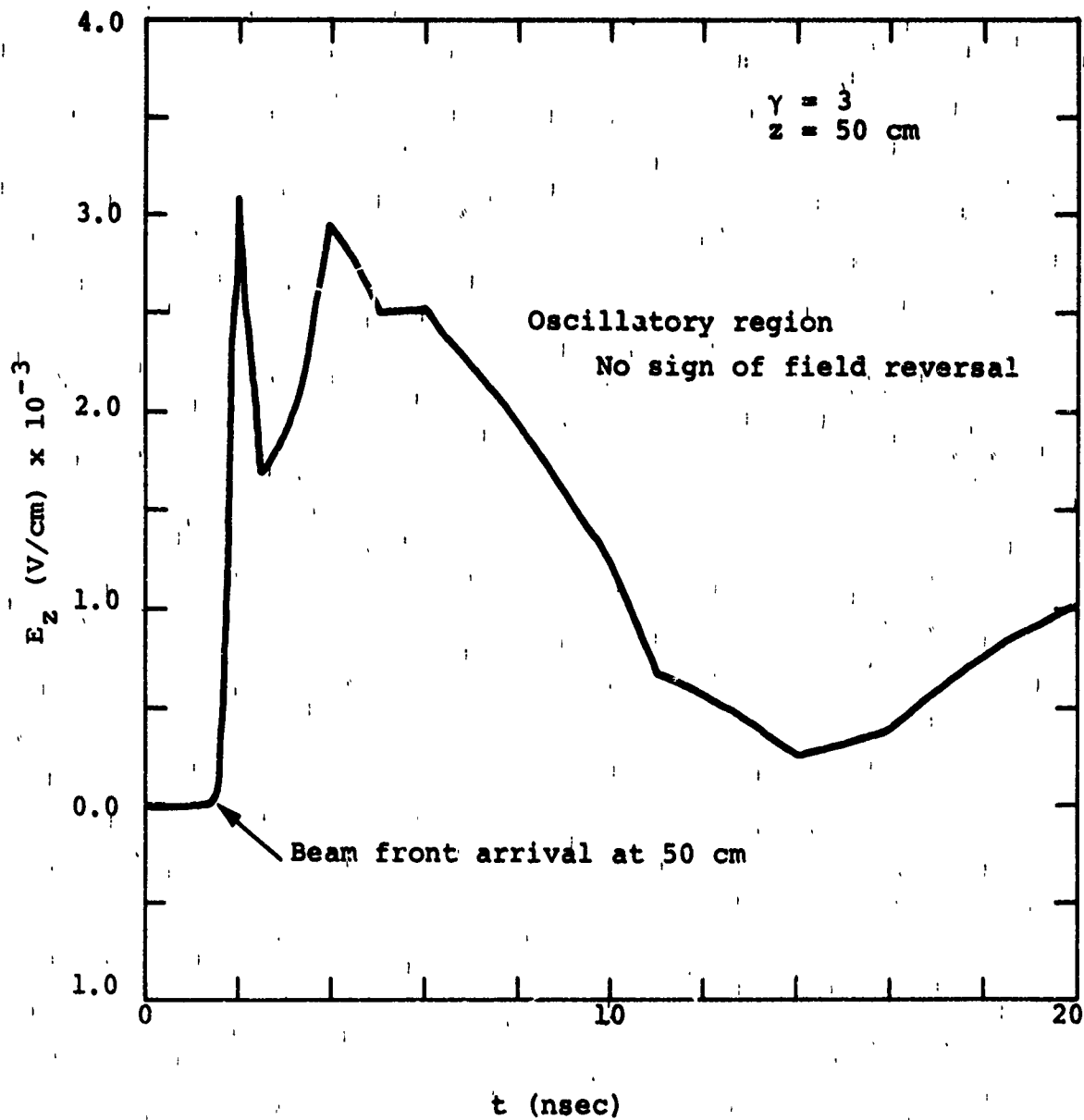


Figure 3.5k

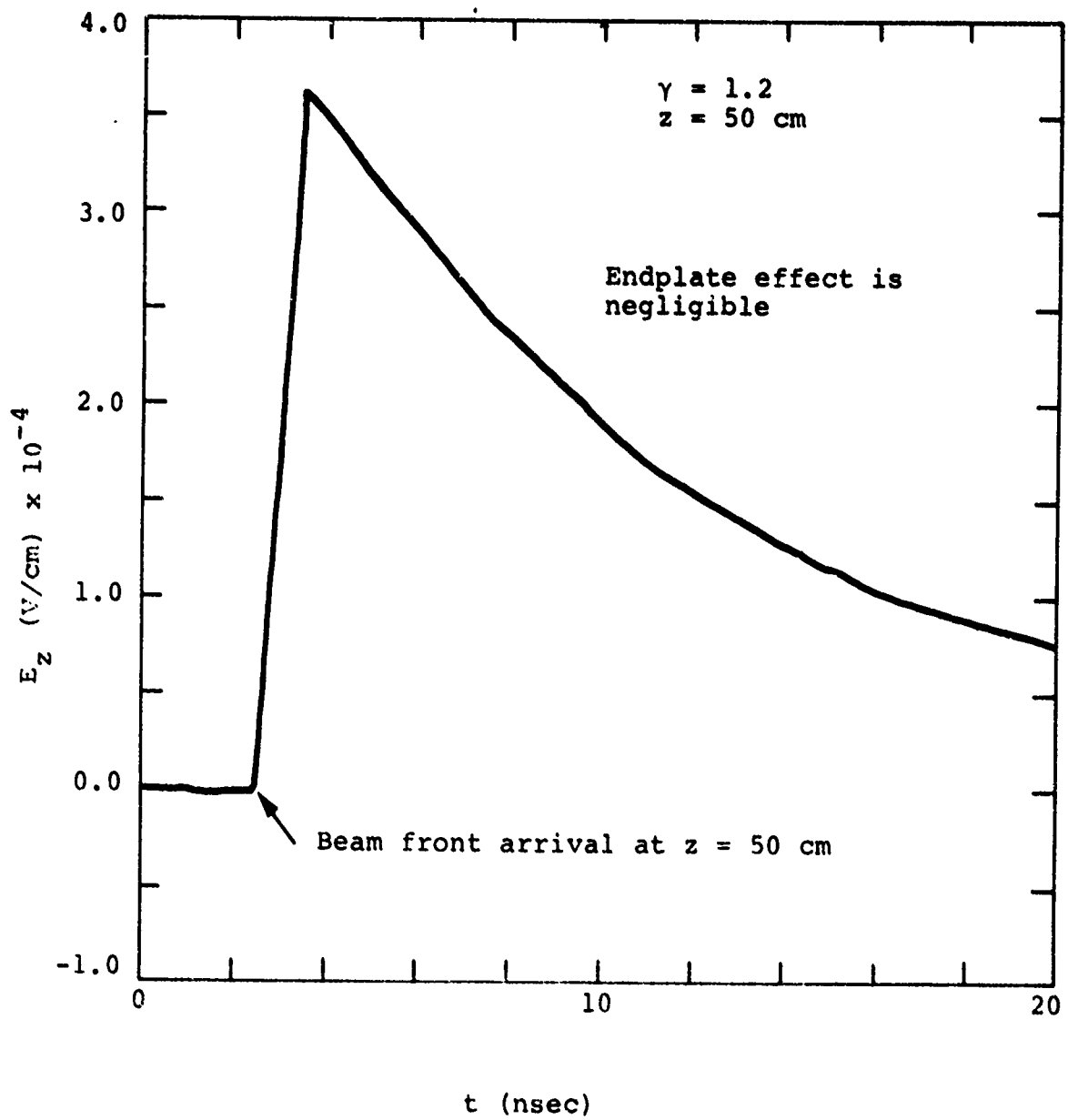


Figure 3.6

In Figures 3.7a through 3.7c, we look at the  $E_z$  field on axis as a function of  $z$  for various times after injection. The parameters for these figures are:

$$\begin{aligned}
 I_b^P &= 1.77 \times 10^3 \text{ A} \quad (\text{Corresponds to same beam charge/length at this lower } \beta \text{ as for peak current in cases of Figures 3.5a through k.}) \\
 \gamma &= 1.0005 \quad (\beta \approx \frac{1}{30}) \\
 r &= 0 \\
 R &= 6 \\
 t_r &= 0.1 \text{ nsec}
 \end{aligned}$$

These parameters have been chosen to illustrate the modification of the electrostatic contribution to  $E_z$  as a result of termination of the negative beam charges by positive surface charges at the endplate for small  $z$ . The  $\beta$  value for Figures 3.7 is such that the time in nanoseconds is numerically equal to the  $z$  for the beam front. We have taken a blunt or fast risetime beam to approximate the case where the beam risetime has been shortened by the large  $E_z$  fields near  $z = 0$  in the low-pressure injection problem.

The fields scale linearly with peak current, so the fields have been calculated for all peak currents. Different risetime effects can be approximated from the curves by correcting for different " $L \frac{dI}{dt}$ "; i.e., calculate the inductance/length,  $L$ , in henries/centimeter at the radius of interest, then for  $t_r = t_{r2}$ ,  $\alpha = \alpha_2$ ,

$$E_z \Big|_{t_{r2}} \approx E_z(\text{graph}) + LI^P (\alpha e^{-\alpha t} - \alpha_2 e^{-\alpha_2 t})$$

The time  $t$  is to be calculated as the time after the beam front arrival at the  $z$  value of interest, and  $\alpha$  is the graph value corresponding to  $t_r = 20 \text{ nsec}$ .

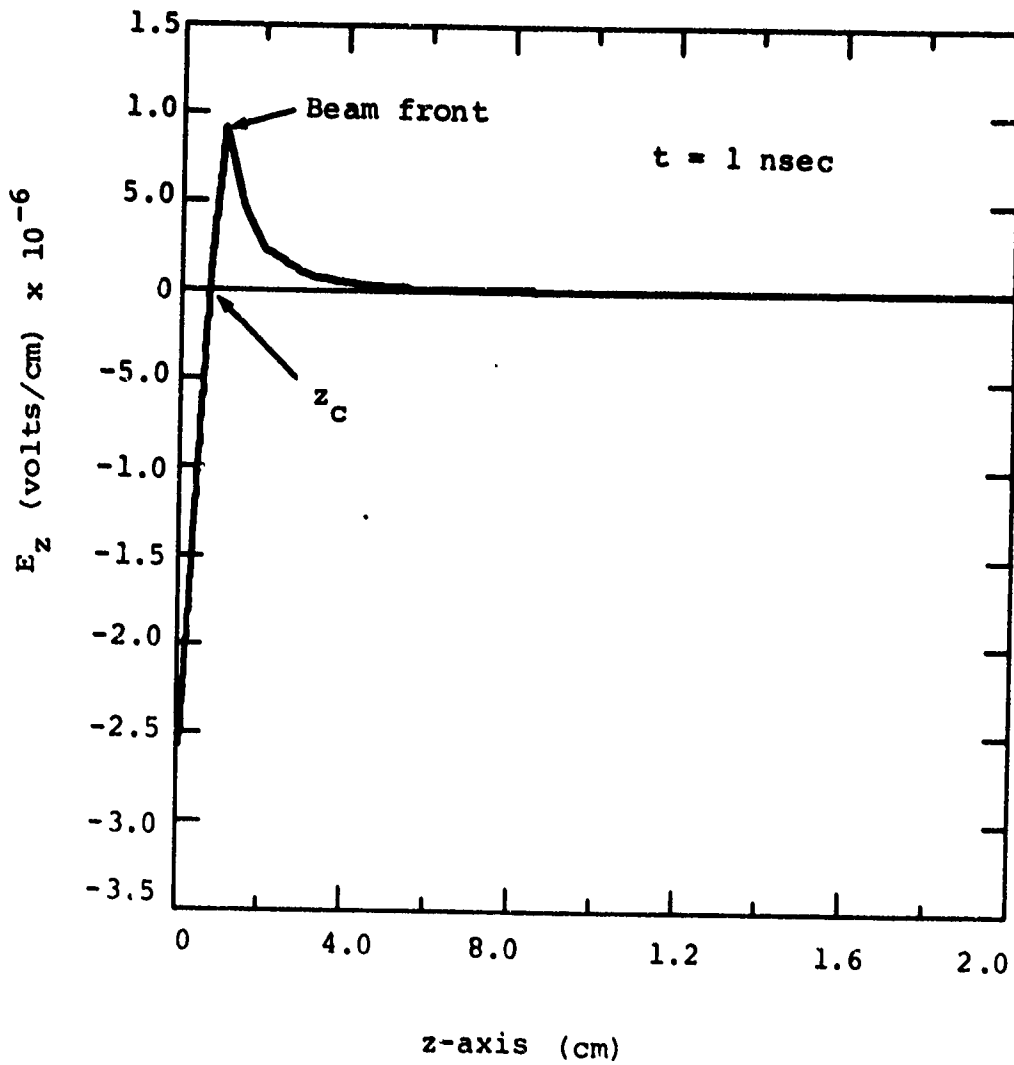


Figure 3.7a The longitudinal electric field ( $E_z$ ) on axis for a beam penetrating an end plate in a finite radius cavity ( $t = 1$  nsec).

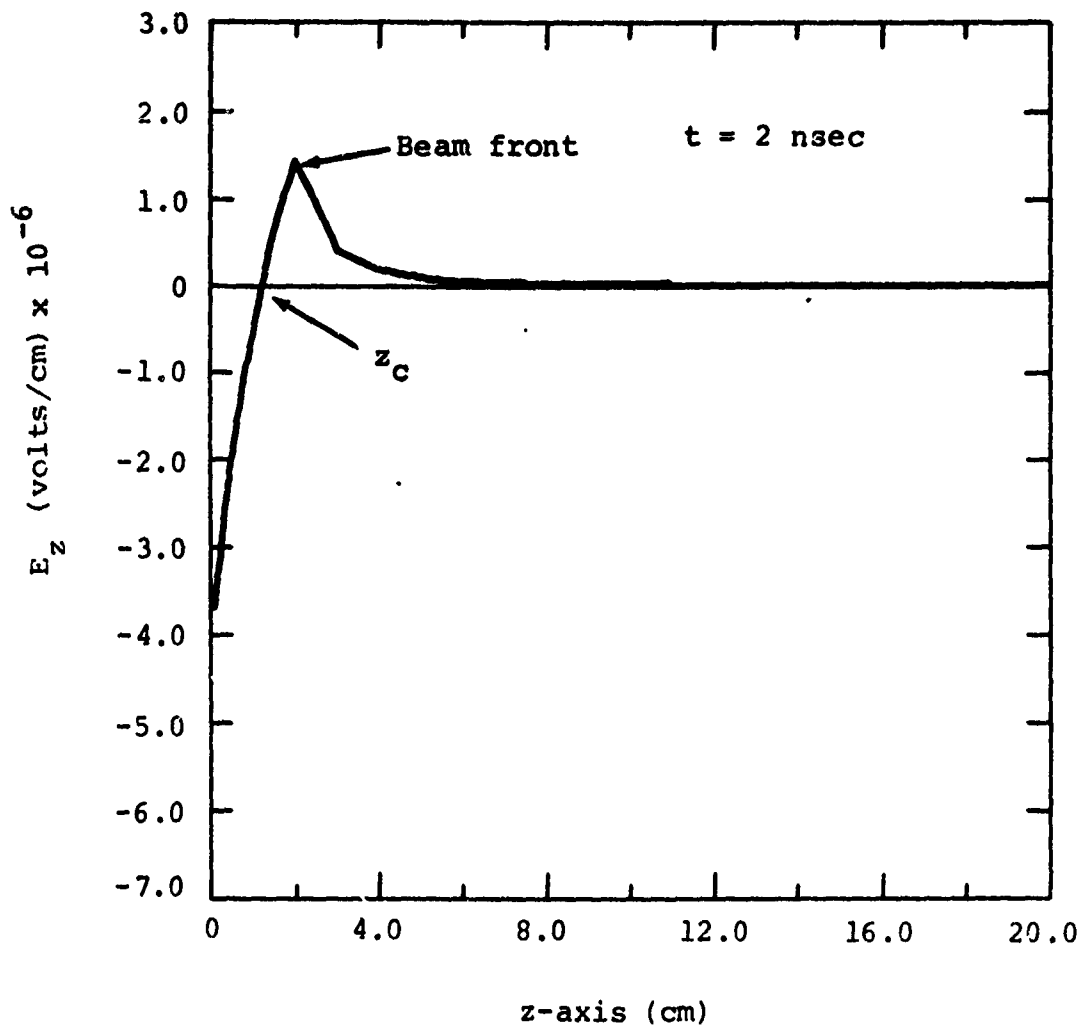


Figure 3.7b The longitudinal electric field ( $E_z$ ) on axis for a beam penetrating an end plate in a finite radius cavity ( $t = 2$  nsec).

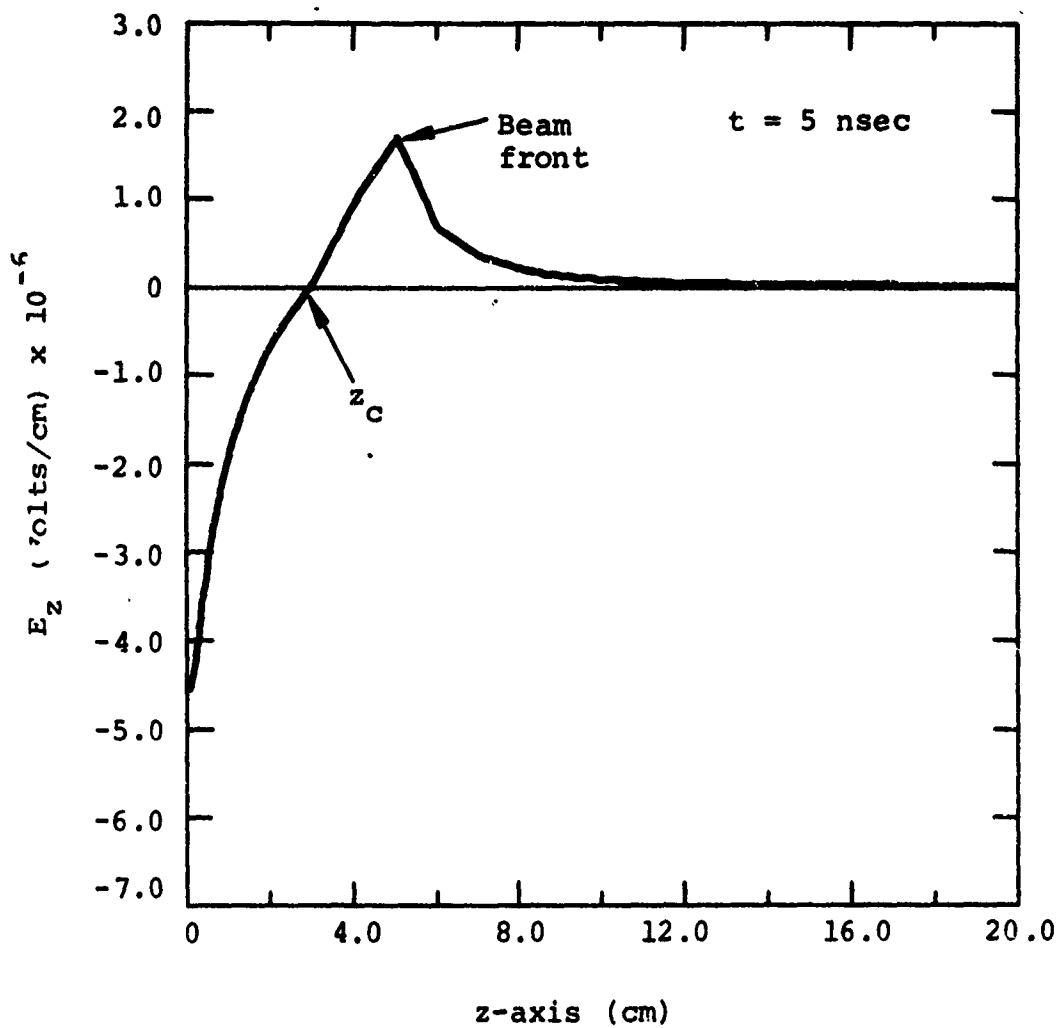


Figure 3.7c The longitudinal electric field  $E_z$  on axis for a beam penetrating an end plate in a finite radius cavity ( $t = 5$  nsec).

3.4.2 Discussion of Calculations. We now discuss some of the physics exhibited by the graphs. The effect of the endplate is primarily electrostatic, leading to a reversal of the direction of  $E_z$  from the case of a beam in a long pipe without endplates, and to an increase in  $E_z$  and a drop in  $E_r$  near  $z = 0$ . By examining the magnitude of  $E_z$  near  $z = 0$  and its dropoff with increasing  $z$ , many of the low pressure beam propagation characteristics may be understood.

First of all, we note from Figures 3.5a and 3.5b that 1-MeV electrons at the peak current level would be stopped within 5 mm in the absence of ions. Alternatively, one can deduce that at about a 3000-A current level, the beam would "shut off" because the  $E_z$  field would be large enough to degrade the electron kinetic energy.

Another important point that the graphs illustrate is the  $\gamma$  dependence of the endplate effect. We note that in Figure 3.6 at 50 cm, the  $E_z$  field has the shape as would be expected without an endplate, i.e., the field is reversed in sign and decays with distance behind the beam front as  $e^{-t/t_r}$ . The  $\gamma = 3$  plot at the same distance downstream (Figure 3.5k), shows that the field has reversed from the  $z = 0$  direction, but that the curve shows an oscillatory behavior near the beam head.\* These oscillations are even more pronounced at  $z = 25$  cm (Figure 3.5j).

To understand these differences, we return to Equation (3.103) and (3.104). We rewrite  $E_z^n$  in terms of  $t$  and  $z$  variables, for the simpler case of  $t_r \rightarrow 0$ .

---

\*The fields are not accurately represented in the oscillatory regions since the graphs are plotted by linear interpolation between specified time points.

$$\bar{E}_z^n = \frac{1}{\gamma\beta} \left\{ e^{\frac{\lambda_n}{R} \gamma(\beta ct - z)} H(z - \beta ct) + e^{-\frac{\lambda_n}{R} \gamma(\beta ct - z)} H(ct\beta - z) \right. \quad (1)$$

$$- \gamma \int_0^{\frac{\lambda_n}{R} \sqrt{(ct)^2 - z^2}} e^{-\beta\gamma \left[ \sqrt{\omega^2 + \left(\frac{\lambda_n z}{R}\right)^2} - ct \frac{\lambda_n}{R} \right]} \frac{\omega J_0(\omega) d\omega}{\sqrt{\omega^2 + \left(\frac{\lambda_n z}{R}\right)^2}} \quad (2)$$

$0, ct < z$

$$+ \gamma \int_0^{\frac{\lambda_n}{R} \sqrt{(ct)^2 - z^2}} e^{-\beta\gamma \left[ \frac{\lambda_n}{R} ct - \sqrt{\omega^2 + \left(\frac{\lambda_n z}{R}\right)^2} \right]} \frac{\omega J_0(\omega) d\omega}{\sqrt{\omega^2 + \left(\frac{\lambda_n}{R}\right)^2 z^2}} \quad (3)$$

$$- 2\gamma \int_0^{\frac{\lambda_n}{R} \sqrt{(ct)^2 - z^2}} \left. \frac{\omega J_0(\omega) d\omega}{\sqrt{\omega^2 + \left(\frac{\lambda_n}{R}\right)^2 z^2}} \right\} \quad (3.104a) \quad (4)$$

The (1) terms give the field without an endplate, the remaining terms are the endplate contributions. When  $\sqrt{(ct)^2 - z^2} \gg R/\lambda_n$  terms (2) and (3) approach zero, and

$$- 2\gamma \int_0^{(\lambda_n/R)\sqrt{(ct)^2 - z^2}} \frac{\omega J_0(\omega) d\omega}{\sqrt{\omega^2 + \left(\frac{\lambda_n}{R} z\right)^2}} + - 2\gamma e^{-\frac{\lambda_n}{R} z}$$

We can now obtain criteria regarding absence of endplate effects by noting that the fundamental mode ( $n = 1$ ) drops off most slowly with increasing  $z$ . Negligible endplate contributions to the  $E_z$  field require for a zero-risetime beam,

$$(a) \quad \sqrt{(ct)^2 - z_f^2} \gg \frac{R}{\lambda_1}, \quad (\text{no field "oscillation"}) \quad (3.107)$$

$$\approx 10 \frac{R}{2.4}$$

where  $z_f$  is the beam front position at time of interest, and

$$(b) \quad e^{-\frac{2.4\gamma}{R}(z_f - z)} \gg 2\gamma e^{-\frac{2.4}{R} z} \quad (\text{no field sign reversal})$$

If  $t_r \approx 0$ , the crossover point,  $z_c$ , for the  $E_z$  field is

$$e^{-\frac{2.4\gamma}{R}(z_f - z_c)} = 2\gamma e^{-\frac{2.4}{R} z_c}$$

$$\text{or } z_c \approx \left( \frac{R}{2.4} \ln 2\gamma + \gamma z_f \right) / (\gamma + 1), \quad z_f, z_c \lesssim \frac{2R}{2.4} \quad (3.108)$$

The criterion for absence of field oscillation simply states that the light signal from the anode at  $z = 0$  has traveled far beyond the beam front. We note that the  $E_z$  sign reversal point in Figures 3.7 is predicted very accurately by the above criterion and we also see that

$$\text{Figure 3.5k} \rightarrow \sqrt{(ct)^2 - z_f^2} \approx \frac{ct}{\gamma} \approx 17 \approx 7 \frac{R}{2.4} \quad (\text{predicts oscillation})$$

$$\text{Figure 3.6} \rightarrow \frac{ct}{\gamma} \approx 42 \approx \frac{17 R}{2.4} \quad (\text{no oscillation})$$

These remarks have been noted on the graphs.

### 3.5 BEAM IN A LONG PIPE WITH PLASMA CONDUCTIVITY VARYING WITH DISTANCE BEHIND BEAM FRONT

As a beam penetrates a nonionized gas at pressures sufficiently high so that the collision frequency is large compared to the inverse beam risetime, and so that the avalanche charge production is negligible, the gas may be characterized by a conductivity which varies with distance behind the beam front. In particular; if the beam fills the pipe radially, a good approximation is

$$\begin{aligned} \sigma &= C_1 (1 - e^{-\alpha u}) + C_2, \quad u > 0 \\ \sigma &= C_2, \quad u < 0 \end{aligned} \tag{3.109}$$

with  $u = \gamma(vt - z)$  (see Figure 3.8).  $C_2 \neq 0$  corresponds to a pre-ionized conductivity level.

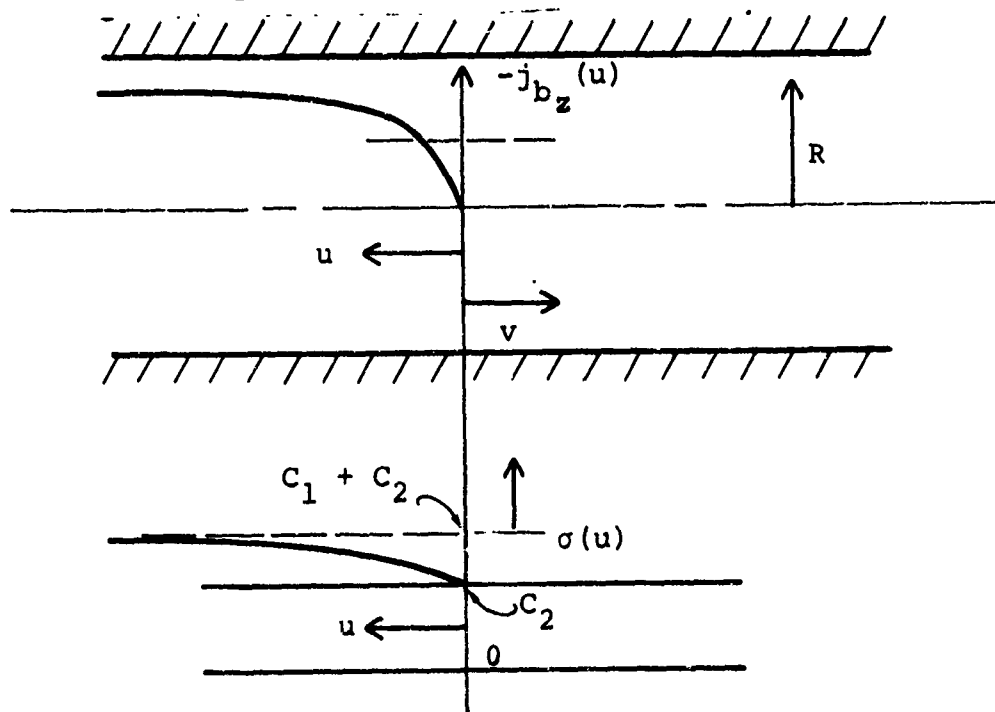


Figure 3.8 The conductivity function.

Recall from part A of this section, Equations (3.11) and (3.12), that if  $\sigma$  has spatial variation, the equations for  $A$  and  $\phi$  do not decouple. If we expand  $A$ ,  $\phi$  and  $j_{b_z}$  in radial modes as in previous sections, the basic Equations (3.11) and (3.12) give for the  $n^{\text{th}}$  mode coefficients:

$$\left[ -\frac{\partial^2}{\partial u^2} + \frac{4\pi\sigma\gamma v}{c^2} \frac{\partial}{\partial u} + \left(\frac{\lambda_n}{R}\right)^2 \right] A_n = S_n + \frac{4\pi\sigma\gamma}{c} \frac{\partial \sigma}{\partial u} \phi_n \quad (3.110)$$

$$\left( \frac{4\pi\sigma}{c} + \frac{\gamma v}{c} \frac{\partial}{\partial u} \right) \phi_n = \gamma \frac{\partial A_n}{\partial u} + \bar{Q}_n \quad (3.111)$$

Here we define  $S_n$  such that

$$\frac{4\pi}{c} j_{b_z}(r, u) = \sum_{n=1}^{\infty} S_n(u) J_0\left(\frac{\lambda_n}{R} r\right),$$

and henceforth drop the "n" subscript. Substituting from Equation (3.109) in Equations (3.110) and (3.111), and defining  $C_3 = C_1 + C_2$ ,

$$\left[ -\frac{\partial^2}{\partial u^2} + \frac{4\pi\gamma v}{c^2} C_3 \frac{\partial}{\partial u} - \frac{4\pi\gamma v}{c^2} C_1 \alpha e^{-\alpha u} \frac{\partial}{\partial u} + \left(\frac{\lambda_n}{R}\right)^2 \right] A = S + \frac{4\pi\gamma}{c} C_1 \alpha e^{-\alpha u} \phi \quad (3.112)$$

and

$$\left( \frac{4\pi C_3}{c} - \frac{4\pi C_1}{c} e^{-\alpha u} + \frac{\gamma v}{c} \frac{\partial}{\partial u} \right) \phi = \frac{\gamma \partial A}{\partial u} + Q \quad (3.113)$$

If we let  $w = \alpha u$  and take the Laplace transform of Equations (3.112) and (3.113) with respect to  $u$ , we obtain

$$\begin{aligned} -\alpha^2 [p^2 A(p) - pA(0) - A(0)] + \frac{4\pi\gamma v}{c^2} C_3 \alpha [pA(p) - A(0)] \\ - \frac{4\pi\gamma v}{c^2} C_1 \alpha [-A(0) + (p+1)A(p+1)] + \left(\frac{\lambda_n}{R}\right)^2 A(p) = S(p) + \frac{4\pi\gamma}{c} C_1 \alpha \phi(p+1) \end{aligned} \quad (3.114)$$

and

$$\begin{aligned} \frac{4\pi C_3}{c} \phi(p) - \frac{4\pi C_1}{c} \phi(p+1) + \frac{\gamma v}{c} \alpha [p\phi(p) - \phi'(0)] \\ = \gamma \alpha [pA(p) - A(0)] + Q(p) \end{aligned} \quad (3.115)$$

Rewriting Equations (3.114) and (3.115), we have

$$\lambda_1 A(p) + \lambda_2 A(p+1) = \bar{S}(p) + \lambda_3 \phi(p+1) \quad (3.116)$$

$$\lambda_4 \phi(p) + \lambda_5 \phi(p+1) = \lambda_6 A(p) + \bar{Q}(p) \quad (3.117)$$

$$\text{with } \lambda_1 \equiv \left(\frac{\lambda_n}{R}\right)^2 - \alpha^2 p^2 + 4\pi \frac{\gamma v}{c^2} C_3 \alpha p$$

$$\lambda_2 \equiv -\frac{4\pi\gamma v}{c^2} C_1 \alpha (p+1)$$

$$\bar{S}(p) \equiv s(p) + \left[ \frac{4\pi\gamma v}{c^2} C_3 \alpha - \alpha^2 p - \frac{4\pi\gamma v}{c^2} C_1 \alpha \right] A(0) - \alpha^2 A(0)$$

$$\lambda_3 \equiv \frac{4\pi\gamma}{c} C_1 \alpha$$

$$\lambda_4 \equiv \frac{4\pi C_3}{c} + \frac{\gamma v}{c} \alpha p$$

$$\lambda_5 \equiv -\frac{4\pi C_1}{c}$$

$$\lambda_6 = \gamma \alpha p$$

$$\bar{Q}(p) = Q(p) - \gamma \alpha A(0) + \frac{\gamma v \alpha}{c} \phi(0) \quad (3.118)$$

Equations (3.116) and (3.117) are two coupled equations with four "unknown" quantities,  $A(p)$ ,  $A(p+1)$ ,  $\phi(p)$ ,  $\phi(p+1)$ . In general, they cannot be decoupled. We proceed by first expressing  $\phi(p)$  and  $\phi(p+1)$  in terms of  $A(p)$ ,  $A(p+1)$ ,  $\bar{S}(p)$  and  $\bar{Q}(p)$ . From Equations (3.116) and (3.117),

$$\phi(p+1) = \frac{\lambda_1}{\lambda_3} A(p) + \frac{\lambda_2}{\lambda_3} A(p+1) - \frac{\bar{S}(p)}{\lambda_3} \quad (3.119)$$

$$\phi(p) = \left( \lambda_6 - \frac{\lambda_1 \lambda_5}{\lambda_3} \right) \frac{1}{\lambda_4} A(p) - \frac{\lambda_2 \lambda_5}{\lambda_3 \lambda_4} A(p+1) + \bar{S}(p) \frac{\lambda_5}{\lambda_4 \lambda_3} - \frac{\bar{Q}(p)}{\lambda_4} \quad (3.120)$$

Now replace  $p+1$  in Equation (3.119) by  $p$  and denote this translation in the  $\lambda$ 's by the subscript  $(p-1)$ . Then

$$\phi(p) = \left( \frac{\lambda_1}{\lambda_3} \right)_{(p-1)} A(p-1) + \left( \frac{\lambda_2}{\lambda_3} \right)_{(p-1)} A(p) - \frac{\bar{S}(p-1)}{\lambda_3} \quad (3.121)$$

Equating (3.120) and (3.121) gives an equation for  $A$  alone:

$$\begin{aligned} \epsilon_1 A(p) + \epsilon_2 A(p+1) + \epsilon_3 A(p-1) = \\ \epsilon_4 \bar{S}(p) + \epsilon_5 \bar{S}(p-1) + \epsilon_6 \bar{Q}(p) \end{aligned} \quad (3.122)$$

with

$$\begin{aligned}
\epsilon_1 &\equiv \left(\frac{\lambda_2}{\lambda_3}\right)_{(p-1)} - \left(\lambda_6 - \frac{\lambda_1 \lambda_5}{\lambda_3} \frac{1}{\lambda_4}\right) \\
\epsilon_2 &\equiv \frac{\lambda_5 \lambda_2}{\lambda_3 \lambda_4} \\
\epsilon_3 &\equiv \left(\frac{\lambda_1}{\lambda_3}\right)_{(p-1)} \\
\epsilon_4 &\equiv \frac{\lambda_5}{\lambda_4 \lambda_3} \\
\epsilon_5 &\equiv \frac{1}{\lambda_3 (p-1)} \\
\epsilon_6 &\equiv -\frac{1}{\lambda_4}
\end{aligned} \tag{3.123}$$

The  $\epsilon$ 's are all rational functions of  $p$  and  $\bar{S}$ ,  $\bar{Q}$  are source functions involving  $A(0)$ ,  $\partial A(0)/\partial u$ ,  $\phi(0)$ , and  $\partial \phi(0)/\partial u$ , the boundary conditions at  $w = 0$ , Equation (3.122) can now be inverted back to  $w$  space giving an integral equation for  $A(w)$ . Let us denote the inverse transform of  $\epsilon_i$  by  $f_i(w)$ . Then

$$\begin{aligned}
&\int_0^w du \left[ A(u) f_1(w-u) + e^{-u} A(u) f_2(w-u) + e^{+u} A(u) f_3(w-u) \right] \tag{3.124} \\
&= \int_0^w du \left[ S(u) f_4(w-u) + e^w \bar{S}(u) f_5(w-u) + \bar{Q}(u) f_6(w-u) \right]
\end{aligned}$$

or

$$\int_0^w du A(u) \left[ f_1(w-u) + e^{-w} f_2(w-u) + e^w f_3(w-u) \right]$$

(3.125)

$$= \int_0^w du \left\{ \bar{S}(u) \left[ f_4(w-u) + e^w f_5(w-u) \right] + \bar{Q}(u) f_6(w-u) \right\}$$

The actual inversion of the  $f_i$ 's is straightforward, but tedious, and we shall not include the algebra here. It turns out that Equation (3.125) is a Volterra integral equation and its solution can be obtained by well-known techniques.

## REFERENCES

### SECTION 3

- 3.1 S. Chandrasekhar; "The EM Wake Following a Pulse of Charged Particles," July 1961; IDA Report; Unclassified.
- 3.2 S. V. Yadavalli; Physics of Fluids, 1965, Vol. 8, Page 956; Unclassified.
- 3.3 S. Zwick; Physics International Company Internal Report, 1967; Physics International Company, San Leandro, California; Unclassified.
- 3.4 D. Hammer and N. Rostoker; Physics of Fluids, 1970, Vol. 13, Page 1831; Unclassified.
- 3.5 J. Cox and W. Bennett; Physics of Fluids, 1970, Vol. 13, Page 182; Unclassified.

## SECTION 4

### COLLECTIVE ION ACCELERATION BY INTENSE ELECTRON BEAMS IN LINEAR GEOMETRY\*

Collective acceleration of ions has attracted a significant amount of interest throughout the world in recent years. The goal of this work has been to find an alternative to present day accelerators in order to achieve ultrahigh energy protons, more than GeV, or GeV heavy ions. The possibilities of collective field acceleration of ions were first outlined by Veksler in 1956 (Reference 4.3). A group or collection of charges (electrons) create accelerating fields, and the magnitude of these fields is proportional to the number of charges. These "second generation" accelerators would be capable of generating accelerating fields in the range of  $10^5$  to  $10^7$  V/cm, or several orders of magnitude higher than fields in conventional accelerators. Moreover, large ion fluxes ( $10^{13}$  to  $10^{15}$  ions/bunch) of different ion species can be expected from a collective accelerator. The collective field concept currently receiving much attention in several laboratories is the electron ring accelerator (ERA) (Reference 4.4). The Dubna Laboratory has reported acceleration of nitrogen ions to about 60 MeV by controlled expansion of a compressed and ion-loaded ring.

A relatively small effort has been directed toward studying collective acceleration of ions by intense relativistic electron beams in linear geometry. This simple technique involves injecting a beam into a drift chamber filled with a neutral gas at low

---

\* Much of the material of this section has been reported in References 4.1 and 4.2.

pressures; the electron beam ionizes the gas and bunches and accelerates the ions. The process was discovered by Graybill and Uglum at Ion Physics Corporation (Reference 4.5) and verified and further studied at Physics International Company by Rander, et al. (References 4.6 and 4.7). To date, ions with an energy up to 8 MeV/Z, Z being the charge state of the ions, have been reported for several ion species. (A  $+14$  is the highest charge state observed--(Reference 4.8).) Minimum average accelerating fields of  $10^5$  V/cm have been experimentally demonstrated. Although several models have been advanced to explain these results (References 4.1, 4.9, 4.10 and 4.11) the acceleration process is at present essentially unconfirmed. The process is therefore probably not optimized from the viewpoints of either efficiency or ion energy. Even so, the experimental data have already established the utility of this ~~mode~~ as a highly-stripped ion source and as an ion source ~~for~~ plasma heating. If the acceleration cutoff ~~process~~ can be identified and the acceleration length ~~extended~~, the technique can be used to directly accelerate heavy ions to GeV energies.

An important use of the acceleration process would perhaps be in the area of plasma heating where more than adequate deuteron energies (2 to 5 MeV) have been attained. The emphasis of further research here should be directed to increasing the ion number/beam pulse, or the efficiency. Reported (energy) efficiencies range from 0.25 to a few percent and, if one extrapolates present data to larger current (5 to 10 MA) electron beam machines presently under development, several kilojoules of deuteron energy/beam pulse can be anticipated. Such a deuteron pulse could be injected into a dense plasma focus, for example, where a  $10^{19}$  to  $10^{20}/\text{cm}^3$  density plasma passes through the focus field for 50 to 100 nsec.\* Without appealing to anomalous range shortening effects, 2-MeV

---

\* See Section 2.11.

deuterons would deposit all of their energy in the small focal plasma volume ( $\sim 10^{-2} \text{ cm}^3$ ), effecting perhaps an order of magnitude increase in ion temperature and a concomitant  $10^3$  increase in thermonuclear D-T burn rate. In short, the narrow ion pulse width ( $\sim 10$  to  $20$  nsec) and the large ion flux make the ions an interesting energy source for heating high-density, high  $\beta$  plasmas. These plasmas would at least provide an intense 14-MeV neutron and kilovolt X-ray source. The deuterons could also be focussed geometrically on a thick tritiated target to directly produce a 14 MeV neutron source ( $\sim 10^{12}$  to  $10^{14}$  neutrons).

The use of heavy ions (nitrogen, neon, argon) of several hundred MeV/nucleon for medical applications (cancer therapy) is currently of great interest in the bio-medical community. One such proposal, the BEVALAC, which is now under study at the Lawrence Berkeley Laboratory in Berkeley, California, would use the Bevatron to accelerate heavy ions (Reference 4.12). Here, as in all heavy ion accelerators, the ion source is perhaps the limiting factor on beam intensity. A linear electron-beam ion source, using demonstrated experimental data, could provide  $10^{13}$  stripped nitrogen ions/electron pulse with  $\sim 2$  MeV/nucleon for injection into a linear accelerator stage. An important aspect of the experimental charge-state distribution for both nitrogen and argon is that the charge state peaks toward more highly stripped states, in contrast to conventional ion sources.

The potential of the acceleration technique for higher energy heavy ions (or protons) is not as clear at this point. Although the energies achieved for  $\text{N}^{+6}$  ( $\sim 30$  MeV) and Ar (mean energy  $\sim 25$  MeV) are within a factor of two or less of ERA results, the extension of heavy ion acceleration to higher energies rests upon obtaining an understanding of the acceleration cutoff mechanism. Several possible cutoff mechanisms have been suggested (Reference 4.2) and present data are encouraging. We

can also cite two features of the accelerating process which are encouraging independently of the details of the accelerating mechanism: (1) the data indicate that the full beam pulse width is not used for ion acceleration--ions are accelerated and the process cuts off rather abruptly--and (2) the electron-beam streaming velocity limit on ion velocity should allow GeV or higher heavy ion energies.

Other techniques for collective ion acceleration have been suggested by various authors, such as ion drag acceleration using high-density electron bunches, impact acceleration of plasmoids, and ion trapping in traveling magnetic mirrors. The reader is referred to the review articles of Sessler (Reference 4.13) and Rabinovich (Reference 4.14) for a discussion of these proposals.

We discuss the experimental results for low-pressure neutral-gas ion acceleration, some proposed acceleration models, and suggest a model which agrees with presently established features of experimental data.

#### 4.1 EXPERIMENTAL RESULTS

An electron beam is injected through a thin metallic anode window into a right-conducting cylindrical cavity with a small hole in the center at the downstream end (see Figure 4.1). The beam and ions pass through the hole into a magnetic field where the beam and ions are separated; the ions are then diagnosed with time-of-flight, magnetic-spectroscopy, and nuclear-emulsion techniques. Various neutral gases at controlled pressures (10 to 200 microns) are ionized by the beam.

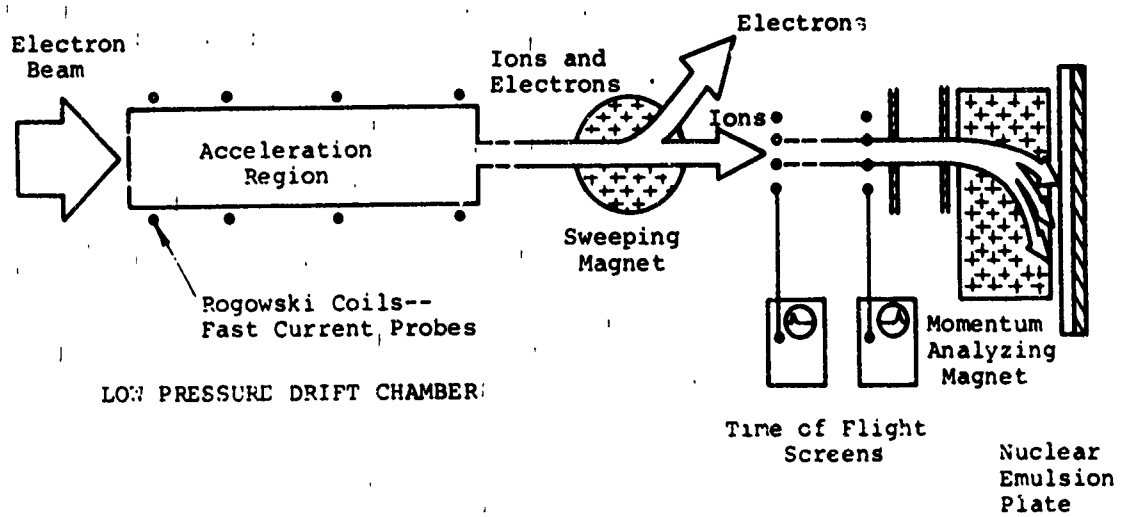


Figure 4.1 Schematic of linear beam experiment

For reference, a summary of the experimental data from the experimental groups of Graybill and Uglum at Ion Physics Corporation (IP) (Reference 4.5) and Rander at Physics International Company (PI) (References 4.6 and 4.7) is given below. We assume that the data refer to the same accelerating process although there are differences in the nature of the beam front propagation:

1. The peak ion energies are proportional to  $Z$ , the ion charge number, as would be the case if ions were accelerated by a stationary electrostatic field. The particle energy per unit charge is proportional to  $I^2$ , where  $I$  is the beam current. The experimental uncertainties allow a current dependence from  $I^{3/2}$  to  $I^{5/2}$ .

2. The ion energy is nearly independent of filling gas pressure over a range of a factor of 6 in pressure. The proton pressure range for IP is from about 50 to 200  $\mu\text{m}$ . Graybill has recently reported a pressure dependence for hydrogen and deuterium (Reference 4.15).

3. The ion pulses are formed and accelerated after the fractional electrical neutralization.

$$f_e \equiv (-) \frac{\text{ion charge density}}{\text{electron charge density}}$$

becomes greater than  $1/\gamma^2 = 1 - \beta_e^2$ , where  $\gamma$  is the electron energy,  $E/m_0 c^2$ . The condition for radial force neutralization and the onset of beam pinching is  $f_e \sim 1/\gamma^2$ .

4. The proton energy spread (full width at half-maximum) is  $< 20$  percent, the limit of the spectrometer resolution. This energy spread for PI covers two proton pulses.

5. The total number of accelerated ions per ion pulse is in the range of  $10^{12}$  to  $10^{15}$  particles. The ion pulse widths range from 3 nsec for protons and 5 nsec for deuterons, to about 10 nsec for helium and nitrogen.

6. Multiple ion pulses (two) have been reported by Rander et al. This feature can be accounted for by approximately twice as long beam pulse width for the PI beam as compared to the IP beam. The pulse separation is inversely proportional to the filling gas pressure for  $H_2$ . The pressure dependence of the pulse separation is shown in Figure 4.2 (Reference 4.16).

7. The first ion pulse may be moving with the beam front (Reference 4.15) or behind the beam front (Reference 4.13). The different behavior of the beam front propagation with respect to the first ion pulse is most likely due to the higher  $v/\gamma$  of the PI beam. The IP beams were typically  $v/\gamma \sim 0.8$ , whereas PI beams were  $v/\gamma \sim 2$ .

The data summary above pertains to ions accelerated by intense relativistic electron beams in neutral-gas-filled drift chambers. Sessler (Reference 4.13) has pointed out the data similarity to the ion acceleration results of Plyutto, et al. (References 4.17 and 4.18), who observed ions of various species in the few MeV range from a vacuum diode with a gap potential of 200 to 300 keV. The similar features of Plyutto's data are:

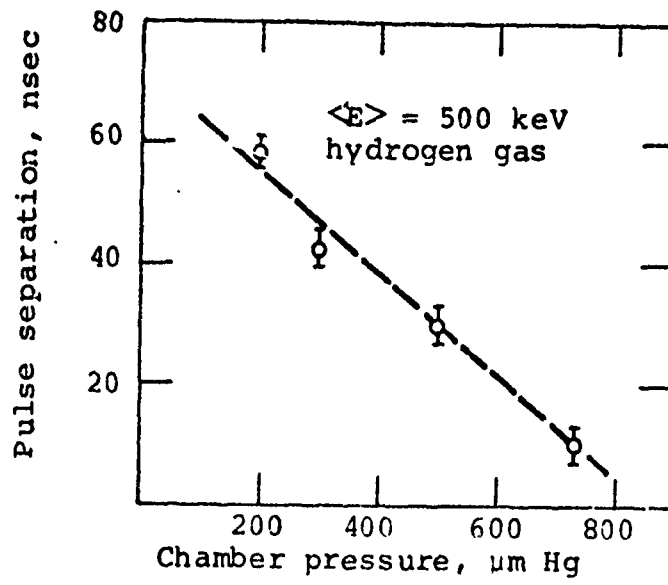


Figure 4.2 Proton pulse separation versus pressure

1. Ions are accelerated in the direction of electron flow, in opposition to the applied field
2. Multiple bursts or pulses of ions
3. Beam pinches when ions are accelerated
4. Same order of magnitude of current density  $\sim 10^4$  A/cm<sup>2</sup>
5. Approximately the same ion energies and number of ions/burst

#### 4.2 SOME SUGGESTED ACCELERATION MODELS

4.2.1 Inverse Cerenkov Radiation. Wachtel and Eastlund (Reference 4.11) have suggested that the "inverse Cerenkov radiation" acceleration mechanism first proposed by Veksler (Reference 4.3) may be responsible for the energetic ion production. Veksler's formula for the average accelerating electric field seen by a bunch of ions of charge number  $N$  in an electron beam plasma is

$$E = \frac{eN\omega_p^2}{v_b^2} F \ln \left( \frac{v_b}{D \omega_p} \right) \quad (4.1)$$

where  $\omega_p^2 = \frac{4\pi n_b e^2}{m_0}$  is the beam plasma frequency (non-relativistic)

$v_b$  = electron longitudinal velocity

$n_b$  = beam electron density

$m_0$  = electron mass

- F = a form factor of order unity for bunch dimensions which are small compared to the resonant plasma oscillation wavelength,  $2\pi v_b/\omega_0$
- D = the Debye length of the electron beam plasma.

The theory requires that the bunch dimensions be small compared to  $2\pi v_b/\omega_p$ , and that the ion bunch perturbation of the beam be small. Thus, for typical beam plasma frequencies of  $10^{11}$  to  $10^{12}$ /sec, the bunch dimensions must be in the millimeter range, and to obtain interesting accelerating fields we would want the bunch number for protons, e.g., to be  $10^{12}$  or more. These requirements are formidable indeed, as was recognized by Veksler.

Equation (4.1) may be derived quite simply by transforming to the beam frame and applying the usual "dE/dx" energy-loss formula for a test particle (the ion bunch) in a plasma (Reference 4.19) for the case where the test particle velocity is much greater than the thermal velocity of the plasma particles.

We present a somewhat different approach to the problem of determining maximum energies attainable by ions in a beam plasma resulting from the electric fields associated with the resonant plasma waves. Though relatively crude, the work does allow a definition of the upper limit and avoids complications of extending a test particle calculation to the resultant ion beam, which we have in the frame where the beam electrons are at rest.

The electrostatic instability calculations of Bludman, Watson, and Rosenbluth (Reference 4.20) are applicable to the situation of practical interest here; namely, to an electron beam traveling through a plasma containing either secondary

electrons and ions or simply ions alone. We obtain the high-frequency instability growth rates and wavelengths from the theory:

$$\begin{aligned} \text{Im } (\omega) &\approx 0.69 (\omega_t \omega_i^2)^{1/3} && \text{(ion plasma)} \\ \text{Im } (\omega) &\approx 0.69 (\omega_t^2 \omega_p)^{1/3} && \text{(electron-ion plasma in collisionless limit)} \end{aligned} \quad (4.2)$$

$$\begin{aligned} \lambda_{\text{instability}} &\approx \frac{2\pi v_b}{\omega_i} && \text{(ion plasma)} \\ &\approx \frac{2\pi v_b}{\omega_p} && \text{(electron-ion plasma)} \end{aligned} \quad (4.3)$$

where  $\text{Im } (\omega)$  is the e-folding rate, and

$$\omega_p^2 \approx \frac{4\pi n_p e^2}{m_o}$$

$$\omega_t^2 = \frac{4\pi n_b e^2}{\gamma m_o}$$

$$\omega_i^2 = \frac{4\pi n_i z_i^2 e^2}{m_i}$$

$n_b$  = beam particle density

$n_i$  = ion particle density

$n_{pe}$  = secondary electron density

$\lambda$  = the wavelength of the fastest growing instability oscillation

$m_0$  = electron rest mass

$m_i$  = ion rest mass

$\gamma$  = the relativistic factor for beam electrons.

In the ion experiments where the beam ionizes the gas, the plasma is first an ion plasma until  $f_e$  is approximately 1, and then the secondary electron density builds up and the plasma effectively becomes an electron-ion plasma. Let us optimistically estimate the growth time for an ion plasma.\* With  $I = 50$  kA, beam radius,  $a$ , = 1 cm,  $v_b = 0.7c$ ,  $f_e = 1$ , and  $Z_i = 1$ , we obtain

$$\omega_t \approx 7.1 \times 10^{10} \text{ rad/sec}$$

$$\omega_i = 2.8 \times 10^9 \text{ rad/sec}$$

$$\text{Im}(\omega) = 2.8 \times 10^9 / \text{sec (ion plasma)}$$

$$\lambda \approx 47 \text{ cm (approximately the experimental chamber length)}$$

---

\*We assume that Landau damping of the oscillations is negligible.

If, on the other hand, we consider later times after gas breakdown, and take  $n_{pe} \approx 10 n_b$ ,

$$\omega_{pe} = 4 \times 10^{11} \text{ rad/sec}$$

$$\text{Im}(\omega) = 8.7 \times 10^{10} / \text{sec},$$

and  $\lambda \approx 0.3 \text{ cm}$

The equation of motion for an ion in the  $E_z$  field associated with the charge density modulation of the instability oscillation is

$$\ddot{z} = \frac{d^2 z}{dt^2} = \frac{Ze}{m_i} \Delta E_z \cos(kz - \omega t), \quad (4.4)$$

$\Delta E_z$  is the amplitude,

and the kinetic energy (non-relativistically) is

$$\text{K.E.} = \frac{1}{2} m_i (\dot{z})^2 \quad (4.5)$$

If we take  $z = \dot{z} = 0$  at  $t = 0$ , the solution of Equation (4.4) for  $z$  gives

$$\text{K.E.} = \frac{m_i}{2k^2} \left[ \omega - \sqrt{\omega^2 + \frac{2Zek}{m_i} \Delta E_z \sin(kz - \omega t)} \right]^2, \quad \omega^2 > 2Ze \frac{\Delta E_z k}{m_i} \quad (4.6)$$

If  $\omega^2 < 2 \frac{Ze \Delta E_z k}{m_i}$ , the ion is trapped in the wave, and

$$(kz - \omega t) < \sin^{-1} \left( - \frac{\omega^2 m_i}{2Ze\Delta E_z k} \right) \quad (4.7)$$

and the maximum K.E. =  $\frac{m_i \omega^2}{2k^2} \approx \frac{m_i}{2} v_b^2$ , which is outside the non-relativistic approximation. We now estimate an upper limit for  $\Delta E_z$ . Assuming the electron beam kinetic energy to be 1 MeV

$$\begin{aligned} \Delta E_z &\approx 10^6 / (\lambda/4) \\ &\approx 8.5 \times 10^4 \text{ V/cm for ion plasma} \\ &\approx 1.0 \times 10^7 \text{ V/cm for electron-ion plasma} \end{aligned}$$

Now 
$$\frac{2Ze\Delta E_z k}{m_i} = \frac{1}{\lambda^2} (4.8) \times 10^{19} \text{ for protons}$$

$$\omega^2 = \frac{1}{\lambda^2} (1.7) \times 10^{22}$$

Thus, in neither case are the protons trapped, as, of course, one would expect since the fields are not high enough to accelerate the protons to  $\beta = 0.7$  in a wavelength. Returning to Equation (4.6), we can obtain the maximum kinetic energy of the ions

$$\text{K.E. max} = \frac{m_i}{2k^2} \left[ \omega - \sqrt{\omega^2 - \frac{2 Zek \Delta E_z}{m_i}} \right]^2$$

$$\frac{\text{K.E. max}}{m_i c^2} = 1.1 \times 10^{-6} \beta_L^2$$

$$\approx 5 \times 10^{-7}$$

For protons the maximum kinetic energy is about 500 V--very small indeed.

We therefore rule out the electrostatic instability fields as the mechanism responsible for the observed 5-MeV proton energies. In any case, an experimental check could be made by injecting the electron beam into a pre-ionized plasma, a condition which would not give rise to ion acceleration in the other models. Then the plasma would exist over the entire beam pulse. Also, one would expect a relatively broad ion energy spectrum from a drift chamber comparable in length to the beam pulse length.

#### 4.2.2 Accelerated Space Charge Potential Well Models.

Rostoker (Reference 4.9) has proposed that ions are accelerated by the moving space-charge potential well associated with the beam front as it moves across the drift chamber, ionizing the neutral gas behind it. Uglum, McNeil, and Graybill (Reference 4.10) have independently suggested essentially the same mechanism with somewhat different assumptions about the beam configuration at the start of the acceleration process and the mechanism of well acceleration. Both theories consider only longitudinal electric fields and one-dimensional beam motion.

In our discussion of low pressure beam propagation (Section 2.10.1) we derived an approximate expression for the distance from the anode,  $\bar{z}_c$ , which an unneutralized beam could propagate:

$$\bar{z}_c \text{ (cm)} \approx \frac{3.4 \times 10^4}{I_b^P \text{ (amps)}} \left( \frac{t_r}{t_v} \right) \frac{\sqrt{1+V^P} \sqrt{V^P}}{1 + 2V^P} \quad (4.8)$$

$$\cdot R/2.4 \frac{1}{1/2 + \ln R/a} , \quad \bar{z}_c \lesssim 2 \text{ (R/2.4)}$$

where

- $t_r$  = the current rise time
- $t_v$  = the electron kinetic energy rise time
- $I_b^p$  = the peak beam current
- $V^p$  = the peak electron kinetic energy in MeV
- $a$  = beam radius
- $R$  = chamber radius

The voltage and current rises were assumed linear in deriving Equation (4.8), and the electrostatic potential (retarding beam electrons) at  $\bar{z}_c$  is equal to the beam kinetic energy. If  $I_b^p = 30$  kA,  $t_r/t_v = 2$ ,  $V^p = 1$  MeV,  $R = 6$  cm, and  $a = 1$  cm,  $\bar{z}_c = 1.2$  cm. Beam electrons are thus reflected back to the anode by the virtual cathode at  $\bar{z}_c$ , and the beam envelope "blows up" radially.

As the beam "hovers" near the conducting plate, the background gas is ionized by collisions and electron avalanche over a time scale  $\tau_N$ . The ions short out the electrostatic field and the beam moves forward. If no ions are created in front of the beam by electrons that have spilled out of the potential well (typically a few kiloamperes) or by radiative ionization, the velocity of the front,  $\beta_f^{ES} c \equiv v_p$ , is approximately  $\bar{z}_c/\tau_N$  and would remain constant, barring substantial changes in the beam energy. The kinetic energy of ions trapped in the advancing front can be estimated from

$$\text{K.E.} \approx \frac{m_i}{2} v_p^2 \approx \frac{m_i}{2} \left( \frac{\bar{z}_c}{\tau_N} \right)^2 \quad (4.9)$$

and if  $\bar{z}_c \approx 1$  cm,  $\tau_N \approx 10$  nsec, protons would achieve the rather uninteresting energy of 50 keV. The maximum energy that protons could attain by a sudden acceleration to a constant beam front velocity would be 1 MeV, corresponding to  $\tau_N \approx 2$  nsec.

We therefore realize that to attain ion energies in excess of the beam energy, ions must be trapped in an accelerating potential well, or, in other words,  $\tau_N$  must decrease in time. Moreover, to obtain ion energies which depend only on the  $Z$  of the ions, the acceleration must be "just right." Let us inquire how  $\tau_N$  must change with time. If

$$v_p \approx \bar{z}_c / \tau_N(t) \quad (4.10)$$

then

$$\frac{dv_p}{dt} = \dot{v}_p \approx \frac{\bar{z}_c}{\tau_N} \left( -\frac{1}{\tau_N} \frac{d\tau_N}{dt} \right) = v_p \left( -\frac{1}{\tau_N} \frac{d\tau_N}{dt} \right) \quad (4.11)$$

Ions will spill out of the well if

$$\dot{v}_p > \dot{v}_{pc} \equiv \frac{ZeE_0}{m_i}, \quad (4.12)$$

where  $E_0$  is the electrostatic field at the ionization front  $\approx 10^6$  V/cm in our example, since the electric field will no longer be strong enough to accelerate ions at the same rate as the beam front. Substituting Equations (4.11) and (4.12) in Equation (4.9),

$$K.E. \text{ max} = \frac{m_i}{2} (v_{pc})^2 = \frac{m_i}{2} (\dot{v}_{pc})^2 \left[ \frac{1}{\frac{1}{\tau_N} \frac{d\tau_N}{dt}} \right]_{t=t_c}^2$$

where  $t_c$  is the time of spillout. Thus

$$K.E. \text{ max} = \frac{z^2}{2m_i} E_0^2 e^2 \left[ \frac{1}{\frac{1}{\tau_N} \frac{d\tau_N}{dt}} \right]_{t=t_c}^2 \quad (4.13)$$

The bracketed term in Equation (4.13) must therefore be  $\propto \sqrt{m_i/Z}$  to have energy dependence only on the  $Z$  of the ion. Another way of expressing this requirement is

$$\dot{v}_{pc} \propto \frac{Z}{m_i} \propto (v_{pc})^2 \quad (4.14)$$

and a way of satisfying Equation (4.14) is to take  $\dot{v}_p \propto v_p^2$  which requires

$$v = \frac{1}{B-At} \approx \frac{z_c}{\tau_N(t)} \quad (4.15)$$

where  $A$  and  $B$  are constants. Then

$$\tau_N \propto B - At \quad (4.16)$$

a not unreasonable form, which is precisely the one proposed by Rostoker. In fact he argues that

$$A = + \frac{n_b^*}{n_b} \quad (4.17)$$

$$B = \tau_e + \tau_I \left( 1 + \frac{n_b^*}{n_b} \right)$$

where  $n_b^*$  is the ion density ahead of the beam front  
 $n_b$  is the beam density  
 $\tau_e$  is the time required for the electrons to escape from the pre-ionized (neutral) region as the beam front advances, [this time is negligible compared to  $\tau_I (1 + n_b^*/n_b)$ ],

and  $\tau_I$  is  $\tau_N$  at  $t = 0$ .

Using Equation (4.17), Rostoker obtains,

$$\text{K.E.}^{\text{max}} \approx \left( \frac{n_b}{n_b^*} \right) \text{ MeV} \tag{4.18}$$
$$t_c \approx \frac{n_b}{n_b^*} \tau_I$$

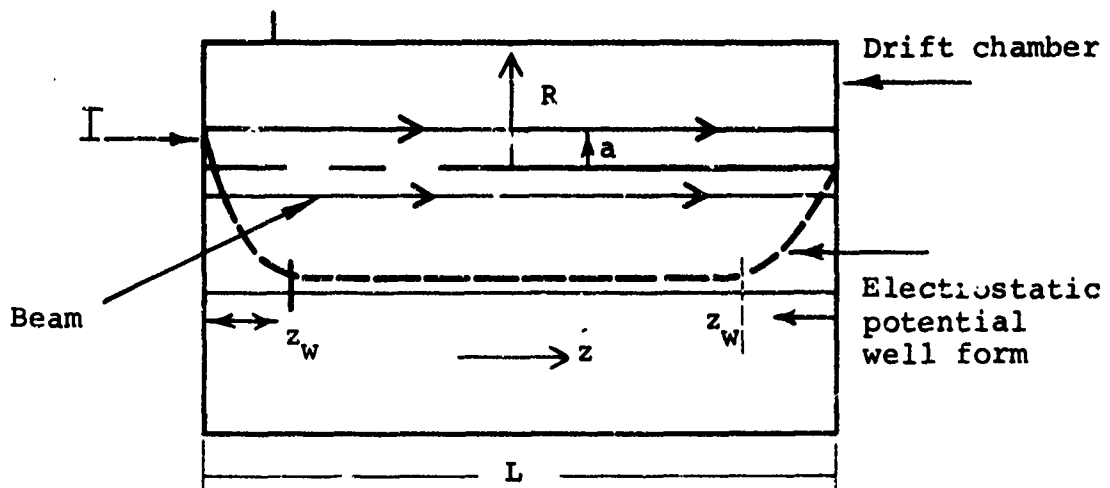
and takes  $n_b/n_b^* = 5$  to obtain agreement with the observed proton energies. However, the assumed ratio of  $n_b/n_b^*$  gives  $t_c = 50$  nsec, which is not in agreement with the data when one uses the acceleration length of 9 cm which follows from the theory.<sup>†</sup> If we assume a smaller ratio  $n_b/n_b^*$  to be more in line with the timing data, we, of course, lower the energy. Estimating  $n_b/n_b^*$ , which is the only parameter entering into the kinetic energy formula, is very difficult a priori. To illustrate the point, one could perhaps argue equally well that  $n_b^*/n_b = 0$ , since radiative ionization is much too slow, even with radiation intensities comparable to those generated when the beam is stopped in the anode. Moreover, as electrons in the region of the well are decelerated and the charge density increases, the beam "blows up" radially over distances comparable to the beam radius. This radial blowup would imply that the front is very sharp and that a significant number of electrons do not precede the front to pre-ionize and decrease  $\tau_N$ .

Ion acceleration in Rostoker's model cuts off because the well acceleration reaches a value such that the electric field is no longer high enough to trap the ions (Equation 4.12). We thus would expect to see a continuously accelerated beam front up to a velocity determined by the electron beam energy (and transverse energy). Moreover, the ion bunch should be very narrow (< 1 cm), although space-charge effects after ion separation from the electron beam could widen the ion bunch, as suggested by Rostoker.

<sup>†</sup>See References 4.5 and 4.10.

Uglum, McNeill and Graybill (UMG) also consider an accelerated-charge potential well, but they assume that the process starts when  $f_e = 1/\gamma^2$ , the condition for radial force neutralization, in accordance with the data, and calculate the electrostatic field for a uniform charge density beam in a right cylindrical cavity. With  $R = 10$  cm,  $I = 5 \times 10^4$  A,  $a = 1$ , they obtain  $E_z \sim 2.5 \times 10^5$  V/cm for  $0 \leq z \leq z_w \cong 5$  cm (see Figure 4.3). However, the potential well depth is then of the order of the beam kinetic energy and the beam would be stopped and be blown up radially. Nevertheless, if the field is assumed to be approximately the same as for  $z \leq z_w$ , the well will move with increasing background ionization, as discussed in the Rostoker model. UMG suggest well acceleration due to gas breakdown and obtain a breakdown time  $t_B$  from extrapolation of the data of Felsenthal and Proud (Reference 4.21). In the opinion of the author, however, they do not argue well acceleration, but a constant velocity well moving with velocity  $\approx \bar{z}_c/t_B$ . One could perhaps argue an acceleration by invoking preionization by the beam ahead of the breakdown front to decrease the effective breakdown time. Also, since the well shorts out over the electrical neutralization time, it would seem that their well velocity is too slow ( $\tau_N < t_B$ ).

In summary, the accelerated-electrostatic space-charge potential-well models can account for the observed ion energies. It is not clear at this time if a more careful and detailed coupled longitudinal-field and beam-motion calculation in the spirit of these models could explain such features of the data such as the current dependence of the ion energy and multiple pulses. We proceed to a different model that offers detailed agreement with experimental data.



$L$  = chamber length

$z_w$  = distance from endplate over which the potential reaches its maximum value

$a$  = beam radius

$R$  = radius of outer conducting walls

Figure 4.3 The beam profile at the start of ion acceleration in the UMG model.

### 4.3 THE LOCALIZED PINCH MODEL

Recently this author has proposed a different ion-acceleration model, the localized pinch model (LPM) (References 4.1 and 4.2). This model features a self-synchronized mechanism to keep the accelerating fields in place with the accelerated ions. Moreover, it is not necessary to invoke pre-ionization in front of the effective beam front, i.e., the acceleration can occur behind or with the beam front, or more precisely, slightly behind the beam front. The following aspects of the acceleration process will be addressed in the LPM:

1. The accelerating mechanism-generation of accelerating fields, synchronization, and bunch stability
2. Ion bunch formation
3. Acceleration cutoff

4.3.1 The Acceleration Mechanism. We first consider an idealized situation to illustrate the physics of the mechanism. Consider Figure 4.4 where we have a beam traveling in a long conducting tube (no endplate effects) with constant radius and charge density. Within the beam envelope we postulate a uniform background ion density such that  $f_e = f_e^0 < 1$ , except within region 1 where we imagine that a slug of ions have been injected at  $t = 0$ , giving a higher ion charge/length,  $\lambda_1 = \lambda_{i0} + \Delta\lambda_i$ .

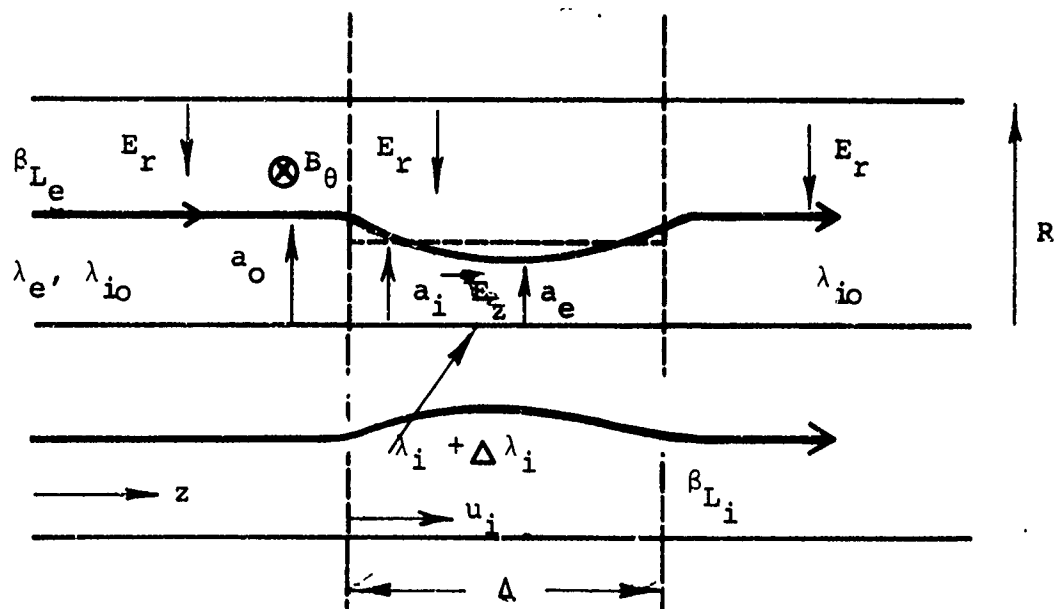


Figure 4.4 The localized pinch acceleration model.

$\beta_{Le}$  = longitudinal  $\beta$  of primary electrons upstream from the ion slug

$\beta_{Li}$  = longitudinal  $\beta$  of ions

$\Delta$  = length of moving ion slug

$I_p$  = primary electron current\*

$a_0$  = radius of beam entering the region (1)

$a_i$  = radius of ion slug

$B_\theta$  = theta component of magnetic field

$E_r$  = radial electric field

$\lambda_{io}$  = background ion charge/length

$\Delta\lambda_i$  = increment in ion charge/length in region (1)

Upstream from the ion "slug" in region 1, the electron beam radius,  $a_o$ , is determined by the electron and ion emittances. In Section 2.7.1, Equation (2.79), we obtained expressions for  $a_o$  and  $f_e^o$  from the Kapchinskij-Vladimirskij (Reference 4.22) equation:

$$a_o^2 = \frac{\gamma}{2v} \left( \frac{1}{1-1/\gamma_L^2} \right) (C_e \gamma m_o + C_i m_i/Z), (v/\gamma < 1) \quad (4.19)$$

$$f_e^o = \frac{1}{\gamma_L^2} + \left( 1 - \frac{1}{\gamma_L^2} \right) \left( \frac{C_e \gamma m_o}{C_i m_i/Z + C_e \gamma m_o} \right)$$

where

$$C_e \equiv \epsilon_e^2 \beta_{L_e}^2 c^2$$

$$C_i \equiv \epsilon_i^2 \beta_{L_i}^2 c^2$$

$$Z = \text{ion charge state}$$

$$m_i = \text{ion mass}$$

$$\epsilon_j = \text{the electron and ion emittances}$$

In region 1 where  $\lambda_i > \lambda_{io}$ , the beam radius will not be equal to the ion radius. Therefore, we really cannot apply the K&V equation since the radial force for beam and/or ion particles is no longer linear in displacement from the axis. Nevertheless we shall use the K&V equations in order to obtain an estimate of new equilibrium radii. Straightforward algebraic manipulation of the K&V equations for electrons and ions gives

$$\begin{aligned}
(a_{e1})^2 = & a_o^2 \left\{ \left[ \frac{(1-f_e^o)}{\gamma_L^2} \frac{-\lambda_e}{\lambda_{io} + \Delta\lambda_i} + \left( f_e^o - \frac{1}{\gamma_L^2} \right) \right] \frac{1}{2 \left( 1 - \frac{1}{\gamma_L^2} \right)} \right. \\
& + \frac{1}{2 \left( 1 - \frac{1}{\gamma_L^2} \right)} \left[ \left( \frac{1-f_e^o}{\gamma_L^2} \left( \frac{-\lambda_e}{\lambda_{io} + \Delta\lambda_i} \right) + f_e^o - \frac{1}{\gamma_L^2} \right)^2 \right. \\
& \left. \left. + 4 \left( 1 - \frac{1}{\gamma_L^2} \right) \left( f_e^o - \frac{1}{\gamma_L^2} \right) (1-f_e^o) \frac{-\lambda_e}{\lambda_{io} + \Delta\lambda_i} \right]^{\frac{1}{2}} \right\} \quad (4.20)
\end{aligned}$$

where  $a_{e1}$  is the electron beam equilibrium radius in region (1), assuming  $\Delta$  is large enough for achievement of equilibrium. Similarly, the ion radius in region (1),  $a_{i1}$ , is given by

$$(a_{i1})^2 = a_o^2 (1-f_e^o)^2 + \left( \frac{\lambda_i + \Delta\lambda_i}{|\lambda_e|} \right) (a_{e1})^2 \quad (4.21)$$

Let us now assume  $C_e \approx 0$ , then  $f_e^o \approx (1/\gamma_L^2)$  from Equation (4.19). Equations (4.20) and (4.21) give

$$a_{e1} \approx \frac{a_o}{\gamma_L} \left( \frac{|\lambda_e|}{\lambda_{io} + \Delta\lambda_i} \right)^{\frac{1}{2}} \quad (4.22)$$

$$a_{i1} \approx a_o$$

If  $\lambda_{io} + \Delta\lambda_i = \lambda_e$ ,  $a_{e1} \approx (a_o/\gamma_L)$ , or, in other words an increase in the ion charge/length to give equal charges/length for ions and electrons in region (1) reduces the beam radius by a factor  $(1/\gamma_L)$ , with the result that

$$f_e^1 = \frac{\lambda_{i0} + \Delta\lambda_i}{|\lambda_e|} \left( \frac{a_{e1}}{a_{i1}} \right)^2 \approx f_e^0$$

Let us now consider the beam envelope motion dynamically. When the beam electrons stream into region (1), the higher ion charge/length shorts out the radial electric field, causing the beam radius to collapse. The radial motion generates an  $E_z$  field, the magnitude of which we now estimate. We assume below that  $\lambda_e$  is constant,  $\Delta\lambda_i$  constant within region (1),  $a_i = a_0 = \text{constant}$ , and  $(\partial\beta_{Le}/\partial z) \approx 0$  in region (1). The  $E_z$  field along the axis generated by the beam radial collapse,  $E_z^1$ , is

$$E_z^1 \approx 2 \frac{\beta_{Le} \lambda_e}{c a_e} \frac{\partial a_e}{\partial t} + \frac{2\lambda_e}{a_e} \frac{\partial a_e}{\partial z} \quad (4.23)$$

in the quasi-static, paraxial approximation.

Transforming Equation (4.23) to the ion rest frame gives (non-relativistically),

$$E_z^1 = - \frac{2\beta_{Le} \beta_{Li}}{a_e} \lambda_e \frac{\partial a_e}{\partial u_i} + \frac{2\lambda_e}{a_e} \frac{\partial a_e}{\partial u_i}, \quad u_i > 0$$

with  $u_i = z_i - \beta_{Li} ct$ . If  $\beta_{Li}$  or  $\beta_{Le} \ll 1$ ,

$$E_z^1 \approx \frac{2\lambda_e}{a_e} \frac{\partial a_e}{\partial u_i}, \quad u_i > 0 \quad (4.24)$$

We use the K&V equation (Equation 2.73) to estimate  $\partial a_e / \partial u_i$  in region (1), assuming that  $a_i \approx a_0$ ,

$$\frac{\partial^2 a_e}{\partial z^2} \approx \frac{\partial^2 a_e}{\partial u_i^2} \approx \frac{2v}{\gamma \beta_{L_e}^2} \left( 1 - f_e - \beta_{L_e}^2 \right) \frac{1}{a_e} + \frac{C_e}{\beta_{L_e}^2 c^2 a_e^3} \quad (4.25)$$

or

$$\begin{aligned} \frac{\partial^2 a_e}{\partial u_i^2} &= - \frac{2v}{\gamma \beta_{L_e}^2} \left[ f_e^o \left( \frac{a_e}{a_0} \right)^2 + \left( \frac{a_e}{a_0} \right)^2 \frac{\Delta \lambda_i}{|\lambda_e|} - \frac{1}{\gamma_L^2} \right] \frac{1}{a_e} + \frac{C_e}{\beta_{L_e}^2 c^2 a_e^3} \\ &= - \frac{2v}{\gamma \beta_{L_e}^2} \left[ \left( f_e^o + \frac{\Delta \lambda_i}{|\lambda_e|} \right) \frac{a_e}{a_0^2} - \frac{1}{\gamma_L^2 a_e} \right] + \frac{C_e}{\beta_{L_e}^2 c^2 a_e^3}, \quad \left( \frac{v}{\gamma} \lesssim 1 \right) \end{aligned} \quad (4.26)$$

A first integral of Equation (4.26) can be obtained analytically:

$$\left( \frac{\partial a_e}{\partial u_i} \right)^2 = K_1 \left[ a_0^2 - a_e^2 + \frac{2K_2}{K_1} \ln \frac{a_e}{a_0} - \frac{K_3}{K_1} \left( \frac{1}{a_e^2} - \frac{1}{a_0^2} \right) \right] \quad (4.27)$$

$$K_1 \equiv \frac{2v}{\gamma \beta_{L_e}^2} \left( f_e^o + \frac{\Delta \lambda_i}{|\lambda_e|} \right) \frac{1}{a_0^2}$$

$$K_2 \equiv \frac{2v}{\gamma \beta_{L_e}^2 \gamma_L^2}$$

$$K_3 \equiv \frac{c_e}{\beta_{L_e}^2 c^2}$$

Equation (4.27) can be written in dimensionless form by defining

$$s = (a_e/a_0), \quad x = u_i \sqrt{K_1}:$$

$$\left(\frac{ds}{dx}\right)^2 = 1 - s^2 + P \ln s^2 - Q \left(\frac{1}{s^2} - 1\right), \quad (4.28)$$

with

$$P \equiv \frac{1}{\gamma_L^2 \left(f_e^0 + \frac{\Delta \lambda_e}{|\lambda_e|}\right)}$$

$$Q \equiv \frac{\left(f_e^0 - \frac{1}{\gamma_L^2}\right)}{f_e^0 + \frac{\Delta \lambda_i}{|\lambda|}}$$

The dimensionless turning radius for the beam envelope,  $s_t$ , defined by

$$\left(\frac{ds}{dx}\right)_{s=s_t} = 0, \text{ can be estimated from Equation (4.28):}$$

$$\begin{aligned} s_t &\approx \sqrt{Q}, \quad \sqrt{Q} \gg e^{-1/2P}, \quad P < 1 \\ &\approx e^{-1/2P}, \quad \sqrt{Q} \ll e^{-1/2P} \end{aligned} \quad (4.29)$$

Let us now determine  $a_{e_t}$  from Equation (4.29) with  $Q \approx 0$ ,  $\gamma_L^2 = 9$ ,

$$\frac{\Delta\lambda_i}{|\lambda_e|} \approx 1 - \frac{1}{\gamma_L^2}, \quad f_e^o \approx \frac{1}{\gamma_L^2},$$

$$\begin{aligned} a_{e_t} = s_t a_o &\approx a_o e^{-\frac{\gamma_L^2}{2} \left( f_e^o + \frac{\Delta\lambda_i}{|\lambda_e|} \right)} \\ &\approx \frac{a_o}{100} \end{aligned}$$

which is a small radius indeed!

Equation (4.28) allows us to obtain an estimate of the turning length,  $x_t$ , by taking  $a_{e_t} \approx 0$ ,  $P \approx Q \approx 0$ ,

$$x_t \approx \int_0^1 \frac{dw}{\sqrt{1-w^2}} \approx \frac{\pi}{2}$$

or

$$u_{i_t} \approx \frac{\pi}{2} \frac{1}{\sqrt{K_1}} = \frac{a_o \pi}{2} \left[ \frac{2v}{\gamma \beta_L e} \left( f_e^o + \frac{\Delta\lambda_i}{|\lambda_e|} \right) \right]^{-\frac{1}{2}} \quad (4.30)$$

A qualitative sketch of  $a_e(u_i)$  is shown in Figure 4.5.

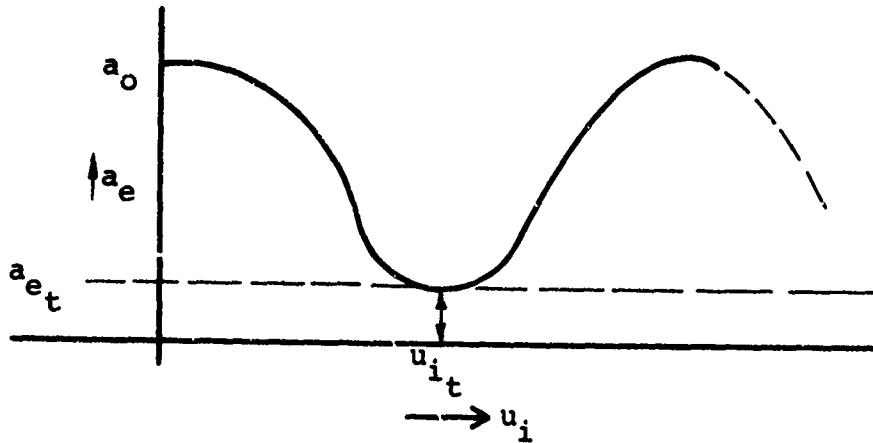


Figure 4.5 Sketch of the beam envelope in region 1.

Let us now examine the implications of the assumption in Equation (4.26) that the ion radius =  $a_0$  = constant. Denoting

$$\left[ \left( f_e^0 + \frac{\Delta\lambda_i}{|\lambda_e|} \right) \left( \frac{a_e}{a_i} \right)^2 - \frac{1}{\gamma_L^2} \right] \frac{1}{a_e}$$

by  $F$ , we see from Equation (4.25) that larger positive  $F$  values correspond to larger inward radial acceleration of the beam envelope.

If

$$\frac{\lambda_{i0} + \Delta\lambda_i}{|\lambda_e|} > \frac{1}{\gamma_L^2} + \frac{Z \gamma m_0 / m_i}{1 + (Z \gamma m_0 / m_i)} \approx \frac{1}{\gamma_L^2}$$

the initial inward radial acceleration for the beam envelope will be greater than that of the ion envelope, so we really need only inquire about the effects of changing ion radius with  $a_i > a_e$ .

When

$$a_i = a_o = \text{const.}, F = \left( f_e^o + \frac{\Delta\lambda_i}{|\lambda_e|} \right) \left( \frac{a_e}{a_o} \right)^2 - \frac{1}{\gamma_L^2 a_e}$$

$$a_i \approx a_e, F = \left( f_e^o + \frac{\Delta\lambda_i}{|\lambda_e|} - \frac{1}{\gamma_L^2} \right) \frac{1}{a_e} > 0,$$

so we see that our calculation gives an estimate of the minimum radial velocity and  $E_z$  field. The maximum radial velocity occurs for  $a_i \approx a_e$ , in which case the dimensionless radial velocity is

$$\left. \begin{aligned} \frac{dp}{dv} &= -p^2 \cdot [\ln p^2 - Q'(p^2 - 1)]^{\frac{1}{2}} \\ \text{where } p &= \frac{a_o}{a_e}, v = \frac{u_1}{a_o} \sqrt{\frac{2v}{\gamma\beta_L} \left( f_e^o + \frac{\Delta\lambda_i}{|\lambda_e|} - \frac{1}{\gamma_L^2} \right)} \end{aligned} \right\} (4.31)$$

$$Q' \equiv \frac{\left( f_e^o - \frac{1}{\gamma_L^2} \right)}{\left( f_e^o + \frac{\Delta\lambda_i}{|\lambda_e|} \right)}$$

The turning radius and length do not appreciably differ from the case  $a_i \approx a_o$  constant.

The  $E_z$  field of Equation (4.24) may now be written as

$$E_z = 2 \lambda_e \sqrt{K_1} \frac{1}{s} \frac{ds}{dx}$$

or

$$\begin{aligned} E_z \text{ (V/cm)} &= - \frac{1.4 \times 10^6}{\beta_{L_e} a_o} \left( \frac{v^{3/2}}{\gamma^{1/2}} \right) \left( f_e^o + \frac{\Delta \lambda_i}{|\lambda_e|} \right)^{1/2} \left( \frac{1}{s} \right) \frac{ds}{dx} \\ &\approx - 1.4 \times 10^6 \left( \frac{v}{\gamma} \right)^{1/2} \frac{v \sqrt{1 + v/\gamma}}{a_o \beta} \left( f_e^o + \frac{\Delta \lambda_i}{|\lambda_e|} \right)^{1/2} \frac{1}{s} \frac{ds}{dx} \end{aligned} \quad (4.32)$$

where we have used

$$\beta_{L_e} \approx \frac{\beta}{\sqrt{1 + v/\gamma}}$$

and

$$\frac{1}{s} \frac{ds}{dx} = \sqrt{\frac{1}{s^2} - 1 + \frac{P}{s^2} \ln s^2 - \frac{Q}{s^2} \left( \frac{1}{s^2} - 1 \right)}$$

An approximate average field,  $\bar{E}_z$ , can be obtained by taking

$$\frac{1}{s} \frac{ds}{dx} \approx - \frac{1}{2} \frac{1}{x_t} \approx - \frac{1}{\pi}$$

giving

$$\bar{E}_z \approx 4.4 \times 10^5 \left( \frac{v}{\gamma} \right)^{1/2} \frac{v \sqrt{1 + v/\gamma}}{a_o \beta} \left( f_e^o + \frac{\Delta \lambda_i}{|\lambda_e|} \right)^{1/2} \text{ (V/cm)}$$

for

$$0 \ll u_i \lesssim u_{i_t} \quad (4.33)$$

Typical experimental parameters of  $I = 5 \times 10^4$  amperes,  $a_0 = 1$  cm,

and 
$$\gamma_L = 3, \quad \frac{\Delta\lambda_i}{|\lambda_e|} = \frac{1}{\gamma_L^2}$$

$$f_e^0 = \frac{1}{\gamma_L^2}$$

give  $\bar{E}_z = 9 \times 10^5$  V/cm, in which case the electrons would essentially lose all their kinetic energy over a distance equal to the beam radius. Our approximation that  $\partial\beta_{Le}/\partial u_i = 0$ ,  $0 < u_i < u_{it}$ , is, of course, violated. This example leads us to the concept of a strong inductance-dominated pinch collapse. Generally speaking if  $v/\gamma \ll 1$ , and the beam enters a region of higher charge neutralization, the pinch rate is slow and  $u_{it} \gg a_0$ , whereas if  $v/\gamma \approx 1$ , the pinch is strong-inductance-dominated, i.e., the magnetically driven beam collapse is so fast that the "I dL/dt"  $E_z$  field degrades the electron kinetic energy over distances of the order of the beam radius. The current drops, retarding further pinching. This condition is a "saturation" condition in the sense that further increases in the charge neutralization or the effective  $v/\gamma$  do not appreciably increase  $E_z$ . Moreover, the strong-inductance dominated pinch is the state where essentially all of the magnetic energy of a beam in a pipe ( $1/2 LI^2$ ) could be extracted by a localized charge density inhomogeneity. The saturated  $E_z$  field value is

$$E_z^{\text{sat}} \approx \frac{60 I (\text{amps})}{a_0} \quad (\text{V/cm}) \quad (4.34)$$

obtained by taking  $\partial a_e/\partial t \approx c$ . For  $I = 5 \times 10^4$  amperes,  $E_z^{\text{sat}} \approx 3 \times 10^6$  V/cm.

\* L is the inductance/length. This analogy to linear pinch phenomenology is somewhat ambiguous. The  $E_z$  pinching field in the ion frame is electrostatic, whereas to a stationary observer in the lab frame, the field appears as an I dL/dt field when the ion bunch passes the observer.

A contribution to  $E_z$  from electron bunching ( $\propto \frac{\partial \lambda_e}{\partial u_i}$ ) therefore arises in the saturation case and this field is required for the mechanism to "work." Roughly speaking, the pinching field gives synchronization and the concomitant electron bunching contributes to longitudinal phase stability. In the saturated case, of course, these components cannot be treated independently. The electron bunching field, which we call  $E_z^2$ , is of the same order of magnitude as  $E_z^1$ , the pinching field. In fact, in the saturation case where the electron streaming velocity is significantly reduced, one might guess that  $E_z^2$  actually exceeds  $E_z^1$  around  $u_i = 0$ . Both  $E_z^1$  and  $E_z^2$  have the same limit, given by Equation (4.34), but the pinching limit is actually necessarily lower inasmuch as a completely radial velocity would cause  $B_\theta$  to vanish, and  $B_\theta$ , of course, "drives" the pinch. That  $E_z^2$  is a maximum around  $u_i \approx 0$  may be argued by analogy with Langmuir-Childs diode theory (Section 2.1). The position  $u_i \approx 0$  corresponds to the anode and  $u_{it}$  to the cathode. The pinching of the beam envelope is analogous to diodes where the current exceeds the critical current.\* (The fact that ions are accelerated in the same direction as the electron flow in our model points to the essential distinction between inertially driven and externally applied fields.)

A further contribution to  $E_z$ ,  $E_z^{\text{ion}}$  comes from the variation in ion charge/length in region 1. If  $l_i$  is the rise length of the  $\Delta\lambda_i$ , and  $\overline{\Delta\lambda_i}$  is the peak value,

$$\frac{\partial \Delta\lambda_i}{\partial u_i} \sim \frac{\overline{\Delta\lambda_i}}{l_i} \quad \text{and}$$

$$E_z^{\text{ion}} = -2 \frac{\overline{\Delta\lambda_i}}{l_i} \left( \frac{1}{2} + \ln R/a_0 \right)$$

\*The experimental observations on beam pinching in diodes with gap spacings of the order of  $u_{it} \lesssim 1$  cm gives us some confidence in our approximate analysis.

In order to use the beam envelope collapse analysis above, we must have  $\ell_i \lesssim a_0$ , otherwise the envelope collapse is adiabatic. To be more precise, the adiabatic limit pertains to envelope changes over a length scale  $\gg \lambda_\beta$ , the betatron wavelength. Equation (4.30) shows that the turning length is  $\sim \lambda_\beta \sim a_0$  when  $v/\gamma \sim 1$  and

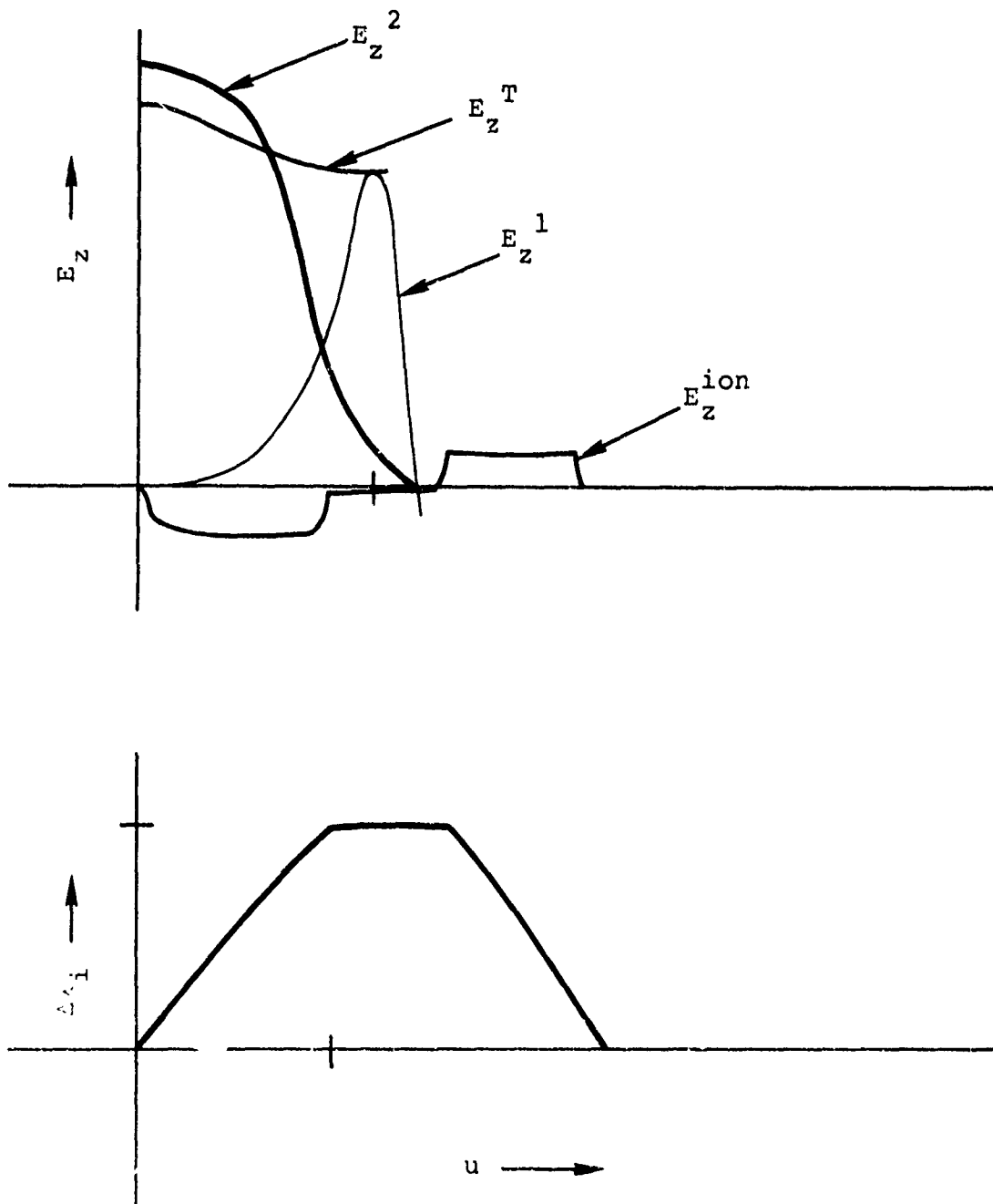
$$\left( f_e^0 + \frac{\Delta\lambda_i}{\lambda_e} \right)^{1/2}$$

is of order unity, as it is with the experimental parameters. Although the beam envelope equation we used above did not include a variation in  $\Delta\lambda_i$  with  $u_i$ , the analysis should be quite good if  $\ell_i \lesssim a_0$ ; i.e., in the non-adiabatic limit.

The total  $E_z$  field about the ion bunch,  $E_z^T$ , is

$$\begin{aligned} E_z^T &= E_z^1 + E_z^2 + E_z^{\text{ion}} \\ &\approx \frac{2\lambda_e}{a_e} \frac{\partial a_e}{\partial u_i} - 2 \left( 1/2 + \ln R/a_e \right) \left( \frac{\partial \lambda_e}{\partial u_i} + \frac{\Delta\lambda_i}{\lambda_i} \right) \end{aligned} \quad (4.35)$$

A sketch of the contributions to  $E_z^T$  is shown in Figure 4.6, reflecting the remarks above regarding  $E_z^1$  and  $E_z^2$ .  $E_z^{(1)}$  rises from zero at  $u_i = 0$  because of electron inertia and keeps the electron bunching leading the tail end of the ion bunch ( $u_i \approx 0$ ).  $E_z^{(2)}$  prevents loss of ions around  $u_i = 0$ . These two components added together maintain a relatively uniform  $E_z^T$ , the one peaking where the other vanishes. This discussion requires further quantitative support, of course, but hopefully at least makes the synchronous mechanism plausible. Part of our motivation for invoking a two-dimensional beam motion in the first place is now perhaps apparent. A one-dimensional model such as Rostoker's



4.6 Longitudinal electric fields of the synchronous ion density enhancement.

which utilizes electron bunching near the beam front (an  $E_z^2$  field) has the desired longitudinal phase stability. However, multiple pulse data, where the beam is definitely extended in front of the second pulse, requires some other way to maintain electron bunching. (It is also difficult to see how a one-dimensional ES well can impart significant net energy to ions of a second pulse. The electrons would gain energy as they approached the bunch and lose energy when they passed it.)

Radial stability of the pulse at least requires that the outward  $v \times B$  force on the ions not be greater than the inward space charge electric field:

$$\beta_{L_i} \leq \frac{\left[1 - \left(f_e^o + \frac{\Delta\lambda_i}{|\lambda_e|}\right)\right]}{\beta_{L_e}} \approx \frac{\left[1 - \left(f_e^o + \frac{\Delta\lambda_i}{|\lambda_e|}\right)\right]}{\beta_e} \sqrt{1 + \frac{v}{\gamma}} \quad (4.36)$$

If  $v/\gamma \sim 1$ ,  $\beta_e \sim 1$ ,

$$\frac{\Delta\lambda_i}{|\lambda_e|} \sim \frac{1}{\gamma_L}, \quad f_e^o \sim \frac{1}{\gamma_L},$$

we have radial stability for  $\beta_{L_i} \leq 1$ .

More quantitative statements regarding the stability are outside the analysis above. A linear stability investigation currently underway should give more insight into the important questions of pulse stability, growth times, and pulse lifetime.

4.3.2 Ion Bunching. Let us now address the question of the initial formation of a non-adiabatic beam collapse condition. An obvious way to do so would be, of course, to inject a pulse with rise length of the order of the beam radius. We can argue bunching in the experimental situation in several ways. Basically we require an electric field gradient or a localized electric field large enough to accelerate ions out of a region faster than collisional ionization can restore an approximately uniform ion density. The electric fields can arise from electron space charge bunching and/or beam pinching. We consider below space charge field bunching and defer pinching effects to an instability analysis.

A bunching arises even in an open-ended potential well (Figure 4.7) simply because ions are formed at various distances within the well by collisional ionization. To illustrate this point, we estimate the ion charge density in an open-ended well assuming uniform ion production over the well and well velocity  $v_p \ll \beta_{Li}^0 c$  where  $\beta_{Li}^0 c$  is the velocity corresponding to an ion accelerated over the full width of the well. Within a width  $dz_0$ ,  $z_1 \leq z_0 \leq z_2$ , the collisional ion density,  $\Delta \rho_{ion}^1$ , is

$$\Delta \rho_{ion}^1 \approx \frac{|\lambda_e|}{\pi a_0^2} \frac{dz_0}{\tau_N}$$

and the density of ions created within the well as a function of  $z$  is

$$\rho_{ion}^1(z) = \left( \sqrt{\frac{m_i}{2Ze}} \right) \frac{|\lambda_e|}{\pi a_0^2} \frac{1}{\tau_N} \int_{z_1}^z dz_0 \frac{1}{\sqrt{|V(z) - V(z_0)|}} \quad (4.37)$$

$$z_1 \leq z \leq z_2$$

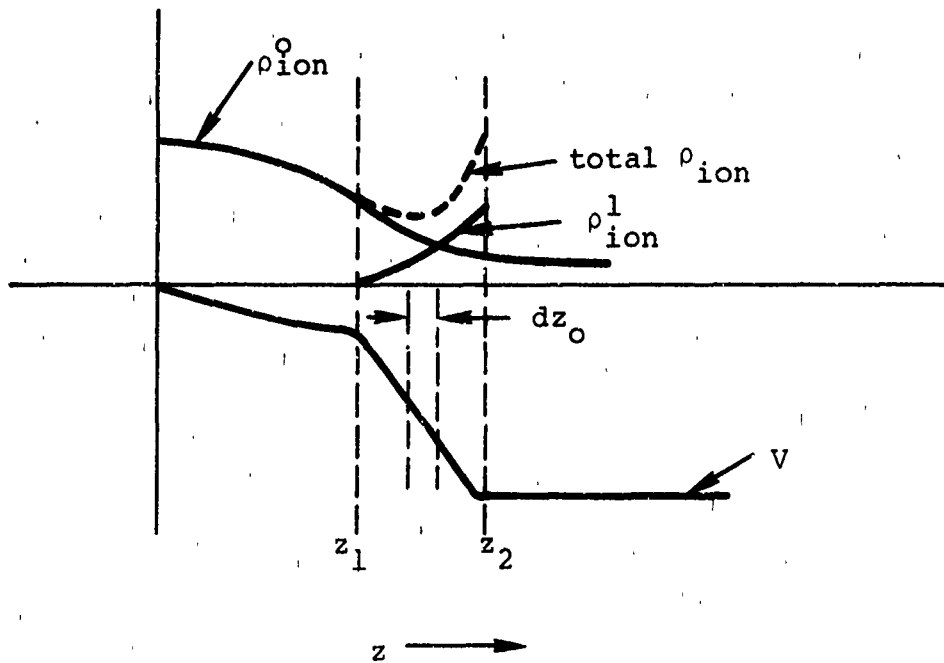


Figure 4.7 Bunching in a slowly moving open-ended potential well

If  $V(z) \approx E_z (z-z_1)$ ,  $E_z$  assumed constant, we obtain

$$\rho_{ion}^1(z) \approx \sqrt{\frac{m_i^0}{2Ze}} E_z \frac{|\lambda_e|}{\pi a_0^2} \frac{2}{\tau_N} \sqrt{z-z_1}, \quad z_1 < z < z_2 \quad (4.38)$$

The total ion density within the well is obtained by adding the contribution of the upstream ion flux incident upon the well,  $\rho_i^0$ . This contribution varies as  $(z_1 - z)^{-1/2}$  by similar arguments. In the actual experimental situation, this relatively weak bunching effect is augmented by the partially closed nature of the well. Because of radial electron loss, the well near the beam front is more like that shown in Figure 4.8. (Recall also from Section 2.10.1 that even without beam loss, the  $E_z$  field reverses direction behind the front in a finite cavity.) We derive a simple criterion for bunching in this case, assuming  $\Delta V/V \ll 1$ .

If  $j_{ion}$  is the  $z$  component of the ion current due to the space charge field and  $\partial \rho_{ion} / \partial t$  is due to collisional ionization, bunching will occur when

$$\frac{\partial j_{ion}}{\partial z} \gg \frac{\partial \rho_{ion}}{\partial t} \quad (4.39)$$

Rewriting this inequality,

$$\frac{|\lambda_e| f_e \beta_{L_i}^0}{\bar{z}_c \pi a^2} \gg \frac{|\lambda_e|}{\pi a^2} \frac{df_e}{dt} = \frac{|\lambda_e|}{\pi a^2} \frac{1}{\tau_N}$$

or

$$\frac{f_e \beta_{L_i}^0}{\bar{z}_c} \gg \frac{1}{\tau_N} \quad (4.40)$$

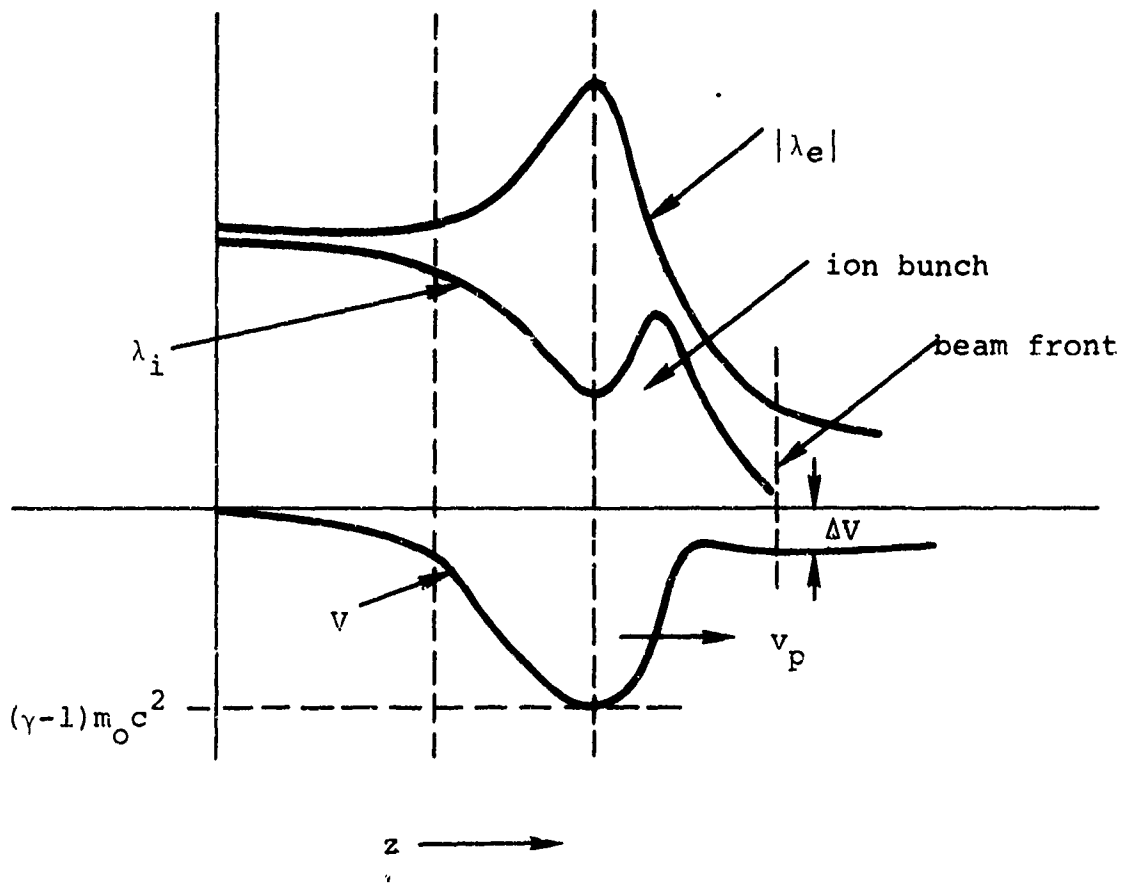


Figure 4.8 Bunching near the anode with a partially closed well

with  $\beta_{L_i}^0 c$ , the velocity an ion obtains after acceleration over the full width of the well. If we use the space-charge limited value for  $\bar{z}_c$ ,

$$\bar{z}_c \text{ (cm)} \approx 85 a \left[ \frac{V \text{ (MeV)}^{3/2}}{I \text{ (amps)}} \right]^{1/2}$$

and with

$$\beta_{L_i}^0 c \text{ (cm/sec)} \approx 1.4 \times 10^9 \left[ \frac{Z m_p}{m_i} V \text{ (MeV)} \right]^{1/2}$$

Equation (4.40) becomes

$$\tau_N \text{ (nsec)} \geq \gamma^2 \left[ \frac{1}{j_b} \left( \frac{m_i}{Z m_p} \right) \sqrt{\frac{\gamma-1}{2}} \right]^{1/2} \quad (4.41)$$

The beam current density  $j_b$  is in kA/cm<sup>2</sup>,  $m_p$  is the proton mass, and  $f_e \approx 1/\gamma^2$  was assumed.

Let us compare this formula with the Graybill-Uglum data on the high pressure cutoff for proton acceleration. If we assume that the experimental beam radius was approximately the cathode radius, their maximum  $j_b \approx 8 \text{ kA/cm}^2$ ,\* Equation (4.41) gives  $\tau_N \geq 3.2 \text{ nsec}$ . In order to obtain direct agreement with the experimental data, the inequality has to be replaced by a factor of  $\sim 10$ . In view of the approximations in our discussion, as well as uncertainties in estimating  $\tau_N$ , it is not worthwhile in pursuing a data fit further.

\* This assumption is strictly valid only until  $I \sim 8500 \sqrt{\gamma^2 - 1} (r_c/d)$ , or until about 15 kA.

We have given a physical argument showing that the longitudinal space charge field is adequate to bunch ions, so when the beam front passes the beginning of the "pinch-active" region,  $z \gtrsim R/2.4$ , the radial electric field is no longer shorted out by the endplate and, if  $f_e > 1/\gamma^2$ , the preformed bunch may begin synchronous acceleration according to the LPM. Growth of the bunch ion density will occur until  $v_p > \beta_{Li}^0 c$ , at which velocity background ions can no longer be picked up by the coherently accelerated bunch.

The LPM model is itself suggestive of an instability growth of bunches; i.e., the beam appears unstable to ion density inhomogeneities when  $1/\gamma^2 < f_e < 1$ . The instability would be two-dimensional EM in contrast to the well-known ES longitudinal streaming instabilities. Moreover, such an instability would not appear to be stabilized by longitudinal beam velocity spreads since the pinching force is magnetically (or current) driven. We defer a detailed treatment of instability bunch growth for later publication.

4.3.3 Acceleration Cutoff Mechanisms. Experimental evidence indicates that the acceleration process rather abruptly terminates at a length  $L_{acc}$  (Figure 4.9). The PI data show  $L_{acc} \lesssim 7$  cm and the IP data suggest  $L_{acc} \lesssim 20$  to 30 cm. We now consider possible cutoff mechanisms and suggest some relatively simple experiments to check these speculations.

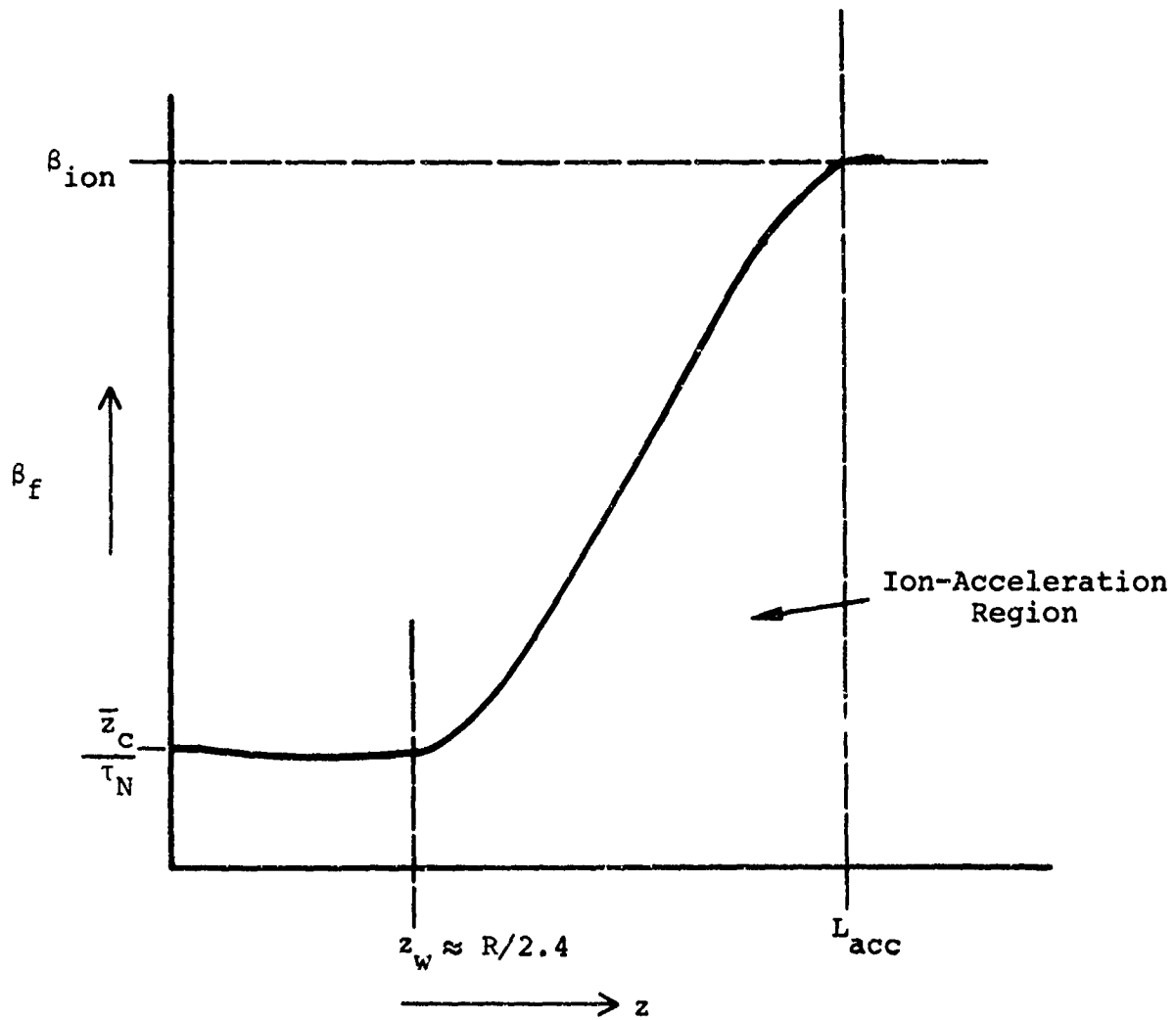


Figure 4.9 Beam-front velocity as a function of distance from the anode for a beam penetrating a neutral gas.

The ion velocity is certainly limited by the electron streaming velocity, and within the context of the LPM, there exists a more restrictive kinematical limitation for the acceleration mechanism since the electron envelope requires time to contract. This limit would roughly correspond to ion velocities of  $\beta_e/\sqrt{2}$ . In view of the constancy of the observed ion energy/charge state for protons as well as nitrogen and argon, this acceleration limitation appears unlikely.

Perhaps the most obvious reason is that the accelerating fields somehow lose synchronization with the ion bunch and accelerate "fresh" background ions. (This would be the case if the potential well reached an acceleration value such that field becomes too low to trap the ions, a cutoff mechanism proposed by N. Rostoker.) The process could terminate acceleration for the IP beam where the beam front precedes the ion bunch, or for the second ion pulse with PI data. In any case, the mechanism is not relevant to the first PI proton bunch since the beam front stays with the ions.

If a well does accelerate and leaves the coherently accelerated bunch behind, one would expect to observe at appropriate pressures a distribution of ions with energies in the tens of keV range generated by the well as it proceeds to the end of the drift chamber. The energy spectrum would, of course, depend on the acceleration history of the well.

Let us consider the IP proton data to illustrate this point. The observed proton energy was  $4.8 \pm 0.9$  MeV, corresponding to an ion velocity  $\approx 0.1c$ ; the drift chamber length was 50 cm and  $L_{acc}$  was approximately equal to 25 cm. We need to know the kinetic energy given an untrapped ion created in a potential well of depth  $V$  as the well moves by it. For simplicity, we consider a well moving with constant velocity,  $\beta c$ , and obtain from relativistic kinematics an expression for the kinetic energy, K.E., imparted to ions as the well moves by:

$$K.E. = M_i c^2 \left\{ \gamma^2 (1-\alpha) - 1 - \beta \gamma \left[ \gamma^2 (1-\alpha)^2 - 1 \right]^{1/2} \right\} \quad (4.42)$$

where  $M_i$  is the ion rest mass,  $\gamma = 1/\sqrt{1-\beta^2}$ ,  $\alpha = ZeV/\gamma M_i c^2$ , and  $V$  is the well depth. If  $\alpha \ll 1$ , Equation (4.42) reduces to  $K.E. \approx [Z^2 (eV)^2 / M_i c^2] 1/2\beta^2$ . Thus, for protons, and  $\beta \geq 0.1$ ,  $eV \approx 1$  MeV, the background ion energy from the accelerating well is  $\leq 53$  keV. The time for such an ion to travel the remainder of the drift chamber ( $\sim 25$  cm) would be  $\approx 78$  nsec, during which time the beam would have certainly neutralized the potential barrier at the downstream end of the chamber at the 300  $\mu$ m pressure value. It would be important in any experiment to rule out background ion acceleration from beam inductive fields which might be important after space charge neutralization.

Another possible acceleration cutoff would obtain if the beam electrons precede the ion pulse by a sufficient distance to give  $f_e \approx 1$  in front of the ion bunch. Secondary electrons then "short out" or damp beam envelope oscillations. This possibility is again relevant to the IP ion pulse and the second pulse for PI. It seems unlikely that this mechanism is operative, however, inasmuch as it would imply ion energies inversely proportional to chamber pressure and would rule out multiple pulses.

A cutoff process relevant to the first PI ion pulse, where the beam front and ions travel together, would occur if the ion velocity eventually reaches values such that  $f_e$  of the background drops below  $1/\gamma^2$ . In other words, the collisional ionization rate due to the beam electrons and accelerated ions is no longer sufficient to maintain the  $f_e^0 \approx 1/\gamma^2$  as the beam front penetrates the neutral gas. One can easily show that for ion energies greater than a few MeV, the accelerated ions themselves can maintain  $f_e^0 \geq 1/\gamma^2$  for typical experimental ion pulse lengths of 10 cm and  $\beta_i \approx 0.1$ . In any case, such a cutoff mechanism would be pressure sensitive and would give a higher energy for the second ion pulse than for the first. Moreover, this cutoff could be overcome by a pressure gradient in the drift tube.

Finally, we come to a mechanism which appears to be a likely possibility in the present experimental configuration--depletion of the ion supply behind the accelerating bunch. The ion supply may be depleted upstream from the pulse since accelerating fields moving in space generate a wake ion current during pulse growth and acceleration. The electrostatic potential well is reestablished near the anode as the ions are removed by the wake ion current, and the electron kinetic energy is degraded downstream, thereby terminating acceleration. Such a mechanism would explain multiple pulse formation; the bunching and accelerating process repeats as the ion charge density again grows near the anode from collisional ionization. Also, this mechanism would explain the inverse dependence of pulse separation upon pressure, since  $\tau_N \propto (\text{pressure})^{-1}$ .

We express these remarks in a slightly more quantitative way:

$$\int_{t_0}^{t_{\text{acc}}} \left[ I_{\text{ion}} - \frac{dQ_{\text{ion}}}{dt} \right] dt = K \quad (4.43)$$

where

$I_{\text{ion}}$  = average wave current behind accelerating bunch

$\frac{dQ_{\text{ion}}}{dt}$  = ion production rate within effective supply volume

$K$  = effective ion supply

$t_0$  = time of start of acceleration

$t_{\text{acc}}$  = duration of acceleration

Let  $\frac{dQ_{ion}}{dt} = C_1/\tau_N$ , and

$$I_{ion} \approx \bar{F}_e I_b \frac{\bar{\beta}_{L_i}}{\bar{\beta}_{L_e}} c \approx C_2 \bar{\beta}_{L_i} \propto (Z/m_i)^{1/2}$$

where  $\bar{F}_e$  is the average background ion density during acceleration and  $\bar{\beta}_{L_i} c$  is the average wake ion velocity. Then Equation (4.43) becomes

$$t_{acc} - t_0 \approx \Delta t \cong K \left[ \frac{1}{C_2 \bar{\beta}_{L_i} - C_1/\tau} \right] \quad (4.44)$$

If collisional ion production is negligible compared to the  $I_{ion}$  term over  $\Delta t$ , Equation (4.44) says that  $\Delta t \sim (m_i/Z)^{1/2}$ , which, in turn, implies that the final ion energy is independent of the ion mass, in accordance with the data.

An experimental check of the ion depletion hypothesis can be made by measuring the electron kinetic energy as a function of time. The number of beam electrons with energies of the order of the injected energy should drop significantly when the acceleration is terminated.\* It is important that these measurements be performed in the chamber interior to the electron-accelerating space charge fields near the downstream chamber end-plate.

If the ion supply depletion hypothesis is experimentally verified, the obvious question remains as to how to extend  $L_{acc}$ ; i.e., how can the ion supply be enhanced? A method of

\*The beam current cannot "shut off," however, because of inductive effects.

effectively doing this would be to inject an accelerated ion bunch into a second accelerating stage. The wake ion current is inversely proportional to the injected ion velocity, and the acceleration time in the second stage proportional to the injected velocity. In principle, the average wake current could be reduced until  $C_L \bar{\beta}_{Li} \approx C_1/\tau_N$  in Equation (4.44), a condition where acceleration would no longer be supply limited.

## REFERENCES

### SECTION 4

- 4.1 S. Putnam; Physical Review Letters, 1970, Vol. 25, Page 1129; Unclassified.
- 4.2 S. Putnam; IEEE Transactions on Nuclear Science, 1971, Vol. NS-18, No. 3, Page 496; Unclassified.
- 4.3 V. Veksler, "CERN Symposium for High Energy Accelerators and Particle Physics"; June 1956, Page 80; Unclassified.
- 4.4 E. Lofgren; Transactions on Nuclear Science, 1971, Vol. NS-18, No. 3, Page 456; Unclassified: M. Reiser; IEEE Transactions on Nuclear Science, 1971, Vol. NS-18, No. 3, Page 460; Unclassified.
- 4.5 S. Graybill and J. Uglum; J. Applied Physics, 1970, Vol. 41, Page 236; Unclassified.
- 4.6 J. Rander and others; Physical Review Letters, 1970, Vol. 24, Page 283; Unclassified.
- 4.7 J. Rander; Physical Review Letters, 1970, Vol. 25, Page 893; Unclassified.
- 4.8 S. Graybill and others; "Conference on Heavy Ion Sources"; 1970; U. S. Atomic Energy Commission, Washington, D. C.; Page 219; Unclassified.
- 4.9 N. Rostoker; Report No. LPS 21, 1969; Laboratory for Plasma Studies, Cornell University, Ithaca, New York; Unclassified.
- 4.10 S. Graybill and others; DASA Report 2477, June 1970; Defense Nuclear Agency, Washington, D. C.; Unclassified.
- 4.11 B. Eastlund and J. Wachtel; Bulletin of the American Physical Society, 1969, Vol. 14, Page 1047; Unclassified.

REFERENCES (cont.)

- 4.12 H. Grunder and J. Peterson; Private Communication, June 1971; Unclassified.
- 4.13 A. Sessler; UCRL-19242, July 1969; Lawrence Berkeley Laboratory, Berkeley, California; Unclassified.
- 4.14 M. Rabinovich; Preprint No. 36 of the Plasma Accelerator and Plasma Physics Laboratory, Lebedev Physics Institute, Moscow, USSR, March 1969; UCRL-Translation No. 1398, Lawrence Berkeley Laboratory, Berkeley, California; Unclassified.
- 4.15 S. Graybill; IEEE Transactions on Nuclear Science, June 1971, Vol. NS-18, Page 438; Unclassified.
- 4.16 J. Rander and others; PIFR-2-71, July 1971; Physics International Company, San Leandro, California; Unclassified.
- 4.17 A. Plyutto; JETP Letters, 1967, Vol. 6, Page 540; Unclassified.
- 4.18 E. Korop and A. Plyutto; Soviet Physics-Technical Physics, 1971, Vol. 15, Page 1986; Unclassified.
- 4.19 A. J. Prentice; Plasma Physics, 1967, Vol. 9, No. 4, Page 433; Unclassified.
- 4.20 S. Bludman and others; Physics of Fluids, 1960, Vol. 3, No. 5, Page 757; Unclassified.
- 4.21 P. Felsenthal; Physical Review, 1965, Vol. 139, Page A1796; Unclassified.
- 4.22 I. Kapchinskij and V. Vladimirkij; "Proceedings of the International Conference on High Energy Accelerators and Instrumentation-CERN,"; 1959; Page 274; Unclassified.

## SECTION 5

### SUMMARY

The theoretical beam research described in this report has been undertaken in support of Defense Nuclear Agency-sponsored experimental research at Physics International Company and has been reported to the beam physics community and Defense Nuclear Agency in a series of papers and reports, notably PIFR-105, April 1970. We briefly summarize the contributions of the program below.

1. Characterization of the Background Gas Plasma. A procedure has been developed to predict gas breakdown charge densities and conductivities and degree of current neutralization as a function of gas pressure, constituency and beam parameters. We can thus predict conditions required for beam pinching or drifting.
2. Definition of High  $v/\gamma$  Beam Propagation Limits. An explanation of the propagation of  $v/\gamma > 1$  beams in terms of current neutralization or  $v_{net}/\gamma$ , and the dominant role of the electromagnetic interpretation of  $v_{net}/\gamma$  were first presented during the program.
3. Explanation of the General Features of Beam Instability. The qualitative character of beam instabilities as a function of background gas pressure has been outlined. In particular, the important "frozen hose" instability of pinched beams at low pressure has been explained and instability wavelengths may now be predicted.
4. Development of the Concept of Plasma Channeling. When a beam breaks down the background gas, a highly conducting plasma channel is formed with a "frozen-in" magnetic field, which serves to guide subsequent beam electrons. Understanding the properties of the plasma channel has important applications in beam bending and combining.

5. Role of Current Density Parameter. The importance of the current density, in addition to the  $v/\gamma$  ratio, has been explicitly exhibited in neutral gas and external field propagation.

6. Transport in Linear Pinch Plasmas. A complete phenomenological exposition of beam transport in linear pinch plasmas has been presented and a model of beam penetration of pinch plasmas in violation of single particle orbit theory has been developed to estimate plasma expansion due to transverse pressure imbalance. Criteria for efficient beam propagation of high  $v/\gamma$ , high current density beams have been presented.

7. Solenoidal Field Transport. A model for determining upper limits on  $B_z$  fields for efficient transport has been proposed along with formulae to estimate beam channel diamagnetism or paramagnetism and its concomitant energy loss effects.

8. Calculations of the Electromagnetic Fields of Beams with Various Boundary Conditions. Exact electromagnetic field expressions for finite beams in drift chambers of finite radius and length filled with a gas of constant conductivity and in long conducting pipes with conductivity varying with distance behind the beam head have been developed. Quasistatic electric field expressions have been derived including variation of beam radius with distance and time, endplates and charge neutralization.

9. Development of Ion Acceleration Models and Analysis of Low Pressure Beam Transport. Ion acceleration mechanisms have been surveyed and a new accelerating process has been proposed which gives detailed agreement with experimental data--the electric fields associated with the non-adiabatic pinch collapse of the beam synchronize the acceleration process.